ANALYSIS AND TEST STRATEGIES FOR STRESS RUPTURE IN UNIDIRECTIONAL CONTINUOUS FIBER COMPOSITE STRUCTURES

A Dissertation

Presented to the Faculty of the Graduate School

of Cornell University

In Partial Fulfillment of the Requirements for the Degree of

Doctor of Philosophy

by

Amy Elspeth Engelbrecht-Wiggans

December 2017

ANALYSIS AND TEST STRATEGIES FOR STRESS RUPTURE IN UNIDIRECTIONAL CONTINUOUS FIBER COMPOSITE STRUCTURES

Amy Elspeth Engelbrecht-Wiggans, Ph. D.

Cornell University 2017

Stress rupture is a catastrophic failure mode in continuous unidirectional fiber composites, such as those used in composite overwrapped pressure vessels (COPVs). COPVs are currently used mainly in aerospace applications, such as storing the reserve oxygen on the International Space Station. Indeed a carbon/epoxy COPV failure caused the September 2016 explosion of the SpaceX Falcon 9 rocket at Cape Canaveral, leading to more than a billion dollars of damage. Currently COPVs are used in relatively small numbers, but the day is rapidly approaching when they will be used in the millions in many aspects of daily life, particularly in automotive applications.

My research seeks to better understand stress rupture and more accurately estimate the probability that a specific composite structure will fail in stress rupture. Prediction of a composite's stress rupture behavior is heavily based on results from extensive testing, as there are not yet methods to predict a composite's stress rupture behavior based on the component materials' properties. Testing results in comparatively small datasets of accelerated test data, which then must be extrapolated to predict a failure probability for a the service life of interest. This dissertation shows that the method used to analyze these datasets is crucial to accurately estimating the probability of a stress

rupture failure, and also presents a data analysis method with lower variance and MSE estimates than current ad-hoc industry methods. Furthermore this dissertation compares current stress rupture models and derives a new, micromechanical stochastic stress rupture model.

BIOGRAPHICAL SKETCH

Amy Engelbrecht-Wiggans grew up in Champaign Urbana IL, attending local Champaign schools. In 2006 Amy began her B.S. in Engineering Mechanics with a specialization in Mechanics of Materials at the University of Illinois at Urbana Champaign. Amy also obtained minors in Computer Science and Mathematics. Amy used her time at the U of I to take as many classes in how things break as possible. While at the U of I, Amy took on many leadership roles, particularly with the Krannert Center Student Association and the Society for Experimental Mechanics. Also during her undergraduate career Amy spent one year studying abroad in Bilbao, Spain. Over the summers she worked to design, organize and teach workshops, design projects and classes for the Girls Adventures in Math, Engineering and Science program, a summer camp for middle school girls interested in STEM.

In 2011 Amy began her doctoral studies with Dr. Stuart Leigh Phoenix in the field of Theoretical and Applied Mechanics at Cornell University. During her time at Cornell Amy enjoyed the opportunity to teach undergraduates, serving as a teaching assistant on seven separate occasions and receiving the H.D. Block Teaching Award for her outstanding service. Amy also twice had the opportunity to be an instructor for the Design and Operations of Composite Overwrapped Pressure Vessels, a five day course sponsored by the International Association for the Advancement of Space Safety. In addition to teaching Amy also published several papers in peer-reviewed journals, reviewed papers, and bought a horse.

ACKNOWLEDGMENTS

I thank my advisor, Dr. Stuart Leigh Phoenix, for his guidance and mentoring in directing my PhD work, as well as taking me on as a student despite the influence of my family. I also thank him for teaching me tact. I would like to thank my committee, Meredith Silberstein and Gennady Samorodnitsky. Thanks also to Michael Kezirian.

I thank Air Products Inc, and NIST Agreement ID 70NANB14H323 for the funds they provided.

I thank my father, Dr. Richard Engelbrecht-Wiggans, for being a second, unofficial advisor. I also thank both my parents for their continued support and encouragement. My Ithacan family is also due for a large dose of thanks for everything they do for me.

More generally I would like to thank all the people who have offered assistance, moral support, friendship and inspiration over the past many years. Your friendship has meant the world to me.

Finally I'd like to thank Lacy for keeping me sane and grounded throughout the past three years.

TABLE OF CONTENTS

LIST OF FIGURES

LIST OF TABLES

CHAPTER 1

INTRODUCTION

Stress rupture is a failure mode in continuous, unidirectional fiber composites subjected to a constant load over long time periods. It can occur at normal operating stresses and temperatures at maintained stresses well below the ultimate strength for an extended time. Stress rupture is catastrophic and explosive, and occurs with little or no advance warning. Its occurrence is also highly variable: two otherwise identical specimens, under identical loading and environmental conditions, can fail at times that differ by orders of magnitude.

Prediction of a composite's stress rupture behavior is heavily based on results from extensive testing. These tests fall into two categories: strength testing and lifetime testing. Strength testing consists of applying a linearly increasing load until failure. Strength failures typically occur in under a minute. Lifetime testing consists of applying a steady load, higher than the service load, until either the specimen fails or the test is ended. Lifetime testing typically spans months to years and involves groups of specimens loaded at different load levels. Variance in failure times is high for lifetime tests, ranging from immediate failure to specimens that have not failed after over a decade of testing, leading to censored data sets. Strength testing is required to determine the load levels used in lifetime tests, even though stress rupture failures only occur in lifetime testing.

Extrapolation is required to predict a composite structure's resistance to stress rupture based on test results. This is for two reasons: first, the design life, which can sometimes be decades, is generally longer than the amount of time available for testing, and second, the desired probability that a structure will fail in the designed service life is very small (frequently less than

one in a million). Thus even if tests could be run for the length of the desired service life, an infeasible number (perhaps ten million) of specimens would need to be tested to guarantee such a small probability of failure. Because of cost and equipment limitations, real stress rupture data sets generally contain fewer than two hundred specimens, thus requiring higher load levels and a modeling approach.

With stress rupture, a probabilistic stress rupture model is used to extrapolate from the limited data. The data is analyzed to determine model parameters, which in turn are used to predict the failure probability under a given load profile. Much of my research to date has been in developing statistical estimation procedures for such probabilistic stress rupture models for composite structures. I used Monte-Carlo simulation techniques to choose between different maximum likelihood estimation (MLE) based approaches for analyzing stress rupture data sets, as is described in Chapter 2. Chapter 3 then details the procedure resulting in the least error when estimating failure probabilities, complete with implementation on an example dataset. An estimate of the failure probability alone is not the full answer, however, and Chapter 4 gives one method for determining the amount of uncertainty in the failure probability estimate, as well as a method for removing the bias in the failure probability estimate, for the same example dataset.

Several probabilistic stress rupture models exist that can be used to extrapolate with. The oldest and most commonly used model is the classic power-law model in a Weibull framework (CPL-W). Coleman developed the CPL-W model in the 1950s using Tobolsky-Eyring theory for molecular bond breakage in a single fiber. Other models include a functional form proposed in 1979 by Phoenix, a Paris-law style crack-growth based model proposed in 1981 by Kelly and McCartney, a strength decay model by Reeder in 2012, and a micro-mechanical based model, termed the ‘stochastic fiber breakage model’, proposed by Phoenix and myself. A comparison of

all but the last of these models is given in Chapter 5, while the stochastic fiber breakage model itself is derived in Chapter 6.

The combination of an accurate model and estimation procedure allows for prediction of a composite's stress rupture behavior from test data. The research presented in this dissertation aims to discover these two things.

CHAPTER 2

COMPARISON OF MAXIMUM LIKELIHOOD APPROACHES FOR ANALYSIS OF COMPOSITE STRESS RUPTURE DATA

The following chapter is published in the Journal of Mechanical Science and reprinted here with permission. The reference to the published work is:

Engelbrecht-Wiggans A, Phoenix SL (2016) Comparison of maximum likelihood approaches for analysis of composite stress rupture data, J Mater Sci DOI 10.1007/s10853-016-9950-3

2.1 Introduction

When a unidirectional continuous fiber, polymer-matrix composite is placed under a steady tensile load for a long period of time, it may fail suddenly and catastrophically with little or no warning. The phenomenon is known as stress rupture. Examples of structures susceptible to stress rupture are composite overwrapped pressure vessels (COPVs), composite flywheels for energy storage and long tension members used in civil engineering structures, all of which are essentially unidirectional in function.

Mechanistically, stress-rupture is a time dependent failure process where individual fibers fail successively until the specimen fails. Individual fibers inherently have high variability in strength, and are considered to be strong except for randomly distributed flaws. On initial loading, the flaws with strength less than the applied load will fail. The load that had been carried by a broken fiber is transferred to its neighbors in shear causing stress concentrations. This may immediately cause more broken fibers around the break, ending when the specimen becomes temporarily stable or when the specimen fails due to a cascade of broken fibers.

If the specimen is stable, two further failure mechanisms may occur over time: thermally activated fiber breakdown at the nanoscale and matrix creep. In matrix creep the distance over which the neighboring fibers are overloaded increases over time until one of the neighboring fibers has a flaw in the overload region and thus fails. Either way, clusters of broken fibers grow over time, ultimately leading to sudden instability and thus failure of the specimen in stress-rupture.

While the stress rupture process is thus describable in mechanistic terms, a practicable mechanical model requires a large number of assumptions. Furthermore, randomness in both thermal activation events and the location and severity of flaws in a given specimen are not knowable. Thus instead of being able to predict exactly when a particular specimen will fail, parametric models must be used to characterize the distribution of failures of otherwise identical specimens.

Work has been done to model stress rupture failure based on the properties of the constituent materials and the known micromechanics as previously described [1-5]. These types of stochastic models have the potential to predict strength and lifetime distributions for a composite with minimal testing of the full-scale composite. With these models strength and lifetime distributions are predicted based solely on knowledge of the mechanics and constituent material. In contrast, this paper will look at a statistical model to interpret data from full-scale extensive testing. These statistical models may, to varying extents, be based on the micromechanics, but are more concerned with using test results to predict failures for different load profiles. With statistical models the challenge is to accurately estimate the unknown parameters and thus failure probabilities.

The oldest and most commonly used statistical model is the classic power law model in a Weibull probabilistic framework (CPL-W). In this model, a power law is used to describe the sensitivity of mean lifetime (time to failure) with respect to the stress level in the composite. For a given stress level, the Weibull distribution is then used to characterize the distribution of failure times. These failure times may be highly variable, with variance larger than the mean. Furthermore, the strength of the material (as measured in tension or burst tests) also follows a Weibull distribution, though with different parameters from the lifetime version and with much less variability. The simplest interpretation of the CPL-W model has five unknown parameters, but there are two constraints, leaving only three independent parameters. These constraints are sometimes omitted, leading to variations on the CPL-W model.

This paper investigates eight methods for estimating the parameters for various implementations of the CPL-W model based on Monte-Carlo simulated data sets. Some of these methods have appeared in the literature; others are included for insight. Monte Carlo simulation is particularly appropriate for such comparisons since we know the correct parameter values in advance and can see how accurately the various methods estimate the correct parameter values and failure probabilities.

In practices the failure probabilities are actually are more important than parameter estimates. The goal in data collection and estimation is to be able to estimate the probability that a specimen will not fail under a given load profile by a certain time. Thus the failure probabilities are ultimately a more important metric for estimation method comparison than the parameter estimates. As we will see they are also more accurately estimated than the parameter values. Thus failure probabilities will also be estimated and used as the primary metric of comparison

for various estimation methods.

This paper investigates which of eight maximum likelihood methods for the CPL-W model produces the smallest estimation error. These methods are readily applicable to any set of stress rupture data, and the aim is to determine which method results in the tightest confidence bounds on both parameter and failure probability estimates.

No actual experimental data are analyzed. Instead statistical analysis is carried out on large replications of Monte Carlo simulated data sets. These data sets are typical of those seen in practice, including having various degrees of censoring. The parameter values used in the simulations are typical of various carbon/epoxy and aramid/epoxy fiber composite systems. While only a limited number of parameter values are studied in this paper, there is every reason to believe that these results are broadly applicable, and at the very least that parameter estimation will still be a concern for different materials than those simulated here.

In "Models" we introduce stress rupture models in general and the CPL-W model and its repercussions in particular. "Testing" relates what typical stress-rupture testing consists of and describes a typical data set. "Methods" describes current methods used to estimate model parameters, the procedure used in this paper to investigate the accuracy of a method, effects of distorting a key constraint and the measures of estimation error used in this paper. In "Results" estimation error for the eight methods is given for two different materials-T1000 carbon epoxy tows and Kevlar 49-with references to general trends seen in other materials. Findings are summarized in the "Discussion and Conclusions" section.

2.2 Models

The CPL-W model for polymer based fibers and fibrous composites has its roots in the classical *Tobolsky-Eyring* theory of thermally activated bond breakage developed in the 1940s

[6]. In the context of polymer fibers and fiber bundles, seminal theoretical and experimental work on the model appeared in many papers by B.D. Coleman while at DuPont in the 1950s [7-13]. Further development of the model, as well as variations, and theoretical justification for the Weibull lifetime form (arising from molecular and fiber load-sharing) was developed by S.L. Phoenix and co-workers the late 1970's and early 1980's [14-15]. The following outlines the structure of various versions of the model that have appeared in the literature.

The cumulative distribution function (CDF) of the most general functional form of the model we assume for the lifetime of unidirectional composites is

$$F\left(t\middle|\sigma\right)=\sup_{0\le\tau\le t}\left\{\psi\left(\sigma\left(\tau\right),\, Z\left(t,\sigma\left(t\right)\right)\right)\right\}. \tag{2.1}$$

Here $\psi\left(\sigma,Z\right)$ is the shape function in terms of the non-negative stress profile, $\sigma\left(t\right),\ t\ge 0$, where Z provides for the introduction of degradation over time, reminiscent of Miner's rule [16-17], through the integral form

$$Z=\int_0^t \kappa\left(\sigma\left(s\right)\right)ds \tag{2.2}$$

This model was actually introduced by Phoenix [18] for the lifetime of individual fibers within a fiber bundle. In this application the 'supremum' function is equivalent to the maximum, except when the maximum is undefined. This assures that the cumulative distribution function is monotone non-decreasing in t.

Two specific assumptions are generally made for stress rupture. First, the power-law breakdown rule

$$\kappa\left(\sigma\left(s\right)\right)=\left(\frac{\sigma\left(s\right)}{\sigma_{\text{ref}}}\right)^{\rho},\quad \sigma\ge 0, \tag{2.3}$$

where the constant $\rho > 0$ is the power-law exponent and the constant $\sigma_{\text{ref}} > 0$ is a strength scale parameter. Second, a 'generalized' Weibull shape function is given by

$$\psi(\sigma, Z) = 1 - \exp\left\{-\left(\left(\frac{\sigma}{\sigma_{\text{ref}}}\right)^r + \frac{Z}{t_{\text{ref}}}\right)^\beta\right\}, \tag{2.4}$$

where $r > 0$ is a constant, the constant $\beta > 0$ is a shape parameter and the constant, $t_{\text{ref}} > 0$, is a lifetime scale parameter. Combining (2.1) through (2.4) we obtain the lifetime distribution function

$$F(t|\sigma) = 1 - \exp\left\{-\sup_{0 \le \tau \le t}\left\{\left[\left(\frac{\sigma(\tau)}{\sigma_{\text{ref}}}\right)^r + \int_0^\tau \left(\frac{\sigma(s)}{\sigma_{\text{ref}}}\right)^\rho \frac{ds}{t_{\text{ref}}}\right]^\beta\right\}\right\}, \; t \ge 0. \tag{2.5}$$

This is a particular version of the 1979 functional form (2.1) that is applicable to the stress-rupture failure of composites. This gives the probability of failure by time t under load history $\sigma(t)$ as a function of five parameters: σ_{ref}, r, ρ, t_{ref} and β. Examples of models for stress-rupture in the 1979 functional form are the CPL-W model, the stress decay model [19], and the crack-growth model [20]. For a given set of values of the four parameters, σ_{ref}, ρ, t_{ref} and β, these models differ in terms of the specific values of r they assume, as discussed in Appendix I.

Of these models the CPL-W model is the oldest (predating the 1979 functional description) and the most commonly used. The CPL-W model is also the most conservative, in that for the same values of σ_{ref}, ρ, t_{ref} and β the CPL-W model gives the highest probability of failure across all r values. The CPL-W model is obtained by taking $r \to \infty$, thus yielding the

distribution function:

$$F\left(t\middle|\sigma\right)=1-\exp\left\{-\left[\int_0^t\left(\frac{\sigma\left(\tau\right)}{\sigma_{\text{ref}}}\right)^{\rho}\frac{d\tau}{t_{\text{ref}}}\right]^{\beta}\right\}. \tag{2.6}$$

In the simplest case of stress-rupture, the load profile is taken as a constant over time

$$\sigma\left(t\right)=\bar{\sigma},\ t\geq 0 \tag{2.7}$$

where the constant $\bar{\sigma}\geq 0$ is the fixed stress level, so that (2.6) simplifies to

$$F\left(t\middle|\sigma\left(t\right)=\bar{\sigma}\right)=F_{\bar{\sigma}}\left(t\right)=1-\exp\left\{-\left[\left(\frac{\bar{\sigma}}{\sigma_{\text{ref}}}\right)^{\rho}\frac{t}{t_{\text{ref}}}\right]^{\beta}\right\}. \tag{2.8}$$

We can also write this in the form

$$F_{\bar{\sigma}}\left(t\right)=1-\exp\left\{-\left[\frac{t}{t_{\bar{\sigma}}}\right]^{\beta}\right\} \tag{2.9}$$

where

$$t_{\bar{\sigma}}=t_{\text{ref}}\left(\frac{\bar{\sigma}}{\sigma_{\text{ref}}}\right)^{-\rho} \tag{2.10}$$

is the Weibull scale parameter for lifetime at given stress level $\bar{\sigma}$, and β is the Weibull shape parameter for lifetime common to all stress levels.

In the case of a strength test under a linearly increasing load profile,

$$\sigma\left(t\right)=Rt,\ t\geq 0 \tag{2.11}$$

where the constant $R>0$ is the loading or stress rate, then by integration in (2.6) we have the

time to failure distribution

$$F_R(t) = 1 - \exp\left\{-\left[\left(\frac{Rt_{\text{ref}}}{\sigma_{\text{ref}}(\rho+1)^{1/\rho}}\right)^{\rho}\left(\frac{t}{t_{\text{ref}}}\right)^{\rho+1}\right]^{\beta}\right\}. \tag{2.12}$$

However, at time t, the stress level is $s = Rt$, so by making the substitution $t = s/R$, we obtain the distribution function for strength as

$$\overline{F}_R(s) = 1 - \exp\left\{-\left(\frac{\sigma_{\text{ref}}}{R(\rho+1)t_{\text{ref}}}\right)^{\beta}\left(\frac{s}{\sigma_{\text{ref}}}\right)^{\beta(\rho+1)}\right\}, \quad s \geq 0. \tag{2.13}$$

Note that this result collapses to the accepted Weibull distribution for strength, which is

$$\overline{F}_R(s) = 1 - \exp\left\{-\left(\frac{s}{\sigma_{\text{ref}}}\right)^{\alpha}\right\} \tag{2.14}$$

provided that we define

$$\beta = \frac{\alpha}{\rho+1} \tag{2.15}$$

and also take

$$t_{\text{ref}} = \frac{\sigma_{\text{ref}}}{R(\rho+1)}. \tag{2.16}$$

Some interpretation of the strength distribution (2.14) and lifetime distribution (2.9), as well as the relationships (2.15) and (2.16), is in order. The strength distribution (2.14) is of the commonly accepted Weibull form with α being the Weibull shape parameter and σ_{ref} being the Weibull scale parameter for strength. The lifetime distribution (2.9) has a shape parameter β,

and scale parameter $t_{\bar{\sigma}}$, which in turn depends on a normalizing parameter t_{ref}, as well as the stress ratio $\bar{\sigma}/\sigma_{\text{ref}}$, and power-law exponent ρ. The parameter t_{ref} can be interpreted as the scale parameter for lifetime when $\bar{\sigma}$ is exactly σ_{ref}. Note also that the constraint (2.16) for t_{ref} involves the loading rate R. Thus there are five related quantities (α, σ_{ref}, β, t_{ref} and ρ) to be estimated. According to the CPL-W model, however, t_{ref} and β are not independent of the remaining parameters but are related through the definition of α in (2.15) and the constraint for t_{ref} in (2.16). Taking into account these two equations, there are really only three basic parameters.

Similar definitions to (2.15) can be seen in other models with the 1979 functional form, as discussed in Appendix A. While the exact constraint varies somewhat among them we always find that

$$\frac{\alpha}{\rho+1} \le \beta \le \frac{\alpha}{\rho-2} \tag{2.17}$$

Since ρ is typically large, the practical differences are slight. This definition links the strength and lifetime shape parameters. Removing this definition, and thus adding another parameter, could be physically explained by different failure mechanisms in strength and lifetime testing.

In contrast to (2.15), constraint (2.16) for t_{ref} does not appear in the other members of the 1979 family as detailed in Appendix A. There is also an implicit assumption in (2.16), namely that strength testing will only occur at one loading rate R, as is typically the case. If strength testing is done at different loading rates the mean strength will differ for the different loading rates. However these differences are small, unless R is changed by several orders of magnitude (the difference in the strength scale parameter is less than one percent for Kevlar 49/epoxy

aramid tows when R is changed by one order of magnitude). If strength testing is done for more than one loading rate, this can still be handled while using (2.16) by scaling the Weibull strength distribution (2.14) by the ratio $\left(R / \hat{R}\right)^{1/(\rho+1)}$. Thus both (2.15) and (2.16) are direct consequences of the functional form (2.5) when specialized to yield Weibull strength and lifetime distributions, i.e. when using the CPL-W model.

Given values for all the parameters, failure probabilities can be calculated for various lifetimes, t, and load levels, $\bar{\sigma}$. In fact (2.6) can be used to calculate failure probabilities for more complex load histories, including calculating conditional lifetime probabilities for specimens that have survived proof tests. The problem we address in this paper is that of efficiently estimating the five parameters from strength and lifetime test data.

2.3 Testing

In practice large numbers of identical specimens are tested to obtain data from which the various parameters may be estimated. The specimens may, for instance, be epoxy-impregnated strands (tows) or small-scale COPVs. Testing is generally of two types: strength testing and lifetime testing. Strength testing involves a set of specimens subject to a linearly increasing load (or pressure) over time, culminating in failure of each specimen on the order of seconds to minutes. The ultimate strengths are recorded, ideally along with the loading rate, R. Lifetime testing consists of sustaining a fixed tensile load (or fixed pressure) on a set of specimens until failure. Generally two or more load (or pressure) levels are used. The individual loadings are assumed to be step functions in time, and the failure times of the specimens are recorded along with the corresponding load levels. Often a specimen will not fail within the time allotted for a test. In this case the end time of the test is recorded along with a note that the specimen survived. This produces what is known as 'right censored' lifetime data, which almost always

occurs in practice and must be accommodated. The strength and lifetime data sets together make up the overall data set used to estimate model parameters.

2.4 Methods

This paper compares eight different MLE-based methods for analyzing strength and lifetime data sets in order to come to conclusions on how data sets ought to be treated. This was done through Monte Carlo simulation of multiple sets of strength and lifetime data, using the CPL-W model with parameter values representative of various materials. The model parameters, as well as failure probability, were estimated from each set of simulated strength and lifetime data for each different MLE based method. Errors of estimation were determined and compared using statistical analysis of the estimates for each method. By distorting the constraint equation (2.16), non CPL-W model data sets were also simulated in order to test the robustness of the methods.

2.4.1 Maximum likelihood vs. rank regression

There are two commonly used procedures for estimating parameters for the Weibull distribution in the case of right-censored data (i.e. a set of lifetime data at one load level): rank regression (RR), and maximum likelihood estimation (MLE). These two methods have been compared for censored Weibull data by many investigators [21-23], with the general consensus that MLE is superior, if only by a slight margin in terms of the errors of estimation, or if only because it is more flexible. The flexibility of MLE lies in its being able to analyze not only right-censored data, but also left-censored and mid-censored data. Furthermore, in our application involving a complex data set, MLE allows the possibility of analyzing all strength and lifetime data at once, which cannot be done with RR.

Various approaches have been taken in implementing MLE for a complex data set that includes both strength and lifetime data. These approaches focus on how to partition the data in terms of which MLE equations are used to estimate which key parameters; that is, which portion of the data is analyzed at each step in a sequential approach. These different approaches will be described below in the "MLE CPL-W analysis methods" section.

2.4.2 Simulation procedure

Monte Carlo simulations were performed around five different points (5 sets of the three quantities σ_{ref}, α and ρ) in the CPL-W model's three-dimensional parameter space. These points were chosen to reflect parameter value sets for five composite materials of interest, namely a) T1000 carbon fiber/epoxy tows, b) T1000 carbon fiber/epoxy pressure vessels (COPVs), c) generic carbon fiber/epoxy tows of modest performance, such as AS4, d) Vectran aromatic polyester yarns and e) Kevlar 49/epoxy aramid tows. For each material, the point chosen for running simulations becomes what is called as the "true" parameter set, which we know at the outset – unlike the situation in experimental testing. These parameter values are referred to as "true values" only in the sense that the simulations use them as a starting point so we can assess estimation errors in the eight particular MLE methods. We assess the estimation errors as a function of such things as sample sizes, censor times, chosen stress levels in the lifetime tests, and specific lifetime/load level combinations for which failure probabilities are desired.

Once a set of 'true' parameter values has been chosen (i.e., a parameter set for one of the materials of interest), the simulation procedure is as follows:

(i) An individual data set is created by simulation using the CPL-W model. Each set contains n_s specimen strength values given a loading rate, R, and n_j, $j = 1,\ldots m$ specimen lifetime values for the m different load levels. For this paper we typically use $n_s = 30$, $m = 3$ and thirty specimens per lifetime load level; these values are similar to those in some real-world data sets. In the simulation the set of n_s strength values σ_i, $i = 1,...,n_s$ for a given loading rate R, is obtained using the "inverse CDF method"; specifically by solving $\bar{F}_R(\sigma_i) = U_i$ using the 'true' parameter values, where $\bar{F}_R(\sigma_i)$ is given in (14), and where U_i, $i = 1,...,n_s$ are independently sampled, uniform random numbers on $[0,1]$. Likewise for each separate load level, $\bar{\sigma}_j$, a set of n_j lifetimes t_i, $i = 1,...,n_j$ can be obtained by solving $F_{\bar{\sigma}}(t_i) = U_i$, using (2.8) together with the 'true' parameter values, and where U_i, $i = 1,...,n_j$, are also independently sampled, uniform random numbers on $[0,1]$.

(ii) This data set is then analyzed, *without censoring*, using each of the eight MLE-based methods described below, the result being eight sets of parameter estimates as well as calculated failure probabilities for certain lifetimes of interest under specific load levels.

(iii) This same data set is then censored using a censor time, t_l, typical of 'real world' testing, that is, a particular time when the lifetime testing is permanently suspended (which can differ from specimen to specimen since test stations are often reloaded after specimens fail); the lifetimes of specimens still surviving at the 'censor time',

are characterized in terms of time interval (t_1, ∞). To mimic 'real-world' measurements all lifetime data are rounded: failure times within the first five hours are rounded to the nearest second, while all others are rounded to the nearest minute.

(iv) This censored data set is then reanalyzed using each of the eight MLE-based methods, the result again being eight sets of parameter estimates as well as calculated failure probabilities for the same lifetimes of interest under specific load levels, as in (ii).

(v) The simulation process in (i) through (iv) is replicated N times, where N is large (at least 1,000 and as much as 50,000). Each replication, therefore, yields sixteen different sets of parameter estimates and calculated failure probabilities corresponding to the time and load level combinations of interest (i.e., eight for the uncensored data and eight for the censored version).

Originally we used N = 500 or 1000. This size of run typically took two hours, and was used to understand the general trends. When further refinement was required, N was increased, up to a maximum of 50 thousand-equivalent to two weeks of computation time.

This process is repeated for each of the five sets of parameter values corresponding to the five material systems mentioned above and described later in Table 2.1. These five material systems are widely different, so that there are many other material systems, such as IM7 carbon/epoxy, that fall within the range of parameter values tested.

Simulation is used in this paper to compare estimation approaches, but also has an important place in interpreting any real data set. Any estimation approach on a single dataset will only give one estimate of the probability of failure and/or parameters. To also understand the amount of error in the estimate requires more work. This could take the form of analytical error

estimation, e.g. using the t-distribution to determine a confidence interval. Alternatively, simulation can be used to estimate the error in an estimate, following the exact same procedure used in this paper to compare estimation methods.

2.4.3 MLE CPL-W analysis methods

The eight different MLE-based methods were used to obtain estimates of the CPL-W model parameters from a single data set, which consisted of multiple simulated observations of both strength and lifetime data at several load levels. The MLE is obtained by maximizing the likelihood function: $L\left(\underline{\theta};x_1,...,x_n\right)=\prod_{i=1}^{n} f\left(x_i\middle|\underline{\theta}\right)$, where $x_1,...,x_n$ represent a sample of observed values; the vector $\underline{\theta}$ is the set of model parameters of interest, and where $f\left(x\middle|\underline{\theta}\right)$ is the underlying probability density function. For example, when estimating σ_{ref} and α from strength data $x_1,...,x_n$ are observed strengths, $\underline{\theta}=\left(\sigma_{\text{ref}},\alpha\right)$ and $f\left(x\middle|\underline{\theta}\right)$ is the derivative of (14). In the maximization process, typically it is more convenient to work in terms of the log-likelihood (i.e., the natural logarithm of the likelihood function), $\log L\left(\underline{\theta};x_1,...,x_n\right)$, as the point where the log-likelihood function is maximized will be the same as that for the likelihood function. The result of this maximization is a specific numerical value for the vector $\underline{\theta}=(\sigma_{\text{ref}},\alpha)$, i.e. the parameter set of interest.

This section will first lay out current common practice, then give notation with which the eight MLE CPL-W methods will be described in, and finally describe those methods.

2.4.4 Common practice

Common practice in industry is to take a three-step approach. This procedure will be termed Method 1, as mentioned below. First, the strength data by itself is analyzed to estimate

the parameters σ_{ref} and α. Second, lifetimes for each load level are individually analyzed to obtain the lifetime shape parameter, β, and scale parameter, $t_{\bar{\sigma}}$, which depends on the stress ratio, $\bar{\sigma}/\sigma_{\text{ref}}$. Third, the multiple estimates for β are combined, most often through a direct average. Finally a linear regression is performed on the corresponding $t_{\bar{\sigma}}$ values to calculate t_{ref} and ρ using

$$\ln t_{\bar{\sigma}} = \ln t_{\text{ref}} - \rho \ln\left(\frac{\bar{\sigma}}{\sigma_{\text{ref}}}\right) = b + mx \tag{2.18}$$

where $b = \ln t_{\text{ref}}$, $m = -\rho$ and $x = \ln\left(\bar{\sigma}/\sigma_{\text{ref}}\right)$. At the end of this process, five parameters have been estimated, σ_{ref}, α, β, t_{ref} and ρ; typically these do not naturally satisfy the constraints (2.15) and (2.16). The purpose of this paper is to investigate whether there is a better approach, in terms of errors of estimation and bias, for obtaining the three independent CPL-W parameters, σ_{ref}, α and ρ, and more importantly, the failure probability for some specific lifetime and load level.

2.4.5 Data set notation

Notation for data sets (as described in the "Testing" section above) is as follows: There are n_{s} strength specimens, and their strengths σ_i, $i = 1,...,n_{\text{s}}$ are entries in an n_{s}-component vector. For the lifetime tests, there are m different load levels $\bar{\sigma}_i, i = 1,\ldots,m$, and n_i lifetime specimens subject each to load level $\bar{\sigma}_i$. For each load level $\bar{\sigma}_i$ there may be various censor times leading to multiple censor intervals indexed by $j = 1,\ldots,k_i$, where $k_i \geq 0, i = 1,\ldots,m$ reflects the number of different censoring intervals corresponding to load level, $\bar{\sigma}_i$. Also $j = 0$

corresponds to the special uncensored case where all the exact failure times are known, in contrast to the other intervals. Thus $n_{ij}, i = 1,\ldots,m; j = 0,\ldots,k_i$ describes the number of lifetime specimens at load level, $\bar{\sigma}_i$, corresponding to censor interval index j, and the number of uncensored specimens at load level, $\bar{\sigma}_i$, is given by n_{i0} (i.e. $j = 0$). For load level, $\bar{\sigma}_i$, the total number of specimens, censored and uncensored, must sum to n_i.

For uncensored specimens with known failure times (those indexed by $j = 0$), these times are entries $t_{ir}, i = 1,\ldots,m; r = 1,\ldots,n_{i0}$. For censored specimens, i.e. $j > 0$, there are n_{ij} specimens in censoring interval $\left[t_{ij}^{\ell}, t_{ij}^{\mathrm{u}}\right)$, where lower censor bounds are $t_{ij}^{\ell}, i = 1,\ldots,m; j = 1,\ldots,k_i$, and t_{ij}^{u} gives the upper censor bounds. These bounds t_{ij}^{ℓ} and t_{ij}^{u} as well as n_{ij} can be presented as 'matrices', with the understanding that there may be empty entries. This can be seen in the example below.

As an example, we describe a lifetime data set having two load levels ($m = 2$), with six specimens at the first load level ($n_1 = 6$) and nine at the second ($n_2 = 9$). At the first load level there are three uncensored specimens (with failure times 2, 153, and 632 hours, respectively, such that $n_{10} = 3$), as well as one left censored specimen failing between 0 and 0.5 hours ($n_{11} = 1$), and two right censored specimens both having unknown failure times exceeding 1000 hours ($n_{12} = 2$). At the second load level there are four uncensored specimens (failure times 25, 67, 890 and 2500 hours respectively, thus $n_{20} = 4$), as well as two left censored specimens failing between 0 and 1.5 hours ($n_{21} = 2$), one mid-censored specimen ($n_{22} = 1$) failing between 50 and 350 hours, and two right censored specimens with unknown failure times exceeding two different times, 1000 and 2000 hours, respectively ($n_{23} = 1, n_{24} = 1$), which count as two distinct

censor intervals. Following the above notation, we have

$$\left[k_i\right]=\begin{bmatrix} 2 \\ 4 \end{bmatrix},\ \left[n_{ij}\right]=\begin{bmatrix} 3 & 1 & 2 & & \\ 4 & 2 & 1 & 1 & 1 \end{bmatrix},\ \left[t_{ir}\right]=\begin{bmatrix} 2 & 153 & 632 & \\ 25 & 67 & 890 & 2500 \end{bmatrix}\text{hrs},$$

$$\left[t_{ij}^{\ell}\right]=\begin{bmatrix} 0 & 1000 & & \\ 0 & 50 & 1000 & 2000 \end{bmatrix}\text{hrs},\ \text{and}\ \left[t_{ij}^{\text{u}}\right]=\begin{bmatrix} 0.5 & \infty & & \\ 1.5 & 350 & \infty & \infty \end{bmatrix}\text{hrs}$$

2.4.6 Likelihood equations

The likelihood structure of the eight different estimation methods is described as follows:

Method 1: This three-step procedure is the method referred to in the "Common practice" section. In this case, the strength portion of a data set and each of the lifetime portions (obtained for different load levels) are all treated separately in terms of constructing separate likelihood equations. For the strength portion of a data set, the likelihood equation is:

$$L_{\text{s}}\left(\sigma_{\text{ref}},\alpha\right)=\left[\prod_{j=1}^{n_{\text{s}}}\left(\frac{\alpha}{\sigma_{\text{ref}}}\right)\left(\frac{\sigma_j}{\sigma_{\text{ref}}}\right)^{\alpha-1}\right]\exp\left\{-\sum_{j=1}^{n_{\text{s}}}\left(\frac{\sigma_j}{\sigma_{\text{ref}}}\right)^{\alpha}\right\} \tag{2.19a}$$

and the corresponding log-likelihood equation is

$$\log L_{\text{s}}\left(\sigma_{\text{ref}},\alpha\right)=n_{\text{s}}\left(\ln\alpha-\alpha\ln\sigma_{\text{ref}}\right)+\left(\alpha-1\right)\sum_{j=1}^{n_{\text{s}}}\ln\sigma_j-\sum_{j=1}^{n_{\text{s}}}\left(\frac{\sigma_j}{\sigma_{\text{ref}}}\right)^{\alpha} \tag{2.19b}$$

where the two parameters to be estimated are σ_{ref} and α. (When writing out log-likelihood equations throughout the paper, we will suppress, on the left-hand side, notation referring to observed strengths σ_j, and/or observed failure times t_i, though dependence on these will be understood.) For the lifetime portions of a data set, the set is partitioned into m sets associated

with each of the stress levels, $\bar{\sigma}_r$, $r = 1,...,m$, and the likelihood for the r^{th} lifetime set is:

$$L_{1,r}\left(t_{\bar{\sigma}_r},\beta\right) = \prod_{i=1}^{n_{r0}} \frac{\beta}{t_{\bar{\sigma}_r}}\left(\frac{t_i}{t_{\bar{\sigma}_r}}\right)^{\beta-1} \exp\left\{-\left(\frac{t_i}{t_{\bar{\sigma}_r}}\right)^{\beta}\right\} \prod_{j=1}^{k_r}\left[\exp\left\{-\left(\frac{t_{rj}^{\ell}}{t_{\bar{\sigma}_r}}\right)^{\beta}\right\} - \exp\left\{-\left(\frac{t_{rj}^{\text{u}}}{t_{\bar{\sigma}_r}}\right)^{\beta}\right\}\right]^{n_{rj}} \tag{2.20}$$

where the two parameters to be estimated are β and $t_{\bar{\sigma}_r}$. As described in connection with (2.18), the r different estimates for these two parameters are consolidated using linear regression to get estimates for t_{ref}, β and ρ, for a total of three different steps.

Method 2: Though not realistic and achievable in practice, but useful as an investigative exercise, Method 2 is a modification of Method 1 that takes the "true" value for σ_{ref}, as though it were known, and uses this value in the last two steps of Method 1. To complete the estimated parameter set, (2.19) is still used as in Method 1 to estimate α, though this has no effect on the failure probability estimates.

Method 3: This is a two-step procedure. The first step is to analyze the strength data to obtain estimates of σ_{ref} and α, again using (2.19). Then in the second step, the lifetime data from the m stress levels is analyzed all at once, using the likelihood function:

$$L_3\left(t_{\text{ref}},\beta,\rho;\sigma_{\text{ref}}\right) = \prod_{r=1}^{m}\left[\left(\prod_{i=1}^{n_{r0}} \frac{\beta}{t_{\text{ref}}}\left(\frac{\bar{\sigma}_r}{\sigma_{\text{ref}}}\right)^{\rho\beta}\left(\frac{t_i}{t_{\text{ref}}}\right)^{\beta-1} \exp\left\{-\left(\frac{\bar{\sigma}_r}{\sigma_{\text{ref}}}\right)^{\rho\beta}\left(\frac{t_i}{t_{\text{ref}}}\right)^{\beta}\right\}\right) \left(\prod_{j=1}^{k_r}\left[\exp\left\{-\left(\frac{\bar{\sigma}_r}{\sigma_{\text{ref}}}\right)^{\rho\beta}\left(\frac{t_{rj}^{\ell}}{t_{\text{ref}}}\right)^{\beta}\right\} - \exp\left\{-\left(\frac{\bar{\sigma}_r}{\sigma_{\text{ref}}}\right)^{\rho\beta}\left(\frac{t_{rj}^{\text{u}}}{t_{\text{ref}}}\right)^{\beta}\right\}\right]^{n_{rj}}\right)\right] \tag{2.21}$$

Upon maximizing the likelihood function, estimates for t_{ref}, β and ρ are obtained (with σ_{ref} treated as known from the first step). This method is more or less equivalent to the MLE method presented in [23].

Method 4: As with Method 2, Method 4 is an unrealistic modification of Method 3 whereby the "true" σ_{ref} is used in the second step instead of an estimated σ_{ref} value from (2.19). Again (2.19) is used to estimate α, though again this has no effect on the failure probability estimates.

Method 5: This a one-step process in which all strength and lifetime data are analyzed in one step for the five parameters, σ_{ref}, α, ρ, t_{ref} and β through optimizing the compound likelihood equation:

$$L_5\left(\sigma_{\text{ref}},\alpha,\rho,t_{\text{ref}},\beta\right)=L_s\left(\sigma_{\text{ref}},\alpha\right)L_3\left(t_{\text{ref}},\beta,\rho;\sigma_{\text{ref}}\right) \tag{2.22}$$

Method 6: This is also a one-step process whereby all data are analyzed at once for the four parameters σ_{ref}, α, ρ and t_{ref}, but also imposes constraint (15), i.e., $\beta=\alpha/\left(\rho+1\right)$. The likelihood equation is:

$$L_6\left(\sigma_{\text{ref}},\alpha,\rho,t_{\text{ref}}\right)=L_s\left(\sigma_{\text{ref}},\alpha\right)L_3\left(t_{\text{ref}},\beta,\rho;\sigma_{\text{ref}}\right)\Big|_{\beta=\frac{\alpha}{\rho+1}} \tag{2.23}$$

Recall from (2.17) that this constraint is well agreed upon across models of the 1979 functional form.

Method 7: This is also a one-step process whereby all data are analyzed at once for the four parameters σ_{ref}, α, ρ and β, and imposing constraint (2.16) which is $t_{\text{ref}}=\sigma_{\text{ref}}/\left(R\left(\rho+1\right)\right)$. The likelihood equation is:

$$L_7\left(\sigma_{\text{ref}},\alpha,\rho,\beta\right)=L_s\left(\sigma_{\text{ref}},\alpha\right)L_3\left(t_{\text{ref}},\beta,\rho;\sigma_{\text{ref}}\right)\Big|_{t_{\text{ref}}=\frac{\sigma_{\text{ref}}}{R\left(\rho+1\right)}} \tag{2.24}$$

Method 8: This is also a one-step process, whereby all data are analyzed at once for the fundamental three parameters σ_{ref}, α, ρ, this time imposing both constraints (2.15) and (2.16). The likelihood equation is:

$$L_8\left(\sigma_{\text{ref}},\alpha,\rho\right)=L_s\left(\sigma_{\text{ref}},\alpha\right)L_3\left(\rho,t_{\text{ref}},\beta;\sigma_{\text{ref}}\right)\Big|_{\beta=\frac{\alpha}{\rho+1},\,t_{\text{ref}}=\frac{\sigma_{\text{ref}}}{R\left(\rho+1\right)}} \tag{2.25}$$

2.4.7 Estimator robustness to time scale distortion

To address concerns that Method 8 would outperform the other methods, if only because it takes advantage of constraints that reduce the dimension of the parameter space, the Monte Carlo data simulation was repeated based on "true" parameter values that did not satisfy one of the CPL-W constraints (2.15) and (2.16). Specifically, instead of simulating data based on the constraint, $t_{\text{ref}}=\sigma_{\text{ref}}\Big/\left(R\left(\rho+1\right)\right)$, we simulated data based on values of t_{ref} chosen to satisfy

$$t_{\text{ref}}=K_{\text{D}}\,\sigma_{\text{ref}}\Big/\left(R\left(\rho+1\right)\right) \tag{2.26}$$

where the distortion factor, K_{D}, was given 17 specific values spanning the range, $1/100\le K_D\le 100$. Such a distortion is similar in effect to misreporting the loading rate, R, in the strength tests, by a factor, K_{D}. Also, data generated from other models in the 1979 functional form, such as the strength decay or crack growth models described in the Appendix, could potentially look similar to data generated from the CPL-W model using the distortion (2.26), particularly at higher loading rates R.

2.4.8 Measures of estimation error across the eight MLE-based methods

The various methods were judged primarily in terms of the amounts of bias and variance in estimates of failure probabilities corresponding to certain desired lifetime/load level combinations. Mean squared error (MSE) was also used in comparing methods. For a given MLE method, error in calculated failure probability relative to the known exact one is used as the primary metric of accuracy for two reasons: it reduces the number of error estimates to compare across the eight methods (i.e., one estimated probability versus three, four, or even five parameter estimates), and in practice, is the most important quantity to estimate. The underlying parameter values are useful indirectly, in that the failure probability may be predicted using them, but they are less important to estimate accurately than the failure probability. Perhaps surprisingly, the predicted failure probability corresponding to a desired lifetime/load level combination is frequently known much more accurately than the model parameters.

Estimated failure probability is compared across methods using, primarily, bias and variance in the estimates to see where trade-offs exist. However, MSE is also provided when bias and variance measures are less definitive. Bias and standard deviation measures will often be normalized by the "true" values to provide a measure of relative error, particularly for parameter estimates. Bias will be given as estimated value minus "true" value, so that a negative bias on failure probability corresponds to an optimistic estimate, while positive bias corresponds to a conservative estimate, and when dividing by the true value provides a relative bias.

2.5 Results

Monte Carlo simulations were performed for five different sets of parameter values that we call "true parameter values". These values reflect the behavior of five different fiber systems, as detailed in the "Simulation procedure" section, for which sufficient data exists to determine

representative parameter values that are the basis for our simulations. The systems are a) T1000 carbon fiber/epoxy tows, b) T1000 carbon fiber/epoxy pressure vessels (COPVs), c) generic carbon fiber/epoxy tows of modest performance, d) Vectran aromatic polyester yarns and e) Kevlar 49/epoxy aramid tows. The sets of parameter values corresponding to these systems are given in Table 2.1. Note that the ranges of values, particularly for β and ρ, are especially wide-most commonly used fiber/epoxy systems will have β and ρ values within these ranges. Thus it is likely that any results that hold true for all five parameter sets tested will also hold for other material systems with β and ρ values in these ranges.

Comparisons of results from the various MLE analysis methods will be presented for two material systems. In particular, the comparisons will involve (i) failure probabilities corresponding to different load levels and lifetimes, (ii) the reductions in accuracy resulting from having censored data versus uncensored data, and (iii) the effects of t_{ref} distortion on overall estimation accuracy. The presented results make up a small portion of simulation results obtained over the overall parameter space and 'test' conditions considered. However, lessons learned from the results presented here are consistent across all simulated data sets.

2.5.1 T1000 carbon/epoxy tows

Extensive simulations were done for parameters corresponding to T1000 carbon/epoxy tows. Here the "true" parameters were chosen to correspond to T1000 carbon/epoxy prepreg tows tested at Lawrence Livermore National Laboratory [24], as shown in Table 2.1.

2.5.1.1 Simulation parameters for T1000 carbon/epoxy tows

For T1000 carbon/epoxy tows, the model parameters ("true" parameter values) are given in Table 2.1, and the testing variables are:

- $R = 251.4$ GPa/hr $(4.19$ GPa/min$)$, loading rate
- $n_s = 30$, number of strength specimens
- $[n_1\ n_2\ n_3] = [30\ 30\ 30]$, number of specimens at each of three load levels
- $[0.85\ 0.80\ 0.75]$, stress ratios, i.e., load levels, $\bar{\sigma}_r$, $r = 1,2,3$, divided by σ_{ref}
- upper censor time $t^{\text{u}} = 10^{4.5} = 31{,}623$ hrs (~ 3.6 years)
- failure probability of interest 7.595×10^{-5} calculated for a lifetime of $t_{\text{failure}} = 10^6$ hrs (114.16 yrs) under service stress ratio $\bar{\sigma}/\sigma_{\text{ref}} = 0.50$.
- $N = 5000$, unless otherwise stated, and is the number of simulated datasets analyzed

2.5.1.2 General results for T1000 carbon/epoxy tows

The following results correspond to the parameters given above for T1000 carbon/epoxy tows. Tables 2.2-2.9 present the following quantities with notation in parenthesis: mean failure probability (mean), standard deviation of failure probability (SD), the coefficient of variance (CV) being the standard deviation divided by correct probability of failure based on the "true" parameters, the bias (bias) being the mean minus the correct probability of failure, and the normalized bias (NB) being the bias divided by the correct probability of failure. Other quantities are previously defined in the text.

Table 2.1 Material parameter sets ("true" values for the Monte Carlo simulations) assumed for the five different fiber/epoxy material systems.

	σ_{ref} [a]	α	ρ	t_{ref}	β
T1000/epoxy tows	6.2 GPa	16	235	0.000104 hrs	0.0678
T1000/epoxy vessels	5.1 GPa	24	150	0.000280 hrs	0.159
Generic carbon/epoxy tows	4.0 GPa	18	75	0.000125 hrs	0.237
Vectran yarns	3.5 GPa	28	35	0.000231 hrs	0.778
Kevlar 49/epoxy tows	3.5 GPa	28	24	0.000333 hrs	1.12

[a] Units shown are for effective fiber strength (force divided by cross-sectional area of the fiber material only, or, fiber strain times effective fiber Young's modulus).

From Table 2.2 it is evident that Methods 1 through 5 do a very poor job of estimating the true failure probability, 7.595×10^{-5} as is clear from the very large bias and standard deviation. Method 8 performs best, albeit with an optimistic estimate (negative bias). Methods 6 and 7 do fairly well, and method 7 is also optimistic.

Table 2.2 Failure probability for T1000 tows, based on Monte Carlo simulated data at stress ratios 0.85, 0.80 and 0.75

	Method 1	Method 2	Method 3	Method 4	Method 5	Method 6	Method 7	Method 8
mean	$1.52\text{x}10^{-1}$	$1.52\text{x}10^{-1}$	$6.07\text{x}10^{-3}$	$6.06\text{x}10^{-3}$	$6.07\text{x}10^{-3}$	$1.08\text{x}10^{-4}$	$5.41\text{x}10^{-5}$	$7.07\text{x}10^{-5}$
SD	$3.40\text{x}10^{-1}$	$3.40\text{x}10^{-1}$	$5.64\text{x}10^{-2}$	$5.62\text{x}10^{-2}$	$5.64\text{x}10^{-2}$	$1.27\text{x}10^{-4}$	$8.47\text{x}10^{-5}$	$7.12\text{x}10^{-5}$
CV	4479	4476	742	740	742	1.68	1.11	0.937
bias	$1.52\text{x}10^{-1}$	$1.52\text{x}10^{-1}$	$5.99\text{x}10^{-3}$	$5.98\text{x}10^{-3}$	$5.99\text{x}10^{-3}$	$3.20\text{x}10^{-5}$	$-2.18\text{x}10^{-5}$	$-5.29\text{x}10^{-6}$
NB	2005	2003	78.9	78.7	78.9	0.421	-0.287	-0.070

With respect to estimating the 'true' parameter values, Table 2.3 reveals more complex behavior. All eight methods do well estimating σ_{ref}, and α, but β is relatively poorly estimated by Methods 1 and 2, and Methods 1 through 5 have difficulty accurately estimating ρ. Also, t_{ref} is reasonably well estimated only by Methods 7 and 8.

Table 2.3 Parameter estimates for T1000 tows, based on Monte Carlo simulated data at stress ratios 0.85, 0.80 and 0.75

		σ_{ref}	α	ρ	t_{ref}	β
Method 1	mean	6.195	16.7	198.9	$5.72\text{x}10^{104}$	0.2021
	CV	0.0120	0.1565	1.01	$1.72\text{x}10^{110}$	21.36
	NB	$-7.28\text{x}10^{-4}$	$4.50\text{x}10^{-2}$	$-1.54\text{x}10^{-1}$	$5.47\text{x}10^{108}$	1.98
Method 2	mean	6.200	16.7	198.7	$5.18\text{x}10^{112}$	0.2021
	CV	0	0.1565	1.01	$1.55\text{x}10^{118}$	21.36
	NB	0	$4.50\text{x}10^{-2}$	$-1.55\text{x}10^{-1}$	$4.95\text{x}10^{116}$	1.98
Method 3	mean	6.195	16.7	201.0	$1.45\text{x}10^{18}$	0.1004
	CV	0.0120	0.1565	0.84	$4.20\text{x}10^{23}$	0.41
	NB	$-7.28\text{x}10^{-4}$	$4.50\text{x}10^{-2}$	$-1.45\text{x}10^{-1}$	$1.38\text{x}10^{22}$	$4.81\text{x}10^{-1}$
Method 4	mean	6.200	16.7	198.4	$3.92\text{x}10^{18}$	0.1004
	CV	0	0.1565	0.77	$1.16\text{x}10^{24}$	0.41
	NB	0	$4.50\text{x}10^{-2}$	$-1.56\text{x}10^{-1}$	$3.75\text{x}10^{22}$	$4.81\text{x}10^{-1}$
Method 5	mean	6.195	16.7	185.4	$1.45\text{x}10^{18}$	0.1006
	CV	0.0121	0.1570	0.41	$4.20\text{x}10^{23}$	0.41
	NB	$-7.53\text{x}10^{-4}$	$4.47\text{x}10^{-2}$	$-2.11\text{x}10^{-1}$	$1.38\text{x}10^{22}$	$4.84\text{x}10^{-1}$
Method 6	mean	6.195	16.7	173.9	$1.89\text{x}10^{6}$	0.1001
	CV	0.0120	0.1489	0.18	$5.66\text{x}10^{11}$	0.41
	NB	$-7.48\text{x}10^{-4}$	$4.09\text{x}10^{-2}$	$-2.60\text{x}10^{-1}$	$1.80\text{x}10^{10}$	$4.76\text{x}10^{-1}$
Method 7	mean	6.198	16.7	200.0	$1.26\text{x}10^{-4}$	0.0969
	CV	0.0119	0.1562	0.14	$1.81\text{x}10^{-1}$	0.38
	NB	$-3.07\text{x}10^{-4}$	$4.61\text{x}10^{-2}$	$-1.49\text{x}10^{-1}$	$2.03\text{x}10^{-1}$	$4.29\text{x}10^{-1}$
Method 8	mean	6.213	17.3	207.0	$1.23\text{x}10^{-4}$	0.0862
	CV	0.0106	0.1074	0.18	$1.98\text{x}10^{-1}$	0.26
	NB	$2.21\text{x}10^{-3}$	$8.36\text{x}10^{-2}$	$-1.19\text{x}10^{-1}$	$1.74\text{x}10^{-1}$	$2.71\text{x}10^{-1}$

Despite its inability to estimate t_{ref}, Method 6 still does a fair job of estimating the failure probability. This is seen repeatedly across the methods, and demonstrates the dependence among the parameters. Specifically note that $t_{ref}^{1/\rho}$ is approximately constant, since positive bias on t_{ref} corresponds to negative bias on ρ. Thus failure probabilities are unaffected since failure probabilities depend on t_{ref} and ρ heavily via $t_{ref}^{1/\rho}$.

Table 2.4 Failure probability estimates for T1000 tows, based on Monte Carlo simulated data at different sets of stress ratios.

Tests simulated at stress ratios of 0.85, 0.80 and 0.75								
	Method 1	Method 2	Method 3	Method 4	Method 5	Method 6	Method 7	Method 8
mean	$1.52\text{x}10^{-1}$	$1.52\text{x}10^{-1}$	$6.07\text{x}10^{-3}$	$6.06\text{x}10^{-3}$	$6.07\text{x}10^{-3}$	$1.08\text{x}10^{-4}$	$5.41\text{x}10^{-5}$	$7.07\text{x}10^{-5}$
SD	$3.40\text{x}10^{-1}$	$3.40\text{x}10^{-1}$	$5.64\text{x}10^{-2}$	$5.62\text{x}10^{-2}$	$5.64\text{x}10^{-2}$	$1.27\text{x}10^{-4}$	$8.47\text{x}10^{-5}$	$7.12\text{x}10^{-5}$
CV	4479	4476	742	740	742	1.68	1.11	0.937
bias	$1.52\text{x}10^{-1}$	$1.52\text{x}10^{-1}$	$5.99\text{x}10^{-3}$	$5.98\text{x}10^{-3}$	$5.99\text{x}10^{-3}$	$3.20\text{x}10^{-5}$	$-2.18\text{x}10^{-5}$	$-5.29\text{x}10^{-6}$
NB	2005	2003	78.9	78.7	78.9	0.421	-0.287	-0.070
Tests simulated at stress ratios of 0.90, 0.85 and 0.80								
	Method 1	Method 2	Method 3	Method 4	Method 5	Method 6	Method 7	Method 8
mean	$4.16\text{x}10^{-2}$	$4.15\text{x}10^{-2}$	$1.10\text{x}10^{-3}$	$1.10\text{x}10^{-3}$	$1.10\text{x}10^{-3}$	$1.13\text{x}10^{-4}$	$3.54\text{x}10^{-5}$	$5.65\text{x}10^{-5}$
SD	$1.44\text{x}10^{-1}$	$1.44\text{x}10^{-1}$	$5.29\text{x}10^{-3}$	$5.36\text{x}10^{-3}$	$5.29\text{x}10^{-3}$	$1.32\text{x}10^{-4}$	$5.32\text{x}10^{-5}$	$5.66\text{x}10^{-5}$
CV	1897	1895	70	71	70	1.74	0.70	0.745
bias	$4.15\text{x}10^{-2}$	$4.14\text{x}10^{-2}$	$1.02\text{x}10^{-3}$	$1.02\text{x}10^{-3}$	$1.02\text{x}10^{-3}$	$3.69\text{x}10^{-5}$	$-4.05\text{x}10^{-5}$	$-1.94\text{x}10^{-5}$
NB	547	545	13.4	13.5	13.4	0.486	-0.533	-0.256
Tests simulated at stress ratios of 0.95, 0.90 and 0.85								
	Method 1	Method 2	Method 3	Method 4	Method 5	Method 6	Method 7	Method 8
mean	$1.76\text{x}10^{-2}$	$1.77\text{x}10^{-2}$	$5.02\text{x}10^{-4}$	$5.02\text{x}10^{-4}$	$5.02\text{x}10^{-4}$	$1.17\text{x}10^{-4}$	$2.86\text{x}10^{-5}$	$5.03\text{x}10^{-5}$
SD	$6.79\text{x}10^{-2}$	$6.80\text{x}10^{-2}$	$2.06\text{x}10^{-3}$	$2.01\text{x}10^{-3}$	$2.06\text{x}10^{-3}$	$1.44\text{x}10^{-4}$	$6.75\text{x}10^{-5}$	$6.21\text{x}10^{-5}$
CV	894	895	27	26	27	1.90	0.89	0.817
bias	$1.75\text{x}10^{-2}$	$1.76\text{x}10^{-2}$	$4.26\text{x}10^{-4}$	$4.26\text{x}10^{-4}$	$4.26\text{x}10^{-4}$	$4.11\text{x}10^{-5}$	$-4.74\text{x}10^{-5}$	$-2.57\text{x}10^{-5}$
NB	231	232	5.6	5.6	5.6	0.541	-0.623	-0.338

The 'testing variables' were varied relative to those given above to demonstrate that the general character of the results is independent of the 'testing variables'. Table 2.4 shows the effects of testing at different load level combinations, and similar trends are seen as in Table 2.2. Tables 2.5 and 2.6 show the results of doing the analysis on uncensored data. As expected the estimates are substantially improved, however, the parameter estimates for t_{ref} remain highly inaccurate in Methods 1 through 6, even with the advantage of complete data without censoring. Thus, for these six methods, poor parameter estimates are not improved by lengthening the test time. Table 2.7 shows failure probability estimates based on simulated data for fewer specimens, and as expected, the error is worse but the same trends remain.

Table 2.5 Failure probability estimates for T1000 tows, based on Monte Carlo simulated data with no censoring

Uncensored: tests simulated at stress ratios of 0.85, 0.80 and 0.75								
	Method 1	Method 2	Method 3	Method 4	Method 5	Method 6	Method 7	Method 8
mean	$3.41\text{x}10^{-4}$	$3.44\text{x}10^{-4}$	$1.38\text{x}10^{-4}$	$1.39\text{x}10^{-4}$	$1.38\text{x}10^{-4}$	$8.66\text{x}10^{-5}$	$1.10\text{x}10^{-4}$	$8.75\text{x}10^{-5}$
SD	$1.67\text{x}10^{-3}$	$1.68\text{x}10^{-3}$	$2.54\text{x}10^{-4}$	$2.48\text{x}10^{-4}$	$2.54\text{x}10^{-4}$	$8.44\text{x}10^{-5}$	$1.42\text{x}10^{-4}$	$7.56\text{x}10^{-5}$
CV	22.0	22.1	3.34	3.27	3.34	1.11	1.86	0.995
bias	$2.65\text{x}10^{-4}$	$2.68\text{x}10^{-4}$	$6.22\text{x}10^{-5}$	$6.29\text{x}10^{-5}$	$6.22\text{x}10^{-5}$	$1.07\text{x}10^{-5}$	$3.44\text{x}10^{-5}$	$1.16\text{x}10^{-5}$
NB	3.49	3.53	0.819	0.828	0.820	0.141	0.453	0.152

Table 2.6 Parameter estimates for T1000 tows, based on Monte Carlo simulated data with no censoring

		σ_{ref}	α	ρ	t_{ref}	β
Method 1	mean	6.195	16.7	240.1	7.67×10^{16}	0.0710
	CV	0.0120	0.1564	0.27	2.32×10^{22}	0.09
	NB	-7.26×10^{-4}	4.49×10^{-2}	2.15×10^{-2}	7.34×10^{20}	4.73×10^{-2}
Method 2	mean	6.200	16.7	240.1	3.38×10^{16}	0.0710
	CV	0	0.1564	0.27	1.02×10^{22}	0.09
	NB	0	4.49×10^{-2}	2.15×10^{-2}	3.23×10^{20}	4.73×10^{-2}
Method 3	mean	6.195	16.7	236.3	1.23×10^{5}	0.0692
	CV	0.0120	0.1564	0.13	2.87×10^{10}	0.09
	NB	-7.26×10^{-4}	4.49×10^{-2}	5.47×10^{-3}	1.17×10^{9}	2.13×10^{-2}
Method 4	mean	6.200	16.7	236.3	5.97×10^{3}	0.0692
	CV	0	0.1564	0.13	1.04×10^{9}	0.09
	NB	0	4.49×10^{-2}	5.47×10^{-3}	5.71×10^{7}	2.13×10^{-2}
Method 5	mean	6.195	16.7	236.2	1.23×10^{5}	0.0692
	CV	0.0120	0.1565	0.13	2.87×10^{10}	0.09
	NB	-7.19×10^{-4}	4.51×10^{-2}	5.30×10^{-3}	1.17×10^{9}	2.12×10^{-2}
Method 6	mean	6.195	16.4	237.4	1.45×10^{3}	0.0691
	CV	0.0119	0.1117	0.11	2.93×10^{8}	0.08
	NB	-7.50×10^{-4}	2.66×10^{-2}	1.04×10^{-2}	1.39×10^{7}	1.88×10^{-2}
Method 7	mean	6.195	16.7	235.5	1.05×10^{-4}	0.0688
	CV	0.0111	0.1558	0.06	6.70×10^{-2}	0.09
	NB	-8.13×10^{-4}	4.12×10^{-2}	2.10×10^{-3}	8.93×10^{-4}	1.50×10^{-2}
Method 8	mean	6.195	16.3	235.7	1.04×10^{-4}	0.0688
	CV	0.0098	0.0831	0.05	5.53×10^{-2}	0.08
	NB	-9.26×10^{-4}	1.72×10^{-2}	3.17×10^{-3}	-1.47×10^{-3}	1.47×10^{-2}

Table 2.7 Failure probability estimates for T1000 tows, based on Monte Carlo simulated data with fewer 'test' samples

Number of samples = 20 per load level: tests simulated at stress ratios of 0.90, 0.85 and 0.80								
	Method 1	Method 2	Method 3	Method 4	Method 5	Method 6	Method 7	Method 8
mean	3.41×10^{-4}	3.44×10^{-4}	1.38×10^{-4}	1.39×10^{-4}	1.38×10^{-4}	8.66×10^{-5}	1.10×10^{-4}	8.75×10^{-5}
SD	1.67×10^{-3}	1.68×10^{-3}	2.54×10^{-4}	2.48×10^{-4}	2.54×10^{-4}	8.44×10^{-5}	1.42×10^{-4}	7.56×10^{-5}
CV	22.0	22.1	3.34	3.27	3.34	1.11	1.86	0.995
bias	2.65×10^{-4}	2.68×10^{-4}	6.22×10^{-5}	6.29×10^{-5}	6.22×10^{-5}	1.07×10^{-5}	3.44×10^{-5}	1.16×10^{-5}
NB	3.49	3.53	0.819	0.828	0.820	0.141	0.453	0.152

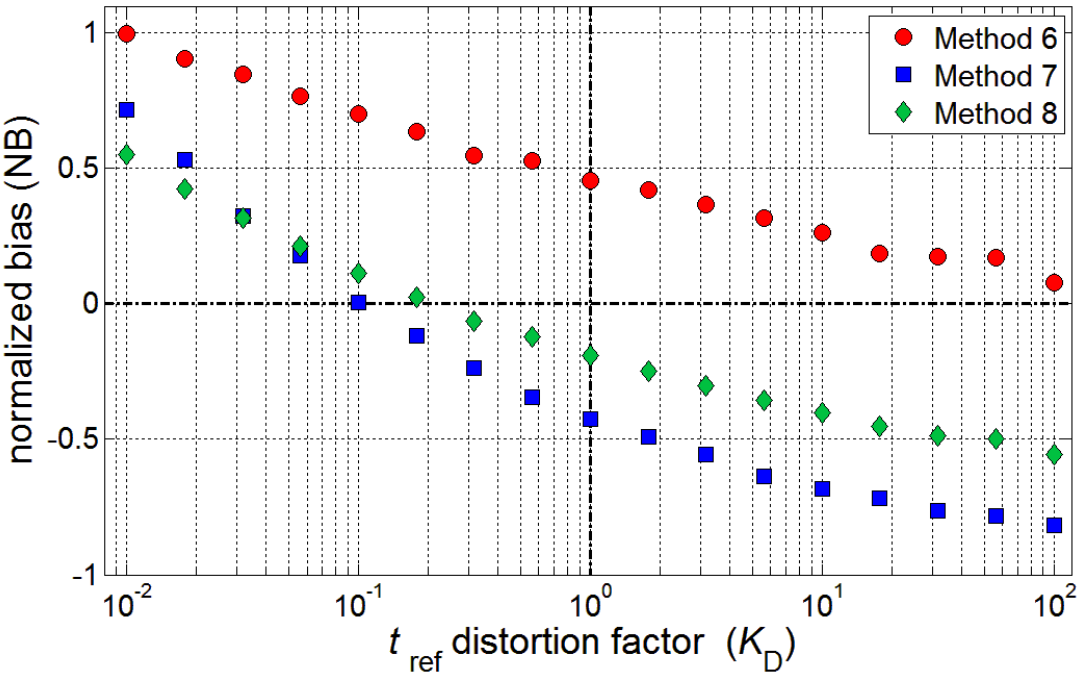

Figure 2.1 Effects of distorting t_{ref} on the normalized bias for failure probability

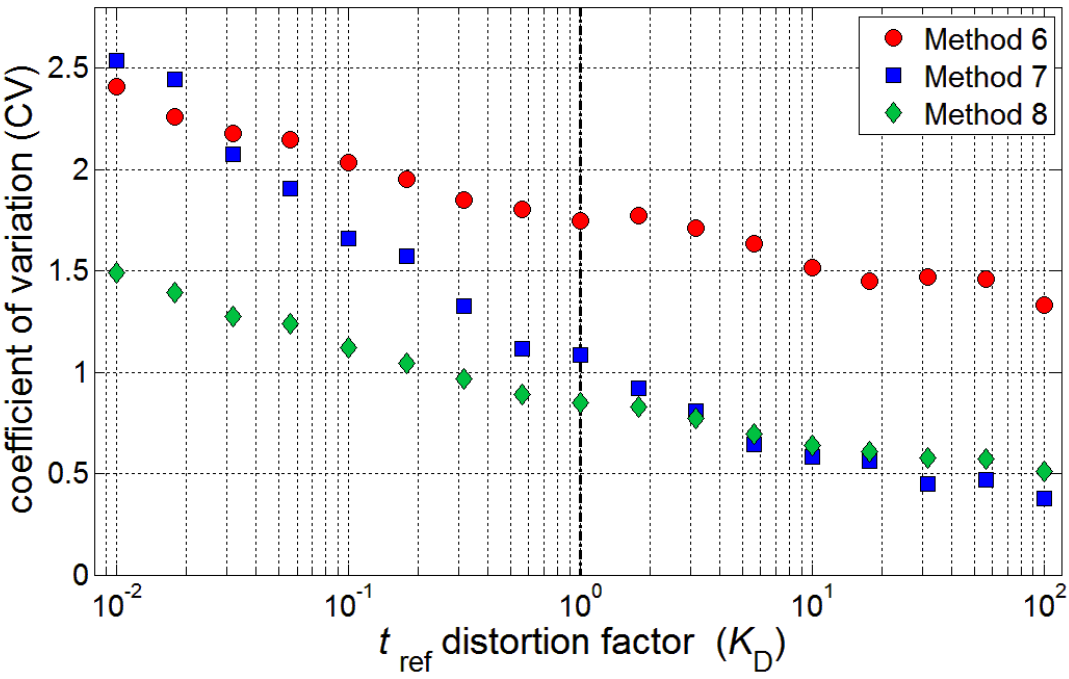

Figure 2.2 Effects of distorting t_{ref} on the coefficient of variation for failure probability

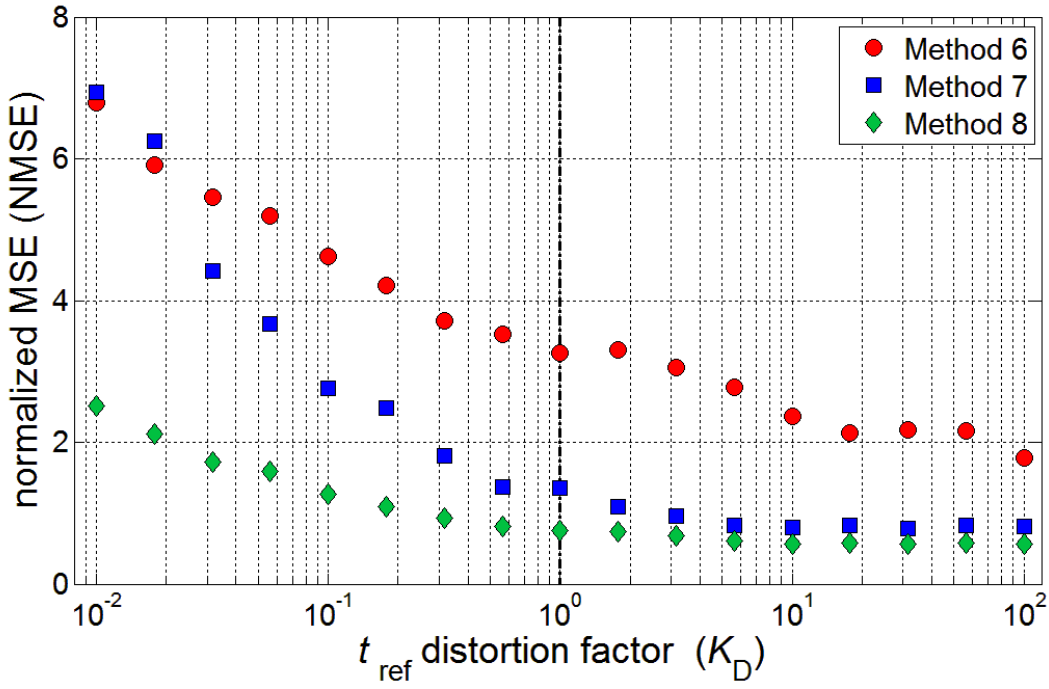

Figure 2.3 Effects of distorting t_{ref} on mean squared error failure probability

Simulations for Figures 2.1 through 2.3 were run with $N \geq 10000$ different simulated data sets, so that the curve would be relatively smooth. Figures 2.1 through 2.3 shows the effect that distorting t_{ref} has on Methods 6 through 8. Figure 2.1 shows normalized bias (NB) as defined previously. Of the three methods, there is no method that consistently has less bias than the others. Figure 2.2 shows the coefficient of variation (CV) as defined previously. Method 8 has the smallest standard deviation through most of the range, though Method 7 has a smaller standard deviation with large distortion factors. Figure 2.3 shows the normalized mean squared error, namely the MSE divided by the correct probability of failure squared (NMSE). While the bias and standard deviation have no method that is consistently better, Figure 2.3 shows that Method 8 has the lowest MSE, despite implementing a distortion factor, K_{D} in (2.26) as large as two orders of magnitude. This illustrates marked robustness of the estimator for failure probability, in three ways: first, knowing precisely the loading rate, R is not essential; second Method 8 outperforms the other methods even when the data does not appear to support constraint (2.16); and third, the superior performance of Method 8 is not merely the consequence of a reduction in the dimension of the parameter space.

2.5.2 Other material systems

Extensive simulations were also performed for the remaining material systems in Table 2.1, and the general trends observed were similar to those for the T1000/epoxy tows in the previous section. Of particular interest was the effect of having a much larger value of β (which is typically associated with a lower value for ρ). Thus we present details for the case of the Kevlar 49/epoxy tow system for which $\beta = 1.12$ [25] as compared to $\beta = 0.0678$ for the T1000/epoxy tow system. The full set of parameter values is given in Table 2.1.

2.5.2.1 Simulation parameters for Kevlar 49/epoxy tow system

For the Kevlar 49/epoxy tow system, the model parameters ("true" parameter values) are given in Table 2.1, and the testing variables are:

- $R = 420$ GPa/hr $\left(7 \text{ GPa/min}\right)$, loading rate
- $n_s = 30$, number of strength specimens
- $\left[n_1 \; n_2 \; n_3\right] = \left[30 \; 30 \; 30\right]$, number of specimens at each of three load levels
- $\left[0.75 \; 0.70 \; 0.65\right]$, stress ratios i.e., load levels, $\bar{\sigma}_r$, $r = 1,2,3$, divided by σ_{ref}
- censor time $t^{\text{u}} = 10^{4.5} = 31{,}623$ hrs (~ 3.6 years)
- failure probability of interest 3.625×10^{-4} calculated for a lifetime of $t_{\text{failure}} = 10^6$ hrs (114.16 yrs) under service stress ratio $\bar{\sigma}/\sigma_{\text{ref}} = 0.30$.

2.5.2.2 General results for Kevlar 49/epoxy tow system

Table 2.8 shows an example of failure probability estimates for Kevlar 49/epoxy tows, and Table 2.9 shows the associated MLE parameter estimates. Clearly accurate failure probability estimation and parameter estimation are much easier when β is larger, as the resulting error in the estimates is much less. In fact, the estimation problem has become less demanding to the point that it is possible for all methods to estimate the parameters reasonably well. However, the same basic trends are seen as in the T1000/epoxy tow system, whereby Method 8 has the lowest bias and variance, Methods 6 and 7 the next lowest, and Methods 1 through 5 noticeably higher bias and variance.

Table 2.8 Failure probability estimates for Kevlar 49/epoxy tows based on Monte Carlo simulated data

	Method 1	Method 2	Method 3	Method 4	Method 5	Method 6	Method 7	Method 8
mean	$7.77\text{x}10^{-3}$	$7.83\text{x}10^{-3}$	$1.30\text{x}10^{-3}$	$1.30\text{x}10^{-3}$	$1.30\text{x}10^{-3}$	$8.67\text{x}10^{-4}$	$5.37\text{x}10^{-4}$	$4.50\text{x}10^{-4}$
SD	$4.47\text{x}10^{-2}$	$4.57\text{x}10^{-2}$	$3.18\text{x}10^{-3}$	$3.20\text{x}10^{-3}$	$3.18\text{x}10^{-3}$	$1.54\text{x}10^{-3}$	$6.98\text{x}10^{-4}$	$4.53\text{x}10^{-4}$
CV	123.3	126.0	8.78	8.83	8.78	4.24	1.92	1.250
bias	$7.40\text{x}10^{-3}$	$7.47\text{x}10^{-3}$	$9.33\text{x}10^{-4}$	$9.39\text{x}10^{-4}$	$9.33\text{x}10^{-4}$	$5.04\text{x}10^{-4}$	$1.75\text{x}10^{-4}$	$8.72\text{x}10^{-5}$
NB	20.43	20.60	2.575	2.589	2.575	1.390	0.483	0.241

Table 2.9 Parameter estimates for Kevlar 49/epoxy tows based on Monte Carlo simulated data

		σ_{ref}	α	ρ	t_{ref}	β
Method 1	mean	3.50	29.3	23.8	$6.68\text{x}10^{-4}$	1.176
	CV	$7.01\text{x}10^{-3}$	$1.53\text{x}10^{-1}$	$1.24\text{x}10^{-1}$	3.00	$9.03\text{x}10^{-2}$
	NB	$-4.31\text{x}10^{-4}$	$4.49\text{x}10^{-2}$	$-7.09\text{x}10^{-3}$	1.00	$4.97\text{x}10^{-2}$
Method 2	mean	3.50	29.3	23.8	$6.50\text{x}10^{-4}$	1.176
	CV	0	$1.53\text{x}10^{-1}$	$1.24\text{x}10^{-1}$	2.84	$9.03\text{x}10^{-2}$
	NB	0	$4.49\text{x}10^{-2}$	$-7.09\text{x}10^{-3}$	$9.50\text{x}10^{-1}$	$4.97\text{x}10^{-2}$
Method 3	mean	3.50	29.3	23.9	$4.22\text{x}10^{-4}$	1.147
	CV	$7.01\text{x}10^{-3}$	$1.53\text{x}10^{-1}$	$6.71\text{x}10^{-2}$	$8.31\text{x}10^{-1}$	$8.59\text{x}10^{-2}$
	NB	$-4.31\text{x}10^{-4}$	$4.49\text{x}10^{-2}$	$-5.43\text{x}10^{-3}$	$2.67\text{x}10^{-1}$	$2.44\text{x}10^{-2}$
Method 4	mean	3.50	29.3	23.9	$4.10\text{x}10^{-4}$	1.147
	CV	0	$1.53\text{x}10^{-1}$	$6.71\text{x}10^{-2}$	$7.65\text{x}10^{-1}$	$8.59\text{x}10^{-2}$
	NB	0	$4.49\text{x}10^{-2}$	$-5.43\text{x}10^{-3}$	$2.31\text{x}10^{-1}$	$2.44\text{x}10^{-2}$
Method 5	mean	3.50	29.3	23.9	$4.22\text{x}10^{-4}$	1.147
	CV	$7.01\text{x}10^{-3}$	$1.53\text{x}10^{-1}$	$6.71\text{x}10^{-2}$	$8.31\text{x}10^{-1}$	$8.59\text{x}10^{-2}$
	NB	$-4.31\text{x}10^{-4}$	$4.49\text{x}10^{-2}$	$-5.43\text{x}10^{-3}$	$2.67\text{x}10^{-1}$	$2.44\text{x}10^{-2}$
Method 6	mean	3.50	28.6	23.9	$4.12\text{x}10^{-4}$	1.147
	CV	$6.75\text{x}10^{-3}$	$8.77\text{x}10^{-2}$	$6.26\text{x}10^{-2}$	$7.83\text{x}10^{-1}$	$7.62\text{x}10^{-2}$
	NB	$-4.59\text{x}10^{-4}$	$1.99\text{x}10^{-2}$	$-3.71\text{x}10^{-3}$	$2.37\text{x}10^{-1}$	$2.44\text{x}10^{-2}$
Method 7	mean	3.50	29.2	24.0	$3.34\text{x}10^{-4}$	1.139
	CV	$6.56\text{x}10^{-3}$	$1.52\text{x}10^{-1}$	$2.42\text{x}10^{-2}$	$2.90\text{x}10^{-2}$	$8.47\text{x}10^{-2}$
	NB	$-1.92\text{x}10^{-4}$	$4.44\text{x}10^{-2}$	$-1.13\text{x}10^{-4}$	$5.83\text{x}10^{-4}$	$1.74\text{x}10^{-2}$
Method 8	mean	3.50	28.5	24.0	$3.33\text{x}10^{-4}$	1.140
	CV	$6.06\text{x}10^{-3}$	$7.58\text{x}10^{-2}$	$2.20\text{x}10^{-2}$	$2.63\text{x}10^{-2}$	$7.40\text{x}10^{-2}$
	NB	$-2.47\text{x}10^{-4}$	$1.81\text{x}10^{-2}$	$2.73\text{x}10^{-4}$	$4.06\text{x}10^{-5}$	$1.79\text{x}10^{-2}$

2.6 Discussion and conclusions

One of the concerns with the industry method, Method 1, was the use of three separate steps, each introducing its own bias. However from these results we see that the biases tend to offset one another when calculating failure probability, meaning that Methods 1 and 3 often have slightly less bias and variability than Methods 2 and 4, respectively. Thus a biased estimate of σ_{ref} in the first step does not seem to cause large inaccuracies in estimates of the failure probability. In comparing a one-step versus two-step estimation procedure, Methods 3 and 5 give almost identical results. Whether or not σ_{ref} and α are estimated in conjunction with the other parameters does not affect the estimates. This is most likely due to an overwhelming influence of the strength data in anchoring these two estimation procedures. Thus in comparing results from Methods 3, 4 and 5, it can be seen that the number of steps is not the driver of estimation errors. Nonetheless the overall poor performance of Method 1 is due to its ad-hoc lifetime estimation procedure, namely in the use of a linear regression of maximum likelihood estimates for lifetime parameters vs. load level. This procedure clearly induces a large amount of estimation error compared to Method 3 and Methods 5 through 8, which are firmly based on maximum likelihood methods.

The differences in Methods 5 through 8 lie in which constraint(s) are enforced. Method 8 implements both (2.15) and (2.16), and has the least bias and variance, while Method 5 has the most and enforces no constraints. Methods 6 and 7 each implement one constraint, (2.15) and (2.16) respectively and Method 7 on average matches or outperforms Method 6. Thus (2.16) is integral to good estimation, even though (2.15) is better agreed upon. Even when data is generated with a t_{ref} value distorted by several orders of magnitude (see (2.26)), estimation

procedures that use the undistorted constraint (2.16) result in less bias and variance in the estimates.

Method 8 takes advantage of the constraints inherent in the CPL-W model and solves the maximum likelihood equations for both strength and lifetime data in one step. This results in the least bias and variance compared to the seven other estimation methods studied. This work was done specifically with five highly dissimilar sets of parameters. Given that the results were consistent across the five parameter sets investigated, there is reason to believe that the results will hold for material systems other than the five discussed here. Furthermore, the question of how parameters should be estimated is fundamental, and should be carefully considered. The current industry method to estimate parameters, Method 1, may work passably for materials such as Kevlar 49/epoxy tows, for which parameter and failure probability estimation is easier, but for T1000 tows and other materials with a low β value, Method 1 has unreasonable amounts of bias and variance. It is also important to recognize that the parameters are not independent; while the parameter estimates can have significant bias and variance, paradoxically the estimates of failure probability often are still accurate with low bias.

2.7 Appendix

The original functional form for the lifetime distribution function, as proposed by Phoenix in 1979 [18], and specialized to forms of interest in the current paper in (2.5), is rewritten here as:

$$F\left(t\middle|\sigma\right)=1-\exp\left\{-\sup_{0\le\tau\le t}\left\{\left[\left(\frac{\sigma\left(\tau\right)}{\sigma_{\text{ref}}}\right)^{r}+\int_{0}^{\tau}\left(\frac{\sigma\left(s\right)}{\sigma_{\text{ref}}}\right)^{\rho}\frac{ds}{t_{\text{ref}}}\right]^{\beta}\right\}\right\} \tag{2.A1}$$

2.7.1 Strength decay model

Setting $r = \rho$, the functional form (2.A1) becomes

$$F\left(t\middle|\sigma\right) = 1 - \exp\left\{-\sup_{0\le\tau\le t}\left\{\left[\left(\frac{\sigma(\tau)}{\sigma_{\text{ref}}}\right)^{\rho} + \int_0^{\tau}\left(\frac{\sigma(s)}{\sigma_{\text{ref}}}\right)^{\rho}\frac{ds}{t_{\text{ref}}}\right]^{\beta}\right\}\right\} \tag{2.A2}$$

Under a constant stress over time $\sigma(t) = \bar{\sigma}$, $t \ge 0$, (2.A2) reduces to

$$\begin{aligned} F_{\bar{\sigma}}(t) &= 1 - \exp\left\{-\sup_{0\le\tau\le t}\left\{\left[\left(\frac{\bar{\sigma}}{\sigma_{\text{ref}}}\right)^{\rho} + \int_0^{\tau}\left(\frac{\bar{\sigma}}{\sigma_{\text{ref}}}\right)^{\rho}\frac{ds}{t_{\text{ref}}}\right]^{\beta}\right\}\right\} \\ &= 1 - \exp\left\{-\left(\frac{\bar{\sigma}}{\sigma_{\text{ref}}}\right)^{\alpha}\left(1 + \frac{t}{t_{\text{ref}}}\right)^{\beta}\right\} \end{aligned} \tag{2.A3}$$

where $\alpha = \rho\beta$. For large t, such that $\frac{t}{t_{\text{ref}}} \gg 1$, (2.A3) simplifies to the CPL-W lifetime distribution of:

$$F_{\bar{\sigma}}(t) = 1 - \exp\left\{-\left(\frac{\bar{\sigma}}{\sigma_{\text{ref}}}\right)^{\alpha}\left(\frac{t}{t_{\text{ref}}}\right)^{\beta}\right\} \tag{2.A4}$$

For a linearly increasing load $\sigma(t) = Rt$, $t \ge 0$, (2.A2) becomes

$$\begin{aligned} F_R(t) &= 1 - \exp\left\{-\sup_{0\le\tau\le t}\left\{\left[\left(\frac{R\tau}{\sigma_{\text{ref}}}\right)^{\rho} + \int_0^{\tau}\left(\frac{Rs}{\sigma_{\text{ref}}}\right)^{\rho}\frac{ds}{t_{\text{ref}}}\right]^{\beta}\right\}\right\} \\ &= 1 - \exp\left\{-\left[\left(\frac{Rt}{\sigma_{\text{ref}}}\right)^{\rho}\left(1 + \frac{t}{(\rho+1)t_{\text{ref}}}\right)\right]^{\beta}\right\} \end{aligned} \tag{2.A5}$$

At the point of failure, the failure stress follows $s = Rt$, so (2.A5) becomes:

$$\bar{F}_R(s) = 1 - \exp\left\{-\left[\left(\frac{s}{\sigma_{\text{ref}}}\right)^{\rho}\left(1+\frac{s}{R(\rho+1)t_{\text{ref}}}\right)\right]^{\beta}\right\} \tag{2.A6}$$

Note that this is not a Weibull distribution, except in the limit as $R \to \infty$. In this limit (2.A6) becomes

$$\lim_{R\to\infty} \bar{F}_R(s) = 1 - \exp\left\{-\left[\left(\frac{s}{\sigma_{\text{ref}}}\right)^{\rho}\right]^{\beta}\right\}, \tag{2.A7}$$

which is the standard Weibull strength distribution. The loading rate R is generally picked such that the failure time in the strength testing for tows is about 30 seconds, and for COPVs as fast as the COPV can be pressurized. Thus (2.A7) is generally a reasonable approximation to (2.A6) for tows, but not always for COPVs, due to typically slower loading rates.

2.7.1.1 Origins of strength decay model

James Reeder developed the strength decay model [19] in response to the fiber breakage model [5]. The underlying assumption is that the strength of the specimen decreases as a function of time. The function

$$s(t) = \bar{\sigma}\left[\left(\frac{s_0}{\bar{\sigma}}\right)^{\rho} - \frac{t}{t_{\text{ref}}}\right]^{1/\rho} \tag{2.A8a}$$

was chosen to represent this decay as it has many different possible shapes. In this function, $s(t)$ is the strength of the specimen at time $t \geq 0$, $s(0) = s_0$, and $\bar{\sigma}$, ρ and t_{ref} are the same as before. Note that (2.A8a) can also be written as

$$s(t) = s_0\left[1-\left(\frac{\bar{\sigma}}{s_0}\right)^{\rho}\frac{t}{t_{\text{ref}}}\right]^{1/\rho} \tag{2.A8b}$$

Failure is said to occur when the strength decays enough to finally equal $\bar{\sigma}$; i.e. $s(t_f) = \bar{\sigma}$ where t_f is the failure time. Thus the initial strength can be written in terms of this failure time and the other variables as:

$$s_0 = \bar{\sigma}\left[1+\frac{t_f}{t_{\text{ref}}}\right]^{1/\rho}. \tag{2.A9}$$

The second assumption of the strength decay model is that the initial strength is Weibull distributed with shape parameter α, and scale parameter σ_{ref}, that is, the survival probability is:

$$P(s_0) = P(\text{initial strength} > s_0) = \exp\left\{-\left(\frac{s_0}{\sigma_{\text{ref}}}\right)^{\alpha}\right\}. \tag{2.A10}$$

By substituting (2.A9) into (2.A10) we obtain:

$$P(\text{initial strength}=\hat{s} > s_0) = P\left(\hat{s} > \bar{\sigma}\left[1+\frac{t_f}{t_{\text{ref}}}\right]^{1/\rho}\right) = P\left(t_{\text{ref}}\left[\left(\frac{\hat{s}}{\bar{\sigma}}\right)^{\rho}-1\right] > t_f\right)$$

$$= P(\hat{t} > t_f) = \exp\left\{-\left(\frac{s_0}{\sigma_{\text{ref}}}\right)^{\alpha}\right\} = \exp\left\{-\left(\frac{\bar{\sigma}}{\sigma_{\text{ref}}}\left[1+\frac{t_f}{t_{\text{ref}}}\right]^{1/\rho}\right)^{\alpha}\right\}$$

or:

$$P(t_f > t) = \exp\left\{-\left(\frac{\bar{\sigma}}{\sigma_{\text{ref}}}\left[1+\frac{t}{t_{\text{ref}}}\right]^{1/\rho}\right)^{\alpha}\right\} \tag{2.A11}$$

Letting $\alpha = \rho\beta$, (2.A11) thus becomes (2.A3).

2.7.1.2 Further development of strength decay model

To show more generally that a strength decay model based on (2.A8) is consistent with the integral form given by (2.A2), we must consider a load scheme with many different small step loads. Load σ_n is applied from t_{n-1} to t_n where $n \geq 1$, $t_n > t_{n-1}$, and $t_0 = 0$. Define $\tau_n = t_n - t_{n-1}$. Remember that the strength of a specimen will never increase-it must be a monotonic decreasing function. Thus the strength at t_1 is given by s_1, according to (2.A8), as

$$s_1 = s(t_1) = \sigma_1 \left[\left(\frac{s_0}{\sigma_1} \right)^{\rho} - \frac{t_1}{t_{\text{ref}}} \right]^{\frac{1}{\rho}} \tag{2.A12}$$

where $s_1 > \sigma_1$ for the specimen to survive. Directly after t_1 we have a new load level, σ_2, and in the case of $\sigma_2 < \sigma_1$ we can talk in the spirit of Reeder [19] of a safe time t_{safe}, which is the additional survival time until failure occurs at the new load level σ_2 i.e. $s(t_{\text{safe}} + t_1) = \sigma_2$. Then (2.A8) gives:

$$\begin{aligned} \sigma_2 &= \sigma_2 \left[\left(\frac{s_1}{\sigma_2} \right)^{\rho} - \frac{t_{\text{safe}}}{t_{\text{ref}}} \right]^{\frac{1}{\rho}} \\ t_{\text{safe}} &= t_{\text{ref}} \left(\left(\frac{s_1}{\sigma_2} \right)^{\rho} - 1 \right) \end{aligned} \tag{2.A13}$$

Equation (2.A13) is given for a particular specimen, for which s_0 and thus s_1 are fixed and known. In general s_0 is not known, so a slightly different definition of t_{safe} is generally used–the amount of time that no vessel will fail. Thus we can substitute $\sigma_1 = s_1$ to get a lower bound on the safe time of any particular vessel.

$$\tilde{t}_{\text{safe}} = t_{\text{ref}}\left(\left(\frac{\sigma_1}{\sigma_2}\right)^{\rho} - 1\right) < t_{\text{safe}} \tag{2.A14}$$

provided that $s_1 > \sigma_1$. If for the moment we assume each τ_n is larger than the corresponding t_{safe}, as given in (2.A13), our strength would decay thusly:

$$\begin{aligned}
s(t_1) &= \sigma_1\left[\left(\frac{s_0}{\sigma_1}\right)^{\rho} - \frac{\tau_1}{t_{\text{ref}}}\right]^{\frac{1}{\rho}} = s_1 \\
s(t_2) &= \sigma_2\left[\left(\frac{s_1}{\sigma_2}\right)^{\rho} - \frac{\tau_2}{t_{\text{ref}}}\right]^{\frac{1}{\rho}} = s_2 = \sigma_2\left[\left(\frac{s_0}{\sigma_2}\right)^{\rho} - \left(\frac{\sigma_1}{\sigma_2}\right)^{\rho}\frac{\tau_1}{t_{\text{ref}}} - \frac{\tau_2}{t_{\text{ref}}}\right]^{\frac{1}{\rho}} \\
s(t_3) &= \sigma_3\left[\left(\frac{s_2}{\sigma_3}\right)^{\rho} - \frac{\tau_3}{t_{\text{ref}}}\right]^{\frac{1}{\rho}} = s_3 = \sigma_3\left[\left(\frac{s_0}{\sigma_3}\right)^{\rho} - \left(\frac{\sigma_1}{\sigma_3}\right)^{\rho}\frac{\tau_1}{t_{\text{ref}}} - \left(\frac{\sigma_2}{\sigma_3}\right)^{\rho}\frac{\tau_2}{t_{\text{ref}}} - \frac{\tau_3}{t_{\text{ref}}}\right]^{\frac{1}{\rho}} \\
s(t_n) &= s_n = \sigma_n\left[\left(\frac{s_0}{\sigma_n}\right)^{\rho} - \frac{\tau_n}{t_{\text{ref}}} - \sum_{i=1}^{n-1}\left(\frac{\sigma_i}{\sigma_n}\right)^{\rho}\frac{\tau_i}{t_{\text{ref}}}\right]^{\frac{1}{\rho}}
\end{aligned} \tag{2.A15}$$

If the specimen finally fails at time t_n we have $s(t_n)/\sigma_n = 1$, which from (2.A15) yields the required initial strength value:

$$s_0 = \sigma_n\left[1 + \sum_{i=1}^{n}\left(\frac{\sigma_i}{\sigma_n}\right)^{\rho}\frac{\tau_i}{t_{\text{ref}}}\right]^{\frac{1}{\rho}} = \left[\sigma_n{}^{\rho} + \sum_{i=1}^{n}\sigma_i{}^{\rho}\frac{\tau_i}{t_{\text{ref}}}\right]^{\frac{1}{\rho}} \tag{2.A16}$$

When we now allow each τ_n to be of arbitrary size we must impose an infimum on the sequence in (2.A15) to ensure that $s(t)$ is monotone decreasing, as the strength can at no time increase. Thus (2.A16) is now

$$s_0 = \sup_{0\le s\le n}\left[\sigma_s{}^{\rho} + \sum_{i=1}^{s}\sigma_i{}^{\rho}\,\frac{\tau_i}{t_{\text{ref}}}\right]^{\frac{1}{\rho}} \tag{2.A17}$$

Now that we have characterized the initial strength s_0 resulting in failure at time t_n, we can calculate the probability of survival by substituting (2.A17) into (2.A10):

$$P\left(t > t_n\right) = 1 - \exp\left\{-\left(\sup_{n\ge s\ge 1}\left\{\left[\left(\frac{\sigma_s}{\sigma_{\text{ref}}}\right)^{\rho} + \sum_{i=1}^{s}\left(\frac{\sigma_i}{\sigma_{\text{ref}}}\right)^{\rho}\frac{\tau_i}{t_{\text{ref}}}\right]^{\frac{1}{\rho}}\right\}\right)^{\alpha}\right\} \tag{2.A18}$$

Taking the limit of the step sizes to be small, i.e. $\tau_i \to 0$, such that $t_n \to t_f$, we get

$$P\left(t > t_f\right) = 1 - \exp\left\{-\sup_{0\le s\le t}\left\{\left[\left(\frac{\sigma(s)}{\sigma_{\text{ref}}}\right)^{\rho} + \int_0^{s}\left(\frac{\sigma(v)}{\sigma_{\text{ref}}}\right)^{\rho}\frac{dv}{t_{\text{ref}}}\right]^{\beta}\right\}\right\}, \tag{2.A19}$$

which is equivalent to (2.A2).

2.7.2 Crack-growth model

The crack growth model is another stress rupture model dating from at least 1981. Based in fracture mechanics, this model also is of the Phoenix functional form [18]. Setting $r = \rho - 2$ in (2.A1) gives this crack growth model:

$$F\left(t\middle|\sigma\right) = 1 - \exp\left\{-\sup_{0\le\tau\le t}\left[\left(\frac{\sigma(\tau)}{\sigma_{\text{ref}}}\right)^{\rho-2} + \int_0^{\tau}\left(\frac{\sigma(s)}{\sigma_{\text{ref}}}\right)^{\rho}\frac{ds}{t_{\text{ref}}}\right]^{\beta}\right\} \tag{2.A20}$$

When evaluated at a constant stress $\sigma(t) = \bar{\sigma}, \quad t \ge 0$, (2.A20) can be written as

$$F_{\bar{\sigma}}(t) = 1 - \exp\left\{-\left(\frac{\bar{\sigma}}{\sigma_{\text{ref}}}\right)^{\alpha}\left(1+\left(\frac{\bar{\sigma}}{\sigma_{\text{ref}}}\right)^{2}\frac{t}{t_{\text{ref}}}\right)^{\beta}\right\}$$
$$= 1 - \exp\left\{-\left(\frac{\bar{\sigma}}{\sigma_{\text{ref}}}\right)^{\rho\beta}\left(\left(\frac{\bar{\sigma}}{\sigma_{\text{ref}}}\right)^{-2}+\frac{t}{t_{\text{ref}}}\right)^{\beta}\right\} \qquad (2.A21)$$

where $\alpha = (\rho - 2)\beta$ and we have given two alternate forms for the lifetime distribution in (2.A21). For the crack growth model, as $t \to \infty$ we again get the basic CPL-W Weibull lifetime load distribution, as in the stress decay model (2.A4). However, since $\left(\bar{\sigma}/\sigma_{\text{ref}}\right)^{-2} > 1$ it takes longer for the crack growth model to converge to CPL-W than it does for the stress decay model.

For a linearly increasing load $\sigma(t) = Rt$, $t \geq 0$, upon integrating (2.A20) reduces to

$$F_R(t) = 1 - \exp\left\{-\left[\left(\frac{Rt}{\sigma_{\text{ref}}}\right)^{\rho-2}+\left(\frac{Rt}{\sigma_{\text{ref}}}\right)^{\rho}\frac{t}{(\rho+1)t_{\text{ref}}}\right]^{\beta}\right\} \qquad (2.A22)$$

At the point of failure, the failure stress is $s = Rt$, so (2.A22) yields the strength distribution:

$$\bar{F}_R(s) = 1 - \exp\left\{-\left(\frac{s}{\sigma_{\text{ref}}}\right)^{\alpha}\left(1+\left(\frac{s}{\sigma_{\text{ref}}}\right)^{2}\frac{s}{R(\rho+1)t_{\text{ref}}}\right)^{\beta}\right\} \qquad (2.A23)$$

again using $\alpha = (\rho - 2)\beta$. Note that this is not a Weibull distribution, but in the limit $R \to \infty$ (2.A23) approaches the standard Weibull strength distribution. This mimics the behavior of the strength decay model.

2.7.2.1 Development of crack growth model

This model was fully developed by Kelly and McCartney [20], and is based on Paris law crack growth. What follows is an alternate and more general derivation, in order to allow illumination of physical assumptions inherent in the strength decay model.

Let $\hat{\sigma}_0$ be the strength of a specimen at time $t = 0$ and assume $\hat{\sigma}_0$ is a random variable that follows a Weibull distribution function, that is, $\Pr\{\hat{\sigma}_0 \le \sigma\} = F_0(\sigma)$, where

$$F_0(\sigma) = 1 - \exp\left(-\left(\frac{\sigma}{\sigma_{\text{ref}}} \right)^{\alpha} \right), \quad \sigma \ge 0 \tag{2.A24}$$

and where the positive constants σ_{ref} and α are the Weibull shape and scale parameters, respectively. We also assume that this initial specimen strength, $\hat{\sigma}_0$, is governed by the existence of a critical Mode I crack of size, a_0, through the fracture mechanics relationship

$$K_{\text{Ic}} \equiv \hat{\sigma}_0 (\pi a_0)^{\eta} \tag{2.A25}$$

where K_{Ic} is called the critical stress intensity factor in Mode I, and η is a positive constant typically taken as $1/2$ for a homogeneous isotropic material, though η can take other values depending on material heterogeneity and crack configuration circumstances. Relationship (2.A25) further implies that for a given stress, σ, a crack of size, a, is catastrophically unstable if $a \ge (K_{\text{Ic}}/\sigma)^{1/\eta}/\pi$ and stable if $a < (K_{\text{Ic}}/\sigma)^{1/\eta}/\pi$.

We consider a time varying stress history on the specimen, $\sigma(t)$, $t \ge 0$ and associated crack, $a(t)$, $t \ge 0$, in the specimen that grows in time starting at size $a(0) = a_0$. We assume a growth

law that is given in integral form as

$$\int_{a_0}^{a(t)} a^{-\rho\eta}\,da = \varphi(\pi)^{\rho\eta} \sup_{0\le\tau\le t}\left[\sigma(\tau)^{\zeta}\int_0^{\tau}\sigma(s)^{\rho}\,ds\right],\ t\ge 0 \qquad \text{(2.A26)}$$

where the constants, $\rho > 0$, and $\zeta \ge 0$ are power law exponents governing the crack growth rate, $\varphi > 0$, is a material constant and $\eta > 0$ was defined previously. Thus the crack size at time t, depends not only on the time evolution of an integral involving stress history but also on the instantaneous value of the stress along the way. The purpose of the supremum function is to prevent the crack from appearing to decrease in size should the stress drop. In the case of a stress decrease the crack will remain at the same size for some period of time before continuing to grow.

In the case where $\zeta = 0$, taking time derivatives of both sides of (2.A26) yields

$$da(t)/dt = \varphi\pi^{\rho\eta}a(t)^{\rho\eta}\sigma(t)^{\rho},\ t\ge 0 \qquad \text{(2.A27)}$$

Defining $K_1 \equiv \sigma(\pi a)^{\eta}$, which is referred to as the stress intensity factor in terms of current crack size a and stress level σ, we rewrite (2.A27) more simply as

$$da/dt = \varphi(K_1)^{\rho},\ t\ge 0 \qquad \text{(2.A28)}$$

which when combined with $\eta = 1/2$ is the Paris-Erdogan crack growth law.

Returning to (2.A26) we integrate the left-hand side to yield

$$a(t)^{1-\rho\eta} = a_0^{1-\rho\eta} + (1-\rho\eta)\varphi\pi^{\rho\eta}\sigma_{\text{ref}}^{\zeta+\rho} \sup_{0\le\tau\le t}\left[\left(\frac{\sigma(\tau)}{\sigma_{\text{ref}}}\right)^{\zeta}\int_0^{\tau}\left(\frac{\sigma(s)}{\sigma_{\text{ref}}}\right)^{\rho} ds\right] \qquad \text{(2.A29)}$$

We can use this result to determine the strength, $\hat{\sigma}(t)$, of a crack of length $a(t)$ at time t, given that it began as a crack of size a_0 with strength $\hat{\sigma}_0$. Initially (2.A25) gives $a_0 = \left(K_{\mathrm{Ic}}/\hat{\sigma}_0\right)^{1/\eta}/\pi$, and at time t this extends to $a(t) = \left(K_{\mathrm{Ic}}/\hat{\sigma}(t)\right)^{1/\eta}/\pi$ so that

$$\left[\left(K_{\mathrm{Ic}}/\hat{\sigma}(t)\right)^{1/\eta}/\pi\right]^{1-\eta\rho} = \left[\left(K_{\mathrm{Ic}}/\hat{\sigma}_0\right)^{1/\eta}/\pi\right]^{1-\eta\rho} + (1-\eta\rho)\varphi\pi^{\eta\rho}\sigma_{\mathrm{ref}}^{\zeta+\rho}\sup_{0\le\tau\le t}\left[\left(\frac{\sigma(\tau)}{\sigma_{\mathrm{ref}}}\right)^{\zeta}\int_0^{\tau}\left(\frac{\sigma(s)}{\sigma_{\mathrm{ref}}}\right)^{\rho} ds\right] \quad \text{(2.A30)}$$

Rearranging (2.A30) results in

$$\hat{\sigma}(t) = \left[\hat{\sigma}_0^{\rho-1/\eta} - \sigma_{\mathrm{ref}}^{\rho-1/\eta}\sup_{0\le\tau\le t}\left[\left(\frac{\sigma(\tau)}{\sigma_{\mathrm{ref}}}\right)^{\zeta}\int_0^{\tau}\left(\frac{\sigma(s)}{\sigma_{\mathrm{ref}}}\right)^{\rho}\frac{ds}{t_{\mathrm{ref}}}\right]\right]^{\frac{1}{\rho-1/\eta}} \quad \text{(2.A31)}$$

where we have set

$$t_{\mathrm{ref}} \equiv \left(\frac{1}{\eta\rho-1}\right)\frac{K_{\mathrm{Ic}}^{1/\eta-\rho}\sigma_{\mathrm{ref}}^{-(\zeta+1/\eta)}}{\varphi\pi} \quad \text{(2.A32)}$$

We let $F\left(t;\sigma(\cdot)\right)$ be the distribution function for the lifetime of the specimen under stress history $\sigma(\tau)$, $0 \le \tau \le t$, and let $\hat{\sigma}(\tau)$ be the strength of the weakest flaw at time, τ, where $0 \le \tau \le t$. The probability that the specimen is surviving at time t is $\Pr\left\{\inf_{0\le\tau\le t}\left\{\hat{\sigma}(\tau)-\sigma(\tau)\right\} > 0\right\}$, that is, the probability that the specimen strength is greater than the stress over time period $0 \le \tau \le t$. However, the specimen initially had strength $\hat{\sigma}_0$, and by rearranging (2.A31) we have

$$
\begin{aligned}
1-F\left(t;\sigma\left(\cdot\right)\right) &= \Pr\left\{\inf_{0\le\tau\le t}\left\{\hat{\sigma}\left(\tau\right)-\sigma\left(\tau\right)\right\}>0\right\} \\
&= \Pr\left\{\hat{\sigma}_0 > \sup_{0\le\tau\le t}\left[\sigma\left(\tau\right)^{\rho-1/\eta}+\sigma_{\text{ref}}^{\rho-1/\eta}\left(\frac{\sigma\left(\tau\right)}{\sigma_{\text{ref}}}\right)^{\zeta}\int_0^{\tau}\left(\frac{\sigma\left(s\right)}{\sigma_{\text{ref}}}\right)^{\rho}\frac{ds}{t_{\text{ref}}}\right]^{\frac{1}{\rho-1/\eta}}\right\} \\
&= 1-F_0\left(\sup_{0\le\tau\le t}\left[\sigma\left(\tau\right)^{\rho-1/\eta}+\sigma_{\text{ref}}^{\rho-1/\eta}\left(\frac{\sigma\left(\tau\right)}{\sigma_{\text{ref}}}\right)^{\zeta}\int_0^{\tau}\left(\frac{\sigma\left(s\right)}{\sigma_{\text{ref}}}\right)^{\rho}\frac{ds}{t_{\text{ref}}}\right]^{\frac{1}{\rho-1/\eta}}\right)
\end{aligned}
\tag{2.A33}
$$

which by (2.A24) yields

$$
F\left(t;\sigma\left(\cdot\right)\right)=1-\exp\left(-\sup_{0\le\tau\le t}\left[\left(\frac{\sigma\left(\tau\right)}{\sigma_{\text{ref}}}\right)^{\rho-1/\eta}+\left(\frac{\sigma\left(\tau\right)}{\sigma_{\text{ref}}}\right)^{\zeta}\int_0^{\tau}\left(\frac{\sigma\left(s\right)}{\sigma_{\text{ref}}}\right)^{\rho}\frac{ds}{t_{\text{ref}}}\right]^{\frac{\alpha}{\rho-1/\eta}}\right),\quad t\ge 0 \tag{2.A34}
$$

The supremum in (2.A33) and (2.A34) is to prevent the argument from ever decreasing since F must be non-decreasing in time, $t\ge 0$, and note that the supremum in (2.A31) becomes absorbed by the new one generated in (2.A33) and (2.A34).

Next we let

$$
\beta\equiv\alpha/\left(\rho-1/\eta\right), \tag{2.A35}
$$

so that

$$
\alpha/\beta=\rho-1/\eta \quad \text{or} \quad \alpha=\left(\rho-1/\eta\right)\beta \tag{2.A36}
$$

and we note that

$$
\rho=\rho-1/\eta+1/\eta=\alpha/\beta+1/\eta=\left(\alpha+\beta/\eta\right)/\beta \tag{2.A37}
$$

Then we rewrite (2.A34) as

$$F\left(t;\sigma\left(\cdot\right)\right)=1-\exp\left(-\sup_{0\le\tau\le t}\left[\left(\frac{\sigma\left(\tau\right)}{\sigma_{\text{ref}}}\right)^{\alpha/\beta}+\left(\frac{\sigma\left(\tau\right)}{\sigma_{\text{ref}}}\right)^{\zeta}\int_0^{\tau}\left(\frac{\sigma\left(s\right)}{\sigma_{\text{ref}}}\right)^{\rho}\frac{ds}{t_{\text{ref}}}\right]^{\beta}\right),\ t\ge 0 \tag{2.A38}$$

For the simpler case of a constant stress history, $\sigma\left(t\right)=\bar{\sigma},\ t\ge 0$, where $\bar{\sigma}$ is a positive constant, we can reduce (2.A38) to

$$F\left(t;\bar{\sigma}\right)=1-\exp\left(-\left[\left(\frac{\bar{\sigma}}{\sigma_{\text{ref}}}\right)^{\alpha/\beta}+\left(\frac{\bar{\sigma}}{\sigma_{\text{ref}}}\right)^{\rho+\zeta}\frac{t}{t_{\text{ref}}}\right]^{\beta}\right),\ t\ge 0 \tag{2.A39}$$

which can also be written as

$$F\left(t;\bar{\sigma}\right)=1-\exp\left(-\left(\frac{\bar{\sigma}}{\sigma_{\text{ref}}}\right)^{\alpha}\left[1+\left(\frac{\bar{\sigma}}{\sigma_{\text{ref}}}\right)^{\zeta+1/\eta}\frac{t}{t_{\text{ref}}}\right]^{\beta}\right) \tag{2.A40}$$

where again α is the Weibull shape parameter for strength. At time $t=0$ we have $F\left(0;\bar{\sigma}\right)=F_0\left(\sigma\right)$ so that (2.A40) yields

$$F_0\left(\sigma\right)=1-\exp\left(-\left(\frac{\bar{\sigma}}{\sigma_{\text{ref}}}\right)^{\alpha}\right),\ \sigma\ge 0 \tag{2.A41}$$

in agreement with (2.A24).

In the special case where $\zeta=0$, the crack grows according to the Paris-Erdogan law, and we reduce (2.A38) to

$$F\left(t;\sigma\left(\cdot\right)\right)=1-\exp\left(-\sup_{0\le\tau\le t}\left[\left(\frac{\sigma\left(\tau\right)}{\sigma_{\text{ref}}}\right)^{\alpha/\beta}+\int_0^{\tau}\left(\frac{\sigma\left(s\right)}{\sigma_{\text{ref}}}\right)^{\rho}\frac{ds}{t_{\text{ref}}}\right]^{\beta}\right),\ t\ge 0 \tag{2.A42}$$

This is of the same form as (2.A20), although to get (2.A20) we must take $\eta = 1/2$ in (2.A35).

Under constant stress history, $\sigma(t) = \bar{\sigma},\ t \geq 0$, (2.A42) becomes

$$F(t;\bar{\sigma}) = 1 - \exp\left(-\left(\frac{\bar{\sigma}}{\sigma_{\text{ref}}} \right)^{\alpha} \left[1 + \left(\frac{\bar{\sigma}}{\sigma_{\text{ref}}} \right)^{1/\eta} \frac{t}{t_{\text{ref}}} \right]^{\beta} \right) \tag{2.A43}$$

Note that the value of the exponent, η, affects the influence of increasing time. When $\eta = 1/2$, the formulation is the standard crack growth formulation (2.A20). A useful way to view this formulation is to interpret the specimen strength, $\hat{\sigma}(t)$, as decaying according to

$$\hat{\sigma}(t) = \frac{\hat{\sigma}_0}{\left[1 + \left(\bar{\sigma}/\sigma_{\text{ref}} \right)^2 \left(t/t_{\text{ref}} \right) \right]^{1/(\rho-2)}} \tag{2.A44}$$

As expected, strength decay cannot occur unless the specimen is under stress, $\bar{\sigma}$.

In the special case where $\zeta = -1/\eta$ we reduce (2.A38) to

$$F(t;\sigma(\cdot)) = 1 - \exp\left(-\sup_{0 \leq \tau \leq t} \left[\left(\frac{\sigma(\tau)}{\sigma_{\text{ref}}} \right)^{\alpha/\beta} + \left(\frac{\sigma(\tau)}{\sigma_{\text{ref}}} \right)^{-1/\eta} \int_0^{\tau} \left(\frac{\sigma(s)}{\sigma_{\text{ref}}} \right)^{\rho} \frac{ds}{t_{\text{ref}}} \right]^{\beta} \right),\ t \geq 0 \tag{2.A45}$$

Under constant stress history, $\sigma(t) = \bar{\sigma},\ t \geq 0$, (2.A45) becomes

$$F(t;\bar{\sigma}) = 1 - \exp\left(-\left(\frac{\bar{\sigma}}{\sigma_{\text{ref}}} \right)^{\alpha} \left[1 + \frac{t}{t_{\text{ref}}} \right]^{\beta} \right) \tag{2.A46}$$

This is the strength decay model, where the strength can be viewed as decaying according to

$$\hat{\sigma}(t) = \frac{\hat{\sigma}_0}{\left(1 + t/t_{\text{ref}} \right)^{\beta/\alpha}} = \frac{\hat{\sigma}_0}{\left(1 + t/t_{\text{ref}} \right)^{\frac{1}{\rho - 1/\eta}}} \tag{2.A47}$$

irrespective of whether there is stress on the specimen or not. This circumstance may be relevant to environmentally driven strength decay but is not the result of a crack growth mechanism of the Paris-Erdogan type and is not stress rupture.

In the case where $\eta \to \infty$, from (A36) we have $\alpha/\beta = \rho$ and (2.A47) becomes

$$\hat{\sigma}(t) = \frac{\hat{\sigma}_0}{\left(1 + t/t_{\text{ref}}\right)^{1/\rho}} \tag{2.A48}$$

which is the stress decay model of Reeder. However, taking $\eta \to \infty$ in (A25) removes all connection to fracture mechanics concepts.

REFERENCES

[1] Blassiau S, Thionnet A, Bunsell A. (2006) Micromechanisms of load transfer in a unidirectional carbon fibre–reinforced epoxy composite due to fibre failures. Part 1: Micromechanisms and 3D analysis of load transfer: The elastic case, Compos Struct 74:303–18.

[2] Blassiau S, Thionnet A, Bunsell A. (2006) Micromechanisms of load transfer in a unidirectional carbon fibre–reinforced epoxy composite due to fibre failures. Part 2: Influence of viscoelastic and plastic matrices on the mechanisms of load transfer, Compos Struct 74:319–31.

[3] Blassiau S, Thionnet A, Bunsell A. (2008) Micromechanisms of load transfer in a unidirectional carbon fibre–reinforced epoxy composite due to fibre failures. Part 3: Multiscale reconstruction of composite behaviour, Compos Struct 83:312–23.

[4] Chou HY, Thionnet A, Mouritz A, Bunsell AR. (2016) Stochastic factors controlling the failure of carbon/epoxy composites, J Mater Sci 51:311-333.

[5] Phoenix SL and Murthy PLN (2007) Pro's and Cons of Proof Testing Carbon Composite Overwrapped Pressure Vessels: A Comparison of Two Mathematical Models, AIAA Paper No. 2007-2325, presented at 48th AIAA/ASME/ASCE/AHS/ASC Structures, Structural Dynamics, and Materials Conference. Honolulu, HI.

[6] Tobolsky A and Eyring H (1943) Mechanical Properties of Polymeric Materials. J Chem Phys 11:125-134.

[7] Coleman BD (1956) Application of the theory of absolute reaction rates to the creep failure of polymeric filaments, J Polym Sci 20:447-455. doi:10.1002/pol.1956.120209604

[8] Coleman BD (1956) Time dependence of mechanical breakdown phenomena, J Appl Phys 27:862-866.

[9] Coleman BD (1957) A stochastic process model for mechanical breakdown phenomena, Trans Soc Rheol 1:153-168.

[10] Coleman BD and Knox AG (1957) The interpretation of creep failure in textile fibers as a rate process, Text Res J 27:393-399.

[11] Coleman BD (1958) Time dependence of mechanical breakdown in bundles of fibers. III. The power law breakdown rule, Trans Soc Rheol 2:195-218.

[12] Coleman BD (1958) Statistics and time dependence of mechanical breakdown in fibers, J Appl Phys 29:968-983.

[13] Coleman BD, Knox AG and McDevit WF (1958) The effect of temperature on the rate of creep failure for 66 Nylon, Text Res J 28:393-399.

[14] Phoenix SL and Tierney LJ (1983) A statistical model for the time dependent failure of unidirectional composite materials under local elastic load-sharing among fibers, Eng Fract Mech 18:193-215.

[15] Phoenix SL (1978) Stochastic strength and fatigue of fiber bundles, Int J Fract 14:327-344. doi:10.1007/BF00034692

[16] Miner MA (1945) Cumulative damage in fatigue. ASME J Appl Mech 12(3):159–164.

[17] Liang Y and Chen W (2015) A regularized Miner's rule for fatigue reliability analysis with Mittag-Leffler statistics, Int J Damage Mech doi:10.1177/1056789515607610

[18] Phoenix SL (1979) The Asymptotic Distribution for the Time to Failure of a Fiber Bundle, Adv Appl Probab 11:153-187

[19] Reeder J (2012) Composite Stress Rupture: A New Reliability Model Based on Strength Decay. Report NASA/TM-2012-217566, L-20122, NF1676L-14234

[20] Kelly A and McCartney LN (1981) Failure by Stress Corrosion of Bundles of Fibres, P Roy Soc Lond A Mat 374:1759.

[21] Genschel U and Meeker WQ (2010) A Comparison of Maximum Likelihood and Median-Rank Regression for Weibull Estimation, Qual Eng 22(4):236-255.

[22] Olteanu D and Freeman L (2010) The Evaluation of Median-Rank Regression and Maximum Likelihood Estimation Techniques for a Two-Parameter Weibull Distribution, Qual Eng 22(4):256-272.

[23] Knoester H, Hulshof and Meester (2015) Modeling failure of high performance fibers: on the prediction of long-term time-to-failure, J Mater Sci 50(19):6277-6290.

[24] DeTeresa SJ and Groves SE (2001) Properties of Fiber Composites for Advanced Flywheel Energy Storage Devices, SAMPE Symp 2001-01-12.

[25] Phoenix SL, Grimes-Ledesma L, Thesken JC and Murthy PLN (2006) Reliability Modeling of the Stress-Rupture Performance of Kevlar 49/Epoxy Pressure Vessels: Revisiting a Large Body Stress Rupture Data to Develop New Insights, Proc Am Soc Compos, 21st Annual Technical Conference, University of Michigan-Dearborn, Dearborn, MI.

CHAPTER 3

ANALYSIS OF STRESS RUPTURE DATA ON FIBER COMPOSITES: PART 1- A UNIFIED MAXIMUM LIKELIHOOD METHOD

The following chapter is published in the Journal of Space Safety Engineering and reprinted here with permission. The reference to the published work is:

Engelbrecht-Wiggans, A., Phoenix, S.L. Analysis of stress rupture data on fiber composites: Part 1- A unified maximum likelihood method, The Journal of Space Safety Engineering (2017), http://dx.doi.org/10.1016/j.jsse.2017.03.002

3.1 Introduction

Stress rupture is a failure mode in continuous unidirectional fiber composites, particularly in composite overwrapped pressure vessels (COPVs), flywheels and tension members in civil engineering subjected to a constant load over long time periods. It can occur at normal operating stresses and temperatures at maintained stresses well below the ultimate strength for an extended time. Stress rupture is catastrophic and explosive, and occurs with little or no advance warning. Its occurrence is also highly variable, with two otherwise identical specimens under identical loading and environmental conditions failing at widely differing times (sometimes by several orders of magnitude). Stress rupture is of increasing concern, particularly in COPVs, as the impetus to increase service loads and times has increased, thus increasing the risk of stress rupture failure.

Prediction of a composite's stress rupture behavior is based heavily on extensive testing at loads considerably higher than the design load. These tests fall into two categories: strength testing and lifetime testing. Strength testing consists of a linearly increasing load until failure.

Strength failures typically occur in under a minute. Lifetime testing consists of a steady load held until either specimen failure or the test is ended. Lifetime testing typically spans months to years and uses multiple different load levels. The variance in failure times is high for lifetime tests, so while some specimens may fail quickly others may be destined to take decades or centuries to fail, which leads to censored data sets as the test is often stopped before all the specimens have failed. This censoring adds complexity to predicting a specimen's behavior at the design load.

Extrapolation is required to predict a composite's resistance to stress rupture based on test results. This is for two reasons; first, the design life is generally longer than the amount of time available for testing. Second, the desired probability that a composite will fail in its lifetime is generally less than one in a million. Thus even if tests could be run for the length of the desired service life, an infeasible number (perhaps ten million) of specimens would need to be tested to guarantee such a small probability of failure. Real stress rupture data sets generally contain fewer than two hundred specimens, thus requiring a modeling approach.

Extrapolation typically requires some form of a probabilistic stress rupture model. Several models exist, the oldest and most commonly used being the classic power-law model in a Weibull framework (CPL-W) which was developed by Coleman using Tobolsky-Eyring theory for thermally activated molecular bond breakage [7-13, 26]. In this model stress rupture failure times at different load levels are related using a power-law, and failure times at any given load level are Weibull distributed. The CPL-W model allows for prediction of a composite's probability of failure in stress rupture for any load profile in terms of three material constants. These three constants must be determined from a combination of strength and lifetime testing.

This paper presents a procedure for predicting the probability of stress rupture failure using the CPL-W model together with a maximum likelihood estimation (MLE) based method.

This method analyzes all the strength and lifetime data together in one unified procedure. Current industry standard analysis approaches are sequential and often 'ad hoc'. Typically strength and lifetime data are treated separately, and often the lifetime data sets at each load level are treated individually and then the model parameters estimated using some form of regression and averaging. Relative to other current approaches, the unified approach presented here avoids such data partitioning and provides much tighter estimates on typical stress rupture data sets for the key quantity of interest, namely the failure probability at a given lifetime and given load level [27].

To illustrate the details of this approach we use an existing stress-rupture data set on model cylindrical COPVS, generated by NASA at their White Sands Testing Facility. These vessels consisted of an aluminum liner overwrapped with T1000 carbon fiber in an epoxy matrix. More details on these vessels are provided in a later section.

3.2 CPL-W model

The CPL-W model describes the probability of failure of a composite as having a cumulative distribution function given by:

$$F\left(t\middle|\sigma\left(t\right)\right)=1-\exp\left\{-\left[\int_0^t\left(\frac{\sigma\left(\tau\right)}{\sigma_{\text{ref}}}\right)^{\rho}\frac{d\tau}{t_{\text{ref}}}\right]^{\beta}\right\} \tag{3.1}$$

where $\sigma\left(t\right)$ denotes an applied composite stress (or load) profile over time, and there are four material constants: σ_{ref} is the Weibull scale parameter for strength, t_{ref} is the Weibull scale parameter for lifetime (corresponding to stress level σ_{ref}), ρ is the power-law exponent relating behavior at different stress levels, and β is the Weibull shape parameter. These four material

constants are interconnected and dependent. In fact, since strength data is known to follow a Weibull distribution, these four constants are reduced to three as follows.

In strength testing the stress is linearly increasing:

$$\sigma(t) = Rt, \quad t \geq 0 \tag{3.2}$$

where the constant $R > 0$ is the loading or stress rate. Thus by integrating (3.1) we get the cumulative distribution function for time to failure in a strength test:

$$F_s(t) = 1 - \exp\left\{-\left[\left(\frac{R\,t_{\text{ref}}}{\sigma_{\text{ref}}}\right)^{\rho} \frac{1}{(\rho+1)}\left(\frac{t}{t_{\text{ref}}}\right)^{\rho+1}\right]^{\beta}\right\}. \tag{3.3}$$

However we are interested in the failure load or stress, and note that at any time t prior to failure, the stress level is $s = Rt$. Thus (3.3) can be re-written in terms of stress level upon substituting $t = s/R$, giving:

$$\bar{F}_s(s) = 1 - \exp\left\{-\left(\frac{\sigma_{\text{ref}}}{R(\rho+1)t_{\text{ref}}}\right)^{\beta}\left(\frac{s}{\sigma_{\text{ref}}}\right)^{\beta(\rho+1)}\right\}, \quad s \geq 0\,. \tag{3.4}$$

It is generally accepted that strength is Weibull distributed following the form:

$$\bar{F}_s(s) = 1 - \exp\left\{-\left(\frac{s}{\sigma_{\text{ref}}}\right)^{\alpha}\right\}, \quad s \geq 0 \tag{3.5}$$

where α and σ_{ref} are, respectively, the Weibull shape and scale parameter for strength. For this to be true in the context of the CPL-W model, a comparison of (3.4) and (3.5) yields an added constraint, namely

$$\left(\frac{\sigma_{\text{ref}}}{R(\rho+1)t_{\text{ref}}}\right)^{\beta}=1 \quad \text{requiring} \quad t_{\text{ref}}=\frac{\sigma_{\text{ref}}}{R(\rho+1)}. \tag{3.6}$$

Furthermore α is defined in terms of the existing material parameters such that

$$\alpha=\beta(\rho+1). \tag{3.7}$$

The importance of (3.6) and (3.7) is that we can describe all stress rupture failures within the CPL-W model in terms of only three material constants: σ_{ref}, α, and ρ rather than five (σ_{ref}, α, ρ, t_{ref}, and β). We choose these particular three parameters because the estimators of these happen to be the least correlated (compared to other possible choices of three parameters) when analyzing real data sets.

Stress rupture lifetimes can also be characterized in terms of these three parameters. In lifetime testing the load is held constant:

$$\sigma(t)=\bar{\sigma}, \quad t>0, \tag{3.8}$$

so in this case (3.1) simplifies to:

$$F\left(t\middle|\sigma(t)=\bar{\sigma}\right)\equiv F_{\bar{\sigma}}(t)=1-\exp\left\{-\left[\left(\frac{\bar{\sigma}}{\sigma_{\text{ref}}}\right)^{\rho}\frac{t}{t_{\text{ref}}}\right]^{\beta}\right\}, \tag{3.9}$$

or in terms of (3.6) and (3.7):

$$F_{\bar{\sigma}}(t)=1-\exp\left\{-\left[\left(\frac{\bar{\sigma}}{\sigma_{\text{ref}}}\right)^{\rho}\frac{R(\rho+1)t}{\sigma_{\text{ref}}}\right]^{\alpha/\rho+1}\right\}. \tag{3.10}$$

3.3 MLE method

Maximum likelihood estimation (MLE) is a statistical estimation procedure for estimating parameters. By maximizing the likelihood function, MLE finds the parameters that are 'most likely' to result in the given sample dataset. MLE produces consistent estimators that generally converge in distribution to a standard normal distribution (useful for constructing confidence intervals), and are asymptotically unbiased. In addition MLE is often recommended by statisticians for Weibull distributions with the level of censoring that is common for stress rupture. [21-22] The likelihood function for a set of parameters, given a particular dataset, is equivalent to the probability of obtaining that dataset (in comparison to other possible data sets) given those parameter values, namely:

$$L\left(\underline{\theta}\middle|x_1,\cdots,x_n\right)=P\left(x_1,\cdots,x_n\middle|\underline{\theta}\right) \tag{3.11}$$

where $\underline{\theta}=\left\{\sigma_{\text{ref}},\alpha,\rho\right\}$ is the set of parameters, and $x_1,\cdots,x_n$ constitutes the dataset.

To illustrate the MLE approach, we consider a dataset wherein each specimen is assumed to be statistically independent of the other specimens. The probability of obtaining a given dataset given the parameter values is the product of the probabilities for each individual data point. When either the failure times or stresses are known precisely, we can write (3.11) as:

$$P\left(x_1,\cdots,x_n\middle|\underline{\theta}\right)=\prod_{i=1}^{n}f\left(x_i\middle|\underline{\theta}\right) \tag{3.12}$$

where $f\left(x\middle|\underline{\theta}\right)$ is the appropriate probability density function (pdf). For strength data, this is the derivative of (3.5), namely:

$$f_s\left(x\middle|\underline{\theta}\right)=\frac{\alpha}{\sigma_{\text{ref}}}\left(\frac{x}{\sigma_{\text{ref}}}\right)^{\alpha-1}\exp\left\{-\left(\frac{x}{\sigma_{\text{ref}}}\right)^{\alpha}\right\}, \tag{3.13}$$

whereas for lifetime data the pdf is given by the derivative of (3.10), namely:

$$f_{\bar{\sigma}_i}\left(x\middle|\underline{\theta}\right)=\frac{\alpha}{(\rho+1)x}\left[\left(\frac{\bar{\sigma}_i}{\sigma_{\text{ref}}}\right)^{\rho}\frac{R(\rho+1)x}{\sigma_{\text{ref}}}\right]^{\frac{\alpha}{\rho+1}}\exp\left\{-\left[\left(\frac{\bar{\sigma}_i}{\sigma_{\text{ref}}}\right)^{\rho}\frac{R(\rho+1)x}{\sigma_{\text{ref}}}\right]^{\frac{\alpha}{\rho+1}}\right\}. \tag{3.14}$$

In reality lifetime data consists of some known failure times as well as censored or interval data. Censored and interval data happen when the specimen either had not failed by the time the experiment was terminated, or is only known to have failed at some point between two times (for instance because of recording equipment failure). When the failure time is known, we use the pdf (3.14) to calculate the probability for that data point. However when the failure time is known only to have occurred within a time interval, say $\left(t^{\ell}, t^{u}\right)$, the contribution to the likelihood function is obtained from the cumulative distribution function (10) as

$$P\left(x\middle|\underline{\theta}\right)=F_{\bar{\sigma}}\left(t^{u}\right)-F_{\bar{\sigma}}\left(t^{\ell}\right),\qquad x\in\left(t^{\ell},\,t^{u}\right). \tag{3.15}$$

For censored data where the test was stopped before the specimen failed, the interval of interest is $\left(t^{\ell},\infty\right)$, where t^{ℓ} is now the time that had elapsed when the test was stopped. In this case:

$$P\left(x\middle|\underline{\theta}\right)=F_{\bar{\sigma}}\left(\infty\right)-F_{\bar{\sigma}}\left(t^{\ell}\right)=1-F_{\bar{\sigma}}\left(t^{\ell}\right). \tag{3.16}$$

Note that t^{ℓ} can vary between surviving specimens, as test stations are often reloaded with new specimens when specimens fail early. Accounting for all these situations, the likelihood function (12) involves the product of terms in the form of (3.13), (3.14), (3.15) and (3.16) as appropriate.

3.3.1 Example dataset: T1000 carbon fiber/epoxy COPVs

To illustrate this method we use an example stress-rupture data set for COPVs, generated by NASA at the White Sands Testing Facility. General Dynamics manufactured these model

vessels, which had an aluminum 6061-T6 liner and T1000 carbon fiber/epoxy overwrap. The overwrap was designed to fail in the hoop wraps of the cylindrical section. In this paper the system of interest is the T1000/epoxy portion of the pressure vessel, so to this end the pressure component supported by the metal liner (assumed to be 1195 psig) was subtracted from the original pressure data both from the burst pressures and the three pressures in the lifetime tests. (Note that the liner had gone into plastic yielding for all vessel pressures of interest.) This modified data is what will be used throughout to illustrate the notation, as well as to provide an example use of this method. In using the model for this data set, $\sigma(t)$ is interpreted as the modified vessel pressure, with the understanding that composite stress is proportional to pressure [28-29].

3.3.2 Dataset values and notation

For the strength data, there are n_s test specimens with strengths σ_i, $i = 1,\cdots,n_s$ that become entries in an n_s-component vector. For the T1000 carbon fiber/epoxy COPVs dataset there are thirty strength specimens, so $n_s = 30$. These specimens were loaded at approximately $R = 144{,}000$ psi/hr. The burst strengths of the overwrap portion of the vessels are:

$$\begin{aligned}\sigma = \big[&6191, 6317, 6403, 5611, 5952, 5284, 6288, 5994, 6258, 6385,\\ &5449, 5607, 6307, 5873, 6010, 6054, 5782, 5843, 6058, 5878,\\ &5536, 5413, 5843, 5704, 5597, 5612, 6119, 6081, 6115, 5872\big] \text{ psi}\end{aligned}$$

For the lifetime tests, there are m different load levels $\bar{\sigma}_i$, $i = 1,\cdots,m$, and n_i lifetime specimens each subject to load level $\bar{\sigma}_i$. At each load level $\bar{\sigma}_i$ there may be several known lifetimes but also various censor times leading to multiple censor intervals indexed by $j = 1,\cdots,k_i$, where k_i

reflects the number of different censoring intervals corresponding to load level, $\bar{\sigma}_i$. Also at each load level we use the index $j = 0$ when referring to the group of samples whose exact failure times are known. Thus $n_{ij}, i = 1,\cdots,m;\ j = 0,\cdots,k_i$ describes the number of lifetime specimens at load level, $\bar{\sigma}_i$, that lie within censor interval index j, when $j \geq 1$, and the number of uncensored lifetime specimens, when $j = 0$. At load level $\bar{\sigma}_i$ the total number of specimens, censored and uncensored, is the sum $n_i = n_{i,0} + n_{i,1} + \cdots + n_{i,k_i}$.

For the T1000 COPV lifetime tests there are three different pressure levels, i.e. $m = 3$, with pressures $\bar{\sigma}_i = [5205, 4845, 4505]$ psi. The associated numbers of censored and uncensored specimens, n_{ij}, can be presented as a 'matrix', with the understanding that there may be empty entries. Thus the numbers of specimens at the three load levels are descried in the matrix:

$$\left[n_{ij}\right] = \begin{bmatrix} 7 & 15 & 2 & - \\ 2 & 28 & 1 & 1 \\ 0 & 30 & - & - \end{bmatrix} \text{ where } \left[k_i\right] = \begin{bmatrix} 2 \\ 3 \\ 1 \end{bmatrix}.$$

To elaborate, at the first load level 7 specimens have exact failure times, 15 specimens lie in one censoring interval and 2 specimens lie in a second. At the second load level 2 specimens have exact failure times and there are three different censoring intervals with 28 specimens in one interval, and 1 specimen in each of the other two. At the third load level there are 0 exact failure times (no specimens failed during the test) and all 30 specimens lay in a single censoring interval.

The known failure times for the uncensored specimens (those indexed by $j = 0$), are presented as a 'matrix' with entries $t_{ir}, i = 1,\cdots,m;\ r = 1,\cdots,n_{i0}$. For the T1000 COPV dataset the

known failure times are:

$$\left[t_{ir}\right]=\begin{bmatrix} \frac{1}{30} & 12.1 & 19 & 192 & 730 & 1830 & 8770 \\ 730 & 1830 & - & - & - & - & - \\ - & - & - & - & - & - & - \end{bmatrix} \text{ hrs}.$$

For the censored specimens, indexed by $j>0$, there are n_{ij} specimens in censoring interval $\left[t_{ij}^{\ell},t_{ij}^{\mathrm{u}}\right)$, where t_{ij}^{ℓ} and t_{ij}^{u} correspond to the lower and upper censor bound respectively, and where $i=1,\cdots,m;\ j=1,\cdots,k_i$. These bounds t_{ij}^{ℓ} and t_{ij}^{u} can also be presented as 'matrices', again with the understanding that there may be empty entries, as in the case of n_{ij} above. In the case of the T1000 COPV dataset the bounds are given by

$$\left[t_{ij}^{\ell}\right]=\begin{bmatrix} 20400 & 16800 & - \\ 18300 & 16800 & 16100 \\ 18300 & - & - \end{bmatrix} \text{ hrs} \quad \text{and} \quad \left[t_{ij}^{\mathrm{u}}\right]=\begin{bmatrix} \infty & \infty & - \\ \infty & \infty & \infty \\ \infty & - & - \end{bmatrix} \text{ hrs}.$$

A subtle aspect of the censor intervals is that at given stress level, $\bar{\sigma}_i$, these intervals can overlap. This often occurs since there are a limited number of sample test stations, and testing is often performed on the higher pressure levels first. When such a specimen fails, the test station is reloaded with a specimen at a lower test pressure. This results in differing elapsed times on specimens.

3.3.3 Likelihood equation

We can now write a likelihood equation for the strength and lifetime data. The likelihood will be given as the product of the probability of each specimen failing according to the its type of data:

$$L\left(\sigma_{\text{ref}},\alpha,\rho\right)=\left(\prod_{i=1}^{n_s} f_s\left(\sigma_i\middle|\underline{\theta}\right)\right)\left(\prod_{i=1}^{m}\left\{\left[\prod_{r=1}^{n_{i0}} f_{\bar{\sigma}_i}\left(t_{ir}\middle|\underline{\theta}\right)\right]\left[\prod_{j=1}^{k_i}\left\{F_{\bar{\sigma}_i}\left(t_{ij}^{u}\middle|\underline{\theta}\right)-F_{\bar{\sigma}_i}\left(t_{ij}^{\ell}\middle|\underline{\theta}\right)\right\}^{n_{ij}}\right]\right\}\right). \tag{3.17}$$

Substituting (13), (14) and (3.15) into (17) gives:

$$\begin{aligned}L\left(\sigma_{\text{ref}},\alpha,\rho\right)=&\left(\prod_{i=1}^{n_s}\frac{\alpha}{\sigma_{\text{ref}}}\left(\frac{\sigma_i}{\sigma_{\text{ref}}}\right)^{\alpha-1}\exp\left\{-\left(\frac{\sigma_i}{\sigma_{\text{ref}}}\right)^{\alpha}\right\}\right)\\&\times\left(\prod_{i=1}^{m}\left\{\left[\prod_{r=1}^{n_{i0}}\frac{\alpha}{\left(\rho+1\right)t_{ir}}\left[\left(\frac{\bar{\sigma}_i}{\sigma_{\text{ref}}}\right)^{\rho}\frac{R\left(\rho+1\right)t_{ir}}{\sigma_{\text{ref}}}\right]^{\frac{\alpha}{\rho+1}}\exp\left\{-\left[\left(\frac{\bar{\sigma}_i}{\sigma_{\text{ref}}}\right)^{\rho}\frac{R\left(\rho+1\right)t_{ir}}{\sigma_{\text{ref}}}\right]^{\frac{\alpha}{\rho+1}}\right\}\right]\right.\right.\\&\left.\left.\times\left[\prod_{j=1}^{k_i}\left\{\exp\left\{-\left[\left(\frac{\bar{\sigma}_i}{\sigma_{\text{ref}}}\right)^{\rho}\frac{R\left(\rho+1\right)t_{ij}^{\ell}}{\sigma_{\text{ref}}}\right]^{\alpha/\rho+1}\right\}-\exp\left\{-\left[\left(\frac{\bar{\sigma}_i}{\sigma_{\text{ref}}}\right)^{\rho}\frac{R\left(\rho+1\right)t_{ij}^{u}}{\sigma_{\text{ref}}}\right]^{\alpha/\rho+1}\right\}\right\}^{n_{ij}}\right]\right)\right\}\end{aligned} \tag{3.18}$$

The log-likelihood equation is the natural logarithm of (3.18):

$$\begin{aligned}\ln L\left(\sigma_{\text{ref}},\alpha,\rho\right)=&\left(n_s\ln\left\{\frac{\alpha}{\sigma_{\text{ref}}}\right\}+\left(\alpha-1\right)\sum_{i=1}^{n_s}\ln\left\{\frac{\sigma_i}{\sigma_{\text{ref}}}\right\}-\sum_{i=1}^{n_s}\left(\frac{\sigma_i}{\sigma_{\text{ref}}}\right)^{\alpha}\right)\\&+\sum_{i=1}^{m}\left[\sum_{r=1}^{n_{i0}}\ln\left(\frac{\alpha}{\left(\rho+1\right)t_{ir}}\left[\left(\frac{\bar{\sigma}_i}{\sigma_{\text{ref}}}\right)^{\rho}\frac{R\left(\rho+1\right)t_{ir}}{\sigma_{\text{ref}}}\right]^{\frac{\alpha}{\rho+1}}\right)-\sum_{r=1}^{n_{i0}}\left[\left(\frac{\bar{\sigma}_i}{\sigma_{\text{ref}}}\right)^{\rho}\frac{R\left(\rho+1\right)t_{ir}}{\sigma_{\text{ref}}}\right]^{\frac{\alpha}{\rho+1}}\right.\\&\left.+\sum_{j=1}^{k_i}n_{ij}\ln\left\{\exp\left\{-\left[\left(\frac{\bar{\sigma}_i}{\sigma_{\text{ref}}}\right)^{\rho}\frac{R\left(\rho+1\right)t_{ij}^{\ell}}{\sigma_{\text{ref}}}\right]^{\alpha/\rho+1}\right\}-\exp\left\{-\left[\left(\frac{\bar{\sigma}_i}{\sigma_{\text{ref}}}\right)^{\rho}\frac{R\left(\rho+1\right)t_{ij}^{u}}{\sigma_{\text{ref}}}\right]^{\alpha/\rho+1}\right\}\right\}\right]\end{aligned} \tag{3.19}$$

Maximizing either (3.18) or (3.19) across $\underline{\theta}=\left\{\sigma_{\text{ref}},\alpha,\rho\right\}$ thus gives the 'most likely' estimate for the CPL-W model parameters for the given dataset.

3.3.3.1 Example dataset: T1000 carbon fiber/epoxy COPVs

For the example of the T1000 vessel data as given above, we can think of the log-likelihood equation in terms of three parts, represented by the three different summations in equation (3.20):

$$\begin{aligned}\ln L\left(\sigma_{\text{ref}},\alpha,\rho\right)=&\sum_{i=1}^{n_s}\ln\left\{f_s\left(\sigma_i\middle|\underline{\theta}\right)\right\}+\sum_{i=1}^{m}\ln\left\{\prod_{r=1}^{n_{i0}}f_{\bar{\sigma}_i}\left(t_{ir}\middle|\underline{\theta}\right)\right\}\\&+\sum_{i=1}^{m}\ln\left\{\prod_{j=1}^{k_i}\left\{F_{\bar{\sigma}_i}\left(t_{ij}^{u}\middle|\underline{\theta}\right)-F_{\bar{\sigma}_i}\left(t_{ij}^{\ell}\middle|\underline{\theta}\right)\right\}^{n_{ij}}\right\}\end{aligned}\tag{3.20}$$

The first part is the contribution from the strength testing. For the T1000 vessel data this portion of the log-likelihood equation is:

$$
\begin{aligned}
\ln\left(\prod_{i=1}^{n_s} f_s\left(\sigma_i\middle|\underline{\theta}\right)\right) = 30\ln\left\{\frac{\alpha}{\sigma_{\text{ref}}}\right\} + (\alpha-1)\Bigg[& \ln\left\{\frac{6191}{\sigma_{\text{ref}}}\right\} + \ln\left\{\frac{6317}{\sigma_{\text{ref}}}\right\} + \ln\left\{\frac{6403}{\sigma_{\text{ref}}}\right\} \\
& + \ln\left\{\frac{5611}{\sigma_{\text{ref}}}\right\} + \ln\left\{\frac{5952}{\sigma_{\text{ref}}}\right\} + \ln\left\{\frac{5284}{\sigma_{\text{ref}}}\right\} + \ln\left\{\frac{6288}{\sigma_{\text{ref}}}\right\} \\
& + \ln\left\{\frac{5994}{\sigma_{\text{ref}}}\right\} + \ln\left\{\frac{6258}{\sigma_{\text{ref}}}\right\} + \ln\left\{\frac{6385}{\sigma_{\text{ref}}}\right\} + \ln\left\{\frac{5449}{\sigma_{\text{ref}}}\right\} \\
& + \ln\left\{\frac{5607}{\sigma_{\text{ref}}}\right\} + \ln\left\{\frac{6307}{\sigma_{\text{ref}}}\right\} + \ln\left\{\frac{5873}{\sigma_{\text{ref}}}\right\} + \ln\left\{\frac{6010}{\sigma_{\text{ref}}}\right\} \\
& + \ln\left\{\frac{6054}{\sigma_{\text{ref}}}\right\} + \ln\left\{\frac{5782}{\sigma_{\text{ref}}}\right\} + \ln\left\{\frac{5843}{\sigma_{\text{ref}}}\right\} + \ln\left\{\frac{6058}{\sigma_{\text{ref}}}\right\} \\
& + \ln\left\{\frac{5878}{\sigma_{\text{ref}}}\right\} + \ln\left\{\frac{5536}{\sigma_{\text{ref}}}\right\} + \ln\left\{\frac{5413}{\sigma_{\text{ref}}}\right\} + \ln\left\{\frac{5843}{\sigma_{\text{ref}}}\right\} \\
& + \ln\left\{\frac{5704}{\sigma_{\text{ref}}}\right\} + \ln\left\{\frac{5597}{\sigma_{\text{ref}}}\right\} + \ln\left\{\frac{5612}{\sigma_{\text{ref}}}\right\} + \ln\left\{\frac{6119}{\sigma_{\text{ref}}}\right\} \\
& + \ln\left\{\frac{6081}{\sigma_{\text{ref}}}\right\} + \ln\left\{\frac{6115}{\sigma_{\text{ref}}}\right\} + \ln\left\{\frac{5872}{\sigma_{\text{ref}}}\right\}\Bigg] - \left(\frac{6191}{\sigma_{\text{ref}}}\right)^{\alpha} \\
& - \left(\frac{6317}{\sigma_{\text{ref}}}\right)^{\alpha} - \left(\frac{6403}{\sigma_{\text{ref}}}\right)^{\alpha} - \left(\frac{5611}{\sigma_{\text{ref}}}\right)^{\alpha} - \left(\frac{5952}{\sigma_{\text{ref}}}\right)^{\alpha} - \left(\frac{5284}{\sigma_{\text{ref}}}\right)^{\alpha} \\
& - \left(\frac{6288}{\sigma_{\text{ref}}}\right)^{\alpha} - \left(\frac{5994}{\sigma_{\text{ref}}}\right)^{\alpha} - \left(\frac{6258}{\sigma_{\text{ref}}}\right)^{\alpha} - \left(\frac{6385}{\sigma_{\text{ref}}}\right)^{\alpha} \\
& - \left(\frac{5449}{\sigma_{\text{ref}}}\right)^{\alpha} - \left(\frac{5607}{\sigma_{\text{ref}}}\right)^{\alpha} - \left(\frac{6307}{\sigma_{\text{ref}}}\right)^{\alpha} - \left(\frac{5873}{\sigma_{\text{ref}}}\right)^{\alpha} - \left(\frac{6010}{\sigma_{\text{ref}}}\right)^{\alpha} \\
& - \left(\frac{6054}{\sigma_{\text{ref}}}\right)^{\alpha} - \left(\frac{5782}{\sigma_{\text{ref}}}\right)^{\alpha} - \left(\frac{5843}{\sigma_{\text{ref}}}\right)^{\alpha} - \left(\frac{6058}{\sigma_{\text{ref}}}\right)^{\alpha} - \left(\frac{5878}{\sigma_{\text{ref}}}\right)^{\alpha} \\
& - \left(\frac{5536}{\sigma_{\text{ref}}}\right)^{\alpha} - \left(\frac{5413}{\sigma_{\text{ref}}}\right)^{\alpha} - \left(\frac{5843}{\sigma_{\text{ref}}}\right)^{\alpha} - \left(\frac{5704}{\sigma_{\text{ref}}}\right)^{\alpha} \\
& - \left(\frac{5597}{\sigma_{\text{ref}}}\right)^{\alpha} - \left(\frac{5612}{\sigma_{\text{ref}}}\right)^{\alpha} - \left(\frac{6119}{\sigma_{\text{ref}}}\right)^{\alpha} - \left(\frac{6081}{\sigma_{\text{ref}}}\right)^{\alpha} - \left(\frac{6115}{\sigma_{\text{ref}}}\right)^{\alpha} - \left(\frac{5872}{\sigma_{\text{ref}}}\right)^{\alpha}
\end{aligned}
\tag{3.21}
$$

The second part of (3.20) comes from the exact failure times. For the T1000 vessel data this is:

$$\sum_{i=1}^{m}\ln\left\{\prod_{r=1}^{n_{i0}} f_{\bar{\sigma}_i}\left(t_{ir}\middle|\underline{\theta}\right)\right\} = 9\ln\left\{\frac{\alpha}{(\rho+1)}\left[\frac{R(\rho+1)}{\sigma_{\text{ref}}}\right]^{\frac{\alpha}{\rho+1}}\right\} + \ln\left(30\left[\left(\frac{5205}{\sigma_{\text{ref}}}\right)^{\rho}\frac{1}{30}\right]^{\frac{\alpha}{\rho+1}}\right)$$
$$+\ln\left(\frac{1}{12.1}\left[\left(\frac{5205}{\sigma_{\text{ref}}}\right)^{\rho}12.1\right]^{\frac{\alpha}{\rho+1}}\right)+\ln\left(\frac{1}{19}\left[\left(\frac{5205}{\sigma_{\text{ref}}}\right)^{\rho}19\right]^{\frac{\alpha}{\rho+1}}\right)$$
$$+\ln\left(\frac{1}{192}\left[\left(\frac{5205}{\sigma_{\text{ref}}}\right)^{\rho}192\right]^{\frac{\alpha}{\rho+1}}\right)+\ln\left(\frac{1}{730}\left[\left(\frac{5205}{\sigma_{\text{ref}}}\right)^{\rho}730\right]^{\frac{\alpha}{\rho+1}}\right)$$
$$+\ln\left(\frac{1}{1830}\left[\left(\frac{5205}{\sigma_{\text{ref}}}\right)^{\rho}1830\right]^{\frac{\alpha}{\rho+1}}\right)+\ln\left(\frac{1}{8770}\left[\left(\frac{5205}{\sigma_{\text{ref}}}\right)^{\rho}8770\right]^{\frac{\alpha}{\rho+1}}\right)$$
$$+\ln\left(\frac{1}{730}\left[\left(\frac{4845}{\sigma_{\text{ref}}}\right)^{\rho}730\right]^{\frac{\alpha}{\rho+1}}\right)+\ln\left(\frac{1}{1830}\left[\left(\frac{4845}{\sigma_{\text{ref}}}\right)^{\rho}1830\right]^{\frac{\alpha}{\rho+1}}\right)$$
$$+\left[\left(\frac{5205}{\sigma_{\text{ref}}}\right)^{\rho}\frac{R(\rho+1)}{30\sigma_{\text{ref}}}\right]^{\frac{\alpha}{\rho+1}}+\left[\left(\frac{5205}{\sigma_{\text{ref}}}\right)^{\rho}\frac{R(\rho+1)12.1}{\sigma_{\text{ref}}}\right]^{\frac{\alpha}{\rho+1}}$$
$$+\left[\left(\frac{5205}{\sigma_{\text{ref}}}\right)^{\rho}\frac{R(\rho+1)19}{\sigma_{\text{ref}}}\right]^{\frac{\alpha}{\rho+1}}+\left[\left(\frac{5205}{\sigma_{\text{ref}}}\right)^{\rho}\frac{R(\rho+1)192}{\sigma_{\text{ref}}}\right]^{\frac{\alpha}{\rho+1}}$$
$$+\left[\left(\frac{5205}{\sigma_{\text{ref}}}\right)^{\rho}\frac{R(\rho+1)730}{\sigma_{\text{ref}}}\right]^{\frac{\alpha}{\rho+1}}+\left[\left(\frac{5205}{\sigma_{\text{ref}}}\right)^{\rho}\frac{R(\rho+1)1830}{\sigma_{\text{ref}}}\right]^{\frac{\alpha}{\rho+1}}$$
$$+\left[\left(\frac{5205}{\sigma_{\text{ref}}}\right)^{\rho}\frac{R(\rho+1)8770}{\sigma_{\text{ref}}}\right]^{\frac{\alpha}{\rho+1}}+\left[\left(\frac{4845}{\sigma_{\text{ref}}}\right)^{\rho}\frac{R(\rho+1)730}{\sigma_{\text{ref}}}\right]^{\frac{\alpha}{\rho+1}}$$
$$+\left[\left(\frac{4845}{\sigma_{\text{ref}}}\right)^{\rho}\frac{R(\rho+1)1830}{\sigma_{\text{ref}}}\right]^{\frac{\alpha}{\rho+1}} \tag{3.22}$$

The third part is the contribution from the failure intervals. For the T1000 vessel data this is:

$$\sum_{i=1}^{m} \ln\left\{ \prod_{j=1}^{k_i} \left\{ F_{\bar{\sigma}_i}\left(t_{ij}^{u} \middle| \underline{\theta}\right) - F_{\bar{\sigma}_i}\left(t_{ij}^{\ell} \middle| \underline{\theta}\right) \right\}^{n_{ij}} \right\} =$$

$$15 \ln\left\{ \exp\left\{ -\left[\left(\frac{5205}{\sigma_{\text{ref}}} \right)^{\rho} \frac{R(\rho+1)20400}{\sigma_{\text{ref}}} \right]^{\frac{\alpha}{\rho+1}} \right\} \right\}$$

$$+ 2 \ln\left\{ \exp\left\{ -\left[\left(\frac{5205}{\sigma_{\text{ref}}} \right)^{\rho} \frac{R(\rho+1)16800}{\sigma_{\text{ref}}} \right]^{\frac{\alpha}{\rho+1}} \right\} \right\}$$

$$+ 28 \ln\left\{ \exp\left\{ -\left[\left(\frac{4845}{\sigma_{\text{ref}}} \right)^{\rho} \frac{R(\rho+1)18300}{\sigma_{\text{ref}}} \right]^{\frac{\alpha}{\rho+1}} \right\} \right\} \qquad (3.23)$$

$$+ \ln\left\{ \exp\left\{ -\left[\left(\frac{4845}{\sigma_{\text{ref}}} \right)^{\rho} \frac{R(\rho+1)16800}{\sigma_{\text{ref}}} \right]^{\frac{\alpha}{\rho+1}} \right\} \right\}$$

$$+ \ln\left\{ \exp\left\{ -\left[\left(\frac{4845}{\sigma_{\text{ref}}} \right)^{\rho} \frac{R(\rho+1)16100}{\sigma_{\text{ref}}} \right]^{\frac{\alpha}{\rho+1}} \right\} \right\}$$

$$+ 30 \ln\left\{ \exp\left\{ -\left[\left(\frac{4505}{\sigma_{\text{ref}}} \right)^{\rho} \frac{R(\rho+1)18300}{\sigma_{\text{ref}}} \right]^{\frac{\alpha}{\rho+1}} \right\} \right\}$$

By summing (3.21), (3.22) and (3.23) we get (3.20), which is equivalent to (3.19). This is the log-likelihood expression for this particular T1000 data set. The parameter estimate is obtained by maximizing this log-likelihood function for the three parameters $\underline{\theta} = \{\sigma_{\text{ref}}, \alpha, \rho\}$.

For this data set the maximum value of the log-likelihood equation is -305 and occurs at $\hat{\theta} = \{6076 \text{ psi}, 25, 157\}$. The value of the log-likelihood equation at this point is not meaningful

in itself, but any other set of parameter values, $\tilde{\theta}$, will give a smaller value (in this case more negative) for the log-likelihood equation. The point that the equation is maximized at, namely $\hat{\theta} = \{6076 \text{ psi}, 25, 157\}$, is our estimated values for the three parameters.

3.4 Discussion

This paper presents a maximum likelihood method for analyzing a stress-rupture data set using the CPL-W model. In other words, given a data set for stress rupture failure consisting of both strength and lifetime tests, this paper presents a method for analyzing that data assuming the classic power law model in a Weibull framework (CPL-W model). This analysis method has been shown to be better than currently used methods in terms of amounts of bias, variance and mean squared error as shown in [27].

This paper demonstrates the proposed method using an example data set of T1000 carbon fiber/epoxy COPVs tested by NASA. The method consists of maximizing the maximum likelihood equation (3.18) or its log (3.19), which must be done numerically as there is no closed form solution for finding the maximum. The numerical maximization is fast and accurate however, so this is not a limitation in practice. A code for performing this unified MLE analysis is provided in the Appendix.

It is worth remembering that the net result of this method is an estimate of the parameter values, with no error bounds. There is also some bias in this estimate. The error bounds may be obtained in various ways. A brief sketch of two methods to determine error bounds follows, along with one method of quantifying the bias.

First, asymptotic error bounds may be obtained from the Fisher information matrix. This $\tilde{\alpha}$ is a matrix of second partial derivatives of the negative of the log-likelihood function, with respect to the parameters, σ_{ref}, α and ρ. An approximate asymptotic confidence interval can

be constructed for any function, $h(\theta)$, of the parameters $\underline{\theta} = \{\sigma_{\text{ref}}, \alpha, \rho\}$. In particular $h(\theta)$ can be the failure probability from the cumulative distribution function, (3.1), for the desired time and loading profile. Then the asymptotic confidence interval, assuming asymptotic normality of the estimator, is thus given by:

$$h(\hat{\theta}) - z_{\tilde{\alpha}/2}\sqrt{\hat{\mathrm{V}}\left(h(\hat{\theta})\middle|\underline{\theta}\right)} \le h(\underline{\theta}) \le h(\hat{\theta}) + z_{\tilde{\alpha}/2}\sqrt{\hat{\mathrm{V}}\left(h(\hat{\theta})\middle|\underline{\theta}\right)} \tag{3.24}$$

where

$$\hat{\mathrm{V}}\left(h(\hat{\theta})\middle|\underline{\theta}\right) \approx H\left(\underline{\theta}\middle|\mathbf{x}\right)\left[h'(\underline{\theta})\right]^2\Big|_{\underline{\theta}=\hat{\theta}} \tag{3.25}$$

and $H\left(\underline{\theta}\middle|\mathbf{x}\right)$ is the Hessian matrix evaluated at the point $\underline{\theta} = \hat{\theta}$:

$$H\left(\underline{\theta}\middle|\mathbf{x}\right) = -\left[\frac{\partial^2}{\partial\theta^2}\ln L\left(\underline{\theta}\middle|\mathbf{x}\right)\Big|_{\underline{\theta}=\hat{\theta}}\right]^{-1} \tag{3.26}$$

and $\hat{\theta}$ is the maximum likelihood estimate of the parameters, $\ln L\left(\underline{\theta}\middle|\mathbf{x}\right)$ is equation (3.19), is the 'level of significance', and $z_{\tilde{\alpha}/2}$ is 1.96 for a 95% confidence interval as determined from the normal distribution. While this gives a workable formula for calculating a confidence interval, the accuracy of the resulting interval is dependent on how close to normal the distribution of the estimator actually is.

Second, Monte-Carlo simulation can also be used to obtain error bounds through analysis of simulated data sets. In this case one simulates N data sets using parameter values $\hat{\theta}$, and closely mimicking the test conditions used for the original data (number of specimens, load levels, loading rates, censor times, etc.). The N simulated data sets are then analyzed using the unified MLE approach, as before, yielding N parameter estimates: $\hat{\theta}_1, \hat{\theta}_2, \hat{\theta}_3, \ldots, \hat{\theta}_N$. By

repeating the process N times we obtain a distribution of the parameter estimates, from which we can obtain confidence intervals at a level of significance α. Simulation has the advantage that not only will it give a confidence interval, but it also gives a measure of how much bias there is in the estimation method by comparing the average from the simulated data sets with the original estimate $\hat{\theta}$. Simulation also gives the overall shape of the distribution of estimates and provides an indication on whether the estimates are asymptotically normally distributed, though many runs are needed to get the behavior in the tails of the distribution. For further details on this approach see [27].

3.5 Conclusion

This paper presents a method for analyzing strength and lifetime datasets in the context of stress-rupture in general and the CPL-W model in particular. The method presented is a maximum likelihood based estimation procedure and can be summarized as finding the parameters that maximize equation (3.18) or (3.19). This method has been shown to outperform many other methods, including some currently used in industry. It reliably gives better estimates of both the parameters for the CPL-W model, as well as the final probability of failure as given by the CPL-W model, than other methods tested.

REFERENCES

[26] Tobolsky A and Eyring H (1943) Mechanical Properties of Polymeric Materials. J Chem Phys 11:125-134.

[27] Engelbrecht-Wiggans A, Phoenix SL (2016) Comparison of maximum likelihood approaches for analysis of composite stress rupture data, J Mater Sci DOI 10.1007/s10853-016-9950-3

[28] NASA Stress Rupture Liner and COPV Burst Test Report: Revision A. September 16, 2010, Report No. TR-0242-001

[29] Composite Overwrapped Pressure Vessel (COPV) Stress Rupture Mitigation Strategies. NASA FOIA request REF: 15-JSC-F-00616, May 12, 2015

CHAPTER 4

ANALYSIS OF STRESS RUPTURE DATA ON FIBER COMPOSITES: PART 2- DETERMINING UNCERTAINTY AND REMOVING BIAS IN ESTIMATES

The following chapter is published in the Journal of Space Safety Engineering and reprinted here with permission. The reference to the published work is:

Engelbrecht-Wiggans, A., Phoenix, S.L. Analysis of stress rupture data on fiber composites: Part 2- Determining uncertainty and removing bias in estimates, The Journal of Space Safety Engineering (2017), http://dx.doi.org/10.1016/j.jsse.2017.06.003

4.1. Introduction

Stress rupture is a catastrophic failure mode in continuous unidirectional fiber composites, particularly in composite overwrapped pressure vessels (COPVs), flywheels and tension members in civil engineering subjected to a constant load over long time periods. It can occur at normal operating stresses and temperatures, at sustained stress levels well below the ultimate strength for an extended time. Stress rupture is explosive and occurs with little or no advance warning. Its occurrence is also highly variable, with two otherwise identical specimens under identical loading and environmental conditions failing at widely differing times (sometimes by several orders of magnitude). Stress rupture is of increasing concern, particularly in COPVs, as the impetus to increase service loads and lifetimes has increased, thus increasing the risk of stress rupture failure.

Prediction of a composite's stress rupture behavior is based heavily on extensive testing at loads considerably higher than the actual design load. These tests fall into two categories: strength testing and lifetime testing. Test data is then analyzed to extrapolate from test conditions

to calculate a predicted probability of failure corresponding to a desired service lifetime and load level. This analysis is done using a probabilistic stress rupture model, such as the classic power-law model in a Weibull framework (CPL-W).

An important aspect is that no amount of testing will make it possible to determine a precise failure time for future specimens, such as those to be placed in service. The times to failure are inherently random, such that, at best, we can obtain a highly accurate characterization of the distribution for the lifetime at a given load level, and specifically an estimate of the failure probability at a given load level and lifetime. One problematic aspect is that the failure probabilities of interest are in the deep lower tail of the distribution: so not 1 in 10, nor 1 in 100, but rather 1 in 1,000,000 or more. This creates a challenge in terms of estimation accuracy.

A key issue is that our estimation procedure may provide the gratifying, but potentially misleading, result that the probability of failure is 1 in 10,000,000, when in fact it is actually only 1 in 10,000. Such an error in our estimate of failure probability is the type that can result from testing far too few specimens, or, using a sub-optimal estimation procedure, or, using an incorrect model, or some combination thereof. The challenge is to determine how accurate our estimate of failure probability really is, i.e., to characterize the level of uncertainty.

Part 1 [30] of this paper discusses a unified maximum likelihood estimation (MLE) technique for analyzing stress rupture data using the CPL-W model. This MLE analysis results in estimates for the CPL-W model parameters and, in the process, an estimate of the failure probability at a specified load level and lifetime [27]. As mentioned, there is uncertainty in any estimates (the only way to virtually eliminate estimation uncertainty is to test an unfeasibly large number of specimens.). Quantifying the uncertainty becomes the main challenge addressed in this paper.

Another issue is that, as is the case with many estimation procedures, the MLE technique presented in Part 1 [30] may result in biased estimates, particularly when test sample sizes are small. Bias refers to the tendency of the estimation procedure to consistently over-estimate, or under-estimate, the true value of the parameter. More formally bias is defined as the difference between the expected value of an estimator and the true value of the parameter being estimated. This paper presents a method, using Monte-Carlo (MC) simulation, to quantify the uncertainty in both CPL-W model parameter estimates and failure probability estimates, as well as to quantify and eliminate bias. One useful aspect is to be able to generate confidence intervals on the various estimates. While we focus on analyzing an experimental dataset, this MC approach can also be used to evaluate how much uncertainty can be expected from a given test setup, i.e. a certain number of specimens tested at what load levels.

To illustrate the details of this approach we use an existing stress-rupture data set on laboratory scale cylindrical COPVS, generated by NASA at their White Sands Testing Facility [28, 29]. These vessels consisted of an aluminum liner overwrapped with Toray T1000 carbon fiber in an epoxy matrix. More details on these vessels can be found in Part 1 [30].

4.2. CPL-W model

We begin with a brief summary of the CPL-W model and relevant equations [11, 12, 27, 30]. The CPL-W model describes the lifetime of a composite structure as having a cumulative distribution function of the form:

$$F\left(t\middle|\sigma\left(t\right)\right)=1-\exp\left\{-\left[\int_0^t\left(\frac{\sigma\left(\tau\right)}{\sigma_{\text{ref}}}\right)^{\rho}\frac{d\tau}{t_{\text{ref}}}\right]^{\beta}\right\} \tag{4.1}$$

where $\sigma\left(t\right)$ denotes an applied stress (or load) profile over time, and where σ_{ref} is the Weibull

scale parameter for strength, t_{ref} is the Weibull scale parameter for lifetime (corresponding to stress level σ_{ref}), ρ is the power-law exponent relating behavior at different stress levels, and β is the Weibull shape parameter.

In the case of strength testing the stress is assumed to be linearly increasing:

$$\sigma(t) = Rt, \quad t \geq 0 \tag{4.2}$$

where the constant $R > 0$ is the loading or stress rate. Using the relationships

$$\alpha = \beta(\rho + 1) \quad \text{and} \quad t_{\text{ref}} = \frac{\sigma_{\text{ref}}}{R(\rho + 1)} \tag{4.3}$$

we get the cumulative distribution function for failure stress in a strength test:

$$\bar{F}_s(s) = 1 - \exp\left\{-\left(\frac{s}{\sigma_{\text{ref}}}\right)^{\alpha}\right\}, \quad s \geq 0\,. \tag{4.4}$$

where α and σ_{ref} are, respectively, the Weibull shape and scale parameter for strength, and $s = Rt$ is the stress level at failure.

In the case of stress rupture lifetime testing the load is held constant:

$$\sigma(t) = \bar{\sigma}, \quad t > 0\,. \tag{4.5}$$

Using (4.3), the cumulative distribution function for time to failure simplifies from (3.1) to:

$$F_{\bar{\sigma}}(t) = 1 - \exp\left\{-\left[\left(\frac{\bar{\sigma}}{\sigma_{\text{ref}}}\right)^{\rho} \frac{R(\rho + 1)t}{\sigma_{\text{ref}}}\right]^{\frac{\alpha}{\rho+1}}\right\}. \tag{4.6}$$

Thus for both strength and lifetime, and indeed in general, the CPL-W model can be written in terms of the three parameters $\theta = \{\sigma_{\text{ref}}, \alpha, \rho\}$.

4.3 Experimental data collection

The first step in using the CPL-W model to predict failure probability for a loaded structure is to experimentally generate strength and lifetime data. This data is then analyzed using the MLE method in Part 1 [30] to obtain parameter and failure probability estimates. Then to go further and quantify the uncertainty and bias in these estimates, one powerful approach is to use a Monte-Carlo simulation. This requires simulation of multiple datasets (such as 10,000) mimicking the type of experimental dataset that was originally collected.

The original experimental dataset is generated and analyzed as follows. Strength testing is necessarily the first task, as it is required to determine the various load levels that will be applied in lifetime testing. Such testing is done at a specified loading rate R on some number, n_s, of specimens, which are assumed to follow the Weibull distribution given in (3.3). From this testing the most important result is an estimate for the Weibull scale parameter for strength, as obtained using the standard Weibull MLE procedure. This initial estimate of σ_{ref}, called $\hat{\sigma}_{\text{ref}}$, is used primarily to establish the load levels to be used in lifetime testing. (A more refined estimate of σ_{ref} will be generated later.)

The second task is lifetime testing, which is generally done at various load levels that are chosen as certain percentages of $\hat{\sigma}_{\text{ref}}$ and that vary depending on the material. For each of the m load levels, $\bar{\sigma}_j$, $j = 1,\cdots,m$, there are n_j, $j = 1,\cdots,m$ specimens. Lifetime testing generally starts with loading the specimens at the highest load level first, so that as they fail the loading frames can be re-loaded with the lower load level specimens which will take longer to break. If a test ends before a given specimen has failed (or if interim analysis and results are desired, for instance for a progress report), the elapsed time after loading is its 'censor time'. Thus we know

that the specimen survived at least to its censor time, but have no knowledge of what its true failure time would be. Furthermore, since lifetime testing is almost always ended before all the specimens have failed, this loading procedure generally results in a mix of censor times instead of just one.

This data should then be used to calculate estimates as per Part 1 [30]. For example, the T1000 carbon fiber/epoxy COPVs dataset yields the parameter estimate $\hat{\theta} = \{6076 \text{ psi}, 25, 157\}$. (In this application, 6076 psi refers to the burst strength of the composite overwrap portion of the COPV.) Note that the hat on the theta demarcates this as an estimate of the true parameters $\underline{\theta} = \{\sigma_{\text{ref}}, \alpha, \rho\}$. Furthermore $\hat{\sigma}_{\text{ref}} \neq \hat{\sigma}_{\text{ref}}$, as they are estimates based on different amounts of data. The question remaining is how accurate the $\hat{\theta}$ estimates actually are. This is what we address in the following sections.

4.4 Monte-Carlo (MC) simulation procedure

The MC method for quantifying uncertainty and removing bias from our stress rupture estimates involves simulating many 'typical' data sets, analyzing them, and then interpreting the results. We will use the T1000 carbon fiber/epoxy COPVs dataset to illustrate this procedure. In Part 1 [30] we described how to analyze this particular data set to get the parameter estimate $\hat{\theta} = \{6076 \text{ psi}, 25, 157\}$, which we will use here.

4.4.1 Simulating 'typical' data sets

A 'typical' data set is one that mimics, as much as is possible, the process used in collecting an actual real-world data set. Simulation is done using the 'inverse CDF method' as explained below.

First we simulate, strength data, corresponding to n_s specimens, as follows. Let $U_i, i = 1,\ldots,n_s$ be independently sampled, uniform random numbers on [0,1]. Then simulated strength values, σ_i, $i = 1,\cdots,n_s$, are determined according to the distribution for strength, (3.3), using

$$\overline{F}_s(\sigma_i) = U_i = 1 - \exp\left\{-\left(\frac{\sigma_i}{\hat{\sigma}_{\text{ref}}}\right)^{\hat{\alpha}}\right\}, \tag{4.7}$$

which gives

$$\sigma_i = \left[-\ln(1-U_i)\right]^{\frac{1}{\hat{\alpha}}}\hat{\sigma}_{\text{ref}}. \tag{4.8}$$

Here is an illustration, based on the T1000 data set. This data set had $n_s = 30$ specimens, but to simplify the discussion we will use $n_s = 6$ to illustrate the method. (For the actual MC method, one should mimic the experimental dataset, and thus use $n_s = 30$.) Having sampled from the uniform distribution the six values

$$U_i = \left[0.6557 \quad 0.0357 \quad 0.8491 \quad 0.9340 \quad 0.6787 \quad 0.7577\right],$$

the corresponding simulated strength data is calculated, using (4.8), to be:

$$\sigma_i = \left[6092 \quad 5322 \quad 6233 \quad 6324 \quad 6107 \quad 6161\right] \text{ psi.}$$

This data is now analyzed using the standard Weibull MLE to obtain $\hat{\theta} = \left(\hat{\sigma}_{\text{ref}}, \hat{\alpha}\right)$, and for this particular strength data the analysis gives $\hat{\theta} = (6168\,\text{psi}, 32)$. Note that these estimates of the scale and shape parameters differ from the values, (6076 psi, 25), that were used to simulate them, which is a reflection of the uncertainty and bias inherent in estimates based on such a small sample.

The next step is to use the estimate of $\hat{\sigma}_{\text{ref}}$ to establish the m load levels, $\bar{\sigma}_j$, $j = 1,\cdots,m$, to be used in the lifetime simulations. For the original T1000 data set $m = 3$ was chosen and the corresponding load levels chosen were 86%, 80% and 74% of the original scale parameter estimate $\hat{\sigma}_{\text{ref}}$. Thus in the current example, where $\hat{\sigma}_{\text{ref}} = 6168$ psi, we obtain the load levels $\bar{\sigma}_j = \begin{bmatrix} 5304 & 4934 & 4564 \end{bmatrix}$ psi.

The task now is to simulate lifetime data for each of the above load levels, where there will be n_j specimens at the j^{th} load level, where $j = 1,\cdots,m$, and in the example case $m = 3$. For each load level the lifetimes are simulated as follows. Let U_{rj}, $r = 1,\cdots,n_j$; $j = 1,\cdots,m$ be independently sampled uniform random numbers on [0,1]. Then the corresponding simulated lifetime values, $t_{rj}, r = 1,\cdots,n_j$; $j = 1,\cdots,m$, are calculated according to distribution for lifetime, (3.10), using

$$F_{\bar{\sigma}}\left(t_{rj}\right) = U_{rj} = 1 - \exp\left\{-\left[\left(\frac{\bar{\sigma}_j}{\hat{\sigma}_{\text{ref}}}\right)^{\hat{\rho}} \frac{R\left(\hat{\rho}+1\right)t_{rj}}{\hat{\sigma}_{\text{ref}}}\right]^{\frac{\hat{\alpha}}{\hat{\rho}+1}}\right\}, \tag{4.9}$$

which gives

$$t_{rj} = \left[-\ln\left(1-U_{rj}\right)\right]^{\frac{\hat{\rho}+1}{\hat{\alpha}}} \left(\frac{\hat{\sigma}_{\text{ref}}}{\bar{\sigma}_j}\right)^{\hat{\rho}} \frac{\hat{\sigma}_{\text{ref}}}{R\left(\hat{\rho}+1\right)}. \tag{4.10}$$

In the actual T1000 dataset $n_j = \begin{bmatrix} 26,32,30 \end{bmatrix}$, but again to simplify the discussion we will use a smaller dataset where $n_j = \begin{bmatrix} 6,6,6 \end{bmatrix}$ for the 86%, 80%, and 74% load levels respectively. (Of course, for the actual MC method, one should again mimic the actual experimental dataset, and thus use $n_j = \begin{bmatrix} 26,32,30 \end{bmatrix}$.) Having sampled from the uniform distribution the 18 values

$$U_{jr} = \begin{bmatrix} 0.2769 & 0.8235 & 0.9502 & 0.3816 & 0.1869 & 0.6463 \\ 0.0462 & 0.6948 & 0.0344 & 0.7655 & 0.4898 & 0.7094 \\ 0.0971 & 0.3171 & 0.4387 & 0.7952 & 0.4456 & 0.7547 \end{bmatrix},$$

the corresponded simulated lifetimes are calculated, using (4.10), to be

$$t_{jr} = \begin{bmatrix} \mathbf{395} & \mathit{1.58\times10^{7}} & \mathit{5.06\times10^{8}} & \mathbf{4750} & \mathbf{23.1} & \mathit{6.23\times10^{5}} \\ \mathbf{175} & \mathit{1.23\times10^{11}} & \mathbf{26.4} & \mathit{4.37\times10^{11}} & \mathit{3.40\times10^{9}} & \mathit{1.59\times10^{11}} \\ \mathit{4.73\times10^{9}} & \mathit{1.95\times10^{13}} & \mathit{2.68\times10^{14}} & \mathit{1.59\times10^{17}} & \mathit{3.06\times10^{14}} & \mathit{7.40\times10^{16}} \end{bmatrix} \text{ hours.}$$

Note that the numbers in italics will turn out to be censored specimens according to this example (details of which are described next) while the bold specimens will be ones with exact failure times. Once these specimens are censored the dataset is complete. This concludes the illustration of generating a dataset.

Returning to the general simulation procedure, once we have simulated lifetimes we must choose censoring times that mimic reasonably well those seen in the original dataset. By this we mean we must identify which specimens will be reported as having not failed by a certain elapsed time of termination, and these are termed censored specimens. A simple censoring that can occur is a common censor time for all specimens at a given load level. In practice this could occur either by having one station per specimen ($\sum_{j=1}^{m} n_j$ stations) all loaded and terminated at the same time, in which case the censor times are all the same, or terminating the specimens of any given load level at the same elapsed time, which could differ between load levels. Unfortunately this rarely occurs, yet as a practical approach we often simplify the censoring to a single censor time per load level.

In practice, lifetime data can have a variety of censor times even at each load level. For instance, in the original T1000 carbon/epoxy dataset, at the 86% load level there were 15 out of

26 specimens censored at 20400 hours and 2 out of the 26 specimens censored at 16800 hours. At the 80% load level there were three censor groups corresponding to 18240, 16800, and 16100 hours respectively, with 28 out of 32 specimens in the first and one each in the second and third. Lastly all 30 of the specimens loaded at 74% were censored at 18240 hours. As is common in practice, these censoring times were not predetermined but rather occurred as a result of testing decisions made as the data was collected (often over a period of several years). As mentioned in the experimental data collection section, replacing failed specimens with new specimens inevitably creates an even broader variety of censor times when an experiment is terminated. Thus the process of picking censor times for the MC simulation is complex, and impossible to mimic precisely without an exact knowledge of the testing protocol, hence the need for a practical approach such as one common censor time for all specimens at a given load level.

To investigate the sensitivity to censor times choices for the T1000 carbon/epoxy dataset, the MC method was run using $n_s = 30$ and $n_j = \left[26,32,30\right]$ specimens, and $N = 500{,}000$, where N is the number of simulated datasets. We examined three different choices of common load level censor times: {16000, 16000, 18240} hours as a low end bound, {20400, 18240, 18240} hours as closest to the actual censoring, and {21000, 21000, 18240} hours as a high end bound. A two sample Kolmogorov–Smirnov (K-S) test was used to compare the results (which are detailed in Tables 4.2-4.5, in the Appendix). Three comparisons were made at a significance level of 0.0001 (a highly selective test), and in all cases the result was to fail to reject the null hypothesis, which is that the distributions are the same. In particular, for comparisons of low versus mid, mid versus high, and low versus high, the K-S statistic was 0.000870, 0.000522, and 0.001021, respectively. In other words we effectively get the same results for each of the three choices of censor times.

The lack of sensitivity to these censor times can be understood upon noting that the difference between 16000 and 21000 hours is not particularly large when compared to the amount of time a specimen may take to fail. For example, at the highest load, 86%, where the specimens fail the soonest, the median lifetime is estimated to be 506,242 hours or approximately 57.8 years. In comparison to the median, the difference of 5,000 hours between the censor time options is slight.

To get detectable differences in the mean and standard deviation requires increasing the censor time by at least two orders of magnitude, which is rarely practical in actual experiments. This removes some of the burden to mimic censoring times precisely.

Having now described how to simulate a dataset with strength data and censored lifetime data, the next step is to analyze such a simulated dataset. This process is then repeated a large number of times as follows.

4.4.2 Analyzing simulated datasets

After simulating a dataset, this dataset is then analyzed for its parameter estimates, using the unified MLE method detailed in Part 1 [30]. These parameter estimates are then used to calculate a failure probability, for a particular lifetime and load level of interest. Calculating a failure probability for each simulated dataset is key in estimating uncertainty in this estimated failure probability.

The simulation and estimation is repeated N times, where N is typically on the order of 100,000 or more, resulting in N distinct parameter and failure probability estimates. The larger N is the more information we get regarding the uncertainty in our estimates, but the longer the simulations take to run. We have found that $N = 500{,}000$ is large enough to offer reasonable accuracy and takes 2-3 hours to run on a typical laptop.

4.4.3 Interpreting the simulated datasets

At this point we now have all the information to understand how much uncertainty there is in our failure probability estimate, as well as our parameter estimate $\hat{\theta} = \{\hat{\sigma}_{\text{ref}}, \hat{\alpha}, \hat{\rho}\} = \{6076 \text{ psi}, 25, 157\}$, as well as to remove any bias. Before we can do that though, we need to first understand the character of the distributions for the collection of N estimates. Then we can remove the bias from our parameter estimates and determine the final uncertainty.

4.4.3.1 The distribution of the estimates

Using the individual estimates from the N simulations, we can construct empirical distribution functions for the estimated values. This can be done for each of the parameters, as well as for the failure probability itself, as shown in Figures 4.1-4.4. These can be viewed as cumulative probability plots reflecting the uncertainty in the original estimates, $\hat{\theta}$, interpreted as follows. Note that Figures 4.1-4.4 were generated from five million simulations, such that the plots extend deep into the tails of the distributions.

Figures 4.1a and 4.1b show the cumulative probability plots for uncertainty in $\hat{\sigma}_{\text{ref}}$ on normal and lognormal coordinates, respectively. For the parameter σ_{ref} there is very little difference between the two coordinates. Both are nearly linear, showing that either distribution provides a good representation for the uncertainty in the estimate of σ_{ref}. The estimate $\hat{\sigma}_{\text{ref}}$ = 6076 psi, known as the point estimate, is close to the median, 6074 psi, as may be expected.

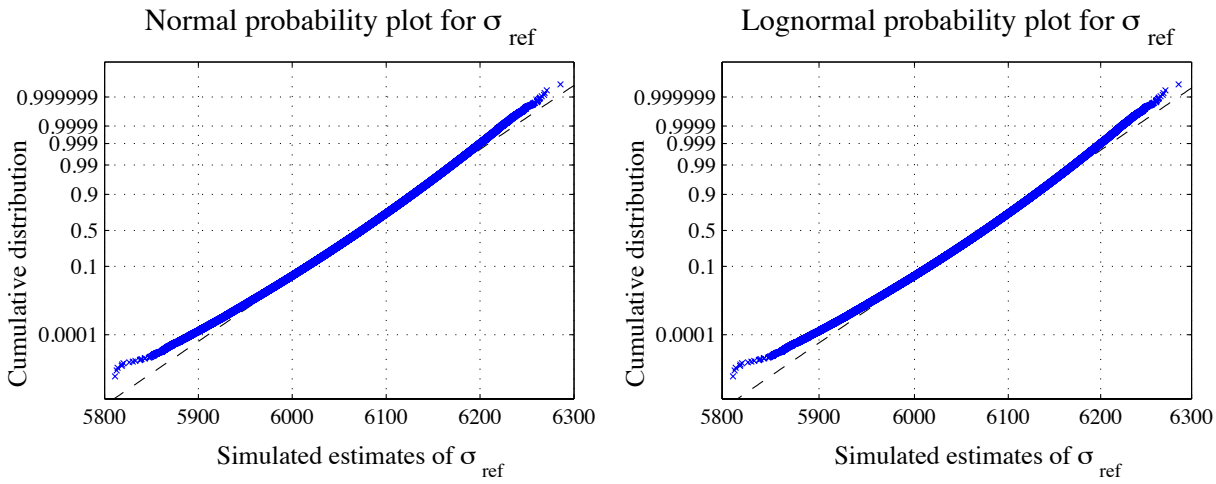

Figure 4.1 Uncertainty distributions for σ_{ref} plotted using normal (a), and lognormal (b) probability coordinates, where $N = 5{,}000{,}000$, using $n_s = 30$ and $n_j = \left[26,32,30\right]$

Repeating the process for α, Figures 4.2a and 4.2b show the cumulative probability plots for uncertainty in $\hat{\alpha}$ on normal and lognormal coordinates, respectively. Here however, the lognormal plot is more linear, showing that the uncertainty distribution for the estimate of α more closely follows a lognormal distribution.

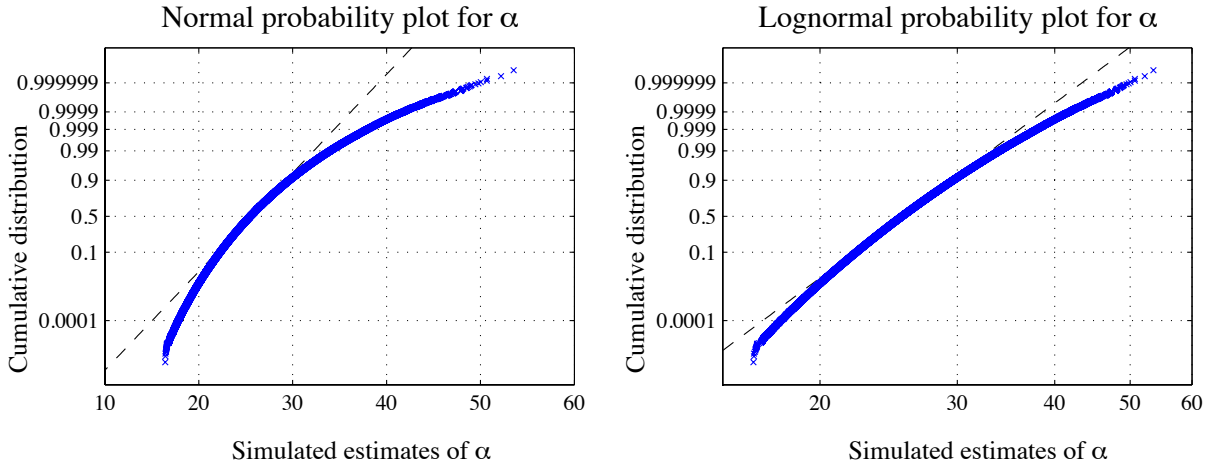

Figure 4.2 Uncertainty distributions for α plotted using normal (a), and lognormal (b) probability coordinates, where $N = 5{,}000{,}000$, using $n_s = 30$ and $n_j = \left[26,32,30\right]$

Repeating the process for ρ, Figures 4.3a and 4.3b show the cumulative probability plots for uncertainty in $\hat{\rho}$ on normal and lognormal coordinates, respectively. Here the lognormal plot is more linear, however there is significant non-linearity in the distribution with respect to either of the plotted coordinate systems. The stretched nature of the upper end of the plot, as compared to the more linear lower tail, indicates that while an estimate for ρ is unlikely to be low by very much (the 1st percentile is 124, compared to the median at 156, and the lowest of the 5 million simulated values is 103), there is a small, yet significant, chance of obtaining a very high ρ value (99th percentile is 250 – more than 60% larger than 156 – and the 99.99th is 550, which is almost four times 156). Thus there is a large spread in the upper tail that goes to many times the actual ρ value. An overly optimistic estimate of ρ can be misleading in assessing COPV reliability.

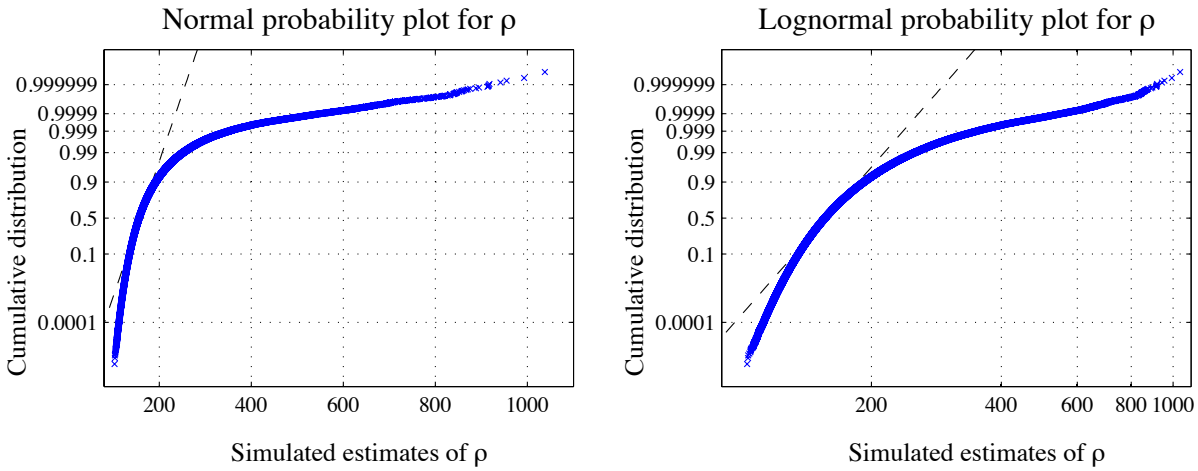

Figure 4.3 Uncertainty distributions for ρ plotted using normal (a), and lognormal (b) probability coordinates, where $N = 5{,}000{,}000$, using $n_s = 30$ and $n_j = \left[26,32,30\right]$

Finally repeating the process for the failure probability at a stress ratio of 50% and a lifetime of 10^5 hours, i.e. $F_{0.5}(10^5)$, Figures 4.4a and 4.4b show the cumulative probability plots

for uncertainty in the estimated failure probability on normal and lognormal coordinates, respectively. Here the lognormal plot is more linear, however again there is significant non-linearity in the distribution with respect to either plotted coordinates. That said the lognormal plot is significantly more linear and informative than the normal probability plot. In contrast to Figure 4.3 for ρ above, Figure 4.4b has a stretched lower tail and compact upper tail. The stretched lower tail suggests a possibility to underestimate the probability of failure (i.e. overestimate the reliability) by a large amount (as much as six orders of magnitude). The interpretation for the lower tail is that the actual probability of failure could well be much lower than the point estimate. However, errors in this direction are of less concern except that the vessel may have been overdesigned.

In contrast, the upper tail characterizes the likelihood that the true failure probability is in fact larger than the point estimate (i.e. the reliability is worse). The fact that in this case the upper tail is compact leads to a very low likelihood that the true failure probability is much higher than the point estimate. For instance, in reading Figure 4.4b we can see that there is a 99% probability that we get an estimate for $F_{0.5}(10^5)$ lower (better) than 10^{-5}, or viewed another way, there is a 1% probability that the true failure probability is larger (worse) than 10^{-5} when our point estimate is 7.63×10^{-7}. Going further, the compact upper tail indicates that the likelihood of the true failure probability being less than 10^{-4} is less than 1 in a million (the lowest value from 5 million simulations was less than 10^{-4}).

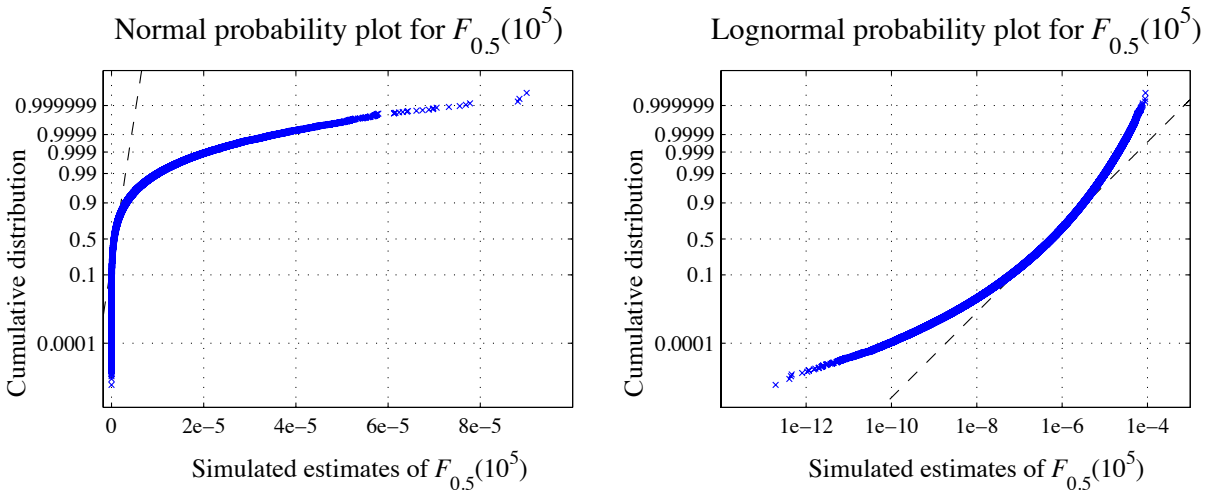

Figure 4.4 Uncertainty distributions for the failure probability at a stress ratio of 50% and a lifetime of 10^5 hours, $F_{0.5}(10^5)$, plotted using lognormal (a), and normal (b) probability coordinates, where $N = 5{,}000{,}000$, using $n_s = 30$ and $n_j = \left[26,32,30\right]$

It is worth noting that not all uncertainty distributions for failure probability have this compact upper tail. In fact it is possible to have the upper tail stretched to a failure probability of 1, such that there is a non-zero chance (from an uncertainty point of view) that the true failure probability is one (reliability of zero), while the point estimate may have been 10^{-4} or less. In this hypothetical case the point estimate is very misleading.

While Figures 4.1 through 4.4 qualitatively show that the uncertainty distributions are closer to lognormal distributed than normal distributed, quantitatively we can perform a Kolmogorov–Smirnov (K-S) test. In this case, the K-S statistics for σ_{ref}, α, ρ and $F_{0.5}(10^5)$ being lognormal distributed are 0.012102, 0.016927, 0.064529, and 0.040072 respectively, as compared to the K-S statistics with regards to the normal distribution of 0.010651, 0.039462, 0.100265, 0.271306 (smaller values of the K-S statistic implies a better match to the distribution). From these K-S statistics we can see that while the distributions are more

lognormal than normal, even the lognormal distribution does not accurately describe the parameter and failure probability uncertainty distributions, as is revealed by doing 5 million simulations.

Most analytical techniques for developing confidence intervals assume that the estimator will be normally distributed centered on the true mean. This is typically a valid assumption due to the asymptotic normality of MLE, as will be discussed next. These analytical techniques can be extended to cover the case of lognormal distributions of estimates, but become less accurate when the distribution is neither normal nor lognormal.

Maximum likelihood estimators are asymptotically normal. This means that the distribution of estimates will become normally distributed as the number of test specimens (in this case) goes to infinity. By performing the MC method for $n_s = 500$ and $n_j = \left[500,500,500\right]$, we get the lognormal probability plots for σ_{ref}, α, ρ and $F_{0.5}(10^5)$ shown in Figure 4.5, as well as the normal probability plots for ρ and $F_{0.5}(10^5)$ shown in Figure 4.6. In this case we can qualitatively see that the distributions in Figure 4.5 and 4.6 are much more linear than in Figures 4.1b through 4.4b, especially for ρ and $F_{0.5}(10^5)$ in Figures 4.3 and 4.4. Quantitatively the K-S statistics for σ_{ref}, α, ρ and $F_{0.5}(10^5)$ being lognormal distributed, when the numbers of specimens is now $n_s = 500$ and $n_j = \left[500,500,500\right]$, are 0.003380, 0.003990, 0.013804, and 0.008685 respectively, as compared to the K-S statistics with regards to the normal distribution of 0.003036, 0.009191, 0.019827, and 0.060947 respectively, all of which are smaller than before.

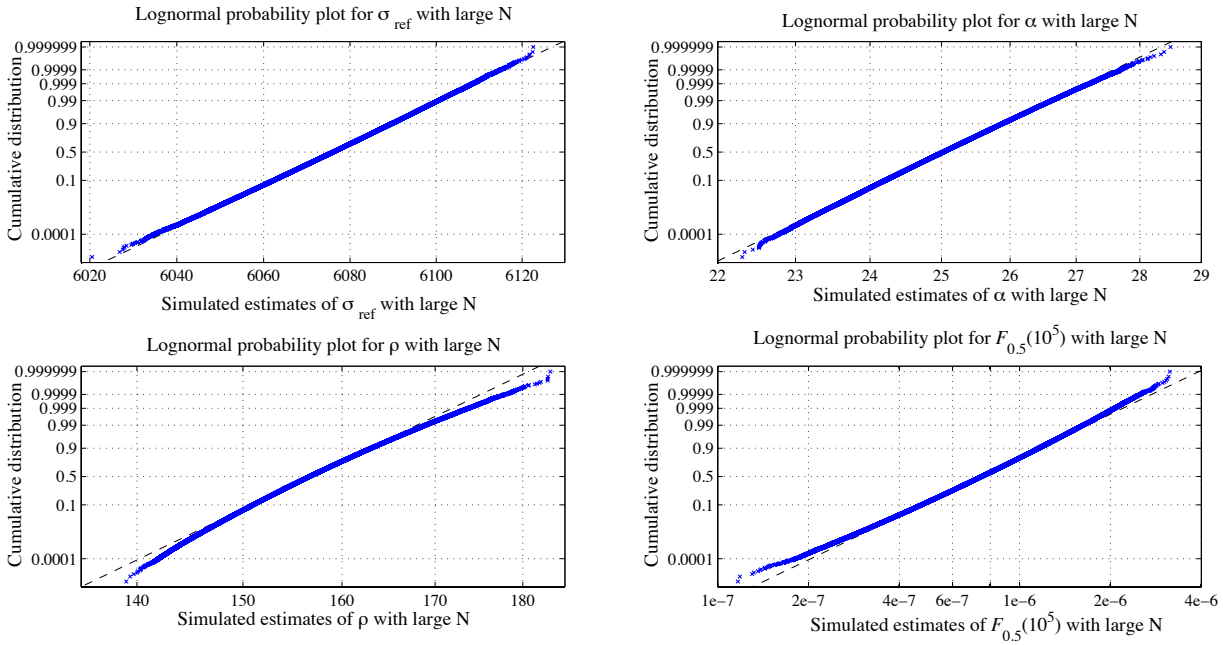

Figure 4.5 Uncertainty distributions for (a) σ_{ref}, (b) α, (c) ρ and (d) $F_{0.5}(10^5)$, plotted using lognormal probability coordinates, where $N = 500{,}000$, using $n_s = 500$ and $n_j = \left[500{,}500{,}500\right]$

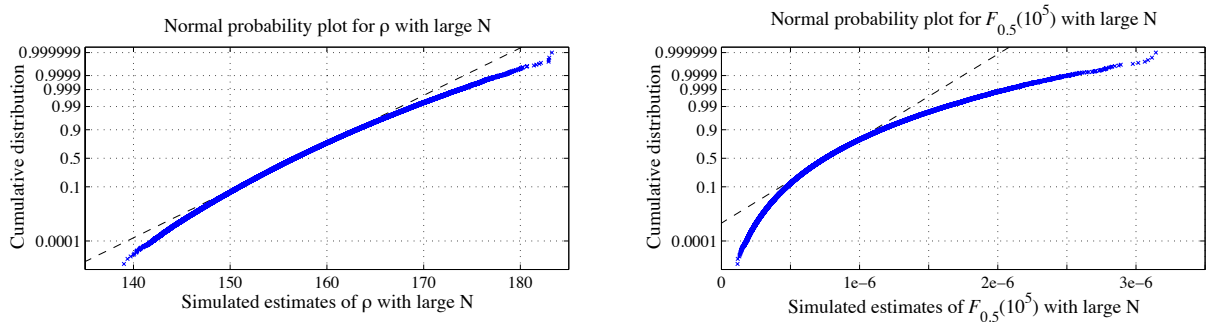

Figure 4.6 Uncertainty distributions for (a) ρ and (b) $F_{0.5}(10^5)$, plotted using normal probability coordinates, where $N = 500{,}000$, using $n_s = 500$ and $n_j = \left[500{,}500{,}500\right]$

As expected, a comparison of Figures 4.1b-4.4b and Figures 4.5 and 4.6 shows that the estimator becomes more normal when the number of specimens increases, so there is no contradiction with the asymptotic normality of maximum likelihood estimators. Unfortunately, it is rare that sample sizes in stress rupture datasets are large enough for a normal approximation of

the estimates to be accurate. Thus we must come up with other ways, described below, to remove the inherent bias in the unified MLE procedure of Part 1 [30] and to calculate the uncertainty in the final unbiased result.

4.4.3.2 Measures for estimate distributions

It is worth discussing for a moment what primary measure to use to describe the uncertainty distribution of estimates. There are three common options: first the average, i.e. the usual expected value of the uncertainty distribution, which has a specific meaning if the data is normally distributed, second the lognormal mean (transformed back into standard coordinates), and thirdly the median. As it turns out, all are biased, as can be seen in Table 4.1.

Table 4.1 Bias in estimates from simulations where $\hat{\theta} = \{6076\,\text{psi}, 25, 157\}$ (the point estimate from the original experimental dataset as well as the starting point for the simulations), and $N = 5{,}000{,}000$, where the failure probability is calculated using SR = 0.5 and t = 1 x 10^5 hours

	σ_{ref} (psi)	α	ρ	$F_{0.5}(10^5)$
Starting point	6076.235	24.995	156.67	7.63 x 10^{-7}
Normal mean	6072.819	25.7695	161.34	1.27 x 10^{-6}
Lognormal mean	6072.819	25.7680	161.22	1.69 x 10^{-6}
Median	6073.981	25.4854	156.15	5.69 x 10^{-7}

The median may be the best choice, as it is unaffected by the distortion in the extreme tails that make the distributions neither lognormal nor normal distributed. The median is also closer to the point estimate than the lognormal or normal mean. However the following sections

will use the lognormal mean to illustrate the procedure, while the provided supplemental Matlab code uses the median.

4.4.3.2 Removing estimator bias

Once we have performed N simulations and calculated for each the parameter values and failure probability estimates, we can calculate the mean for each of the parameters and for the failure probability. For example for the case $N = 5{,}000{,}000$, we calculated the lognormal mean parameter estimates $\hat{\theta}_{sim}$={6072.819 psi, 25.7680, 161.22}, as compared to the initial point estimate from the T1000 dataset, $\hat{\theta} = \{6076.24\,\text{psi}, 25.00, 156.67\}$, which was used to simulate the N datasets (i.e. in equations (4.8) and (4.10)). Clearly $\hat{\theta}_{sim} \neq \hat{\theta}$, and since *N* is large enough for that result to be significant, we can conclude that the estimator (i.e. the unified MLE procedure from [30]) that gave us $\hat{\theta}$ is biased; an estimate of this bias being $\hat{\theta}_{sim} - \hat{\theta} = \{-3.416\text{psi}, 0.7726, 4.55\}$. Thus the point estimate, $\hat{\theta}$, ought to be adjusted to account for the bias. A crude adjustment would be to subtract this bias from $\hat{\theta}$, which should give us parameter values much closer to the true parameters $\underline{\theta}$.

A more sophisticated method of removing bias, however, is to seek parameter values $\breve{\theta}$, for which the lognormal mean from simulated and analyzed datasets comes out to be the original parameter estimates from the experimental data, i.e. $\hat{\theta}$. The value $\breve{\theta}$ then becomes our desired unbiased estimate of the actual material parameters, $\underline{\theta}$. Computationally this effectively requires a search, in parameter space, for the zero of a function, that is the set of parameters, $\breve{\theta}$, to use in equations (4.8) and (4.10) such that the resulting parameter estimates, $\breve{\theta}_{sim}$, satisfies $\breve{\theta}_{sim} - \hat{\theta} \approx 0$. This approach, as described above, is illustrated in Figure 4.7.

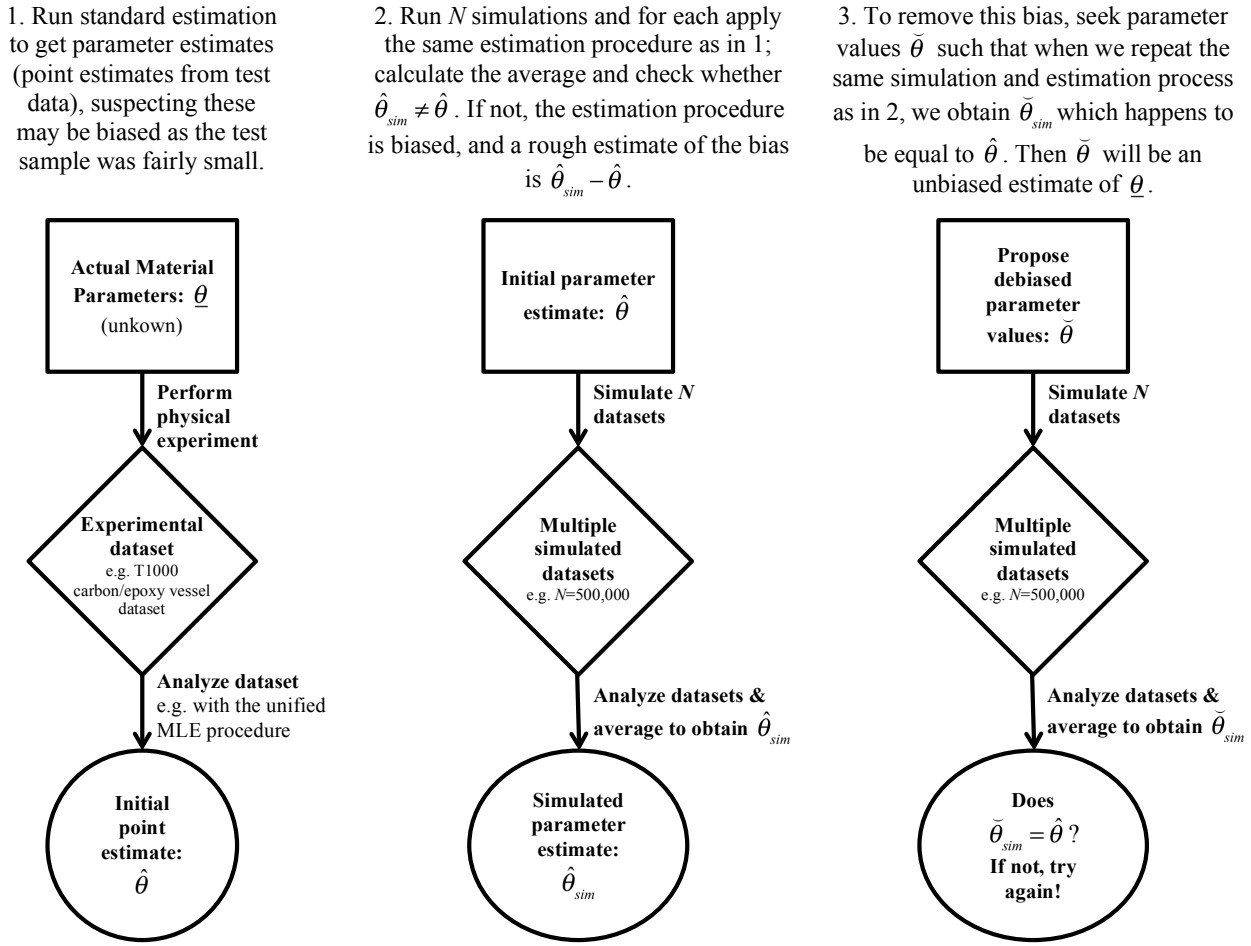

Figure 4.7 Schematic of de-biasing procedure.

The rationale for the process as described in Figure 4.7 is that there are actual, unknown, material parameters, $\underline{\theta}$, and when the experimental testing was done, the statistical analysis of that experimental data resulted in $\hat{\theta}$, known as the point estimate. Yet if we use MC simulation to replicate the testing and statistical evaluation process, and average the resulting parameter estimates, we obtain $\hat{\theta}_{sim}$. Typically $\hat{\theta}_{sim} \neq \hat{\theta}$, and assuming N is sufficiently large, we can conclude that the 'estimator' we used to get $\hat{\theta}$ is biased. To remove this bias we seek (through iteration) parameter values $\breve{\theta}$ that result in estimates $\breve{\theta}_{sim}$, such that $\breve{\theta}_{sim} = \hat{\theta}$. Having found such parameter values $\breve{\theta}$, and noting that typically the simulation procedure is one-to-one, i.e. the

estimate $\breve{\theta}$ is unique, we now have an unbiased estimate for the actual material parameters, $\underline{\theta}$. In finding the zero of the function $\breve{\theta}_{sim} - \hat{\theta} \approx 0$, the supplemental code provided online uses a simple method that nonetheless obtains final estimates $\breve{\theta}$ in about 20 iterations to within the limit of random variation.

For the example of the T1000 dataset, we found that the debiased point estimate $\breve{\theta} = \{6079.857\text{psi}, 24.2619, 152.24\}$ resulted in simulated estimates with a lognormal mean of $\breve{\theta}_{sim} = \{6076.246 \text{ psi}, 24.996, 156.67\}$, which is very close to the original point estimate $\hat{\theta} = \{6076.24\,\text{psi}, 25.00, 156.67\}$. This means that $\breve{\theta} = \{6079.857\text{psi}, 24.2619, 152.24\}$ are now the unbiased point parameter estimate, to within around {0.0024, 0.034, 0.057}% –the uncertainty from the inherent randomness of MC simulation. To elaborate, this uncertainty is equal to three times the standard deviation of the means from nine separate runs of N = 500,000 simulations (the number used in the debiasing iterations to find $\breve{\theta}$), divided by the overall mean from all the simulations. For more details see the Appendix.

4.4.3.3 Calculating uncertainty

Having discussed how to remove the bias from the point estimate, the next step is to calculate the uncertainty for our unbiased parameters. There is every reason to believe that the MC method can be treated as a smooth continuous function, such that the amount of uncertainty around $\breve{\theta}$ should be highly similar to that around $\breve{\theta}_{sim}$. In fact, the percentage of difference from the median to a given percentile is remarkably consistent, at least for parameter choices in the region of $\hat{\theta}$, as can be seen for the example of the T1000 carbon/epoxy dataset from Table 4.6 in the Appendix.

For the example T1000 carbon/epoxy dataset, fifty different sets of parameters were used as starting points for MC simulations involving N = 500,000 (in fact these parameter sets arose as part of the iterative process to remove the bias). Specifically, the starting σ_{ref} values vary from 6076.24 to 6079.90 psi, α values vary from 24.262 to 24.995, and ρ values vary from 152.25 to 156.67; ranges which span both $\hat{\theta}$ and $\breve{\theta}$. Across 50 different sets of parameters in those ranges, the ratio of the 0.05th percentile to the median is 9.27 x 10^{-4}, with a coefficient of variation (standard deviation divided by the mean) of 7.38%. The ratio of the 99.95th percentile and the mean is 37.49, with a coefficient of variation of 2.59%. The larger ratio for the 99.95th percentile is reflective of the skewness in the distribution, as can be seen in Figure 4.4b. These results are presented in the Appendix in Table 4.6.

From the simulated distributions we can now determine the amount of uncertainty in our unbiased parameter estimate $\breve{\theta}$. The failure probability can be calculated from $\breve{\theta}$ using equation (3.1). In our example of the T1000 dataset, where $\breve{\theta} = \{6079.857\text{psi}, 24.2619, 152.24\}$ and for a service lifetime of 10^5 hours at a stress ratio of 0.5, the predicted failure probability is $\breve{F}_{0.5}(10^5)$ = 1.26 x 10^{-6}. The 0.05th percentile is then 9.27 x 10^{-4} $\breve{F}_{0.5}(10^5)$ = 1.17 x 10^{-9}, and the 99.95th percentile is 37.49 $\breve{F}_{0.5}(10^5)$ = 4.72 x 10^{-5}. This means that while the median is only $\breve{F}_{0.5}(10^5)$ = 1.26 x 10^{-6}, there is still a 0.05% chance that the true failure probability is as low as 1.17 x 10^{-9} and a 0.05% chance that it is as large as 4.71 x 10^{-5}.

4.5 Discussion

By using the MC method we can get a distribution of estimates, both for parameters and the failure probability for a given load and lifetime, from which we can quantify the uncertainty and determine the amount of bias. Via an iterative search of parameter space we can then remove

the bias inherent in the estimator by searching for the parameters to use for the simulations that return parameter estimates like the one we received from the actual dataset.

Another use of the MC method presented in this paper is to assess, prior to actual experimental testing, how much uncertainty a certain test protocol will give, assuming preliminary estimates of the parameter values (which is not atypical). Using such rough estimates the MC method can be used to weigh the benefits of testing more specimens or running the tests for longer by evaluating what the effect would be on the distribution of estimates resulting from the MC method. In particular, comparing Figures 4.1-4.4 to Figures 4.5 and 4.6 shows us the difference in uncertainty to expect as we change the number of specimens from $n_s = 30$ and $n_j = \left[26,32,30\right]$, to $n_s = 500$ and $n_j = \left[500,500,500\right]$. In this case the distribution of failure probabilities narrows considerably when the number of specimens in increased this drastically. In Figure 4.4 the failure probability estimates varied by 8 orders of magnitude, but in Figure 4.5d they vary by less than two. Thus by changing the 'testing protocol' (i.e. the number of specimens, loading rate, number and magnitude of the load levels and the censor time) used to simulate the datasets, and comparing the resulting distributions of estimates, we can investigate the sensitivity of the uncertainty to a particular testing protocol. This is a very important secondary use of the MC method, assuming one has preliminary, albeit rough, estimates.

4.6 Conclusion

This paper presents a method for quantifying uncertainty for and removing bias from estimates of parameters from stress rupture datasets, using the CPL-W model. The method is firmly based in Monte-Carlo (MC) simulation techniques and can be summarized as simulating and analyzing datasets that mimic the experimental dataset of interest. A code that implements

this MC method for a sample T1000 carbon/epoxy dataset is provided as supplemental material.

4.7 Appendix: Results for the T1000 dataset

This section presents detailed statistics for the MC simulations, which were all run for $\hat{\theta} = \{6076.24 \text{ psi}, 25.00, 156.67\}$, unless otherwise stated. The number of specimens was either $n_s = 30$ and $n_j = [26,32,30]$, or $n_s = 500$ and $n_j = [500,500,500]$, with the latter case termed 'large *n*'. The different groups of simulations are enumerated in Table 4.2.

Table 4.2 Number of simulations, *N*, run per group

Simulation group	***N***
low censoring: {16000, 16000, 18240}	2499895
mid censoring: {20400, 18240, 18240}	4999831
high censoring: {21000, 21000, 18240}	2497152
'large *n*' applied to mid censoring only	499999

A question of interest was how large to set *N* in the case of the T1000 carbon/epoxy dataset. We ran *N* = 5,000,000 simulations for the mid censor case with $n_s = 30$ and $n_j = [26,32,30]$ and $\hat{\theta} = \{6076.24 \text{ psi}, 25.00, 156.67\}$, as shown in Table 4.2, which enumerates the number of simulations done for a given setup. By grouping the total set of 5 million simulations into different 'batches' of *M* simulations each, we can compare the results of running the identical simulation multiple times. In particular we can look at the standard deviation of our measure of interest (lognormal mean, standard mean, or median), termed 'variability' in this paper. When the variability is divided by the original measure, we get the 'scaled variability' –a

coefficient of variation for the measure of the separate batches. The results are shown in Figure 4.8.

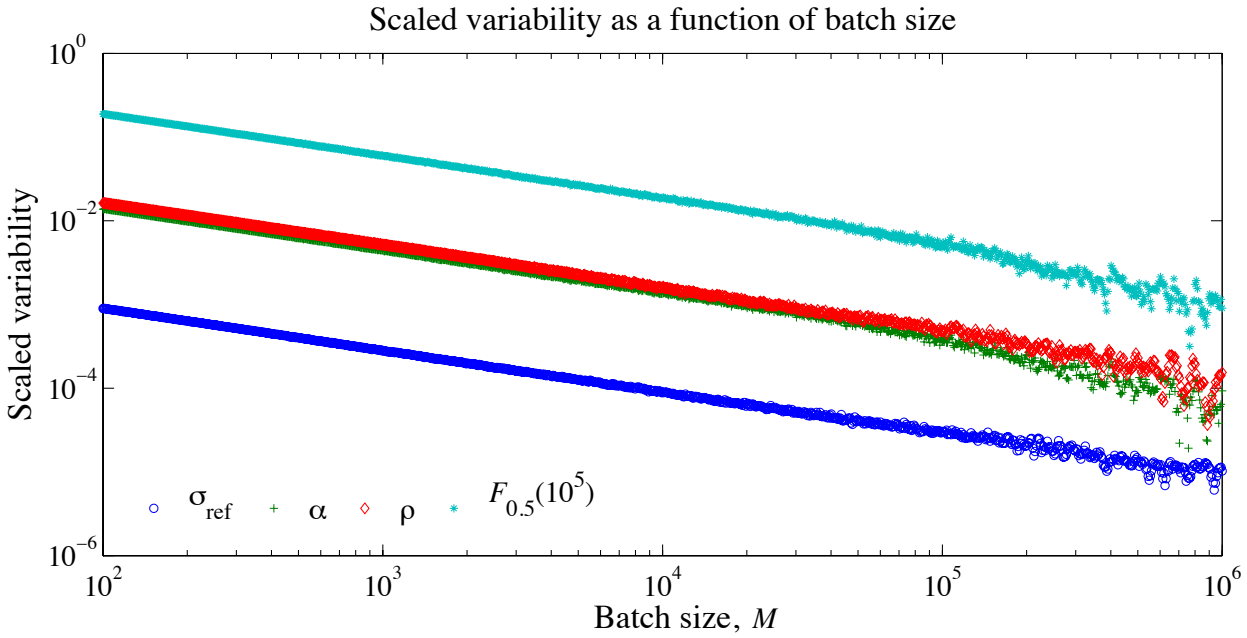

Figure 4.8 Scaled variability in the median as a function of the number of simulations done in a batch, where variability in the median is the standard deviation of the medians from all the batches, and the variability is scaled by the median of all the data.

In Figure 4.8 the lines get bumpy as the batch size goes up because we are pulling from a fixed number of simulations (5 million), so as the batch size goes up the number of batches goes down, and thus the estimate of the variability has more uncertainty, i.e. M times the number of batches equals N.

Figure 4.8 can be used to determine the uncertainty on the de-biasing. The uncertainty that the unbiased parameters are actually the best we can estimate from our simulations can be set as a number of standard deviations around the median. This uncertainty is overwhelmed, however, by the uncertainty in the estimator, which is quantified by the variance and CV. The variability, scaled variability, variance and CV are all shown in Tables 4.3-4.5, for the standard

mean, lognormal mean and median respectively.

Variability, as presented in Tables 4.3-4.5, is defined as the standard deviation across multiple different runs of 100,000 simulations. This metric, and the corresponding scaled version, allow us to see how much difference we might expect to see in different runs where N = 100,000.

Table 4.3 Lognormal results from simulations of different censor times, using $n_s = 30$ and $n_j = \left[26,32,30\right]$ mostly, except 'large n' where $n_s = 500$ and $n_j = \left[500,500,500\right]$, and the number of simulations is given in Table 4.2.

	Censor	Mean:	Variance:	CV:	Variability	Variability / Mean
σ_{ref} (psi)	low	6072.790	1942.4	0.72582%	0.10909	1.796×10^{-3} %
	mid	6072.819	1939.9	0.72524%	0.14852	2.445×10^{-3} %
	high	6072.821	1937.1	0.72476%	0.16755	2.758×10^{-3} %
	large n	6076.022	113.6	0.17545%	0.05477	9.013×10^{-4} %
α	low	25.7727	8.48	11.30%	0.00842	3.269×10^{-2} %
	mid	25.7680	8.40	11.25%	0.00762	2.959×10^{-2} %
	high	25.7727	8.35	11.21%	0.00609	2.367×10^{-2} %
	large n	25.0391	0.43	2.61%	0.00169	6.763×10^{-3} %
ρ	low	161.47	600	15.2%	0.092	5.696×10^{-2} %
	mid	161.22	566	14.8%	0.079	4.930×10^{-2} %
	high	161.16	557	14.6%	0.076	4.687×10^{-2} %
	large n	156.88	22	3.0%	0.015	9.309×10^{-3} %
$F_{0.5}(10^5)$	low	1.69E-06	3.18E-11	333.6%	1.15E-08	0.681%
	mid	1.69E-06	3.11E-11	330.9%	1.13E-08	0.669%
	high	1.67E-06	3.01E-11	328.3%	1.06E-08	0.633%
	large n	7.91E-07	8.12E-14	36.0%	7.63E-10	9.66×10^{-2} %

Table 4.4 Normal results from simulations of different censor times, using $n_s = 30$ and $n_j = \left[26,32,30\right]$ mostly, except 'large n' where $n_s = 500$ and $n_j = \left[500,500,500\right]$, and the number of simulations is given in Table 4.2.

	Censor	Mean:	Variance:	CV:	Variability	Variability / Mean
σ_{ref} (psi)	low	6072.790	1939.9	0.72535%	0.10909	1.796E-05
	mid	6072.819	1937.4	0.72477%	0.14852	2.446E-05
	high	6072.821	1934.6	0.72429%	0.16755	2.759E-05
	large n	6076.022	113.6	0.17544%	0.05477	9.014E-06
α	low	25.7744	8.74	11.47%	0.008428	3.27E-04
	mid	25.7695	8.66	11.42%	0.007643	2.97E-04
	high	25.7744	8.61	11.39%	0.006094	2.36E-04
	large n	25.0391	0.43	2.61%	0.001693	6.76E-05
ρ	low	161.60	759	17.0%	0.093	5.754E-04
	mid	161.34	708	16.5%	0.081	4.997E-04
	high	161.27	693	16.3%	0.076	4.703E-04
	large n	156.88	22	3.0%	0.015	9.308E-05
$F_{0.5}(10^5)$	low	1.27E-06	4.40E-12	165%	4.88E-09	3.83E-03
	mid	1.27E-06	4.38E-12	164%	6.22E-09	4.88E-03
	high	1.25E-06	3.66E-12	153%	5.86E-09	4.69E-03
	large n	7.90E-07	7.74E-14	35%	7.33E-10	9.28E-04

Table 4.5 Percentiles from simulations of different censor times, using $n_s = 30$ and $n_j = \left[26,32,30\right]$ mostly, except 'large n' where $n_s = 500$ and $n_j = \left[500,500,500\right]$, and the number of simulations is given in Table 4.2.

	Censor	**1st**	**50th**	**99th**	Variability in median	Variability / Median
σ_{ref} (psi)	low	5965.162	6073.918	6170.427	0.13752	2.264E-05
	mid	5965.181	6073.981	6170.349	0.19355	3.1865-05
	high	5965.176	6073.993	6170.248	0.20490	3.373E-05
	large n	6050.877	6076.096	6100.470	0.07302	1.20178E-05
α	low	20.1157	25.4898	34.0158	0.00907	3.5591E-04
	mid	20.1209	25.4854	33.9682	0.01018	3.9932E-04
	high	20.1950	25.4875	33.9643	0.00808	3.1696E-04
	large n	23.5805	25.0245	26.6242	0.00222	8.8651E-05
ρ	low	123.52	156.15	255.54	0.0956	6.124E-04
	mid	124.08	156.15	251.57	0.0766	4.908E-04
	high	124.20	156.14	250.60	0.1000	6.405E-04
	large n	146.82	156.65	168.94	0.0178	1.138E-05
$F_{0.5}(10^5)$	low	5.839E-09	5.669E-07	1.000E-05	3.05E-09	5.38E-03
	mid	5.952E-09	5.687E-07	1.001E-05	3.17E-09	5.58E-03
	high	6.023E-09	5.678E-07	9.656E-06	2.11E-09	3.72E-03
	large n	3.185E-07	7.491E-07	1.625E-06	1.13E-9	1.51E-03

Note that while the three censor cases produce similar results, there is a large decrease in variance, the coefficient of variation (CV) and in the variability from changing the number of specimens. The decrease in variance, and thus in CV, comes from the asymptotic normality of the unified MLE method. As the estimator becomes more normal (i.e. the number of specimens increases) the estimates become more accurate, thus also leading to the decrease in variability across batches of simulations, and the lognormal and normal statistics for the results converge.

The final investigation was done to compare the failure probability distributions resulting from slightly different starting points for the simulation. Table 4.6 shows the uncertainty in $F_{0.5}(10^5)$ for various iterations made in the debiasing process. Each of the 50 iterations was done with N = 500,000 and $n_s = 30$ and $n_j = \left[26,32,30\right]$. The percent ratios of the percentiles to the mean are remarkably consistent across these slightly differing starting points.

Table 4.6 Amount of uncertainty at each iteration for $F_{0.5}(10^5)$

Starting Parameters			$F_{0.5}(10^5)$ Percentiles			Ratios	
σ_{ref} (psi)	α	ρ	0.05	50	99.95	0.05 / 50	99.95 /50
6076.235	24.9954	156.669	3.610E-10	5.691E-07	2.436E-05	0.000634	42.81
6077.987	24.6094	153.959	6.194E-10	7.541E-07	2.999E-05	0.000821	39.77
6078.898	24.4291	153.109	7.295E-10	8.494E-07	3.198E-05	0.000859	37.65
6079.312	24.3446	152.696	8.778E-10	9.016E-07	3.437E-05	0.000974	38.12
6079.594	24.3054	152.551	8.612E-10	9.259E-07	3.490E-05	0.000930	37.69
6079.747	24.2851	152.528	8.375E-10	9.366E-07	3.522E-05	0.000894	37.60
6079.771	24.2731	152.484	8.981E-10	9.437E-07	3.545E-05	0.000952	37.57
6079.777	24.2664	152.343	9.440E-10	9.484E-07	3.558E-05	0.000995	37.52
6079.829	24.2660	152.336	8.533E-10	9.491E-07	3.552E-05	0.000899	37.43
6079.870	24.2652	152.383	8.598E-10	9.501E-07	3.543E-05	0.000905	37.29
6079.879	24.2670	152.406	9.375E-10	9.440E-07	3.550E-05	0.000993	37.61
6079.874	24.2640	152.380	8.720E-10	9.490E-07	3.643E-05	0.000919	38.39
6079.898	24.2659	152.376	9.721E-10	9.514E-07	3.486E-05	0.001022	36.64
6079.851	24.2695	152.474	9.373E-10	9.449E-07	3.558E-05	0.000992	37.65
6079.875	24.2676	152.401	8.881E-10	9.476E-07	3.526E-05	0.000937	37.20
6079.757	24.2661	152.489	8.739E-10	9.425E-07	3.550E-05	0.000927	37.67
6079.835	24.2641	152.517	9.487E-10	9.438E-07	3.494E-05	0.001005	37.02
6079.874	24.2647	152.430	7.948E-10	9.452E-07	3.564E-05	0.000841	37.71
6079.847	24.2619	152.416	8.316E-10	9.496E-07	3.596E-05	0.000876	37.87
6079.842	24.2618	152.415	8.392E-10	9.497E-07	3.480E-05	0.000884	36.65
6079.883	24.2628	152.375	9.185E-10	9.509E-07	3.578E-05	0.000966	37.63
6079.823	24.2649	152.387	9.493E-10	9.520E-07	3.538E-05	0.000997	37.16
6079.856	24.2683	152.460	9.322E-10	9.465E-07	3.451E-05	0.000985	36.46
6079.869	24.2648	152.438	8.079E-10	9.456E-07	3.533E-05	0.000854	37.37
6079.808	24.2620	152.430	8.626E-10	9.525E-07	3.448E-05	0.000906	36.20

6079.810	24.2669	152.434	8.423E-10	9.490E-07	3.468E-05	0.000888	36.54
6079.856	24.2682	152.421	9.511E-10	9.461E-07	3.482E-05	0.001005	36.80
6079.833	24.2668	152.433	7.353E-10	9.430E-07	3.579E-05	0.000780	37.96
6079.819	24.2627	152.410	9.040E-10	9.529E-07	3.546E-05	0.000949	37.22
6079.857	24.2653	152.412	9.009E-10	9.468E-07	3.573E-05	0.000952	37.74
6079.863	24.2649	152.457	9.418E-10	9.462E-07	3.490E-05	0.000995	36.88
6079.816	24.2656	152.516	9.520E-10	9.432E-07	3.495E-05	0.001009	37.06
6079.818	24.2646	152.430	9.025E-10	9.486E-07	3.482E-05	0.000951	36.71
6079.837	24.2657	152.346	9.043E-10	9.515E-07	3.535E-05	0.000950	37.15
6079.776	24.2666	152.450	9.459E-10	9.491E-07	3.582E-05	0.000997	37.74
6079.784	24.2662	152.488	8.705E-10	9.503E-07	3.494E-05	0.000916	36.77
6079.823	24.2685	152.459	8.934E-10	9.396E-07	3.524E-05	0.000951	37.50
6079.821	24.2637	152.401	8.350E-10	9.488E-07	3.566E-05	0.000880	37.58
6079.801	24.2624	152.400	9.157E-10	9.501E-07	3.563E-05	0.000964	37.50
6079.813	24.2663	152.397	8.634E-10	9.504E-07	3.499E-05	0.000909	36.82
6079.778	24.2680	152.422	8.968E-10	9.491E-07	3.551E-05	0.000945	37.41
6079.826	24.2675	152.407	9.175E-10	9.504E-07	3.520E-05	0.000965	37.04
6079.810	24.2685	152.432	8.713E-10	9.432E-07	3.615E-05	0.000924	38.32
6079.839	24.2649	152.384	8.956E-10	9.492E-07	3.648E-05	0.000944	38.44
6079.867	24.2682	152.349	9.317E-10	9.480E-07	3.477E-05	0.000983	36.67
6079.847	24.2679	152.387	9.059E-10	9.465E-07	3.508E-05	0.000957	37.06
6079.847	24.2666	152.425	9.069E-10	9.509E-07	3.548E-05	0.000954	37.31
6079.822	24.2689	152.345	8.279E-10	9.464E-07	3.519E-05	0.000875	37.19
6079.825	24.2678	152.248	8.683E-10	9.506E-07	3.566E-05	0.000913	37.51
6079.819	24.2667	152.408	7.909E-10	9.527E-07	3.500E-05	0.000830	36.74

REFERENCES

[30] Engelbrecht-Wiggans A, Phoenix SL (2017) Analysis of stress rupture data on fiber composites: Part 1- A unified maximum likelihood method, The Journal of Space Safety Engineering (2017), http://dx.doi.org/10.1016/j.jsse.2017.03.002

CHAPTER 5

COMPARISON OF PROBABILISTIC MODELS FOR STRESS RUPTURE FAILURE IN CONTINUOUS UNIDIRECTIONAL FIBER COMPOSITE STRUCTURES

5.1 Introduction

Stress rupture is a long-term, catastrophic failure mode in unidirectional continuous fiber composites. Stress rupture failures happen suddenly, with little to no warning, and at present eminent failures cannot be reliably predicted with non-destructive evaluation. Stress rupture occurs at normal operating temperatures and at load levels well below the initial failure load, though stress rupture failures will occur sooner with increased temperature and/or load. Examples of unidirectional continuous fiber composites susceptible to stress rupture are composite overwrapped pressure vessels (COPVs), composite flywheels for energy storage, and long tension members used in civil engineering structures. For COPVs in particular, stress rupture failures are of increasing concern as COPVs are being designed with longer service lives and higher service pressures in mind. Also, the number of COPVs in use is rapidly growing, so even though a stress rupture failure may be a relatively low probability event we can anticipate seeing such failures in applications if stress rupture is not properly understood and accounted for.

Stress rupture failures develop from the randomly distributed flaws that are inherent in any fiber. This causes not only an intrinsic randomness in the fiber strength, including a size effect, but also intrinsic randomness in the strength of corresponding unidirectional continuous fiber composites. Thus the exact strength of a composite specimen cannot be known in advance. Because of this intrinsic randomness, the exact failure time of a specimen also cannot be known

ahead of time. At best, the overall stress rupture behavior for a population of identical specimens must be statistically characterized. From extensive testing as well, as theory, we know that the failure strength is very close to Weibull distributed. The lifetimes under a constant load are also approximately Weibull distributed. A probabilistic model can then be used to relate lifetimes at different loads to each other, as well as to initial strength.

The goal of this paper is to compare various models that have arisen in the literature. In particular, this paper compares what is referred to as (i) the 1979 functional form, (ii) the classic power law model, (iii) the crack-growth model, and (iv) the strength decay model, all of which are cast in a power-law Weibull framework.

5.2 Probabilistic models

The earliest of the existing probabilistic models to describe stress rupture failures date from the 1940s and 1950s. [6, 8-12, 31] These models tend to have a more phenomenological than micro-mechanics basis, though some are well based in the molecular failure processes for a single fiber.

In the literature there are currently three specific probabilistic models, each a parametric variation of a general functional form. The oldest and most commonly used is the classic power-law model in a Weibull framework (CPL-W). [11, 15, 32] Another model is based on Paris law crack growth, termed the crack-growth model. [20, 33] The most recent model is the strength decay model. [19]

5.2.1 1979 functional form

Many currently existing models fit into a functional form proposed by Phoenix in 1979 [18]:

$$F\left(t\middle|\sigma\right)=\sup_{0\le\tau\le t}\left\{\psi\left(\sigma\left(\tau\right),\, Z\left(\tau;\sigma\left(\tau\right)\right)\right)\right\}. \tag{5.1}$$

Here $\psi(\sigma, Z)$ is the shape function in terms of the non-negative stress profile, $\sigma(t)$, $t \geq 0$, where Z provides for the introduction of degradation over time. Equation (5.1) was actually proposed for single fiber behavior as an assumption in modeling bundle lifetime.

A useful shape function for stress rupture is:

$$\psi\left(\sigma, Z\left(\tau;\sigma(\tau)\right)\right) = 1 - \exp\left\{-\left(\left(\frac{\sigma}{\sigma_{\text{ref}}}\right)^{r} + \frac{Z\left(\tau;\sigma(\tau)\right)}{t_{\text{ref}}}\right)^{\beta}\right\}, \tag{5.2}$$

where σ_{ref} is a stress scaling parameter, t_{ref} is a time scaling parameter, β is the shape parameter, and r is a parameter reflecting the sensitivity of the material to instantaneous load.

A useful degradation form, reminiscent of Miner's rule [16], takes the integral structure

$$Z\left(\tau;\sigma(\tau)\right) = \int_{0}^{\tau} \kappa\left(\sigma(s)\right) ds \tag{5.3}$$

where $\kappa(\sigma)$ is the breakdown rule. Most current models for stress rupture use a power-law breakdown rule [34], with molecular justification in terms of thermal activation processes in [11, 35-37]:

$$\kappa\left(\sigma(t)\right) = \left(\frac{\sigma(t)}{\sigma_{\text{ref}}}\right)^{\rho}, \quad \sigma(t) \geq 0, \tag{5.4}$$

where ρ is the power-law exponent, controlling sensitivity to variations in the applied stress. Some more recent modeling of stress rupture in fiber systems, using the power-law breakdown rule, is presented in [38, 39].

An alternative is the exponential breakdown rule, with a long history beginning with Coleman [8, 9] and Zhurkov [40]:

$$\kappa\left(\sigma\left(t\right)\right)=\mu\exp\left\{\frac{\sigma\left(t\right)}{\sigma_{\text{ref}}}\right\},\ \ \sigma\left(t\right)\geq 0\,, \tag{5.5}$$

where μ is a scaling constant. In many circumstances (5.4) and (5.5) are equally realistic in modeling experimental datasets [15], and with properly chosen parameters both rules give qualitatively similar results [34]. There are some circumstances where (5.5) may be more accurate, such as in [41], however, (5.5) has significant drawbacks mathematically [35].

Combining (5.1), (5.2), (5.3) and (5.4) gives the form of (5.1) that is most applicable to stress-rupture in composites:

$$F_{1979}\left(t\middle|\sigma\right)=1-\exp\left\{-\sup_{0\leq\tau\leq t}\left\{\left[\left(\frac{\sigma\left(\tau\right)}{\sigma_{\text{ref}}}\right)^{r}+\int_{0}^{\tau}\left(\frac{\sigma\left(s\right)}{\sigma_{\text{ref}}}\right)^{\rho}\frac{ds}{t_{\text{ref}}}\right]^{\beta}\right\}\right\},\ t\geq 0 \tag{5.6}$$

This is the version of the functional form that will be considered for the rest of the paper.

In the case of strength testing, the stress is assumed to be linearly increasing:

$$\sigma\left(t\right)=Rt,\quad t\geq 0 \tag{5.7}$$

where the constant, $R>0$, is the loading rate or stress rate. Under this load profile (5.6) simplifies to the cumulative distribution function for failure stress in a strength test:

$$F_{1979,s}\left(s\right)=1-\exp\left\{-\left[\left(\frac{s}{\sigma_{\text{ref}}}\right)^{r}+\left(\frac{s}{\sigma_{\text{ref}}}\right)^{\rho}\frac{s}{R\,t_{\text{ref}}\left(\rho+1\right)}\right]^{\beta}\right\} \tag{5.8}$$

where $s=Rt>0$ is the stress level at failure.

In the case of stress rupture lifetime testing the load is held constant:

$$\sigma\left(t\right)=\bar{\sigma},\quad t>0\,. \tag{5.9}$$

Using (5.9), the cumulative distribution function for time to failure simplifies from (5.6) to:

$$F_{1979,\bar{\sigma}}(t) = 1 - \exp\left\{ -\left[\left(\frac{\bar{\sigma}}{\sigma_{\text{ref}}} \right)^{r} + \left(\frac{\bar{\sigma}}{\sigma_{\text{ref}}} \right)^{\rho} \frac{t}{t_{\text{ref}}} \right]^{\beta} \right\} \tag{5.10}$$

Thus the functional form can be given in general by (5.6), with a strength distribution given by (5.8) and a lifetime distribution given by (5.10). The 1979 functional form has five parameters: σ_{ref}, r, ρ, β, and t_{ref}.

Changing the type of material is likely to change the relationship between r and ρ. A material with a large r, respective to ρ, would have an almost deterministic strength distribution for extremely high loading rates, however at slow loading rates the strength distribution has greatly increased variability. This might be the case where flaws of uniform size inherently grow at differing rates. In contrast, a material with a small r, respective to ρ, would have more variability in the strength distribution at extremely high loading rates than at slow ones. This might be the case where the flaws themselves are highly variable, but grow in a way that ultimately masks the initial variability. This paper will consider $-4 \le r - \rho \le 32$ to illustrate differences between models, whether or not these values correspond specifically to a particular material.

5.2.2 Classic power-law model in a Weibull framework (CPL-W)

The CPL-W model was developed to describe the behavior of a single fiber, but is generally applied to the whole composite structure. CPL-W is mostly phenomenological, though a molecular basis has been established: it has been shown that the model is a consequence of the Tobolsky-Eyring theory of thermally activated bond breakage [11, 14, 35, 36]. The CPL-W model fits strength and lifetime data well, albeit with some small differences in comparison with data in the tails of the distribution, in which the CPL-W model happens to be conservative.

Seeing these differences likely requires very large sample sizes (in the hundreds) [14].

The probability of failure of a specimen in stress rupture is given by the CPL-W model to be:

$$F_{\text{CPL-W}}\left(t\middle|\sigma\right)=1-\exp\left\{-\left[\int_0^t\left(\frac{\sigma\left(\tau\right)}{\sigma_{\text{ref}}}\right)^{\rho}\frac{d\tau}{t_{\text{ref}}}\right]^{\beta}\right\} \tag{5.11}$$

where ρ is the power-law exponent, controlling sensitivity to changes in the applied stress, σ_{ref} is a stress scaling parameter, t_{ref} is a time scaling parameter, and β is the Weibull scale parameter, as before in (5.2) and (5.4). Note that (5.11) can be written as

$$F_{\text{CPL-W}}\left(t\middle|\sigma\right)=1-\exp\left\{-\left[\frac{1}{{\sigma_{\text{ref}}}^{\rho}\,t_{\text{ref}}}\int_0^t\sigma\left(\tau\right)^{\rho}\,d\tau\right]^{\beta}\right\} \tag{5.12}$$

so that there is only one scale parameter, namely ${\sigma_{\text{ref}}}^{\rho}\,t_{\text{ref}}$, albeit an unintuitive one with inconvenient dimensions. Nonetheless, the importance of equation (5.12) is that the four parameters shown in (5.11) are not independent. Instead there is a relationship between σ_{ref}, t_{ref} and ρ, such that ${\sigma_{\text{ref}}}^{\rho}\,t_{\text{ref}}$ is a constant for a given material.

Applying the model, (5.11), to the case of strength testing, the cumulative distribution function for failure stress becomes:

$$F_{\text{CPL-W},s}\left(s\right)=1-\exp\left\{-\left[\left(\frac{s}{\sigma_{\text{ref}}}\right)^{\rho}\frac{s}{R\,t_{\text{ref}}\left(\rho+1\right)}\right]^{\beta}\right\}. \tag{5.13}$$

where again $s=Rt$ is the stress level at failure. This can be written as

$$F_{\text{CPL-W},s}\left(s\right)=1-\exp\left\{-\left(\frac{s}{\sigma_{\text{ref}}}\right)^{\beta\left(\rho+1\right)}\right\} \tag{5.14}$$

by assuming

$$\sigma_{\text{ref}} = R\, t_{\text{ref}}\left(\rho+1\right) \quad \text{or} \quad t_{\text{ref}} = \frac{\sigma_{\text{ref}}}{R\left(\rho+1\right)}. \tag{5.15}$$

Equation (5.14) is a basic two-parameter Weibull distribution with the scale parameter σ_{ref} and shape parameter $\beta\left(\rho+1\right)$, termed α, which is how an experimentalist would be most likely to parameterize the strength distribution. However equation (5.15) is necessary to provide consistency in the modeling framework by recasting the dependent parameter t_{ref} in terms of σ_{ref}, R and ρ.

In the case of stress rupture lifetime testing the cumulative distribution function for time to failure simplifies from (5.11) to:

$$\begin{aligned} F_{\text{CPL-W},\bar{\sigma}}\left(t\right) &= 1-\exp\left\{-\left[\left(\frac{\bar{\sigma}}{\sigma_{\text{ref}}}\right)^{\rho}\frac{t}{t_{\text{ref}}}\right]^{\beta}\right\} \\ &= 1-\exp\left\{-\left[\left(\frac{\bar{\sigma}}{\sigma_{\text{ref}}}\right)^{\rho}\frac{R\left(\rho+1\right)t}{\sigma_{\text{ref}}}\right]^{\beta}\right\} \end{aligned}. \tag{5.16}$$

Thus the CPL-W model can be given in general by (5.11), with a strength distribution given by (3.3) and a lifetime distribution given by (3.10). This model has three parameters: σ_{ref}, ρ, and β. The CPL-W model can be obtained from (5.6) by taking the limit as $r \to \infty$ and assuming $\sigma\left(t\right) < \sigma_{\text{ref}}$.

5.2.3 Crack-growth model

The crack-growth model was also developed in the 1980s for a single fiber and has seen relatively little use. It is based on the mechanics of a crack propagating through a single fiber

following the Paris crack growth law, and assumes an initial distribution for the length of the largest crack and a fixed critical stress intensity factor, all chosen to result in a Weibull strength distribution. While originally derived in [20], an alternate derivation is provided in the appendix of [27]. The crack-growth model has been applied as a model for general composite failure, though without micromechanical justification in terms of cracks physically growing through the overall composite. This model is a special case of (5.6) as it can be obtained by setting $r = \rho - 2$:

$$F_{\text{crack}}\left(t\middle|\sigma\right) = 1 - \exp\left\{-\sup_{0\le\tau\le t}\left[\left(\frac{\sigma(\tau)}{\sigma_{\text{ref}}}\right)^{\rho-2} + \int_0^{\tau}\left(\frac{\sigma(s)}{\sigma_{\text{ref}}}\right)^{\rho}\frac{ds}{t_{\text{ref}}}\right]^{\beta}\right\} \tag{5.17}$$

where all the variables have the same meanings as before.

In the case of strength testing the cumulative distribution function for failure stress is:

$$\begin{aligned} F_{\text{crack},s}(s) &= 1 - \exp\left\{-\left[\left(\frac{s}{\sigma_{\text{ref}}}\right)^{\rho-2} + \left(\frac{s}{\sigma_{\text{ref}}}\right)^{\rho}\frac{s}{R\,t_{\text{ref}}(\rho+1)}\right]^{\beta}\right\} \\ &= 1 - \exp\left\{-\left[\left(\frac{s}{\sigma_{\text{ref}}}\right)^{\rho}\left(\left(\frac{s}{\sigma_{\text{ref}}}\right)^{-2} + \frac{s}{R\,t_{\text{ref}}(\rho+1)}\right)\right]^{\beta}\right\}. \end{aligned} \tag{5.18}$$

where again the stress level at failure is $s = Rt$.

If the constraint (5.15), only required for the CPL-W model, is applied to (5.18) the resulting strength distribution is:

$$F_{\text{crack},s}(s) = 1 - \exp\left\{-\left[\left(\frac{s}{\sigma_{\text{ref}}}\right)^{\rho-2}\left(1 + \left(\frac{s}{\sigma_{\text{ref}}}\right)^{3}\right)\right]^{\beta}\right\}. \tag{5.19}$$

In the case of stress rupture lifetime testing, and ignoring the constraint (5.15), the cumulative distribution function for time to failure simplifies from (5.17) to:

$$F_{\text{crack},\bar{\sigma}}(t) = 1 - \exp\left\{-\left[\left(\frac{\bar{\sigma}}{\sigma_{\text{ref}}}\right)^{\rho-2} + \left(\frac{\bar{\sigma}}{\sigma_{\text{ref}}}\right)^{\rho}\frac{t}{t_{\text{ref}}}\right]^{\beta}\right\}$$
$$= 1 - \exp\left\{-\left[\left(\frac{\bar{\sigma}}{\sigma_{\text{ref}}}\right)^{\rho}\left(\left(\frac{\bar{\sigma}}{\sigma_{\text{ref}}}\right)^{-2} + \frac{t}{t_{\text{ref}}}\right)\right]^{\beta}\right\}. \tag{5.20}$$

In general, the strength decay model is given by (5.17), with a strength distribution given by (5.18) and a lifetime distribution given by (5.20). Thus, in general this model has four parameters: σ_{ref}, ρ, β, and t_{ref}.

5.2.4 Strength decay model

The most recently proposed model for stress rupture is the strength decay model [19]. This model is purely a phenomenological model. There has been no statistical analysis to show whether it fits experimental data any better or worse than CPL-W. The strength decay model is also of the form (5.6), (as shown in the appendix of [27]), which is for a single fiber, and as with the previous models there is no compelling rationale as to why it should be applicable to a general composite structure. The strength decay model is obtained from (5.6) by setting $r = \rho$:

$$F_{\text{decay}}(t|\sigma) = 1 - \exp\left\{-\sup_{0\le\tau\le t}\left\{\left[\left(\frac{\sigma(\tau)}{\sigma_{\text{ref}}}\right)^{\rho} + \int_0^{\tau}\left(\frac{\sigma(s)}{\sigma_{\text{ref}}}\right)^{\rho}\frac{ds}{t_{\text{ref}}}\right]^{\beta}\right\}\right\} \tag{5.21}$$

where all the variables have the same meanings as before.

In the case of strength testing, the cumulative distribution function for failure stress is:

$$F_{\text{decay},s}(s) = 1 - \exp\left\{-\left[\left(\frac{s}{\sigma_{\text{ref}}}\right)^{\rho}\left(1 + \frac{s}{R\,t_{\text{ref}}(\rho+1)}\right)\right]^{\beta}\right\}. \tag{5.22}$$

where again $s = Rt$ is the stress level at failure.

If the constraint (5.15), only required for the CPL-W model, is applied to (5.22) the resulting three-parameter strength distribution is:

$$F_{\text{decay},s}(s) = 1 - \exp\left\{-\left[\left(\frac{s}{\sigma_{\text{ref}}}\right)^{\rho}\left(1+\frac{s}{\sigma_{\text{ref}}}\right)\right]^{\beta}\right\}. \tag{5.23}$$

In the case of stress rupture lifetime testing, and ignoring the constraint (5.15), the cumulative distribution function for time to failure simplifies from (5.21) to:

$$F_{\text{decay},\bar{\sigma}}(t) = 1 - \exp\left\{-\left[\left(\frac{\bar{\sigma}}{\sigma_{\text{ref}}}\right)^{\rho}\left(1+\frac{t}{t_{\text{ref}}}\right)\right]^{\beta}\right\}. \tag{5.24}$$

In general, the strength decay model is given by (5.21), with a strength distribution given by (5.22) and a lifetime distribution given by (5.24). Thus, in general this model has four parameters: σ_{ref}, ρ, β, and t_{ref}.

Note that the constraint, (5.15), applied in (5.19) and (5.23), naturally arose in the special case of the CPL-W model, and is not required by the 1979 functional form in general or any instances of it. Applying the constraint, however, does reduce by one the number of independent parameters to be estimated. In some circumstances, particularly when data are sparse, this may help in estimating failure probabilities.

5.3. Comparing basic model behavior

The current state of probabilistic models, particularly those of the type considered here, is that there are three vying models, plus the overall functional form. These models all give either exactly or approximately a Weibull distributed strength distribution as well as Weibull

distributed lifetime distributions. This is key as actual experimental data for strength and life are typically Weibull distributed. The main point of difference in the models is how the strength distribution relates to the lifetime distribution as is explored below.

5.3.1 Comparing lifetime distributions

The lifetime distributions for the 1979 functional form, the CPL-W model, the crack-growth model and the strength decay model are given by (5.10), (3.10), (5.20) and (5.24) respectively, and can be framed as:

$$F_{\bar{\sigma}}(t) = 1 - \exp\left\{-\left[\left(\frac{\bar{\sigma}}{\sigma_{\text{ref}}}\right)^{\rho}\left(\Phi + \frac{t}{t_{\text{ref}}}\right)\right]^{\beta}\right\} \tag{5.25}$$

where

$$\Phi(\bar{\sigma}) = \begin{cases} \left(\bar{\sigma}/\sigma_{\text{ref}}\right)^{r-\rho}, & \text{1979 functional form} \\ 0, & \text{CPL-W model} \\ \left(\bar{\sigma}/\sigma_{\text{ref}}\right)^{-2}, & \text{crack-growth model} \\ 1, & \text{strength decay model} \end{cases} . \tag{5.26}$$

In applications for moderate $\bar{\sigma}/\sigma_{\text{ref}}$, the factor $\Phi + t/t_{\text{ref}}$ is dominated by the ratio t/t_{ref} at all but the shortest times. If the stress ratio, $\bar{\sigma}/\sigma_{\text{ref}}$, is small (say less than 0.3), and if the exponent arising in two of the versions of Φ, namely $r-\rho$ and -2, is negative, and when t_{ref} happens to be large, then it may take some time before the t/t_{ref} term dominates, though in the meantime no failures will happen at such low stress ratios. Because t/t_{ref} is generally significantly greater than Φ when the failure probability is significant, the lifetime distributions are effectively the same for these four models. Testing strategies for distinguishing amongst the

models will not be discussed here, but nonetheless distinguishing features among the various models are presented below.

To simplify the notation when exploring the behavior of Φ, the stress ratio $\bar{\sigma}/\sigma_{\text{ref}}$ is called SR and the normalized time t/t_{ref} is called T. Figure 5.1 plots Φ, which is SR^{ϖ}, for stress ratios ranging from zero to one and for exponents, ϖ, that vary from -10 to 10. For all positive values of ϖ, Φ is less than or equal one. Even for negative values, such as $\varpi = -2$ as in the crack-growth model, the term $\Phi = \text{SR}^{\varpi}$ remains under 10 for $\text{SR} \geq 0.32$, meaning that $T = t/t_{\text{ref}}$ will start to dominate Φ once $t \geq 10\, t_{\text{ref}}$. On the other hand, for $\text{SR} < 0.32$ when $\varpi \leq -2$, and thus higher values of Φ occur, t must be much larger than t_{ref} for T to dominate Φ. The key observation, once again, is that with such a low load level there are unlikely to be early failures observed experimentally. Thus, experimentally observable differences between the models are very unlikely to occur.

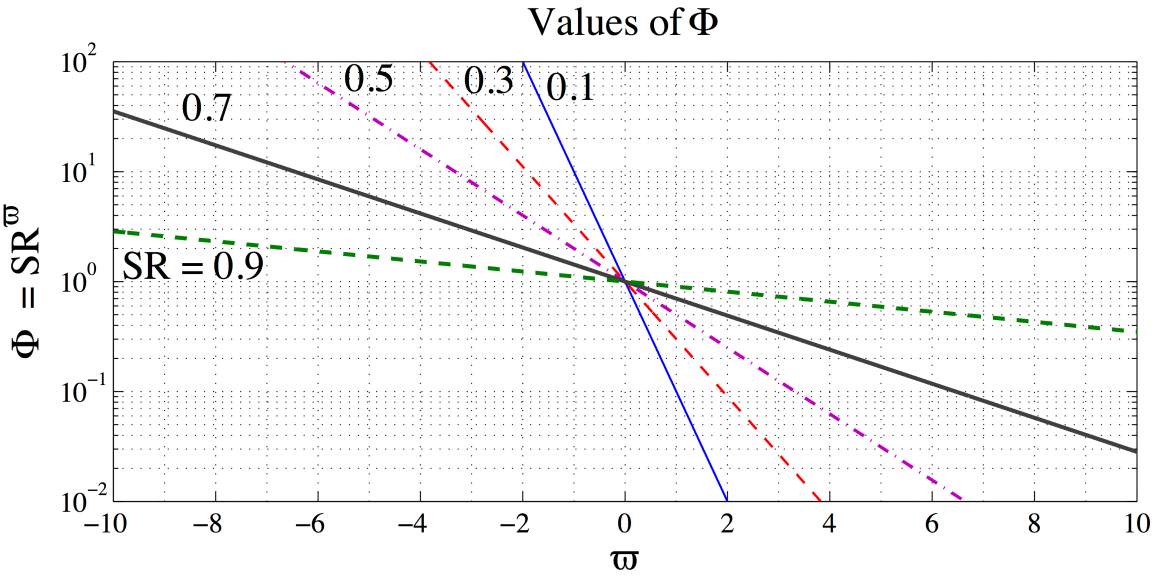

Figure 5.1 Values of $\Phi = \text{SR}^{\varpi}$, where $\text{SR} = \bar{\sigma}/\sigma_{\text{ref}}$, for stress ratios ranging from zero to one, and for ϖ varying from -10 to 10.

Figure 5.2 plots the value of $T = t/t_{\text{ref}}$, the companion to Φ in (5.25), for several values of t_{ref} and for times between 0 and 100 hours. In this figure, T is always greater than 1 for any real time, except when t_{ref} itself is greater than one. Even when $t_{\text{ref}} = 10$, T equals 1 after 10 hours. In practice, rarely is $t_{\text{ref}} > 10$ hours.

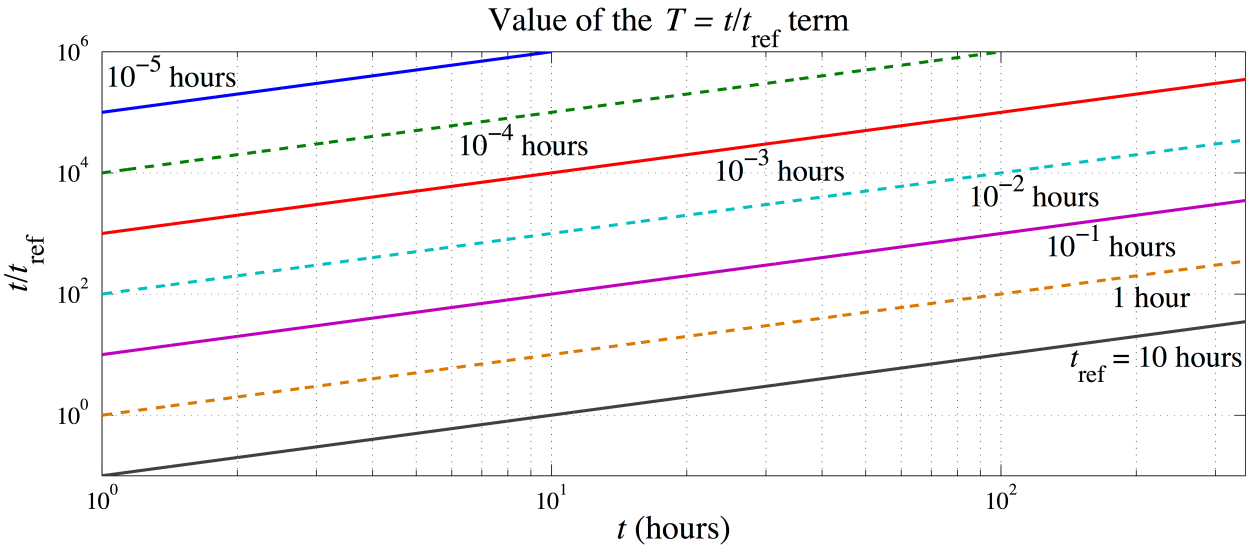

Figure 5.2 Values of $T = t/t_{\text{ref}}$ for t_{ref} values ranging from 1e-5 to 10, and for times, t, between zero and 100 hours.

A comparison of the numerical values for $\Phi = \text{SR}^{\varpi}$ and $T = t/t_{\text{ref}}$, plotted in Figures 5.1 and 5.2 respectively, shows that in most cases SR^{ϖ} is dominated by T, thus the lifetime distributions are effectively the same. This comparison is done in Figure 5.3, which plots the key part of (5.25), $(\Phi + T)\text{SR}^{\rho}$, for scaled time $T = t/t_{\text{ref}}$.

Figure 5.3 shows that, in all plotted cases, the models converge by $T = 10^4$. This convergence happens sooner for larger stress ratios (going from the top of the figure to the bottom), yet as the stress ratio increases the numerical value of $(\Phi + T)\text{SR}^{\rho}$ increases. Thus, when β is held constant, it is more likely for failures to occur at lower times with higher stress

ratios. This is also true as ρ decreases, since smaller ρ values result in larger values of $\left(\Phi+T\right)\mathrm{SR}^{\rho}$.

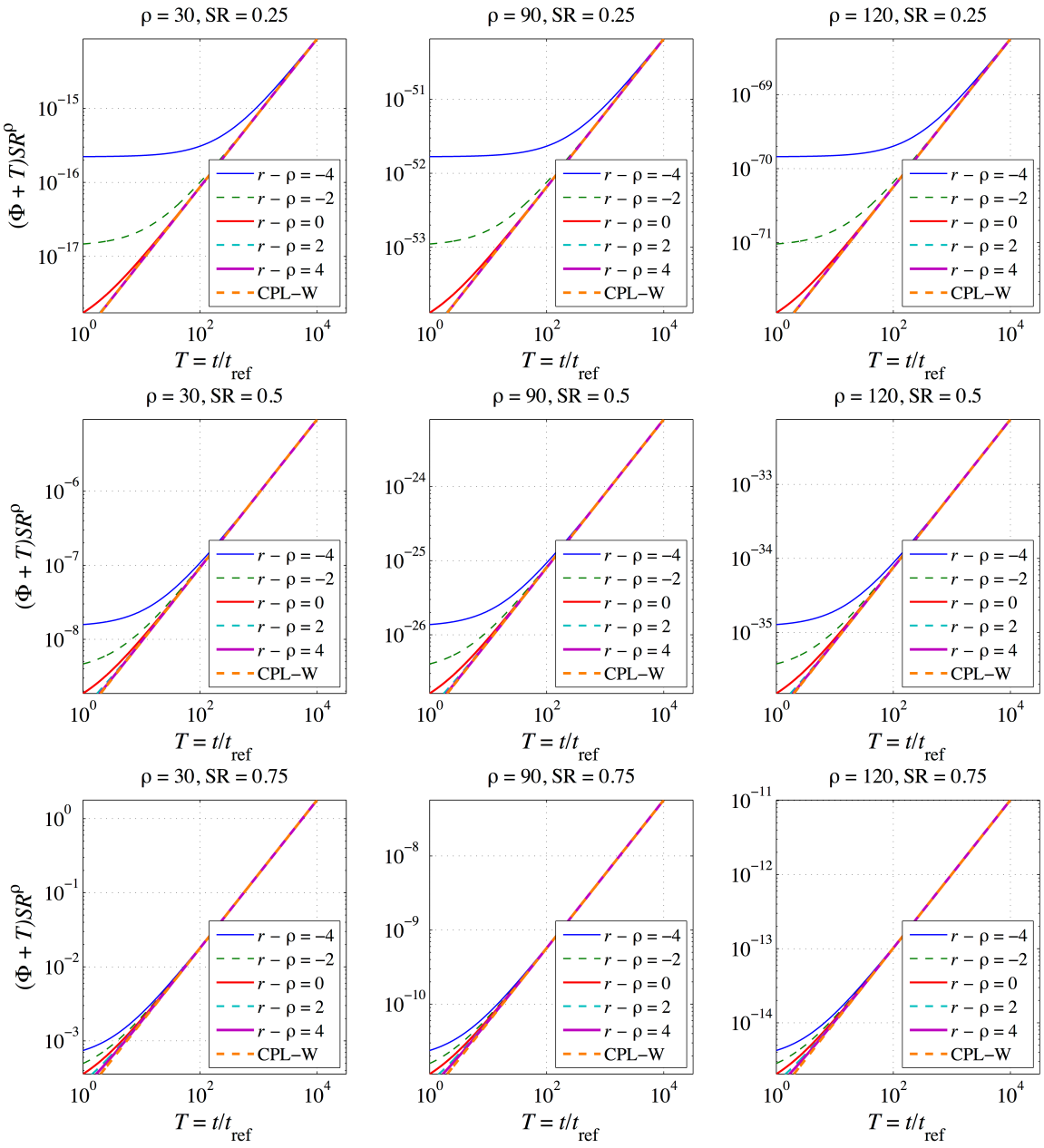

Figure 5.3 Plot of $\left(\Phi+T\right)\mathrm{SR}^{\rho}$, where $T=t/t_{\mathrm{ref}}$ and $\mathrm{SR}=\bar{\sigma}/\sigma_{\mathrm{ref}}$, for values of r including $r=\rho-2$, the crack-growth model, and $r=\rho$, the strength decay model. The term $\mathrm{SR}^{\rho}T$ is also plotted, to correspond with the CPL-W model, wherein $\Phi\equiv 0$.

In carbon fiber composites, where the design stress ratio is typically 0.5, t_{ref} is typically less than one, generally between 10^{-2} and 10^{-5}. In these cases the models mostly converge by the time $T = 10^2$, corresponding to times between 10^{-3} hours and 1 hour. Thus for carbon, under a stress ratio of interest, the models predict the same life behavior for lifetimes of interest, unless β is particularly low. A $\left(\Phi + T\right)\text{SR}^{\rho}$ value of 10^{-7}, when $\beta = 1$ corresponds to a failure probability of 10^{-7}, i.e. almost certain survival. For carbon fiber composites however, β is typically less than 0.3, and for T1000 carbon/epoxy tows can be as low as 0.07, though coupled with a much larger value of ρ, corresponding to the right column in Figure 5.3. Assuming ρ is fixed and small, for low β values the failure probability is higher, e.g. ≈ 0.01 when $\beta = 0.3$ and $\left(\Phi + T\right)\text{SR}^{\rho} = 10^{-7}$, and likely unacceptable from a design point of view. However to obtain $\left(\Phi + T\right)\text{SR}^{\rho} = 10^{-7}$ the stress ratio has to be high and the value of ρ has to be low, i.e. corresponding to the bottom of the left hand column in Figure 5.3. From the point of view of running experiments, however, the models will remain indistinguishable because the probability of getting failures in such short times is so small, even in a relatively large sample.

For Kevlar there is more difference, as t_{ref} for Kevlar may be between 1 and 10 hours, and the stress ratio may be lower, however β for Kevlar is typically greater than 1. Even for a stress ratio of 0.25 though, all models for which $r - \rho \geq -2$ agree fairly well after $T = 100$, and fully by $T = 1000$, where for Kevlar $T = 1000$ corresponds to times between 1000 and 10000 hours.

5.3.2 Comparing strength distributions

The strength distributions for the 1979 functional form, the CPL-W model, the crack-growth model and the strength decay model are given by (5.8), (3.3), (5.18) and (5.22) respectively, and can be framed as:

$$F_s(s) = 1 - \exp\left\{-\left[\left(\frac{s}{\sigma_{\text{ref}}}\right)^{\rho}\left(\Phi + \frac{s}{R\,t_{\text{ref}}(\rho+1)}\right)\right]^{\beta}\right\} \tag{5.27}$$

where the term Φ, defined in (5.26), is here a function of s.

One simplification is to assume the constraint on t_{ref} as given in (5.15), namely $\sigma_{\text{ref}} = R\,t_{\text{ref}}(\rho+1)$, which eliminates t_{ref} as an independent parameter. However, the artificiality of this is that the effect of increasing the loading rate is to change the other parameter values as well. Then Equation (5.27) simplifies to:

$$F_s(s) = 1 - \exp\left\{-\left[\left(\frac{s}{\sigma_{\text{ref}}}\right)^{\rho}\left(\Phi + \frac{s}{\sigma_{\text{ref}}}\right)\right]^{\beta}\right\}. \tag{5.28}$$

However, strictly speaking, the constraint is not a consequence of the structure of the 1979 functional form, and only naturally arises in the CPL-W model.

To help visualize (5.28), with the constraint, Figure 5.4 plots the interior quantity

$$\left(\frac{s}{\sigma_{\text{ref}}}\right)^{\rho}\left(\Phi + \frac{s}{\sigma_{\text{ref}}}\right), \tag{5.29}$$

as a function of the stress ratio, s/σ_{ref}, for several values of ρ. From Figure 5.4 it is clear that the quantity in equation (5.29) varies considerably across the different models, particularly for

low ρ values. (Note that this quantity raised to the power β is approximately the failure probability.) Also, for all models except the CPL-W model, the lines are not straight but rather have a kink around a stress ratio of one, which is typically a bit higher than the mean strength.

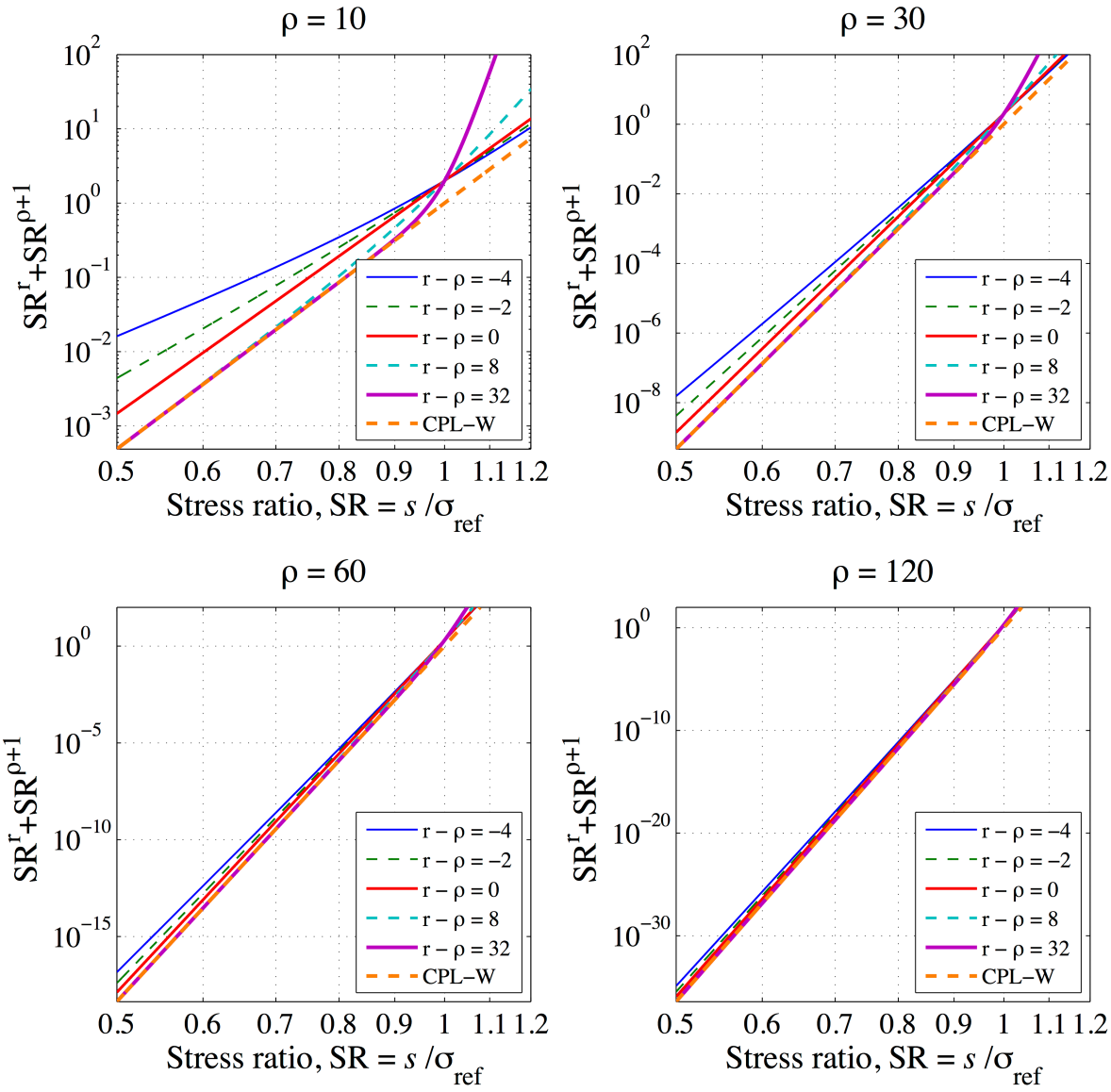

Figure 5.4 Plot of (5.29) for ρ values of a) 10, b) 30, c) 60 and d) 120, comparing the CPL-W model against various instances of the 1979 functional form, including the crack-growth model ($r - \rho = -2$) and the strength decay model ($r = \rho$).

The CPL-W model provides a lower bound to the various instances of the 1979 functional form. For stress ratios less than 1, instances of the 1979 functional form where $r-\rho$ is more negative correspond to the uppermost lines, and all models for which $r-\rho>0$ are approximately equal to the CPL-W model. In contrast, for stress ratios above 1, instances of the 1979 functional form where $r-\rho$ is larger correspond to the uppermost lines.

The constraint (5.15) is applied in Figure 5.4 and equations (5.28) and (5.29). If that constraint is removed, however, (5.27) can be restored to

$$F_s(s)=1-\exp\left\{-\left\{\left[\left(\frac{s}{\sigma_{\text{ref}}}\right)^{\rho}\left(\Phi+\frac{s}{\sigma_{\text{ref}}K}\right)\right]^{\beta}\right\}\right\} \tag{5.30}$$

where

$$K=\frac{R\,t_{\text{ref}}(\rho+1)}{\sigma_{\text{ref}}} \tag{5.31}$$

is now allowed to vary, including in the CPL-W model. Now the key interior part becomes

$$\left(\frac{s}{\sigma_{\text{ref}}}\right)^{\rho}\left(\Phi+\frac{s}{\sigma_{\text{ref}}K}\right). \tag{5.32}$$

Note that K is proportional to the loading rate, R. Experimentally the strength distribution is known to depend on the loading rate, with faster loading generally resulting in a higher experimental value for σ_{ref}.

Figure 5.5 plots (5.32) for various values of K, showing that by allowing K to vary the models become more different when $K>1$ and more similar when $K\le 1$. As before, the CPL-W model provides a lower bound on models from the 1979 functional form. It is interesting to note

that all the models collapse to the same line for small K. The largest difference between the models corresponds to large values of K, i.e. fast loading rates.

For all values of K the CPL-W model retains the same slope, and simply shifts down as K increases. The same is not true for the instances of the 1979 functional form, because while they do shift as K increases, the slope of their central straight regions varies as well. The slope has the most variation for large values of K, but once $K < 1$ the slope has converged, for all instances of the 1979 functional form, to the CPL-W model's slope.

If varying K is viewed as varying the loading rate, this implies that for the CPL-W model changing the loading rate results purely in a different value of the scale parameter. In contrast, for the 1979 models, a change in loading rate can result in both a change of the scale parameter and the shape parameter. These are general observations from Figure 5.5.

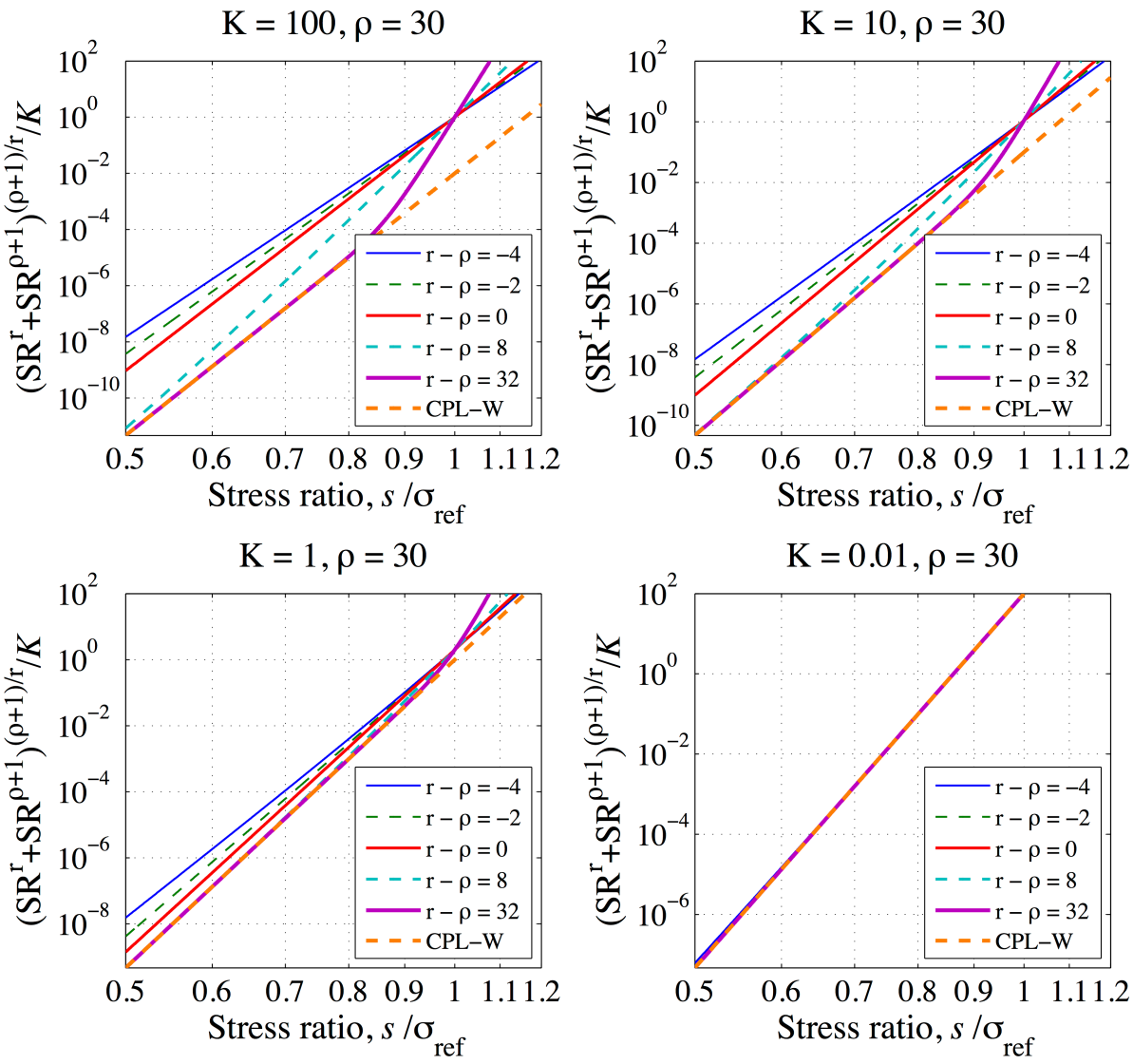

Figure 5.5 Plot of (5.32) for K values of a) 100, b) 10, c) 1, and d) 0.1, comparing the CPL-W model against various instances of the 1979 functional form, including the crack-growth model ($r-\rho=-2$) and the strength decay model ($r=\rho$), where $\rho=30$.

Focusing on the cases K = 10 and K = 100, in the upper straight regions where test data is most likely to occur, a scaling can be chosen to collapse the various instances of the 1979 functional form onto one common line, which happens to be the line for the CPL-W model. If we consider modifying (5.32) to

$$\frac{1}{K}\left[\left(\frac{s}{\sigma_{\text{ref}}}\right)^{\rho}\left(\Phi+\frac{s}{\sigma_{\text{ref}}\,K}\right)\right]^{\frac{\rho+1}{r}}, \tag{5.33}$$

which amounts to a subtle redefinition of several of the parameters, then the lines collapse to the CPL-W model (without the constraint), as desired above, at least for values of (5.33) where data is likely to be easily collected. This is shown in Figure 5.6a.

The rationale for (5.33) is that for $K>1$ the term $s/\left(\sigma_{\text{ref}}K\right)$ becomes small as compared to Φ. Thus (5.33) can be approximated by:

$$\frac{1}{K}\left[\left(\frac{s}{\sigma_{\text{ref}}}\right)^{\rho}\left(\Phi+\frac{s}{\sigma_{\text{ref}}\,K}\right)\right]^{\frac{\rho+1}{r}} \approx \frac{1}{K}\left[\left(\frac{s}{\sigma_{\text{ref}}}\right)^{\rho}\Phi\right]^{\frac{\rho+1}{r}}\left[1+\frac{1}{r}\left(\frac{s}{\Phi\,R\,t_{\text{ref}}}\right)\right]. \tag{5.34}$$

Recalling in the 1979 model that according to (5.26) $\Phi=\left(s/\sigma_{\text{ref}}\right)^{r-\rho}$, and by (5.31) $K=R\,t_{\text{ref}}\left(\rho+1\right)/\sigma_{\text{ref}}$, (5.34) becomes

$$\begin{aligned}
&\frac{1}{K}\left[\left(\frac{s}{\sigma_{\text{ref}}}\right)^{\rho}\Phi\right]^{\frac{\rho+1}{r}}\left[1+\frac{s}{\Phi\,r\,R\,t_{\text{ref}}}\right] \\
&\qquad=\frac{\sigma_{\text{ref}}}{R\,t_{\text{ref}}\left(\rho+1\right)}\left(\frac{s}{\sigma_{\text{ref}}}\right)^{\rho+1}\left[1+\left(\frac{s}{\sigma_{\text{ref}}}\right)^{\rho+1-r}\frac{\sigma_{\text{ref}}}{r\,R\,t_{\text{ref}}}\right], \\
&\qquad\approx\frac{\sigma_{\text{ref}}}{R\,t_{\text{ref}}\left(\rho+1\right)}\left(\frac{s}{\sigma_{\text{ref}}}\right)^{\rho+1}
\end{aligned} \tag{5.35}$$

which is the CPL-W model's interior term. This approximation works well so long as $r-\rho<30$, as can be seen in Figure 5.6a. Whether or not $r-\rho<30$ corresponds to a physical material is unknown.

A different scaling can be done to instead scale the lower straight regions in Figure 5.5, as can be seen in Figure 5.6b. This scaling was done by trial and error.

The implication of Figure 5.6 for $K > 1$, along with Figure 5.5 for $K < 1$, is that all of the models can still be said to have Weibull distributed strength as far as is likely to be discriminated from even a large practical dataset. If one fits a Weibull distribution to experimental data, the Weibull shape and scale parameter values estimated are the same irrespective of any model subtleties. How the values of these estimated parameters will relate to the various model parameters σ_{ref}, r, ρ, β, and t_{ref}, will differ among the models. In particular, for the CPL-W model σ_{ref} is the inherent Weibull scale parameter, yet for the 1979 functional form σ_{ref} varies as a function of K.

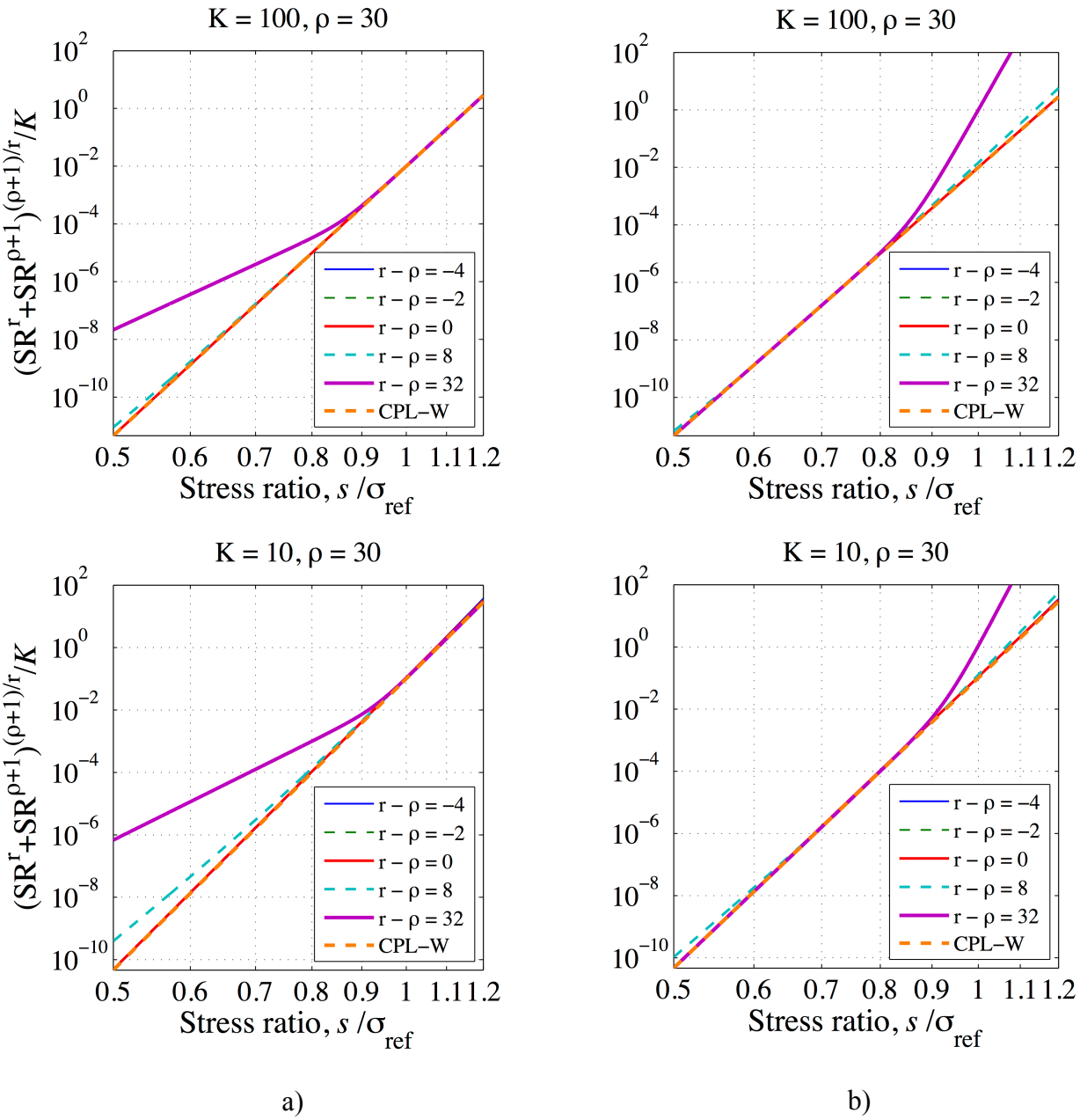

Figure 5.6 Plot of (5.33) for K values of 100, and 10, comparing the CPL-W model against various instances of the 1979 functional form, including the crack-growth model ($r-\rho=-2$) and the strength decay model ($r=\rho$), where $\rho=30$. In a) the upper portions are collapsed, whereas in b) the lower portions are collapsed.

5.4. Proof Testing

In applications, all COPVs typically undergo some form of proof testing (which may be combined with autofrettage), thus model behavior under proof testing is of interest.

In idealized proof testing, the load profile is assumed to be:

$$\begin{aligned} &\sigma(t)=\sigma_p,\ 0\le t<t_p \\ &\sigma(t)=\bar{\sigma},\ t_p\le t \end{aligned}, \tag{5.36}$$

where $t_p>0$ is the proof hold time, $\sigma_p>0$ is the proof load level, and $\sigma_p>\bar{\sigma}$. (In reality there are ramp up and down times, however these have a small effect compared to the proof hold time, largely because of the division by $\rho+1$, as appears in the derivation of equation (5.8).)

The general cumulative distribution function for failure probability of the 1979 functional form is given in (5.6). In the case involving a proof test, substituting (5.36) into (5.6) gives the key quantity in the exponential as:

$$\sup_{0\le\tau\le t}\left[\left(\frac{\sigma(t)}{\sigma_{\text{ref}}}\right)^r+\int_0^t\left(\frac{\sigma(\tau)}{\sigma_{\text{ref}}}\right)^\rho\frac{d\tau}{t_{\text{ref}}}\right]^\beta=\begin{cases}\left(\dfrac{\sigma_p}{\sigma_{\text{ref}}}\right)^r+\left(\dfrac{\sigma_p}{\sigma_{\text{ref}}}\right)^\rho\dfrac{t}{t_{\text{ref}}}, & 0\le t\le t_p \\ \left(\dfrac{\sigma_p}{\sigma_{\text{ref}}}\right)^r+\left(\dfrac{\sigma_p}{\sigma_{\text{ref}}}\right)^\rho\dfrac{t_p}{t_{\text{ref}}}, & t_p\le t\le t_s \\ \left(\dfrac{\bar{\sigma}}{\sigma_{\text{ref}}}\right)^r+\left(\dfrac{\sigma_p}{\sigma_{\text{ref}}}\right)^\rho\dfrac{t_p}{t_{\text{ref}}}+\left(\dfrac{\bar{\sigma}}{\sigma_{\text{ref}}}\right)^\rho\dfrac{t-t_p}{t_{\text{ref}}}, & t\ge t_s \end{cases} \tag{5.37}$$

where t_s is called a 'safe time' as will be described below. The existence of this safe time leads to three distinct time regimes in (5.37), despite there being only two load levels. When the load drops from σ_p to $\bar{\sigma}$ at time t_p, the first term on the left side in (5.37), $\left(\sigma(t)/\sigma_{\text{ref}}\right)^r$, decreases in value, but the accumulated value of the left side cannot decrease since the cumulative

probability of failure cannot decrease. This requirement is mathematically accounted for by using the 'supremum' operator, which essentially means the maximum value achieved up to the given time. It takes some additional time for the left-hand side to increase beyond the value it had at time t_p, i.e. the integral term must accumulate enough to compensate for the decrease in the first term due to the reduction of $\sigma(t)$. This amount of time can be found by equating the middle and last quantities in (5.37) and letting $t = t_s$, giving

$$\left(\frac{\sigma_p}{\sigma_{\text{ref}}}\right)^r + \left(\frac{\sigma_p}{\sigma_{\text{ref}}}\right)^\rho \frac{t_p}{t_{\text{ref}}} = \left(\frac{\bar{\sigma}}{\sigma_{\text{ref}}}\right)^r + \left(\frac{\sigma_p}{\sigma_{\text{ref}}}\right)^\rho \frac{t_p}{t_{\text{ref}}} + \left(\frac{\bar{\sigma}}{\sigma_{\text{ref}}}\right)^\rho \frac{t_s - t_p}{t_{\text{ref}}}. \tag{5.38}$$

Solving for t_s yields

$$\begin{aligned} t_s &= t_{\text{ref}} \left(\frac{\bar{\sigma}}{\sigma_{\text{ref}}}\right)^{-\rho} \left[\left(\frac{\sigma_p}{\sigma_{\text{ref}}}\right)^r - \left(\frac{\bar{\sigma}}{\sigma_{\text{ref}}}\right)^r\right] + t_p \\ &= t_{\text{ref}} \left(\frac{\bar{\sigma}}{\sigma_{\text{ref}}}\right)^{r-\rho} \left[\left(\frac{\sigma_p}{\bar{\sigma}}\right)^r - 1\right] + t_p \end{aligned} \tag{5.39}$$

Thus in the 1979 functional form the cumulative distribution function for time to failure, under the loading given by (5.36), is:

$$F_{1979\,p}(t)=\begin{cases} 1-\exp\left\{-\left[\left(\dfrac{\sigma_p}{\sigma_{\text{ref}}}\right)^{r}+\left(\dfrac{\sigma_p}{\sigma_{\text{ref}}}\right)^{\rho}\dfrac{t}{t_{\text{ref}}}\right]^{\beta}\right\}, & 0<t\le t_p \\ 1-\exp\left\{-\left[\left(\dfrac{\sigma_p}{\sigma_{\text{ref}}}\right)^{r}+\left(\dfrac{\sigma_p}{\sigma_{\text{ref}}}\right)^{\rho}\dfrac{t_p}{t_{\text{ref}}}\right]^{\beta}\right\}, & t_p<t\le t_s \\ 1-\exp\left\{-\left[\left(\dfrac{\bar{\sigma}}{\sigma_{\text{ref}}}\right)^{r}+\left(\dfrac{\sigma_p}{\sigma_{\text{ref}}}\right)^{\rho}\dfrac{t_p}{t_{\text{ref}}}+\left(\dfrac{\bar{\sigma}}{\sigma_{ref}}\right)^{\rho}\dfrac{t-t_p}{t_{\text{ref}}}\right]^{\beta}\right\}, & t>t_s \end{cases} \quad (5.40)$$

where t_s is given in (5.39).

The time t_s is frequently termed the '*safe time*', as the cumulative failure probability does not increase for $t_p < t \le t_s$, thus the probability that a specimen that has survived to time t_p fails inside this range is zero, i.e. the specimens are safe from failures. The length of $t_s - t_p$ increases as the ratio of proof load to sustained load, $\sigma_p / \bar{\sigma}$, increases, and as ρ increases, yet it decreases as r increases.

The magnitude of this safe time can be extremely large in some cases. For instance, for $\rho = 100$, a proof ratio of $\sigma_p / \bar{\sigma} = 1.5$, a lifetime stress ratio of $\bar{\sigma} / \sigma_{\text{ref}} = 0.5$, and $r - \rho \le 40$, then the scaled safe time, t_s / t_{ref}, is predicted to be at least 100,000. However, for $\rho = 100$ and $r - \rho \ge 60$ the scaled safe time becomes negligible.

In contrast to the general 1979 functional form and instances thereof, the CPL-W model (with or without the constraint on t_{ref} as given in (5.15)) has the cumulative distribution function for time to failure, with loading given by (5.36), of:

$$F_{\text{CPL-W}\,p}(t)=\begin{cases} 1-\exp\left\{-\left[\left(\dfrac{\sigma_p}{\sigma_{\text{ref}}}\right)^{\rho}\dfrac{t}{t_{\text{ref}}}\right]^{\beta}\right\}, & 0<t\le t_p \\ 1-\exp\left\{-\left[\left(\dfrac{\sigma_p}{\sigma_{\text{ref}}}\right)^{\rho}\dfrac{t_p}{t_{\text{ref}}}+\left(\dfrac{\bar{\sigma}}{\sigma_{\text{ref}}}\right)^{\rho}\dfrac{t-t_p}{t_{\text{ref}}}\right]^{\beta}\right\}, & t>t_p \end{cases}, \tag{5.41}$$

which has no safe time, but does have a decreased rate of failure for some time after the proof test. Note that for $\sigma(t)<\sigma_{\text{ref}}$, relevant to stress rupture, the CPL-W model can be obtained from the 1979 functional form by letting $r-\rho\to\infty$.

5.4.1 Comparing model behavior in the case of proof testing

The biggest difference between the models, in the case of proof testing, is the behavior of the safe time t_s. Shortly after t_s, all instances of the 1979 functional form, created by varying the value of $r-\rho$, converge to the CPL-W model. Furthermore, the CPL-W model provides a lower bound on the cumulative failure probability, as can be seen in Figure 5.7.

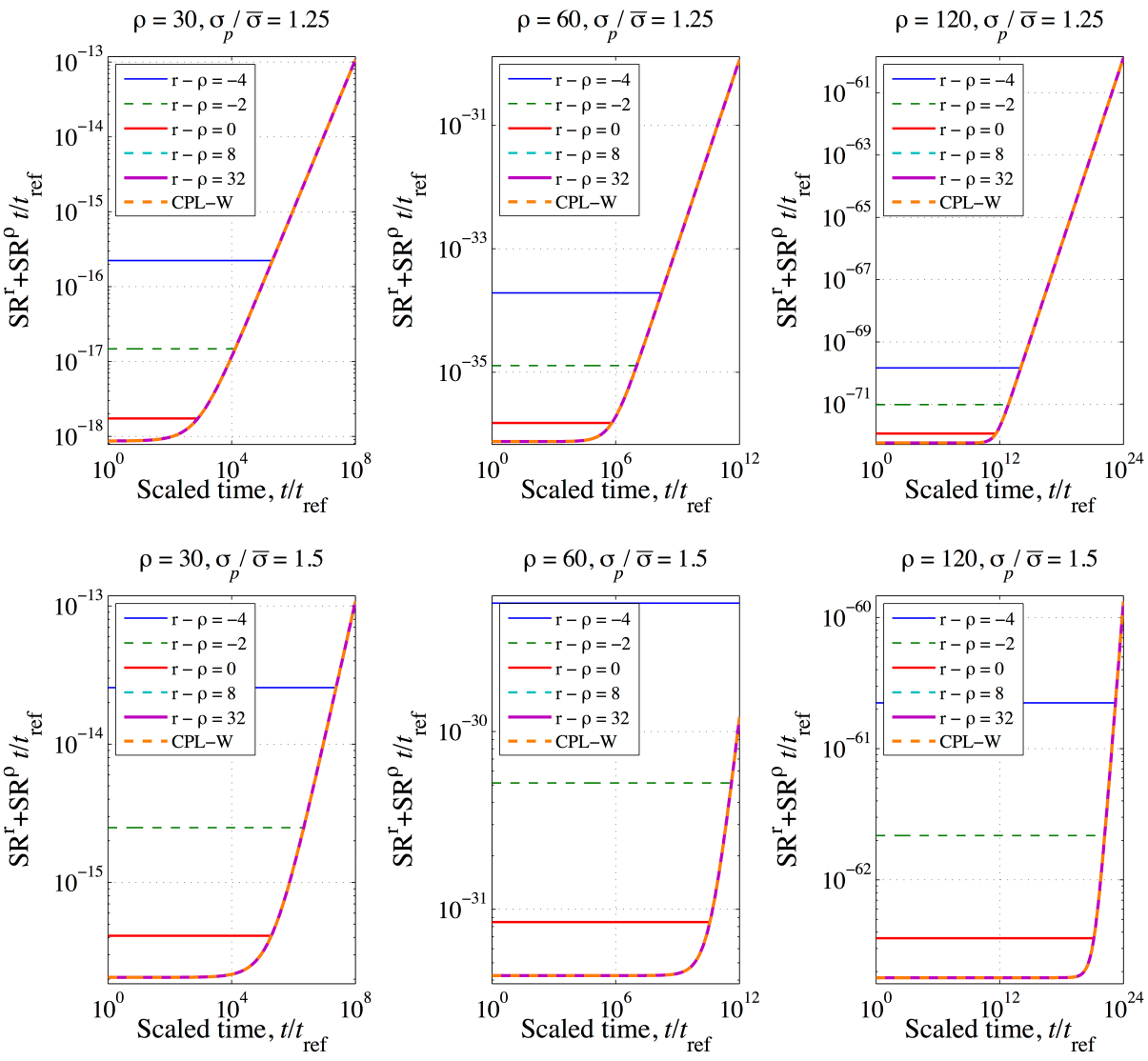

Figure 5.7 Plots of (5.40) and (5.41) for varying values of ρ and $\sigma_p / \bar{\sigma}$, where $\bar{\sigma}/\sigma_{\text{ref}} = 0.5$ and $T_p = t_p / t_{\text{ref}} = 1$, for scaled time $T = t/t_{\text{ref}}$.

In Figure 5.7 the 1979 functional form instances remain flat until $T > T_s = t_s / t_{\text{ref}}$, at which point they sharply increase, and quickly converge to the CPL-W model. As ρ increases, the value of T_s also increases. For instance when $\sigma_p / \bar{\sigma} = 1.5$ and $\rho = 90$, we find that $T_s > 10^{10}$, which corresponds to a time between 10^5 hours and 10^{11} hours, depending on the particular

value of t_{ref}. The sensitivity of T_s to the parameters $\sigma_p / \bar{\sigma}$, ρ, and r can be seen from Figure 5.7. Intuitively what Figure 5.7 is illustrating is that once T_s is known, one can sketch the behavior of each of the models by first drawing the line for the CPL-W model, calculating T_s, and then drawing a horizontal line that intersects the CPL-W line at exactly T_s.

5.4.2 Conditional reliability

The reliability, $R(t)$, for a specimen is defined as one minus the failure probability, $F(t)$, and conditional reliability following a proof test, $R_p(t|\sigma_p)$, is defined as the reliability given that this specimen has survived a proof test. This is, practically, a very useful concept as only COPVs that survive their proof tests can be used. Symbolically, the conditional probability can be calculated using Bayes theorem as:

$$R_p(t|\sigma_p) = \frac{R(t)}{R(t_p)} = \frac{1-F(t)}{1-F(t_p)}. \tag{5.42}$$

For the 1979 functional form, and thus the crack-growth and strength decay models, the reliability at $t > t_p$ given survival of the proof test, is:

$$R_{1979\,p}(t) = \begin{cases} 1, & t_p < t \le t_s \\ \dfrac{\exp\left\{-\left[\left(\dfrac{\bar{\sigma}}{\sigma_{\text{ref}}}\right)^r + \left(\dfrac{\sigma_p}{\sigma_{\text{ref}}}\right)^\rho \dfrac{t_p}{t_{\text{ref}}} + \left(\dfrac{\bar{\sigma}}{\sigma_{ref}}\right)^\rho \dfrac{t-t_p}{t_{\text{ref}}}\right]^\beta\right\}}{\exp\left\{-\left[\left(\dfrac{\sigma_p}{\sigma_{\text{ref}}}\right)^r + \left(\dfrac{\sigma_p}{\sigma_{\text{ref}}}\right)^\rho \dfrac{t_p}{t_{\text{ref}}}\right]^\beta\right\}}, & t > t_s \end{cases} \tag{5.43}$$

or

$$R_{1979\,p}(t)=\begin{cases} 1, & t_p < t \le t_s \\ \exp\left\{\left[\left(\dfrac{\sigma_p}{\sigma_{\text{ref}}}\right)^r+\left(\dfrac{\sigma_p}{\sigma_{\text{ref}}}\right)^\rho\dfrac{t_p}{t_{\text{ref}}}\right]^\beta-\left[\left(\dfrac{\bar{\sigma}}{\sigma_{\text{ref}}}\right)^r+\left(\dfrac{\sigma_p}{\sigma_{\text{ref}}}\right)^\rho\dfrac{t_p}{t_{\text{ref}}}+\left(\dfrac{\bar{\sigma}}{\sigma_{ref}}\right)^\rho\dfrac{t-t_p}{t_{\text{ref}}}\right]^\beta\right\}, & t < t_s \end{cases}$$

(5.44)

For the CPL-W model the conditional reliability for times, t, greater than t_p is given by:

$$\begin{aligned} R_{\text{CPL-W}\,p}(t) &= \exp\left\{\left[\left(\frac{\sigma_p}{\sigma_{\text{ref}}}\right)^\rho\frac{t_p}{t_{\text{ref}}}\right]^\beta-\left[\left(\frac{\sigma_p}{\sigma_{\text{ref}}}\right)^\rho\frac{t_p}{t_{\text{ref}}}+\left(\frac{\bar{\sigma}}{\sigma_{\text{ref}}}\right)^\rho\frac{t-t_p}{t_{\text{ref}}}\right]^\beta\right\} \\ &= \exp\left\{\left[\left(\frac{\sigma_p}{\sigma_{\text{ref}}}\right)^\rho\frac{t_p}{t_{\text{ref}}}\right]^\beta\left(1-\left[1+\left(\frac{\bar{\sigma}}{\sigma_p}\right)^\rho\frac{t-t_p}{t_p}\right]\right)^\beta\right\}, \quad t > t_p \end{aligned} \qquad (5.45)$$

Plots of these conditional reliabilities are given in Figures 5.8 and 5.9, for values of $\sigma_p/\bar{\sigma}$ of 1.5, 1.25 and 1. In the last case, a proof test equivalent to the lifetime loading is the same as the reliability conditional on the vessel surviving loading to the lifetime load. This is the reliability of practical interest, as no vessel in service will be used if it does not survive its initial loading.

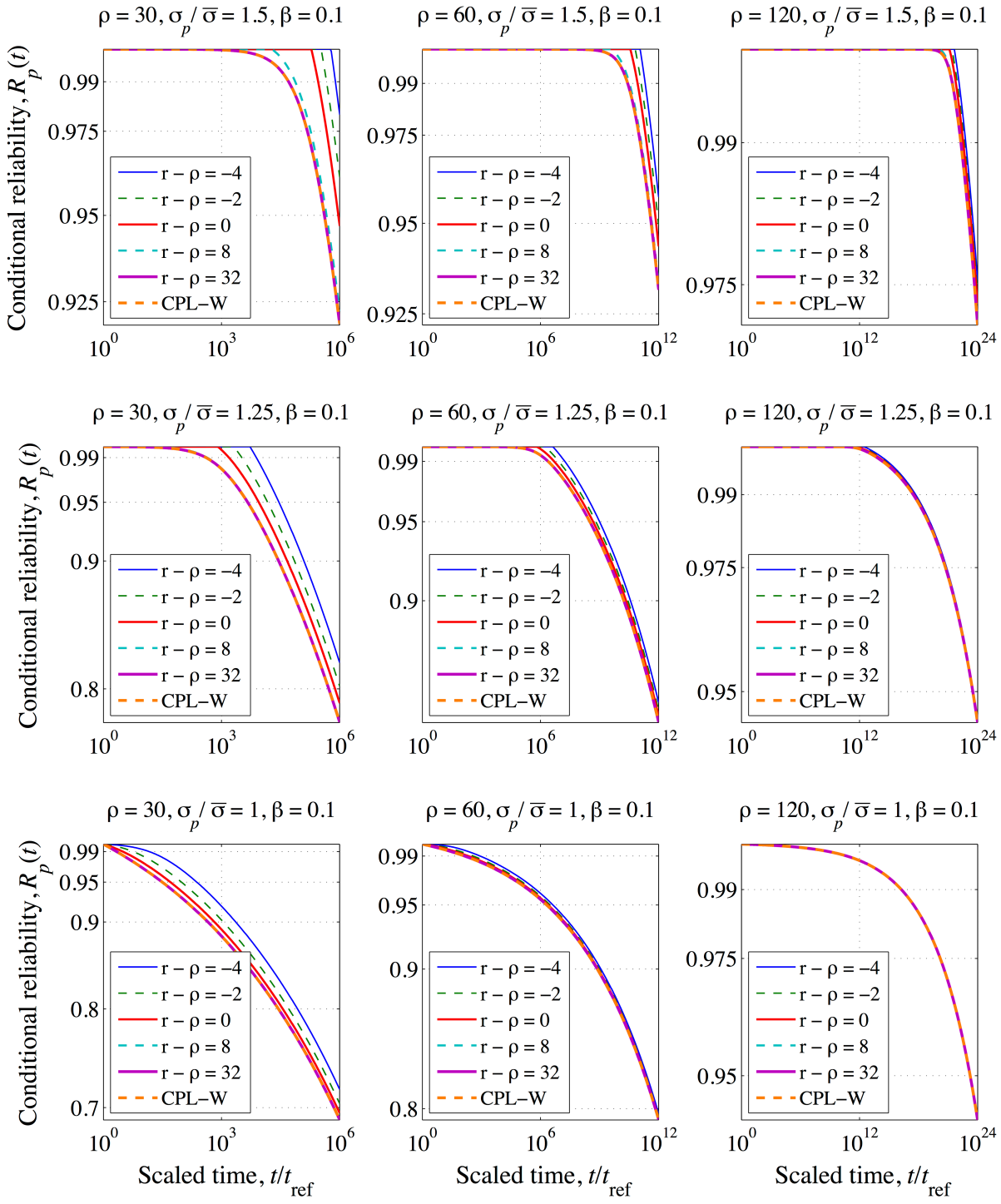

Figure 5.8 Plot of conditional reliabilities (5.43) and (5.45) for varying values of ρ and $\sigma_p / \bar{\sigma}$, where $\bar{\sigma}/\sigma_{\text{ref}} = 0.5$, $T_p = t_p/t_{\text{ref}} = 1$, and $\beta = 0.1$, for scaled time $T = t/t_{\text{ref}}$.

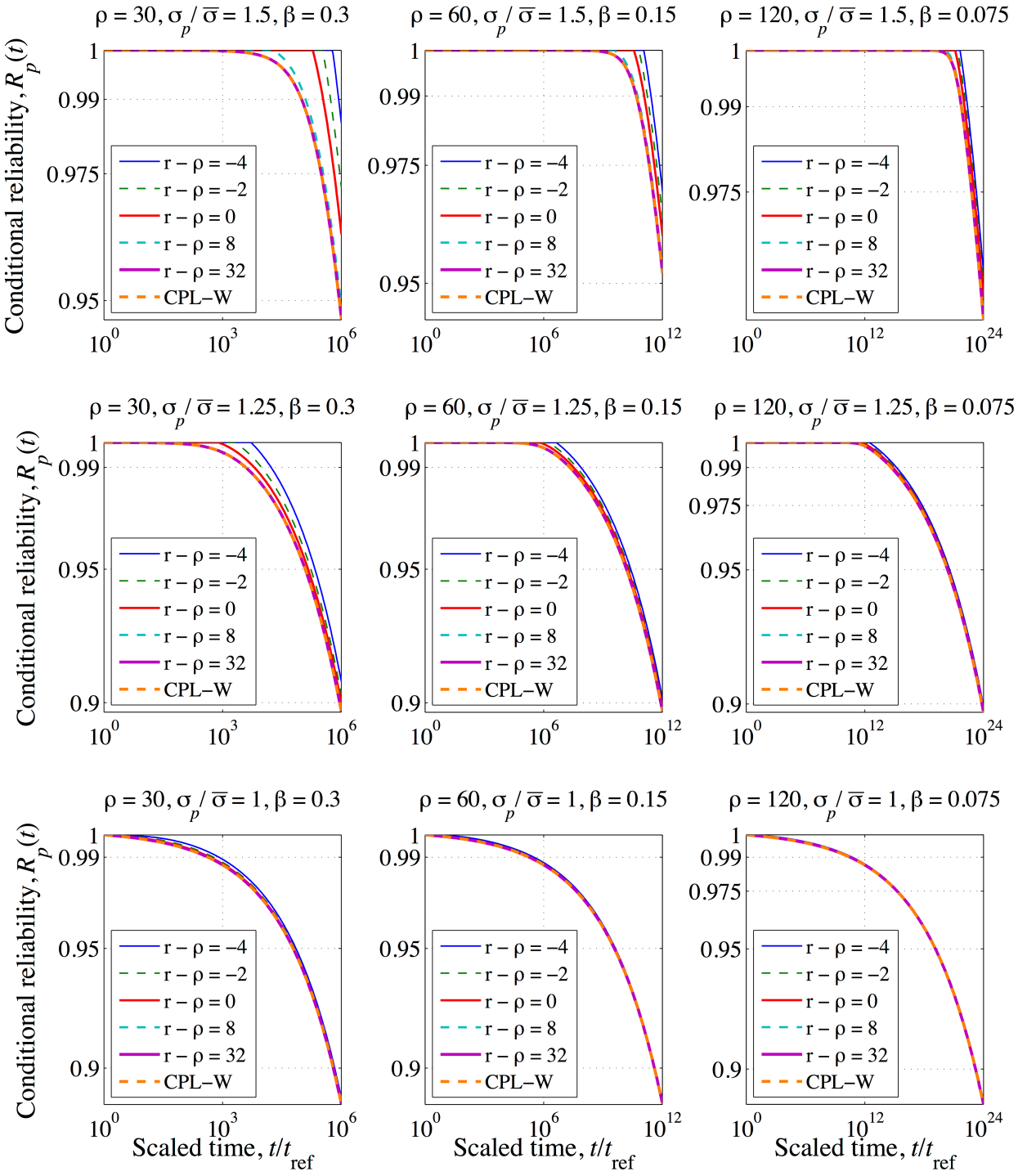

Figure 5.9 Plot of conditional reliabilities (5.43) and (5.45) for varying values of ρ, β, and $\sigma_p / \bar{\sigma}$, where $\rho\beta = 9$, $\bar{\sigma}/\sigma_{\text{ref}} = 0.5$, and $T_p = t_p/t_{\text{ref}} = 1$, for scaled time $T = t/t_{\text{ref}}$.

In Figure 5.8 β is set at 0.1, and ρ varies. In contrast, in Figure 5.9 the product $\rho\beta$ is considered to be a constant, specifically $\rho\beta = 9$, in keeping with an approximately constant Weibull shape parameter for strength. The value for β is then calculated based on the varying ρ value. This study focuses on the case $\beta \leq 1$.

Figure 5.8 shows that the models give remarkably similar results for large ρ values, with the differences between models becoming greater as ρ decreases. Increasing the proof ratio, $\sigma_p / \bar{\sigma}$, increases the conditional reliability in these models, assuming that $\beta \leq 1$. The CPL-W always provides a lower bound on instances of the 1979 functional form, thus the CPL-W is the most conservative, of the models considered, in its conditional reliability predictions.

Figure 5.9 is very similar to Figure 5.8, but shows that for a constant strength distribution, and thus a constant value of $\rho\beta$, as the value of β increases the differences between the models increase. In contrast, if $\rho\beta$ is allowed to vary, then as the value of β increases the differences between the models decrease as then the variability inherent in the material is being reduced. As before in Figure 5.8, increasing the proof ratio increases the amount of difference between models.

To fully see how the conditional reliabilities relate across values of $\sigma_p / \bar{\sigma}$ as well as to the original lifetime reliability, Figure 5.10 plots reliabilities for the CPL-W model. In Figure 5.10 the unconditional lifetime reliability is lowest, followed by the conditional reliabilities for increasing values of $\sigma_p / \bar{\sigma}$. These conditional reliabilities are also shown in Figure 5.8, on separate axes.

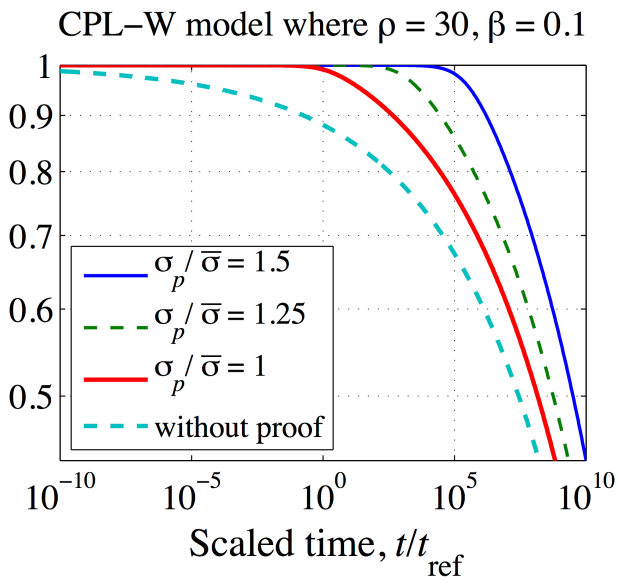

Figure 5.10 Unconditional lifetime reliability and conditional reliabilities for the CPL-W model with $\rho = 30$ and $\beta = 0.1$, for $\sigma_p / \bar{\sigma}$ values of 1.5, 1.25 and 1, and where $\bar{\sigma}/\sigma_{\text{ref}} = 0.5$, and $t_p/t_{\text{ref}} = T_p = 1$, for scaled time $T = t/t_{\text{ref}}$.

The difference between the reliability without a proof test vs. when $\sigma_p / \bar{\sigma} = 1$ is that the second case is conditional on surviving the service load level, $\bar{\sigma}$, that might have been applied to a COPV before placement in a system, even if it was not a true proof test with $\sigma_p > \bar{\sigma}$.

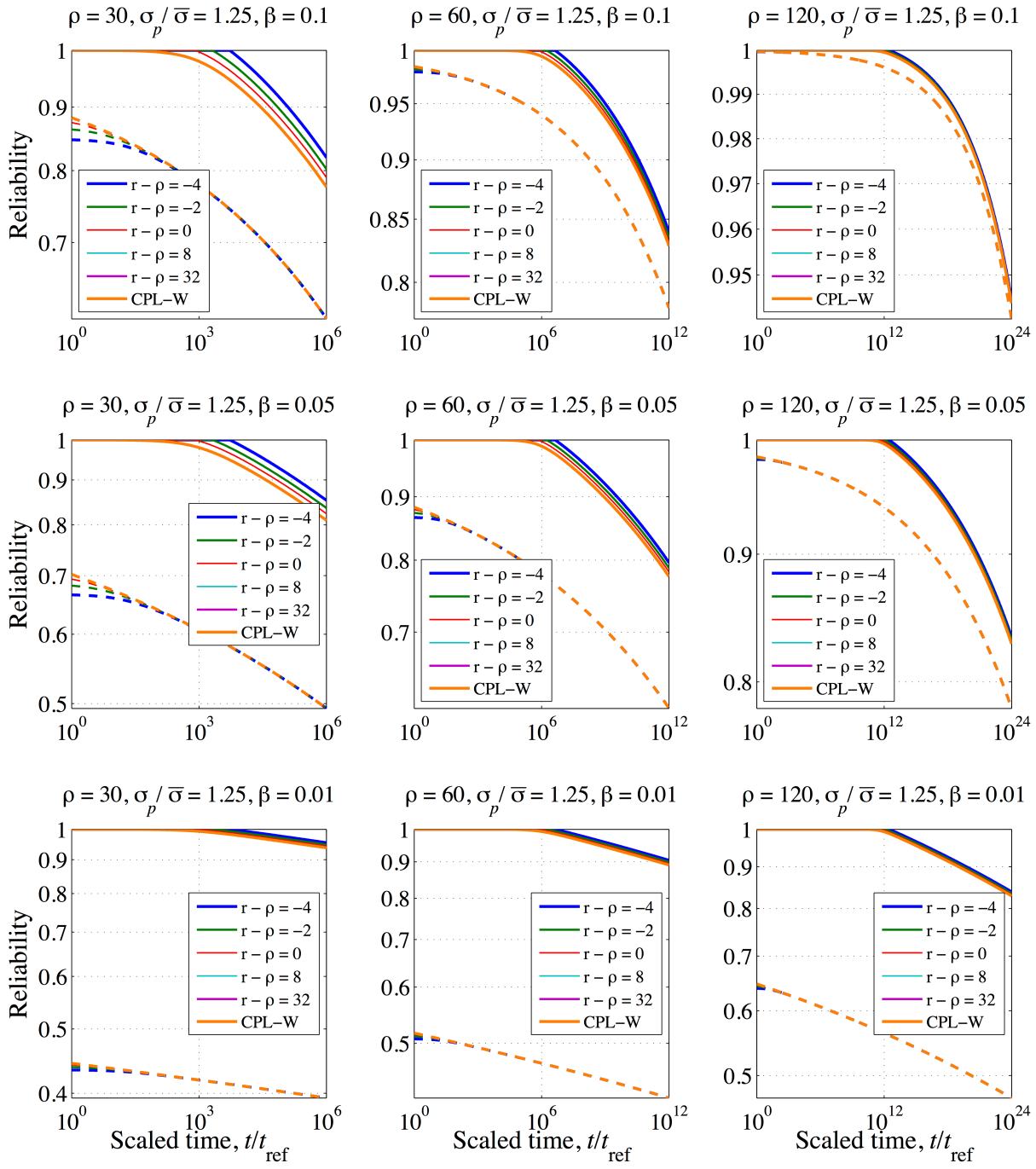

Figure 5.11 Plot of conditional reliabilities (5.43) and (5.45), in solid lines, and sustained lifetime reliabilities (3.10) and (5.25), in dashed lines, for varying values of ρ and β, where $\bar{\sigma}/\sigma_{\text{ref}} = 0.5$, $t_p/t_{\text{ref}} = T_p = 1$, and $\sigma_p/\bar{\sigma} = 1.25$, for scaled time $T = t/t_{\text{ref}}$.

In comparing the plots for long term relability, the conditional reliabilities are larger than or equal to the reliabilities for a constant lifetime load of $\bar{\sigma}/\sigma_{\text{ref}} = 0.5$ (without a proof test). This can be seen in Figure 5.10 in the particular case of the CPL-W model. This is further shown in Figure 5.11 for β values of 0.1, 0.05 and 0.01, where the conditional reliability is shown with the solid lines and the reliability for a simple sustained load is shown in dashed lines.

For larger values of β, all of the models predict indistinguishable conditional reliabilities, as well as indistinguishable reliabilities under sustained loads (without proof testing). In the case where $\beta > 1$, as in composites using polymer fibres such as Kevlar, Vectran and Zylon, the conditional reliabilities and unconditional reliability for a simple sustained load may actually switch places, such that the conditional reliability is less than the sustained load reliability. However carbon fibers are currently more widely used, due to their higher strength, and in carbon $\beta \ll 1$. In this case the conditional reliabilities following a proof test are always higher than the sustained load reliabilities.

Figure 5.11 shows how the difference between the conditional reliability and the reliability for a sustained load increases as β decreases and as ρ increases, as seen before in Figures 5.8 and 5.9. The effect of holding $\rho\beta$ fixed and varying ρ can be seen by comparing the first two figures in the first row with the second two of the second row: the models become more similar as ρ is increased, holding $\rho\beta$ fixed, the difference between the conditional reliabilities and the sustained lifetime reliabilities is similar, but the time scale over which the plots take place is doubled. Figure 5.11 also shows that the difference between the conditional reliability and the reliability for a sustained load also increases as $\sigma_p / \bar{\sigma}$ increases, as expected.

5.5. Discussion

The 1979 functional form, its two particular instances, the crack-growth model and the strength decay model, and the CPL-W model (a limiting case of the 1979 functional form) are more similar than different. The differences between the models focus on the relationship between the strength distribution and the lifetime distribution, and the concept of a 'safe time' after a proof test.

Assuming the models all have similar lifetime distributions, and thus the parameters σ_{ref}, ρ, β, and t_{ref} are consistent across the models, the strength distributions will not be equivalent unless the parameter ρ happens to be quite high, >100. These strength distributions can be collapsed onto one another by choosing different values of the parameters depending on the model.

Experimental evidence shows that the observed strength increases with increased loading rate. All of the models under consideration show this behavior, so long as $t_{\text{ref}} \ll \sigma_{\text{ref}} / (R\rho)$. Otherwise in equation (5.27) the last term will become dominated by the first term, for all models other than the CPL-W model, which eliminates the sensitivity to the loading rate.

Under a simple sustained load, the CPL-W model gives the most optimistic reliability, relative to the other models. In contrast, the CPL-W model gives the most conservative conditional reliability following a proof test. Furthermore, under a sustained load, instances of the 1979 functional form where the quantity $r - \rho$ is more negative give the most conservative reliability, relative to the other models. In contrast, these instances of the 1979 functional form give the most optimistic conditional reliability following a proof test.

All instances of the 1979 functional form have a 'safe time' after a proof test – a time for which the conditional reliability is one. The CPL-W model, being the limit of the 1979 functional form, does not have a true 'safe time', though it does have a decreased rate of failure. According to these models, the safe time can account for the entire desired service life of a specimen.

There is experimental evidence suggesting that for materials where $\beta \ll 1$, the conditional reliability after a proof test can quickly become lower than the reliability at a sustained load. Furthermore, proof testing is known to do damage to the composite, and the occurance of this damage may cancel out any benefits from weeding out weak vessels This concept has great practical importance, yet it is not predicted by any of the models considered in this paper when $\beta \ll 1$, despite there being as many as five parameters. On the other hand, none of these models have a strong physical basis in the micro-mechanics of a composite structure. It is quite possible that all of the current models have shortcomings in predicting composite behavior for load profiles more complex than a sustained or linearly increasing load, or when an excessively high proof load is used.

Determining the conditional reliability after a proof test is an important question. Current models predict only benefits from proof testing, yet they disagree on how much of a benefit. In reality, a proof testing at a high stress level runs the risk of breaking a lot of fibers, which ultimately cannot be good. For the models discussed however, either there is no safe time, or the safe time may encompass the entirety of service life. Either prediction may not be consistent with the experimental evidence.

5.6. Conclusions

The models compared in this paper exhibit many similar characteristics. The only

distinguishing differences between the models tend to be for unrealistic materials or in portions of the distribution where failure is unlikely for typical experimental sample sizes. While these models have a lot of flexibility, none of them allow for the possibility that a proof test may damage the composite through excessive fiber failure to the point where the conditional reliability decreases comparatively rapidly to values below that for a non proof tested specimen.

The current experimental data is not sufficient to determine which of these models may be most accurate. Furthermore there is reason to believe that none of the models accurately predict composite reliability under complex load profiles such as proof tests. None of the models compared here are based in the micro-mechanics of a composite structure, thus there is a need for a micro-mechanics inspired model to deal with the question of proof testing and, in the process, unintended fiber breakage.

REFERENCES

[31] Glasstone, K.J. Laidler and H. Erying, The Theory of Rate Processes. McGraw-Hill, New York (1941)

[32] Phoenix SL (1978) The asymptotic time to failure of a mechanical system of parallel members. SIAM J. Appl. Math 34:227-246

[33] Freudenthal A.M. (1973) Fatigue and fracture mechanics. Eng Fract Mech 2:403-414

[34] Taylor H.M. (1987) A model for the failure process of semicrystalline polymer materials under static fatigue. Prob Eng Inf Sci 1:133-162

[35] Phoenix SL (1982) Statistical modeling of the time and temperature dependent failure of fibrous composites. *Proceedings of the 9th U.S. National Congress of Applied Mechanics*. American Society of Mechanical Engineers

[36] Phoenix SL, Kuo CC (1983) Recent advances in statistical and micromechanical modeling of time dependent failure of fibrous composites. 1983 Advances in Aerospace Structures, Materials and Dynamics – AD-06 ASME Book No. H00272

[37] Tierney, L.-J. (1984). A probability model for the time to fatigue failure of a fibrous composite with local load sharing. Stoch. Processes and Their Applic. 18: 1-14

[38] Newman WI, Phoenix SL (2001) Time-dependent fiber bundles with local load sharing. Phys. Rev. E 63: 021507

[39] Phoenix SL, Newman WI (2009) Time-dependent fiber bundles with local load sharing. II. General Weibull fibers. Phys. Rev. E 80: 066115

[40] Zhurkov, S.N. (1965). Kinetic concept of the strength of solids. International J. of Fracture Mechanics 1: 311-323.

[41] Wu, H.F., Phoenix, S.L. & Schwartz, P. (1988) Temperature dependence of lifetime statistics for single Kevlar 49 filaments in creep-rupture J Mater Sci 23: 1851-1860

CHAPTER 6

STOCHASTIC FIBER BREAKAGE MODEL

6.1. Introduction

Stress rupture is a time dependent failure mode that affects unidirectional continuous fiber composites, such as composite overwrapped pressure vessels (COPVs). It is catastrophic and occurs without warning under sustained loading, at typical operating temperatures and pressures. In stress rupture failures, individual fibers fail successively, some forming clusters of broken fibers. The overall composite fails when one of these clusters becomes too large and goes unstable.

On the micromechanical level, individual fibers inherently have a high variability in strength, with flaws randomly spaced along their length. On initial loading of the composite, fibers fail if they have flaws weaker than the applied load. The load that was carried by a now broken fiber is transferred onto its neighboring fibers through matrix shear, thus causing higher loads in the neighboring fibers in the region near a break. These neighbors may then break, creating a cluster of broken fibers and further overloading the fibers surrounding the cluster, perhaps causing more failures.

A second feature is that the matrix shear load around a fiber break causes the matrix to creep over time, or possibly debond progressively along the fiber-matrix interface, thus lengthening the regions that are overloaded on the neighboring fibers. Ultimately the growing overload region encounters further flaws in neighboring fibers, which causes the neighboring fibers to break adding to the cluster. Eventually a cluster will grow to a size that becomes unstable.

There has been extensive research done into how the micromechanics of stress rupture occurs. Fiber strength has been reviewed in [42, 43] and see references therein for more details, within a Poisson process framework to model both the occurrence and severity of flaws, leading via weakest link statistics to a Weibull model for the strength of a fiber [43]. The incidence of individual fiber failures on loading a composite has been noted using acoustic emissions and is expected based on fiber strength statistics. There has been extensive research, including theoretical [44-48], experimental [49, 50] and with simulations [51-55], into how the matrix transfers the load from a broken fiber to its intact neighbors. The matrix creep in shear has been modeled and experimentally verified [56-58], and the overall process of cluster formation has been extensively simulated [51-54]. What is lacking is a cohesive framework pulling together all of this micromechanical knowledge within a statistical framework for fiber breakage to yield a realistic and robust model for stress rupture.

The models currently used for stress rupture are typically based on the breakdown process in a single fiber, yet, impressively, these models appear to accurately describe the stress rupture behavior for composite materials under a steady sustained load. There is concern, however, that these models break down for load profiles other than a sustained load. Of particular interest is 'proof testing' which is performed on virgin COPVs, where such a COPV is exposed for a limited time to a load much higher than its service load, before being put into service at that load.

Proof testing of COPVs soon after fabrication is conceptually viewed as a process of weeding out weak vessels, thus improving overall reliability in service. However, typically a vessel is weeded out because of liner leakage, instead of failure of composite overwrap. Nevertheless, unlike with metal vessels, proof testing can do considerable damage in terms of

breaking fibers and possibly strands. This is clear from acoustic emission data generated during proof testing and should be expected based on strength data on individual fibers and yarns at fiber stress levels comparable to what occurs in the overwrap. Thus, excessive proof pressure levels above the long-term, service pressure may actually degrade the long term reliability rather than improve it. There is anecdotal evidence of this from tests on COPVs where strands were found to have been broken on the vessel surface after proof testing and before long term testing had commenced. Furthermore, NASA, a major user of COPVs, was concerned enough about the possible degradation of long term reliability to specifically adjust the proof testing guidelines away from higher proof tests, and to lower pressures on COPVs already in service.

While we believe it is possible that proof testing can degrade the long-term reliability, the current stress rupture models cannot predict this for carbon fiber/epoxy composites. The current models are largely phenomenological and are of the mathematical form whereby the conditional reliability upon surviving a proof test is always higher than the reliability for a simple sustained load. These models do a good job of modeling composites with time dependent fibers and load sharing conditions that are closer to global load sharing than local load sharing, however the carbon fiber/epoxy matrix composites currently used have mostly time independent fibers and local load sharing. Thus there is a need for a model that incorporates known micromechanics and fiber flaw statistics and has the potential for the conditional reliability, following an overly aggressive proof test, to be lower than that under a simple sustained load and conditioned on surviving the initial service load level during a system check.

In this paper we develop a model that explicitly accounts for the micromechanical and statistical failure processes in composites consisting of carbon fibers in an epoxy matrix. This model will be called the *stochastic fiber breakage model* and we will find that the long term

benefits and drawbacks of a proof test are very different from those predicted by the classic reliability models depending on the proof pressure level. In developing this model we will draw heavily on the extensive body of research done on the micromechanics of stress rupture and statistical modeling of strength behavior in a local fiber load-sharing framework. Assumptions, where required, will err on the side of being conservative.

As we will show, this stochastic fiber breakage model has much more nuanced behavior following a proof test. We believe this behavior to reflect real world behavior much more accurately than the current stress rupture models.

6.2. Idealized composite

The model we are going to develop is for an idealized composite structure, consisting of an array of n parallel continuous, brittle, elastic fibers embedded in a flexible polymer matrix. The stiffness of the matrix is more than an order of magnitude less than that of the fibers. The role of the matrix is not only to bind the fibers together, but more importantly, to locally transfer load from broken to intact fibers, through shear, when the composite is under high tensile loads. Three fiber configurations will be considered, as shown in figure 6.1: a planar array mimicking tapes used in winding COPVs, a hexagonal array that is a fair approximation of a 3D composite, and a square array for illustrative purposes.

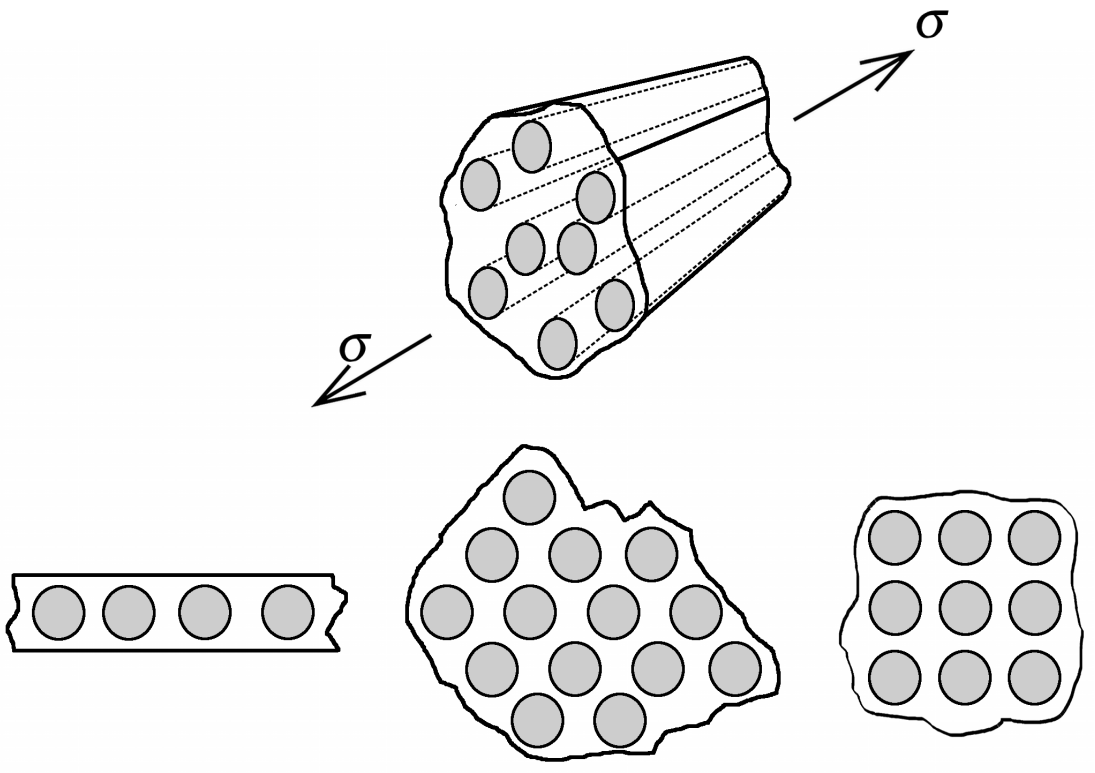

a) planar array b) hexagonal array c) square array

Figure 6.1 The three fiber arrays considered: (a) planar array, (b) hexagonal array, and (c) square array. The fibers nominally support a far-field stress of σ.

6.2.1 The fibers

The fibers are assumed to be stiff, brittle, and elastic, with local flaws that are randomly distributed in both strength and position. In addition, in the current paper, the fibers are assumed to have no time dependency in their failure.

We assume that the occurrence of the flaws along a fiber is well described by a Poisson-Weibull model. In this model the key parameter is $\lambda(\sigma) = \left(\sigma / \sigma_{\ell_0}\right)^{\zeta}$, where σ is the stress level, σ_{ℓ_0} is a reference strength corresponding to the reference length ℓ_0, and ζ is a positive exponent [42]. One interpretation is that $\lambda(\sigma)$ is the average number of flaws per length ℓ_0 with

strength $\leq \sigma$. As a result, the number of flaws in a given length ℓ that have strength $\leq \sigma$ follows a Poisson distribution with parameter $\lambda(\sigma)(\ell/\ell_0)$.

The Poisson distribution implies that the probability that the number of flaws is zero in a given length ℓ, i.e. no flaws occur, is given by $\exp\left(-\lambda(\sigma)\ell/\ell_0\right)$. Then the probability that at least one flaw with strength less than or equal to σ occurs in length ℓ is one minus the probability this probability, which is also the probability that the fiber will fail. Letting $F_\ell(\sigma)$ be the probability that there is at least one flaw and the fiber fails, we get:

$$F_\ell(\sigma) = 1 - \exp\left\{-\left(\frac{\ell}{\ell_0}\right)\left(\frac{\sigma}{\sigma_{\ell_0}}\right)^{\zeta}\right\} \tag{6.1}$$

This is the classic Weibull distribution for fiber strength, whereby the strength of a fiber is equal to that of its worst defect. Furthermore, this Weibull distribution for the strength of a fiber has weakest link scaling in terms of length ℓ/ℓ_0.

In later modeling, we will be interested in the strength distribution for a short fiber element of length δ_e, which is the initial effective length for load transfer (from a statistical point of view) around a fiber break, as will be described in Section 6.2.2. This length δ_e is typically much less than ℓ_0, which in practice is a reference length, typically the tension test gage length for fiber testing (e.g., 1 cm). Furthermore, over time the lengths of interest will grow to become larger than δ_e, as a result of matrix creep.

For the short length δ_e the Poisson-Weibull model still applies, giving:

$$\begin{aligned} F_{\delta_e}(\sigma) &= 1-\exp\left\{-\left(\frac{\delta_e}{\ell_0}\right)\left(\frac{\sigma}{\sigma_{\ell_0}}\right)^{\zeta}\right\} \\ &= 1-\exp\left\{-\left(\frac{\sigma}{\sigma_{\delta_e}}\right)^{\zeta}\right\} \end{aligned} . \tag{6.2}$$

Tension tests are used to estimate the associated Weibull scale parameter σ_{ℓ_0} and shape parameter ζ. Then σ_{δ_e}, the Weibull scale parameter for the strength of a fiber element of length δ_e, can be calculated as

$$\sigma_{\delta_e} = \sigma_{\ell_0}\left(\frac{\delta_e}{\ell_0}\right)^{-1/\zeta} . \tag{6.3}$$

This scaling is consistent with the fact that fibers typically follow Weibull weakest-link statistics [42]. Additionally, $\sigma_{\delta_e} \gg \sigma_{\ell_0}$ as $\left(\delta_e/\ell_0\right)^{-1/\zeta} \approx \left(1/20\right)^{-1/5} \approx 1.82$, and a ratio of 1/20 for δ_e/ℓ_0 is conservative, such that typically $\sigma_{\delta_e} > 2\sigma_{\ell_0}$.

In a large composite approaching failure, the far field applied stress on fiber elements, σ, is small relative to σ_{δ_e}, or even, σ_{ℓ_0}. Thus the failure probability for each individual fiber element is very small, and the lower tail of (6.2) can be accurately approximated by

$$F_{\delta_e}(\sigma) \approx \left(\frac{\sigma}{\sigma_{\delta_e}}\right)^{\zeta}, \quad 0 < \sigma < \sigma_{\delta_e} . \tag{6.4}$$

6.2.2 The matrix

The matrix, being much less stiff than the fibers, supports negligible tensile load. However, around fiber breaks the matrix becomes loaded in shear as it acts to locally transfer load from broken fibers to the nearest intact neighbors over some effective length, proportional to δ_e. In a planar array the load from a broken fiber is shared mainly across its two nearest neighbors, while in a hexagonal array the load from one broken fiber is shared mainly across its six nearest neighbors.

The load transfer process has been successfully described using the classic shear-lag model developed by Hedgepeth and co-workers. [44-46] Extensions and refinements have been developed to improve the accuracy and realism in certain circumstances, [59-66] however, for the purposes of modeling time dependence in this paper, we have chosen to work with the simplest version.

Over time the matrix creeps, giving rise to an increase in the effective length over which load transfer occurs. To model this matrix creep within the shear lag model, we use the power-law creep model, a common and useful creep law, whereby the creep compliance takes the form

$$J_m(t) = J_{m,e}\left[1+\left(\frac{t}{t_c}\right)^{\theta}\right], \quad t \geq 0 \tag{6.5}$$

where $J_{m,e}$ is the instantaneous elastic creep compliance ($J_{m,e} = 1/G_{m,e}$, where $G_{m,e}$ is the instantaneous elastic shear modulus), t_c is the characteristic time for creep to occur (at which time the compliance $J_m(t)$ has effectively doubled), and θ is the creep exponent [67]. The creep exponent is a crucial parameter that governs the growth of the effective length for load transfer, and depends on such factors as the matrix and adhesion chemistry, fiber volume fraction, and

temperature – to name perhaps the most important influences [67]. Typically $0.1 < \theta < 0.5$ for epoxies, [68] and note that, as a reference point, the value $\theta = 1$ corresponds to a Newtonian viscous material.

One characteristic of the power-law creep model in the shear-lag framework is that there is an initial elastic characteristic length, $\hat{\delta}_e$, for load transfer (including regions on both sides of the break along the fiber). This length depends on both mechanical and geometric quantities: the fiber diameter, d_f; the fiber cross sectional area, A_f, (approximately $\pi d_f^2/4$); the fiber Young's modulus, E_f; the matrix shear modulus, G_m; and the fiber volume fraction, V_f, which is manifest in the effective width of matrix between fiber surfaces, w_m, and the effective matrix thickness, h, (which is of order d_f). The latter two quantities depend on the nature of the fiber packing as for instance in Figure 6.1. For fully elastic behavior, $\hat{\delta}_e$ is given by [42, 45, 48]

$$\hat{\delta}_e \approx 2\sqrt{\frac{E_f}{G_m}\frac{A_f w_m}{h}} \tag{6.6}$$

The strongest influences on $\hat{\delta}_e$ are the fiber diameter, d_f, and the square root of the fiber to matrix stiffness ratio, $\sqrt{E_f/G_m}$. The remaining parameters above have a more modest influence through the fiber volume fraction.

In solving the shear lag model under the power-law creep function, (6.5), Lagoudas et. al found that the characteristic load transfer length grows in time and is accurately approximated by [69]

$$\hat{\delta}(t) \approx \hat{\delta}_e \sqrt{1+\left(\frac{t}{t_c}\right)^{\theta}}, \quad t \gg 0$$
$$\approx \hat{\delta}_e \left(\frac{t}{t_c}\right)^{\theta/2}, \qquad t \gg t_c \tag{6.7}$$

Thus, the length depends approximately as the $\theta/2$ root of time, and significantly, the length is independent of stress level, assuming the stress level remains constant.

The overload profile and stress state on a fiber neighboring a broken fiber is roughly triangular in shape. However, its effect can be modeled with an appropriately scaled 'square' overload profile on adjacent fibers over a certain effective length, also growing in time. We assume that only the nearest neighbors are overloaded in the region around the break, and by a constant amount, over some effective length, and that as time passes this effective length increases proportional to (6.7). This effective length is specifically chosen such that the failure probabilities for the true and step overloads are approximately equivalent with respect to probability calculations in the model [42]. Figure 6.2 illustrates the assumed square load profile of effective length, termed $\delta(t)$, in comparison to the actual load profile with its characteristic length $\hat{\delta}(t)$.

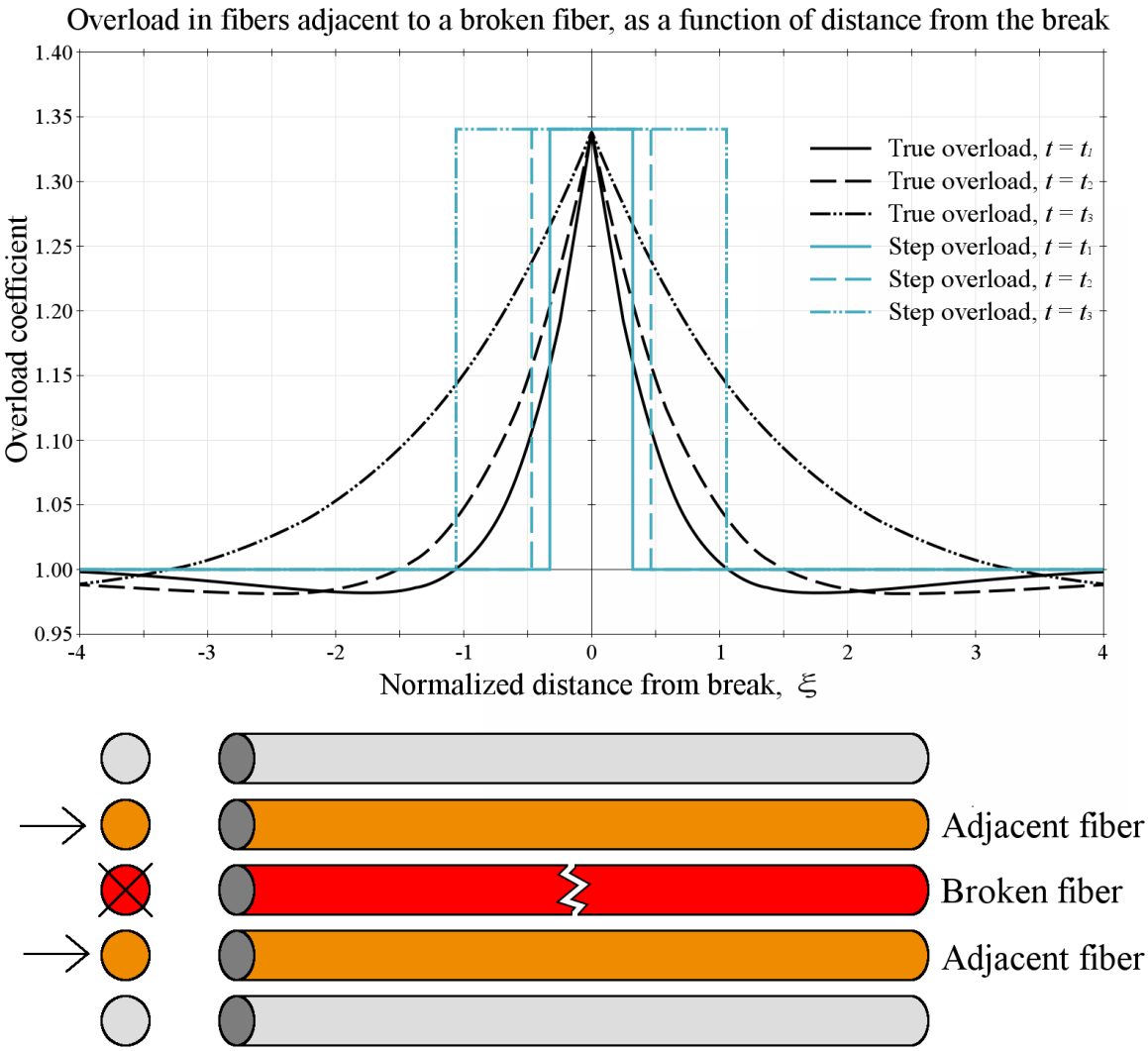

Figure 6.2 Overload profile along the two fibers adjacent to a broken fiber, in a planar fiber array, as shown in the schematic, as a function of the distance from the break and for three different times $t_1 < t_2 < t_3$. Lengths shown for the step overloads are approximate for a fiber scale parameter $\zeta = 5$ using the values from [42].

The proportionality between $\delta(t)$ and $\hat{\delta}(t)$ is governed by the relationship between the initial elastic effective length, termed δ_e, and the initial elastic characteristic length, $\hat{\delta}_e$, which from [42] is approximately given by

$$\delta_e = \frac{2}{\zeta + 1}\hat{\delta}_e . \tag{6.8}$$

This is the result of the fact that the higher the Weibull shape parameter for strength, ζ, the more that only the stress near the peak of the triangular overload region dominates the fiber failure behavior, this region effectively becoming smaller and smaller as ζ increases.

Using (6.7) and (6.8) we then get the time dependent relationship for the effective length:

$$\begin{aligned} \delta(t) &= \frac{2}{\zeta + 1}\hat{\delta}(t) \\ &= \delta_e \sqrt{1 + \left(\frac{t}{t_c}\right)^{\theta}} \end{aligned} \tag{6.9}$$

6.2.3 Idealized failure process

In a strength test, failure is assumed to be triggered when a large enough cluster of broken fibers has formed at a given stress level, and the failure probability for overloaded neighbors becomes of order ½, whereby instability becomes very likely. The process occurs roughly as follows. Upon initial loading, some of fibers will break, even when the load is relatively low. These initial failures tend to be isolated and far apart, but create some level of stress concentration on their neighbors. Upon further increasing of the applied load, the overloaded neighbors of some of these isolated breaks can also fail, creating some small clusters. Further increasing of the load leads to additional failed neighbors to these clusters. Eventually one or more of these clusters reaches a critical, unstable number of broken fibers, triggering the overall failure of the composite.

A strength test, as just described, is presumed to take place quickly enough that there is no time component in the composite failure, such as matrix creep or time dependent breakdown

in the fibers themselves, which would result in additional failures without further increasing the load. In our stress rupture modeling in this paper, however, the overloaded region in fibers neighboring break clusters is allowed to grow over time through matrix creep and/or time dependent debonding. This results in changes to the failure process as described below.

Suppose the idealized composite is loaded under a sudden far-field tensile stress such that each fiber has stress $\sigma \ll \sigma_{\delta_e}$, and the overall tensile load is approximately $\sigma n A_f$. Since the composite strength will turn out to be much less than σ_{δ_e}, the probability of failure of a given fiber element is small and thus the breaks, though numerous, tend to be widely separated.

When such a fiber element breaks, its load is redistributed locally onto its nearest neighbors over some effective length for load transfer, δ_e. In lifetime testing the effective load transfer length becomes $\delta(t)$, following (6.9). In either case, this local load redistribution is modeled as an equivalent uniform overload, over the effective load transfer length, on each of the neighboring fibers, as shown in Figure 6.2.

If all the overloaded fiber elements have strength greater than the stress resulting from the overload, then no fibers fail and the composite is initially stable. In strength testing a stable cluster is made unstable by increasing the load, whereas in lifetime testing the increase in the effective load transfer length can expose new flaws, causing additional fiber breaks.

When these additional fiber breaks occur around isolated breaks, small clusters of broken fibers form, and all fibers adjacent to these clusters now become more severely overloaded. Once again, if all these newly overloaded fiber elements happen to be strong enough, the composite is stable. Otherwise additional fibers break, due to an increase in load or time, and the process repeats itself. Final catastrophic failure of the composite will occur if at least one cluster reaches

a certain critical size, $\hat{k}$, for instability, which we define more precisely later. The same critical size, $\hat{k}$, will apply to both quasi-static strength and time dependent lifetime behaviors. The process of cluster growth is illustrated in Figure 6.3.

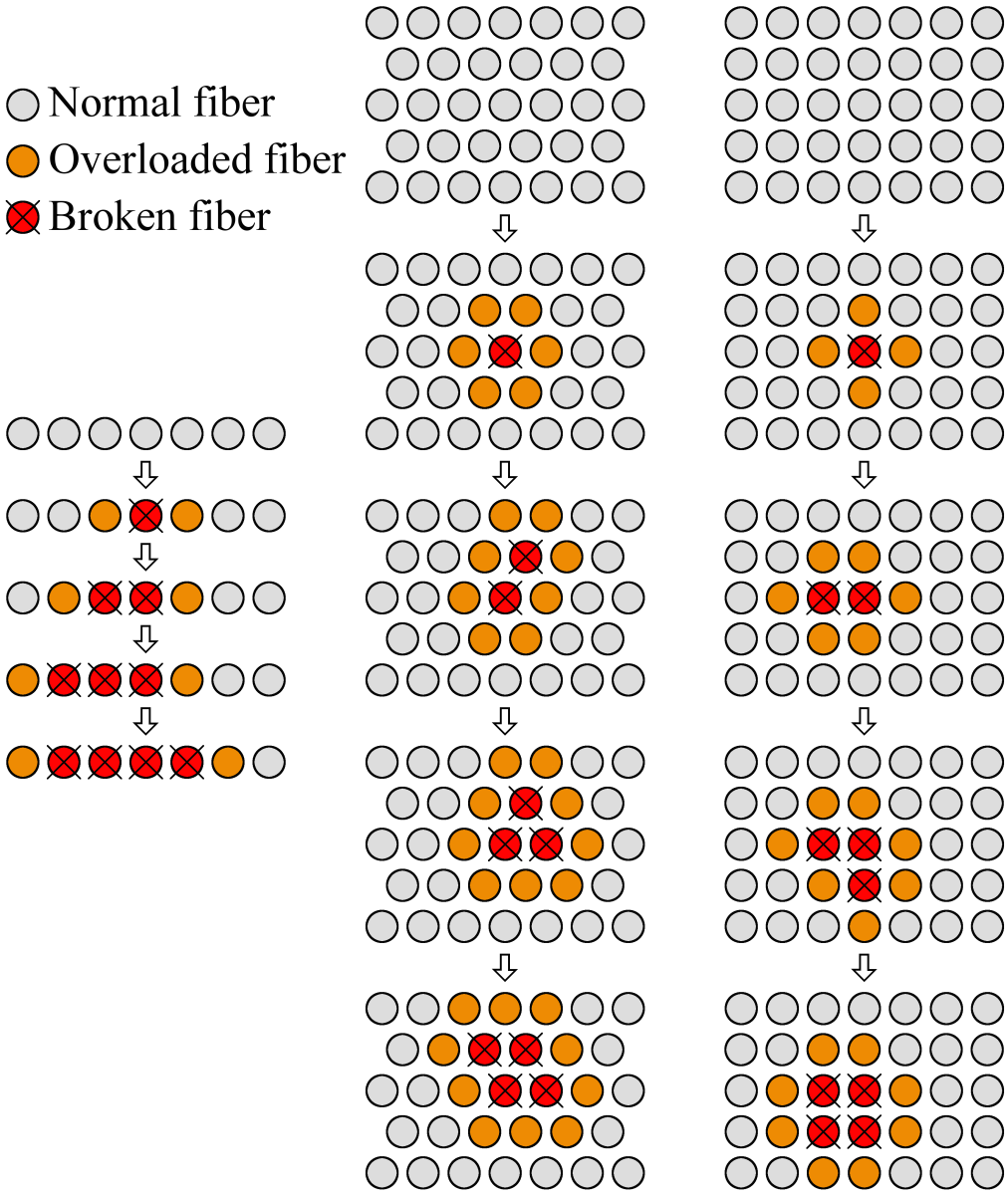

Figure 6.3 A possible scheme for fiber failures in a) a tape, b) a hexagonal array, and c) a square array [70].

Upon loading a composite, initial fiber failures will occur at stress levels far below σ_{δ_e}, the Weibull scale parameter for the strength of a fiber element of length, δ_e. For instance, if σ is just one tenth of σ_{δ_e} and if $\zeta \approx 5$, then the probability of an arbitrary fiber element failing is 10^{-5}, meaning that one in a hundred thousand fiber elements fails. On the other hand, the volume of the composite, V, expressed as the number of fiber elements is easily on the order of 10^{12} for COPVs. Thus, there can be 10^7 initial fiber breaks. However, these breaks are typically widely spaced and for δ_e = 0.1 mm, as is typical in carbon/epoxy systems, the distance along a fiber between breaks would be 10 meters on average. If the stress level σ is doubled to one fifth of σ_{δ_e} and if $\zeta \approx 5$, then the probability of an arbitrary fiber element failing is 3.2×10^{-4}, and fiber breaks are spaced 31.2 cm apart, or 3120 fiber elements apart, which is still a wide spacing.

While there are a large number of single fiber breaks at stresses far less than σ_{δ_e}, there are far fewer clusters of two breaks, even fewer clusters of three breaks and so on, as we shortly show. However, there only needs to be one cluster of critical size $\hat{k}$ to fail the composite. Thus, failure of the composite, starting with failure of a given fiber element under stress σ, is by nature a rare event, even when failure of the entire composite under a stress σ is likely.

In determining the probability of overall composite failure in the case of a quasi-static strength test, we first focus on a quantity $W_k(\sigma)$, which is the probability of a cluster of k fiber breaks forming at a particular location in the composite, and at arbitrary stress σ, and where k is arbitrary. These results are used later in connection with a specific value of k, called $\hat{k}$, the critical cluster size. Any group of k adjacent fiber elements has the potential to become a cluster of k breaks, but as mentioned above this is a rare event for a given group of k fibers. However

the probability of obtaining at least one cluster of size k somewhere in the composite is much larger and takes the weakest link form:

$$H_{V,k}(\sigma) = 1 - \left[1 - W_k(\sigma)\right]^V, \quad \sigma \geq 0 \tag{6.10}$$

where again V is the volume, i.e. the number of fiber elements of length δ_e in the composite. This is true even though two nearby groups of k fiber elements can overlap each other and might ostensibly be viewed as statistically dependent. In reality they satisfy the concept of k-dependence and essentially act independently. (See Smith et al for theorems on the concept of k-dependence associated with rare events [70])

A useful fact is that

$$\exp(x) = \lim_{V\to\infty}\left(1 + \frac{x}{V}\right)^V. \tag{6.11}$$

Letting $x = -VW_k(\sigma)$ we then get

$$\exp\left(-VW_k(\sigma)\right) = \lim_{V\to\infty}\left(1 + \frac{-VW_k(\sigma)}{V}\right)^V. \tag{6.12}$$

Since V is large

$$\exp\left(-VW_k(\sigma)\right) \approx \left(1 - \frac{VW_k(\sigma)}{V}\right)^V = \left(1 - W_k(\sigma)\right)^V \tag{6.13}$$

and equation (6.10) is well approximated by:

$$H_{V,k}(\sigma) \approx 1 - \exp\left[-V\,W_k(\sigma)\right], \tag{6.14}$$

reminiscent of the Weibull form. Once again, see Smith et al. [70]

6.3. Model for strength and lifetime testing

In developing our model for stress rupture, it is instructive to first focus on strength testing, where the loading increases relatively rapidly until failure, e.g., in 30 seconds. Thus, we first consider the process of failure, ignoring time dependence, as was described in Section 6.2.3. After developing a model for strength, we will continue on to modeling stress rupture lifetime behavior.

6.3.1 Strength testing

As a first step towards calculating the failure probability for the overall composite in a strength test, we calculate the probability, $W_k(\sigma)$, a function of stress level σ, that a given group of k fiber elements fails. In so doing we treat the neighbors of this group of k fiber elements as having infinite strength, as shown in Figures 6.15 through 6.18 in the appendix, and do not participate in the failure progression, other than accepting the load of failed fibers at the edge of the cluster, as would occur in the actual composite.

In general, for small clusters of size k, $W_k(\sigma)$ can be written down exactly. For example, in the case where $k=2$, and assuming a planar array of fibers such as in Figure 6.3a,

$$\begin{aligned} W_2(\sigma) &= F_{\delta_e}(\sigma)^2 + 2F_{\delta_e}(\sigma)\left(F_{\delta_e}(K_1\sigma) - F_{\delta_e}(\sigma)\right) \\ &= 2F_{\delta_e}(K_1\sigma)F_{\delta_e}(\sigma) - F_{\delta_e}(\sigma)^2 \end{aligned}, \tag{6.15}$$

where $F_{\delta_e}(\sigma)$, an increasing function of stress $\sigma \geq 0$, is the probability of failure of a fiber with effective length, δ_e, as given in (6.2) and (6.4), and where the multiplier on σ, K_i, is the stress concentration on a fiber element caused by a cluster of i adjacent broken fibers. In equation (6.15) the first term is the probability that both fibers fail under their applied load, σ. The

second term is the probability that only one fiber fails under load σ, and the second fiber, while surviving load σ, fails subsequently under the overload $K_1\sigma$, there being two ways this can happen. Otherwise, the bundle of two fibers survives. This analysis is shown in Figure 6.15 in the appendix.

In the case where $k=3$, and again assuming a planar array of fibers such as in Figure 6.3a, a similar but somewhat more complex sequential fiber failure analysis can be carried out to yield a more complex version of (6.15). This analysis is shown in Figure 6.16 in the appendix, and after summing probabilities for specific failure sequences, expanding products and collapsing by summing similar terms, we obtain

$$\begin{aligned} W_3(\sigma) = {} & 4F_{\delta_e}(K_2\sigma)F_{\delta_e}(K_1\sigma)F_{\delta_e}(\sigma) - F_{\delta_e}(K_2\sigma)F_{\delta_e}(\sigma)^2 \\ & - F_{\delta_e}(K_1\sigma)^2 F_{\delta_e}(\sigma) - 2F_{\delta_e}(K_1\sigma)F_{\delta_e}(\sigma)^2 + F_{\delta_e}(\sigma)^3, \end{aligned} \tag{6.16}$$

with similar interpretation as in (6.15).

In the case where $k=4$, and again assuming a planar array of fibers such as in Figure 6.3a, a similar sequential fiber failure analysis can be carried out, as shown in Figure 6.17 in the appendix. This result when expanded and then collapsed

$$\begin{aligned} W_4(\sigma) = {} & 8F_{\delta_e}(K_3\sigma)F_{\delta_e}(K_2\sigma)F_{\delta_e}(K_1\sigma)F_{\delta_e}(\sigma) - 2F_{\delta_e}(K_3\sigma)F_{\delta_e}(K_2\sigma)F_{\delta_e}(\sigma)^2 \\ & - 2F_{\delta_e}(K_3\sigma)F_{\delta_e}(K_1\sigma)^2 F_{\delta_e}(\sigma) - 2F_{\delta_e}(K_2\sigma)^2 F_{\delta_e}(K_1\sigma)F_{\delta_e}(\sigma) \\ & + F_{\delta_e}(K_2\sigma)^2 F_{\delta_e}(\sigma)^2 - 6F_{\delta_e}(K_2\sigma)F_{\delta_e}(K_1\sigma)F_{\delta_e}(\sigma)^2 + 2F_{\delta_e}(K_2\sigma)F_{\delta_e}(\sigma)^3, \\ & + F_{\delta_e}(K_1\sigma)^2 F_{\delta_e}(\sigma)^2 + 2F_{\delta_e}(K_1\sigma)F_{\delta_e}(\sigma)^3 - F_{\delta_e}(\sigma)^4 \end{aligned} \tag{6.17}$$

Finally, in the case where $k=5$, and again assuming a planar array of fibers such as in Figure 6.3a, a similar analysis, as shown in Figure 6.18 in the appendix, results in

$$
\begin{aligned}
W_5(\sigma) = {} & 16F_{\delta_e}(K_4\sigma)F_{\delta_e}(K_3\sigma)F_{\delta_e}(K_2\sigma)F_{\delta_e}(K_1\sigma)F_{\delta_e}(\sigma) \\
& -4F_{\delta_e}(K_4\sigma)F_{\delta_e}(K_3\sigma)F_{\delta_e}(K_2\sigma)F_{\delta_e}(\sigma)^2 - 4F_{\delta_e}(K_4\sigma)F_{\delta_e}(K_3\sigma)F_{\delta_e}(K_1\sigma)^2F_{\delta_e}(\sigma) \\
& -4F_{\delta_e}(K_4\sigma)F_{\delta_e}(K_2\sigma)^2F_{\delta_e}(K_1\sigma)F_{\delta_e}(\sigma) + 2F_{\delta_e}(K_4\sigma)F_{\delta_e}(K_2\sigma)^2F_{\delta_e}(\sigma)^2 \\
& -4F_{\delta_e}(K_4\sigma)F_{\delta_e}(K_2\sigma)F_{\delta_e}(K_1\sigma)F_{\delta_e}(\sigma)^2 + 2F_{\delta_e}(K_4\sigma)F_{\delta_e}(K_2\sigma)F_{\delta_e}(\sigma)^3 \\
& +4F_{\delta_e}(K_4\sigma)F_{\delta_e}(K_1\sigma)^2F_{\delta_e}(\sigma)^2 - 4F_{\delta_e}(K_4\sigma)F_{\delta_e}(K_1\sigma)F_{\delta_e}(\sigma)^3 + F_{\delta_e}(K_4\sigma)F_{\delta_e}(\sigma)^4 \\
& -4F_{\delta_e}(K_3\sigma)^2F_{\delta_e}(K_2\sigma)F_{\delta_e}(K_1\sigma)F_{\delta_e}(\sigma) + F_{\delta_e}(K_3\sigma)^2F_{\delta_e}(K_2\sigma)F_{\delta_e}(\sigma)^2 \\
& +F_{\delta_e}(K_3\sigma)^2F_{\delta_e}(K_1\sigma)^2F_{\delta_e}(\sigma) + 2F_{\delta_e}(K_3\sigma)^2F_{\delta_e}(K_1\sigma)F_{\delta_e}(\sigma)^2 - F_{\delta_e}(K_3\sigma)^2F_{\delta_e}(\sigma)^3 \\
& -10F_{\delta_e}(K_3\sigma)F_{\delta_e}(K_2\sigma)F_{\delta_e}(K_1\sigma)F_{\delta_e}(\sigma)^2 + 2F_{\delta_e}(K_3\sigma)F_{\delta_e}(K_2\sigma)F_{\delta_e}(\sigma)^3 \\
& -4F_{\delta_e}(K_3\sigma)F_{\delta_e}(K_1\sigma)^2F_{\delta_e}(\sigma)^2 + 8F_{\delta_e}(K_3\sigma)F_{\delta_e}(K_1\sigma)F_{\delta_e}(\sigma)^3 - 2F_{\delta_e}(K_3\sigma)F_{\delta_e}(\sigma)^4 \\
& +4F_{\delta_e}(K_2\sigma)^2F_{\delta_e}(K_1\sigma)F_{\delta_e}(\sigma)^2 - 3F_{\delta_e}(K_2\sigma)^2F_{\delta_e}(\sigma)^3 - 5F_{\delta_e}(K_2\sigma)F_{\delta_e}(K_1\sigma)^2F_{\delta_e}(\sigma)^2 \\
& +10F_{\delta_e}(K_2\sigma)F_{\delta_e}(K_1\sigma)F_{\delta_e}(\sigma)^3 - 2F_{\delta_e}(K_2\sigma)F_{\delta_e}(\sigma)^4 + 4F_{\delta_e}(K_1\sigma)^3F_{\delta_e}(\sigma)^2 \\
& -4F_{\delta_e}(K_1\sigma)^2F_{\delta_e}(\sigma)^3 - 2F_{\delta_e}(K_1\sigma)F_{\delta_e}(\sigma)^4 + F_{\delta_e}(\sigma)^5
\end{aligned}
\qquad (6.18)
$$

Clearly as k increases, the complexity of the calculation and the number of resulting terms drastically increases, and thus we will later establish an accurate approximation for $W_k(\sigma)$. Before doing so, we give an intuitive explanation of the structure of the results.

For instance, in the case where $k=4$, equation (6.17) is the result of expanding and adding together the failure probabilities for all 31 distinct sequences in which a given contiguous group of four fibers can break, as shown in Figure 6.17 in the appendix. Only the first term in (6.17) involves a sequence whereby one fiber fails according to applied stress, σ, a second fiber fails under the first overload, $K_1\sigma$, a third fiber fails due to the second overload, $K_2\sigma$, and the final fiber fails due to the third overload, $K_3\sigma$. Note however that the actual probabilities for such failure sequences are more complicated than simply this first term of (6.17). The constant 8

in front of the first term of (6.17) arises because for a given group of $k = 4$ adjacent failures in a planar array, there are $2^{k-1} = 2^3 = 8$ different ways in which a progressive sequence involving K_1, K_2, and K_3 can occur, as seen in lines 5 and 6 of Figure 6.17.

A critical aspect of the multiplied terms in (6.17) is that $F_{\delta_e}\left(K_3\sigma\right) > F_{\delta_e}\left(K_2\sigma\right) > F_{\delta_e}\left(K_1\sigma\right) > F_{\delta_e}\left(\sigma\right)$, typically by more than a factor of two in each step. Thus any sequence where two or more fibers fail at once, such as depicted in all lines in Figure 6.17 other than lines 5 and 6, involves duplicating one of the lower stress concentrations.

This sequential argument has a further implication. A cluster of more than k adjacent failed fibers in the composite can result from two (or more) clusters growing independently and then joining at the end to create a cluster of more than k breaks. However, this requires (i) at least two fibers to fail under the applied load, σ, (ii) more than k fibers to fail, and (iii) that the clusters are close enough together that they can join. Two fibers failing under the applied load, as discussed above, results in a lower probability than when the fibers fail sequentially in a single cluster. Furthermore, the initial fiber failure is a low probability event, and for each additional broken fiber in a cluster the failure probability gets smaller. Thus, the probability of two sufficiently large clusters forming close enough to each other to join and form a cluster of size at least size k, is much less than that of the formation of a single cluster of size k.

Returning to (6.17), the first term turns out to be the dominant term due to the combination of the higher stress concentrations and the large combinatorial factor. Thus, the first term can be used to approximate $W_k\left(\sigma\right)$ very accurately, as we will show. Thus (6.17) can be approximated by

$$W_4\left(\sigma\right) = 8F_{\delta_e}\left(K_3\sigma\right)F_{\delta_e}\left(K_2\sigma\right)F_{\delta_e}\left(K_1\sigma\right)F_{\delta_e}\left(\sigma\right). \tag{6.19}$$

Note that the remaining terms in (6.17) have both positive and negative signs, giving rise to considerable cancellation in their effects.

To illustrate, if we substitute (6.4) into (6.17), letting $K_1 = 3/2$, $K_2 = 2$, and $K_3 = 5/2$, as well as choosing $\zeta = 5$, as might be the case in an average quality carbon fiber, we get

$$W_k(\sigma) \approx \left(\frac{1.819\sigma}{\sigma_{\delta_e}} \right)^{20} \approx \left(\frac{\sigma}{0.550\sigma_{\delta_e}} \right)^{20}, \quad \sigma < 0.550\sigma_{\delta_e} \tag{6.20}$$

In comparison, our approximation in (6.19) gives:

$$W_k(\sigma) \approx \left(\frac{1.836\sigma}{\sigma_{\delta_e}} \right)^{20} \approx \left(\frac{\sigma}{0.545\sigma_{\delta_e}} \right)^{20}, \quad \sigma < 0.545\,\sigma_{\delta_e}\,. \tag{6.21}$$

A comparison of 0.550 from (6.20) to 0.545 from (6.21) shows that there is less than 1% difference in load required to achieve the same probability of failure. Comparing these two numbers is apt, as any inaccuracies in the approximation will show up as comparable changes to the scale parameter σ_{δ_e}. This comparison is also shown in Figure 6.4, where the ratio of the predicted failure probabilities is about 1.2, however on the scaling of Figure 6.4, in the lower tail this is barely more than the thickness of the plotted lines.

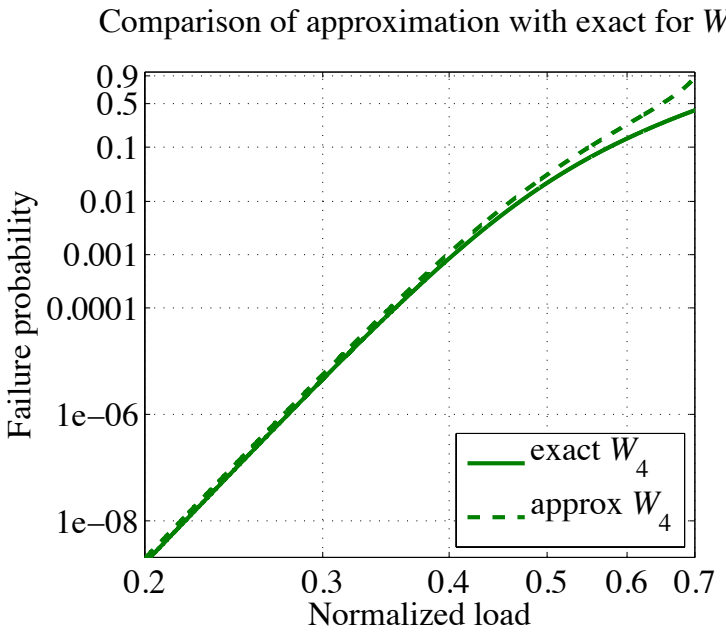

Figure 6.4 A Weibull plot comparison of the exact expression for $W_4(\sigma)$, (6.17), with the approximation used in this paper, (6.19), where $K_1 = 3/2$, $K_2 = 2$, $K_3 = 5/2$, and $\zeta = 5$, using the exact expression for $F_{\delta_e}(\sigma)$.

As stated earlier, as k gets larger the exact expression for $W_k(x)$ becomes orders of magnitude more complex. Fortunately, for the same reasons that (6.17) was well approximated by (6.19), the general expression for the strength of a cluster of k fibers, $W_k(x)$, is well approximated by

$$\begin{aligned} W_k(\sigma) &\approx c_k F_{\delta_e}(\sigma)\left[\prod_{i=2}^{k} F_{\delta_e}(K_{i-1}\sigma)\right] \\ &\approx c_k F_{\delta_e}(\sigma) F_{\delta_e}(K_1\sigma) F_{\delta_e}(K_2\sigma)\cdots F_{\delta_e}(K_{k-1}\sigma) \end{aligned} \tag{6.22}$$

where c_k is a combinatorial factor capturing all the possible configurations (in terms of a growing sequence of fiber breaks) that a cluster can have, and K_i is the stress concentration on a fiber caused by a cluster of i broken fibers.

Figure 6.5 compares approximation (6.22) with the exact expression for $W_k(\sigma)$, (6.15) – (6.18). Of special importance is the behavior of the lower tails. Note that the upper tails for $\sigma > 2\sigma_{\delta_e}/3$ will not superimpose onto $F_{\delta_e}(\sigma)$ for a single fiber but will lie above it. This is because in the group of k fibers the first fiber to fail essentially fails the group since $K_1 = 3/2$ and there are k possible first fiber failures rather than just one. In fact, at such high stress levels, we can see that $W_k(\sigma) \approx 1 - \left[1 - F_{\delta_e}(\sigma)\right]^k = F_{k\delta_e}(\sigma)$, the distribution function for strength of a chain of k fiber elements, that is, of a fiber k times as long.

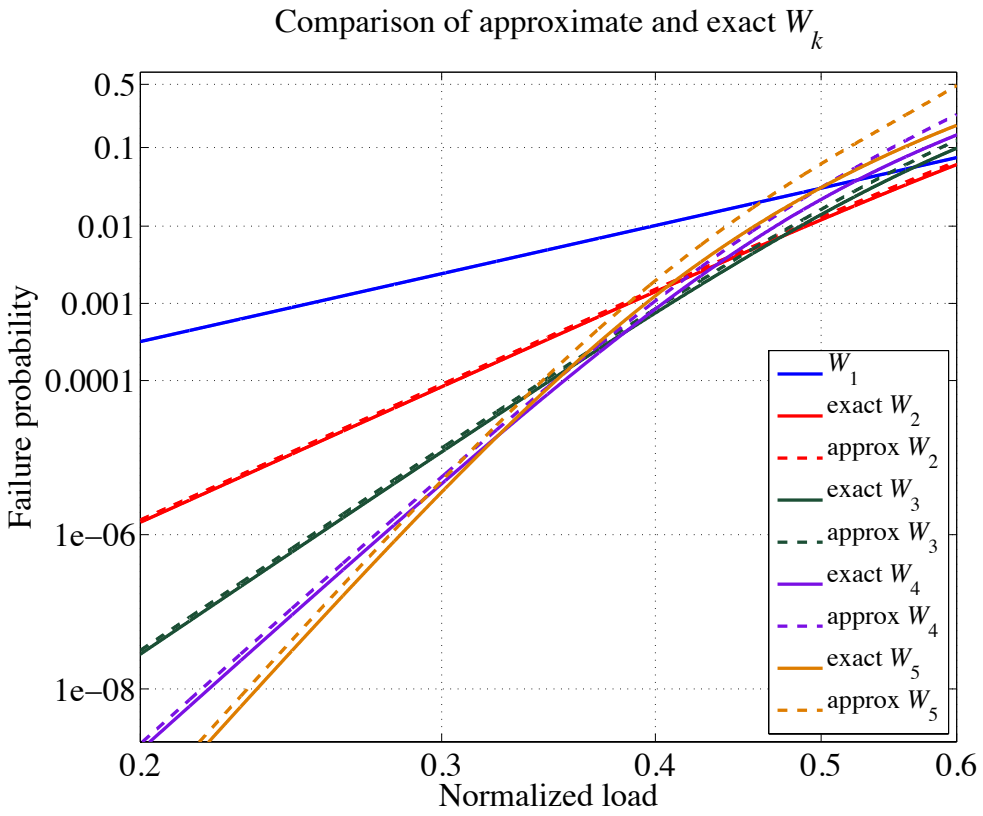

Figure 6.5 A Weibull plot comparison of the exact expression for $W_k(\sigma)$, (6.15) – (6.18), with the approximation used in this paper, (6.22), where $K_1 = 3/2$, $K_2 = 2$, $K_3 = 5/2$, $K_4 = 3$ and $\zeta = 5$, using the exact expression for $F_{\delta_e}(\sigma)$.

The form of (6.22) reflects the fact that for a cluster to grow a neighboring fiber element must fail. There are N_k neighboring fibers around a cluster of k breaks. Each of these fiber elements is exposed to the overload $K_k\sigma$, which increases as k grows. For planar arrays of fibers

$$N_k = 2, \tag{6.23}$$

but for other arrays N_k also increases as k grows. In particular, for a hexagonal array [53]

$$N_j \approx \sqrt{4\pi j} + \pi. \tag{6.24}$$

However this effectively over counts the number of severely overloaded neighbors, as some of the actual neighbors are effectively shielded and loaded to a level significantly lower than others [53, 70].

Thus, the expression

$$c_k = \prod_{j=1}^{k-1} N_k \tag{6.25}$$

captures the fact that, except for the failure of the first fiber element, there are N_k overloaded neighbors next to the growing cluster at any growth step. Since the first failure is excluded from that count, there are $k-1$ growth steps.

Thus, for a planar array of fibers where $N_k = 2$, we get that

$$c_k = 2^{k-1}. \tag{6.26}$$

In a hexagonal array c_k will grow more rapidly than in the planar case and will involve products of increasing numbers of fibers. The cluster, in a hexagonal array, grows approximately circularly [53], leading to the approximation

$$c_k \approx \pi^{k-1} \prod_{j=1}^{k-1} \left(\sqrt{4j/\pi} + 1 \right) \tag{6.27}$$

where $j = \pi D^2/4$ is approximately the number of fiber breaks in the cluster.

The stress concentrations also depend on the fiber arrangement. In this paper henceforth we will use the Hedgepeth stress concentrations, as described in [44, 45, 48]. Thus for the planar array of fibers in Figure 6.1a it can be shown that

$$K_j \approx \sqrt{1 + \pi j/4}, \; j = 0,1,2,\cdots. \tag{6.28}$$

In contrast to the planar case, for the hexagonal case the values of $K_1, K_2, \cdots, K_k, \cdots$ grow more slowly. In fact it has be shown that [52, 53]

$$K_j \approx \sqrt{1 + D/\pi}, \quad D \approx \sqrt{4j/\pi}, \quad j = 0,1,2,\cdots \tag{6.29}$$

where D is approximately the cluster diameter.

By assuming the lower tail approximation for the failure probability of a fiber, (6.4), equation (6.22) becomes:

$$W_k(\sigma) \approx c_k \left(K_1 K_2 \cdots K_{k-1} \right)^{\zeta} \left(\sigma/\sigma_{\delta_e} \right)^{k\zeta}. \tag{6.30}$$

For the approximation in (6.4) to be accurate, we must be in the lower tail of the strength distribution. This may not be the case when the stress concentration factor is high, however any error induced by this approximation has a very tiny impact on the overall value of (6.30). (This behavior is manifest as straight lines in the lower tails seen in Figure 6.5.)

Combining equations (6.14) and (6.30) thus gives the failure probability of the composite at a stress level σ, i.e. the strength distribution, which can be written as the Weibull distribution

$$H_V(\sigma) \approx 1 - \exp\left[-\left(\sigma/\hat{\sigma}_V \right)^{\hat{\alpha}} \right] \tag{6.31}$$

where $H_V(\sigma) \equiv H_{V,k}(\sigma)\big|_{k=\hat{k}}$, and where

$$\hat{\sigma}_V = \sigma_{\delta_e}\left(Vc_{\hat{k}}\right)^{-1/\left(\hat{k}\zeta\right)}\left(K_1 K_2 \cdots K_{\hat{k}-1}\right)^{-1/\hat{k}} \tag{6.32}$$

is the effective Weibull scale parameter for strength, and

$$\hat{\alpha} = \hat{k}\zeta \tag{6.33}$$

is the effective Weibull shape parameter, and where $\hat{k}$ is the critical cluster size, at a particular applied stress, σ, in the stress region where composite specimens are likely to fail (in a strength test). This $\hat{k}$ value is given by

$$K_{\hat{k}-1}\hat{\sigma}_V < \sigma_{\delta_e} < K_{\hat{k}}\hat{\sigma}_V \,. \tag{6.34}$$

Thus, using (34) and (28) for the planar case, $\hat{k}$ satisfies

$$\hat{k} = \left\lceil \frac{4}{\pi}\left[\left(\frac{\sigma_{\delta_e}}{\hat{\sigma}_V}\right)^2 - 1\right]\right\rceil, \tag{6.35}$$

and using (29) for the hexagonal array, $\hat{k}$ is such that:

$$\hat{k} = \left\lceil \frac{\pi^3}{4}\left[\left(\frac{\sigma_{\delta_e}}{\hat{\sigma}_V}\right)^2 - 1\right]^2\right\rceil. \tag{6.36}$$

where '$\lceil \bullet \rceil$' corresponds to the ceiling function, i.e. rounding up the argument to the next integer.

It is important to note that at stress levels, σ, considerably lower than $\hat{\sigma}_V$, the cluster size needed to fail the composite is actually a larger value, k_σ than $\hat{k}$ and satisfying

$K_{k_\sigma - 1}\sigma < \sigma_{\delta_e} < K_{k_\sigma}\sigma$. However, our method of defining a single $\hat{k}$ value for all stress levels yields a Weibull distribution for composite strength, which is both convenient and conservative since the true distribution for composite strength, $H_V(\sigma)$, would tend to curve downward in the lower tail. This is clear from studying the behavior of the governing lower tails of the characteristic distribution functions $W_k(\sigma)$ in Figure 6.5, as k increases. While a larger value k_σ, would be needed to initially fail the composite at stress σ significantly less than $\hat{\sigma}_V$ (say 1/2 to 2/3 of $\hat{\sigma}_V$) the probability of the occurrence of even one such cluster of size k_σ larger than $\hat{k}$ is extremely small (many orders of magnitude less than unity) and even more remote than forming one of exactly size $\hat{k}$, which is already extremely small. However, as time goes on, the situation changes as the smaller, more likely clusters begin to grow as is discussed next. Nevertheless in the model, failure is defined as occurring once a cluster of size $\hat{k}$ as formed irrespective of the stress level.

6.3.2 Lifetime testing

Lifetime testing consists of loading the composite to a specified load and then sustaining that load until the composite fails, presuming that the composite did not already fail during loading (an unlikely event, as the lifetime load level is typically around half the mean strength of a typical specimen). Stress rupture, the dominating failure mode, arises in this paper due to the matrix creeping and/or progressive debonding in shear around fiber breaks, thus increasing the length of the overloaded region on neighboring fibers.

Assuming a classic shear-lag power law creep model as in (6.5), it was shown that the characteristic load transfer length follows equation (6.9), repeated here for convenience:

$$\begin{aligned}\delta(t) &= \delta_e\sqrt{1+(t/t_c)^{\theta}}, \quad t >> 0 \\ &\approx \delta_e(t/t_c)^{\theta/2}, \quad t >> t_c\end{aligned} \tag{6.37}$$

where δ_e is again the characteristic elastic load transfer length.

Materials with high variability in fiber strength, as indicated by low values for the Weibull shape parameter, ζ, are particularly susceptible to such stress rupture failures. This is because as the overloaded region increases in length the probability that it will come to include a very weak flaw also increases, due to the high variability in both the strengths of flaws and their locations.

Carbon fibers particularly have high variability in strength from one segment of length δ_e to the next, meaning that a strong portion of a fiber is unlikely to be followed by equally strong portion (this is not the situation with Kevlar fibers, for instance). This means that Weibull weakest flaw behavior tends to persist down to the length scale of load transfer. Even though the individual fibers themselves are virtually immune to stress rupture, i.e. single carbon fibers under constant stress essentially fail on loading or never fail, carbon/epoxy composites are much more sensitive in comparison. As mentioned, the driving mechanism in the stress rupture of carbon/epoxy composites is the increasing overload length around individual fiber breaks and clusters, thus promoting cluster growth.

To model stress rupture at a fixed stress level, $\bar{\sigma} < \hat{\sigma}_V$, assuming exactly $\bar{\sigma}$ (and no higher load) was applied from $t = 0$, onward (i.e., no proof test) the lifetime distribution function can be derived as a modification of the strength distribution above. Similar to before, the distribution function for composite lifetime follows

$$H_V(t;\bar{\sigma}) \approx 1 - \exp\left[-VW_{\hat{k}}(t;\bar{\sigma})\right], \quad t >> t_c \tag{6.38}$$

where $W_{\hat{k}}\left(t;\bar{\sigma}\right)$ is a characteristic distribution function analogous to (6.22), but with an added time component:

$$\begin{aligned} W_{\hat{k}}\left(t;\bar{\sigma}\right) &\approx c_{\hat{k}} F_{\delta_e}\left(\bar{\sigma}\right)\left[\prod_{i=2}^{\hat{k}} F_{\delta_e}\left(K_{i-1}\bar{\sigma},t\right)\right] \\ &\approx c_{\hat{k}} F_{\delta_e}\left(\bar{\sigma},t\right) F_{\delta_e}\left(K_1\bar{\sigma},t\right) F_{\delta_e}\left(K_2\bar{\sigma},t\right)\cdots F_{\delta_e}\left(K_{\hat{k}-1}\bar{\sigma},t\right) \end{aligned} \tag{6.39}$$

where $\hat{k}$ is defined again by (6.34) and

$$F_{\delta_e}\left(\bar{\sigma},t\right) = 1-\exp\left\{-\frac{\delta\left(t\right)}{\delta_e}\left(\frac{\bar{\sigma}}{\sigma_{\delta_e}}\right)^{\zeta}\right\}. \tag{6.40}$$

Assuming a lower tail approximation, (6.40) becomes

$$F_{\delta_e}\left(\bar{\sigma},t\right) \approx \frac{\delta\left(t\right)}{\delta_e}\left(\frac{\bar{\sigma}}{\sigma_{\delta_e}}\right)^{\zeta}. \tag{6.41}$$

Substituting (6.37) into (6.41) gives:

$$F_{\delta_e}\left(\bar{\sigma},t\right) \approx \sqrt{1+\left(t/t_c\right)^{\theta}}\left(\frac{\bar{\sigma}}{\sigma_{\delta_e}}\right)^{\zeta}. \tag{6.42}$$

Thus, the characteristic distribution function for stress rupture in the composite, (6.39), becomes:

$$\begin{aligned} W_{\hat{k}}\left(t;\bar{\sigma}\right) &\approx c_{\hat{k}}\left[\frac{\delta\left(t\right)}{\delta_e}\left(\frac{\bar{\sigma}}{\sigma_{\delta_e}}\right)^{\zeta}\right]\left[\frac{\delta\left(t\right)}{\delta_e}\left(\frac{K_1\bar{\sigma}}{\sigma_{\delta_e}}\right)^{\zeta}\right]\left[\frac{\delta\left(t\right)}{\delta_e}\left(\frac{K_2\bar{\sigma}}{\sigma_{\delta_e}}\right)^{\zeta}\right]\cdots\left[\frac{\delta\left(t\right)}{\delta_e}\left(\frac{K_{\hat{k}-1}\bar{\sigma}}{\sigma_{\delta_e}}\right)^{\zeta}\right] \\ &\approx c_{\hat{k}}\left(K_1K_2\cdots K_{\hat{k}-1}\right)^{\zeta}\left(\bar{\sigma}/\sigma_{\delta_e}\right)^{\hat{k}\zeta}\left(\sqrt{1+\left(t/t_c\right)^{\theta}}\right)^{\hat{k}-1} \end{aligned} \tag{6.43}$$

For sufficiently large times, i.e. when $t \gg t_c$, (6.43) can be further simplified to

$$W_{\hat{k}}\left(t;\bar{\sigma}\right) \approx c_{\hat{k}}\left(K_1 K_2 \cdots K_{\hat{k}-1}\right)^{\varsigma}\left(\frac{\bar{\sigma}}{\sigma_{\delta_e}}\right)^{\hat{k}\zeta}\left(\frac{t}{t_c}\right)^{\frac{\theta\left(\hat{k}-1\right)}{2}} \tag{6.44}$$

Note that $\hat{k}$ for lifetime was taken to be the same as the $\hat{k}$ used in modeling the strength. The reasonableness of this assumption has been demonstrated in some detailed analysis in related earlier work [71]. Note also that very early in time when $\bar{\sigma} < \hat{\sigma}_V$, being say 1/2 to 2/3 of $\hat{\sigma}_V$, the probability of formation of at least one cluster of size $\hat{k}$ is very remote (and one of initial size k_σ is even more remote). This situation changes, however, as time goes on and clusters grow.

The form of (6.44) again reflects the fact that, for the cluster to grow, a neighboring fiber element must fail. In contrast to the strength distribution, in the lifetime distribution there are N_k neighboring fiber elements to a cluster of size k, nominally of length $\delta\left(t\right)$. As before, each of these fiber elements is exposed to the overload $K_k\bar{\sigma}$, which increases as k grows. However, now the overloaded region of fiber around a fiber element of original length δ_e also increases due to the passage of time, as given in equations (6.9) and (6.37). Thus additional flaws are exposed and additional fiber breaks occur to add to the existing cluster.

An assumption implicit in this is that when a fiber breaks, the overloaded region on the next fiber is not δ_e but instead $\delta_e\sqrt{1+\left(t/t_c\right)^{\theta}}$. In actuality, fiber breaks occur sequentially and there is thus frequently time between breaks, and certainly time between when the initial fiber, $k=1$, broke and when the final fiber, $k=\hat{k}$, breaks. Because of this difference in failure times there is actually some time lag for growth of the new overload length at each new fiber failure site, but this is not reflected in the above formula where time is just the original time, t.

Simulations show, that the effect is small compared to the long timescales involved [67]. This is in large measure the result of the fact that the power law exponent θ is much less than 1, such that, in relative terms, there is rapid growth in $\delta(t)$ right after failure, as is clear from equation (6.37).

The resulting Weibull approximation for long times, $t \gg t_c$, is

$$H_V(t;\bar{\sigma}) \approx 1 - \exp\left[-\left(\left(\frac{\bar{\sigma}}{\hat{\sigma}_V} \right)^{\hat{\rho}} \frac{t}{t_c} \right)^{\hat{\beta}} \right], \qquad t \gg t_c \tag{6.45}$$

where $\hat{\sigma}_V$ is as given in equation (6.32), where

$$\hat{\beta} = (\hat{k} - 1)\theta/2 = \frac{\hat{\alpha}}{\hat{\rho}} \tag{6.46}$$

is the Weibull shape parameter, and

$$\hat{\rho} = \frac{2\zeta \hat{k}}{\theta(\hat{k} - 1)} \tag{6.47}$$

is the power-law exponent for lifetime versus stress level. Equation (6.45) can be re-written in the Weibull form

$$H_V(t;\bar{\sigma}) \approx 1 - \exp\left[-\left(t / \hat{t}_V(\bar{\sigma}) \right)^{\hat{\beta}} \right], \quad t >> t_c \tag{6.48}$$

where

$$\hat{t}_V = t_c \left(\bar{\sigma} / \hat{\sigma}_V \right)^{-\hat{\rho}} \tag{6.49}$$

is the effective Weibull scale parameter for lifetime, and again $\hat{\beta}$ is the associated Weibull shape parameter.

To summarize, the failure probability on loading in lifetime testing is very small, as the applied stress, $\bar{\sigma}$, is much smaller than the scale parameter for tensile strength, $\hat{\sigma}_V$. Instead the concern is for failure at long times, $t \gg t_c$. This is because there are initial fiber failures on loading, causing immediate overloads onto neighboring fiber elements of elastic length $\delta = \delta_e$. Over time these overloaded regions increase in length, thus the remaining $\hat{k}-1$ fibers (needed to create a critical cluster size of $\hat{k}$) eventually fail due to the time dependent matrix creep.

There are two assumptions implicit in the above discussion. The first is that any other initial fiber failures are automatically included in the time dependent failures. The second is that $\hat{k}$ for stress rupture is virtually the same as $\hat{k}$ for strength at times near zero, and the associated K_j values are also preserved, as a result of assuming linear viscoelastic creep behavior.

6.4. Modeling the effect of proof testing

Proof testing consists of loading the composite to some proofing stress, σ_{p}, before reducing the stress to a lifetime maintenance level, $\bar{\sigma}$. For the purposes of this paper we will assume the simplified load profile:

$$\sigma(t) = \begin{cases} \sigma_{\mathrm{p}}, & 0 \le t < t_{\mathrm{p}} \\ \bar{\sigma}, & t \ge t_{\mathrm{p}} \end{cases} . \tag{6.50}$$

that is, the short time spent ramping the load level up and down is ignored.

Proof tests are often applied to COPVs with the implicit goal of filtering out weak vessels. For metal pressure vessels, and many homogeneous materials in general, this process can be argued to be all beneficial with no drawbacks, i.e., the lifetime failure probability conditional on surviving the proof test is lower than the lifetime failure probability without the

proof test. In ductile materials this can be due to crack blunting, and in brittle materials this can be due to weeding out all specimens with cracks above a critical length. In composites, however, the benefits are far less clear.

In reality, proof testing of a COPV may serve the purpose of exposing vessels with flawed liners or some manufacturing defect in the overwrap, such as missing tows or the use of carbon/epoxy prepreg beyond its expiration date for proper resin flow and curing. These aspects of proof testing are not reflected in our modeling, in that as a result of such defects the probability of failure of a freshly manufactured COPV, due to the proof test, may be much higher than our models would suggest.

From the point of view of our modeling, however, it is clear that, because of the proof test, many fiber elements will fail at the higher stress level, σ_{p}, that would not have failed under the lower lifetime stress level, $\bar{\sigma}$, as used in service. These additional fiber failures from the proof test provide many additional locations for subsequent time dependent cluster growth, potentially accelerating the stress rupture process.

For instance, the number, $n\left(\sigma_{\mathrm{p}}\right)$, of fiber breaks at the proof stress level σ_{p}, divided by the number, $n\left(\bar{\sigma}\right)$, at the lifetime load level, $\bar{\sigma}$, is given by

$$n\left(\sigma_{\mathrm{p}}\right)\Big/ n\left(\bar{\sigma}\right)=\left(\sigma_{\mathrm{p}}/\hat{\sigma}_{V}\right)^{\zeta}\Big/\left(\bar{\sigma}/\hat{\sigma}_{V}\right)^{\zeta}=\left(\sigma_{\mathrm{p}}/\bar{\sigma}\right)^{\zeta} \tag{6.51}$$

For the carbon fiber value, $\zeta=5$, and for $\sigma_{\mathrm{p}}/\bar{\sigma}=1.5$, we obtain $n\left(1.5\bar{\sigma}\right)\Big/ n\left(\bar{\sigma}\right)=7.6$. Thus, there are 7.6 times as many single fiber breaks or 'singlets' due to the proof test as without the proof test. These additional singlets provide many more seeds for stress rupture than there would have been without the proof test. The situation is made worse, however, as the proof test will not only cause singlets, but could also form clusters of two or more broken fibers, according to

(6.15) through (6.18). In this way the proof test creates a larger number of broken fiber clusters of all sizes that would not have otherwise occurred on loading, potentially making later stress rupture failure more likely. At the same time, a proof test to stress level σ_p would eliminate any vessels in the lower tail of the strength distribution, which is beneficial, at least in the short run. This raises the potential for trade-offs whereby there are time regimes where proof testing is beneficial and other time regimes (shorter or longer) where it is not. With the appropriate proof level this feature could be exploited.

It is important to appreciate that the fiber itself benefits in some respects from the proof test. This is because any fiber flaws weaker than σ_p, irrespective of their location, will fail in the proof test, and possibly be involved in various clusters. Thus, the remaining unbroken fiber flaws must have strength greater than σ_p. For a stable cluster to grow after the proof test, the overloaded region must expand along the adjacent fibers. This is because the overloaded adjacent fiber elements already have strength greater than $K_j\sigma_p$ where j is the cluster size (otherwise they would have failed in the proof test), and under the subsequent service lifetime stress the overload has been lowered to $K_j\bar{\sigma}$. When this overload expansion along neighboring fiber segments occurs, one of two situations may happen as described next.

The *first situation* is where the cluster formed in proof testing is large enough such that the overload, $K_j\bar{\sigma}$, created in these expanded fiber regions, is greater than the proof stress level, σ_p, to which the fiber was previously exposed. That is, these expanded regions were not exposed to overloads from the cluster during the proof test, and therefore have only been exposed to a stress level of σ_p. In this case further fiber failures, in the newly overloaded neighboring fiber

regions, will be caused by the overload $K_j\bar{\sigma} > \sigma_p$.

The *second situation* is where the cluster is small enough such that over-load stresses after proof testing are now less than or equal to the proof stress, that is $K_j\bar{\sigma} \le \sigma_p$. Thus, as the overload length increases, further cluster growth is initiated from encountering previous fiber breaks from flaws that already failed under σ_p, rather than by creating new failures from flaws of strength of $K_j\bar{\sigma}$ or less, since they would have already failed under the applied load σ_p. Note that when $K_j\bar{\sigma}$ is significantly less than σ_p, it may take several previously broken flaws, say i, to be encountered in succession in order to grow the cluster to the point where $K_{j+i}\bar{\sigma} > \sigma_p$.

For the first situation to occur, there is a minimum size for such a cluster, denoted $k_p = k_p(\bar{\sigma}/\sigma_p)$, that must satisfy

$$K_{k_p-1}\bar{\sigma} < \sigma_p < K_{k_p}\bar{\sigma}, \text{ or } K_{k_p-1} < \sigma_p/\bar{\sigma} < K_{k_p} \tag{6.52}$$

For a planar array, where K_j is given in (6.28) as $K_j \approx \sqrt{1+\pi j/4}$, $j = 0,1,2,\cdots$, this minimum cluster size is

$$k_p = \left\lceil \frac{4}{\pi}\left[\left(\frac{\sigma_p}{\bar{\sigma}}\right)^2 - 1\right]\right\rceil \tag{6.53}$$

while for a hexagonal array, with K_j given in (6.29) as $K_j \approx \sqrt{1+\sqrt{4j/\pi^3}}$, the minimum size is

$$k_p = \left\lceil \frac{\pi^3}{4}\left[\left(\frac{\sigma_p}{\bar{\sigma}}\right)^2 - 1\right]^2\right\rceil. \tag{6.54}$$

where again '$\lceil \bullet \rceil$' corresponds to the ceiling function used earlier.

Note that, depending on the ratio $\sigma_{\mathrm{p}}/\bar{\sigma}$, and the values of various model parameters, it is theoretically possible to obtain a minimum size, k_{p}, that exceeds $\hat{k}$, the critical cluster size that satisfies $K_{\hat{k}-1} < \sigma_{\delta_e}/\hat{\sigma}_V < K_{\hat{k}}$. This threshold in the model would be exceeded if the ratio of the proof test stress to the long-term service stress level exceeds the ratio of the fiber element strength to the Weibull scale parameter for composite strength, that is, $\sigma_{\mathrm{p}}/\bar{\sigma} > \sigma_{\delta_e}/\hat{\sigma}_V$. While k_{p} is a threshold size in the model, it is extremely unlikely that a size anywhere near $\hat{k}$ will physically occur let alone a larger cluster size, k_{p}, when both σ_{p} and $\bar{\sigma}$ are significantly less than $\hat{\sigma}_V$. Nonetheless the probabilities for the various cluster formation paths resulting from a proof test must be assessed and summed systematically, and any potential sequences ruled out only when it is clear they are dominated by probabilities of occurrence of other sequences. In the current case we define the occurrence of a cluster of $\hat{k}$ breaks as equivalent to failure, and thus, considering k values for which $k_{\mathrm{p}} > k > \hat{k}$ is unnecessary.

6.4.1 Failure probability in proof hold time

We consider an initial proof test to stress level, σ_{p}, over time $0 < t < t_{\mathrm{p}}$, where t_{p} is termed the 'proof holding time', and thereafter the stress is $\bar{\sigma}$. This is the stress profile $\sigma(t)$ described by equation (6.50). We let $W_{\hat{k},\mathrm{p}}\left(t;\sigma(t),\sigma_{\mathrm{p}}\right)$ be the characteristic distribution function for lifetime including a proof test, extending the concepts developed earlier.

For failure to occur during the holding time in the proof test, a critical cluster of size $\hat{k}$ must

form, and we must have

$$H_{V,\mathrm{p}}\left(t;\sigma\right)\approx 1-\exp\left\{-VW_{\hat{k},\mathrm{p}}\left(t;\sigma_{\mathrm{p}},\sigma_{\mathrm{p}}\right)\right\},\qquad 0<t<t_{\mathrm{p}} \tag{6.55}$$

where

$$\begin{aligned} W_{\hat{k},\mathrm{p}}\left(t;\sigma_{\mathrm{p}},\sigma_{\mathrm{p}}\right) &\approx c_{\hat{k}}F_{\delta_e}\left(\sigma_{\mathrm{p}}\right)\left[\prod_{i=2}^{\hat{k}}F_{\delta_e}\left(K_{i-1}\sigma_{\mathrm{p}},t\right)\right] \\ &\approx c_{\hat{k}}\left(K_1K_2\cdots K_{\hat{k}-1}\right)^{\zeta}\left(\sigma_{\mathrm{p}}/\sigma_{\delta_e}\right)^{\hat{k}\zeta}\left(\sqrt{1+\left(t/t_c\right)^{\theta}}\right)^{\hat{k}-1},\quad 0<t<t_{\mathrm{p}} \end{aligned} \tag{6.56}$$

The right hand side of (6.56) is identical to (6.45), upon taking $\sigma\left(t\right)=\sigma_{\mathrm{p}}$.

In the case where failure does not occur during the proof test, we continue on for times $t>t_{\mathrm{p}}$, whereby the composite is under the service load, $\sigma\left(t\right)=\bar{\sigma}$. To calculate the failure probability for times after time t_{p}, we must first consider the state of the composite at time t_{p}.

6.4.2 Cluster of size $\hat{k}-1$ forms initially

Suppose that an initial cluster of $\hat{k}-1$ breaks occurs under the proof test, that is, the cluster size is only one short of that required to fail the composite, (since we have defined the occurrence of a cluster of $\hat{k}$ breaks as being equivalent to failure). If, for instance, the stress, σ, were inadvertently increased to above $\hat{\sigma}_V$ then failure would occur. Ruling out this scenario, however, in order then to reach a cluster of critical size of at least $\hat{k}$ at some time $t>t_{\mathrm{p}}$ requires failure of at least one of the nearest neighbors. In the case of a proof test stress satisfying $\sigma_{\mathrm{p}}=\bar{\sigma}$, i.e., no actual proof test, then for failure to occur after a long time, $t\gg t_{\mathrm{p}}$, the overload length eventually must satisfy $F_{\delta_e}\left(K_{\hat{k}}\bar{\sigma},t\right)\approx 1/2$. However, when $\sigma_{\mathrm{p}}>\bar{\sigma}$ we must look more

closely at the two situations described above regarding the cluster size after the proof test, and its relation to the critical threshold k_{p}.

6.4.2.1 Cluster of size $\hat{k}-1$ forms initially, where $\hat{k}-1 \geq k_{\mathrm{p}}$

Continuing with a cluster of $\hat{k}-1$ breaks occurring during the proof test, and considering the first case mentioned above, this cluster size must satisfy $\hat{k}-1 \geq k_{\mathrm{p}}$, the critical threshold. Thus, the overloads caused by the cluster after time t_{p} must be larger than the previously applied load σ_{p}, and the characteristic distribution function takes the form:

$$W_{\hat{k},\mathrm{p},\hat{k}-1}\left(t;\bar{\sigma},\sigma_{\mathrm{p}}\right) \approx c_{\hat{k}-1} F_{\delta_e}\left(\sigma_{\mathrm{p}}\right)\left[\prod_{i=2}^{\hat{k}-1} F_{\delta_e}\left(K_{i-1}\sigma_{\mathrm{p}},t_{\mathrm{p}}\right)\right]\left[1-F_{\delta_e}\left(K_{\hat{k}-1}\sigma_{\mathrm{p}},t_{\mathrm{p}}\right)\right]^{N_{\hat{k}-1}} \times N_{\hat{k}-1}\left[F_{\delta_e}\left(K_{\hat{k}-1}\bar{\sigma},t\right)-F_{\delta_e}\left(K_{\hat{k}-1}\bar{\sigma},t_{\mathrm{p}}\right)\right], \qquad t > t_{\mathrm{p}} \tag{6.57}$$

where as before $N_{\hat{k}-1}$ is the number of nearest neighbors around a cluster of $\hat{k}-1$ breaks.

Equation (6.57) represents that *exactly* $\hat{k}-1$ breaks occurred over time t_{p} (the first term), and then after time t_{p} one of the $N_{\hat{k}-1}$ nearest neighbors fails, causing composite failure since the cluster is now of size $\hat{k}$. In doing this calculation, since the last fiber didn't fail during time t_{p}, we know that the portion of the fiber exposed to the overload at the end of t_{p} is stronger than $K_{\hat{k}-1}\sigma_{\mathrm{p}} > K_{\hat{k}-1}\bar{\sigma}$. Thus when calculating the failure probability for that fiber, we must only consider length that is newly exposed to the overload as the overload grows. This is captured by

$$F_{\delta_e}\left(K_{\hat{k}-1}\bar{\sigma},t\right)-F_{\delta_e}\left(K_{\hat{k}-1}\bar{\sigma},t_{\mathrm{p}}\right), \tag{6.58}$$

which becomes clearer when (6.41) is substituted into (6.58), resulting in

$$F_{\delta_e}\left(K_{\hat{k}-1}\bar{\sigma},t\right)-F_{\delta_e}\left(K_{\hat{k}-1}\bar{\sigma},t_{\mathrm{p}}\right)=\left(\frac{K_{\hat{k}-1}\bar{\sigma}}{\sigma_{\delta_e}}\right)^{\zeta}\left[\frac{\delta\left(t\right)-\delta\left(t_{\mathrm{p}}\right)}{\delta_e}\right]. \tag{6.59}$$

Now we can see that we are only considering newly exposed fiber when calculating the failure probability of the last neighboring fiber in (6.57). Finally, the remaining term in (6.57) is the probability of survival for all of the neighboring fiber elements:

$$\left[1-F_{\delta_e}\left(K_{\hat{k}-1}\sigma_{\mathrm{p}},t_{\mathrm{p}}\right)\right]^{N_{\hat{k}-1}}. \tag{6.60}$$

since in order for exactly $\hat{k}-1$ breaks to occur during the proof test, none of the neighboring fibers can fail during time t_{p}, which is captured in (6.60).

To reduce (6.57) to a more useful form, we substitute in (6.41) to describe the fiber strength distribution, getting:

$$\begin{aligned}W_{\hat{k},\mathrm{p},\hat{k}-1}\left(t;\bar{\sigma},\sigma_{\mathrm{p}}\right)\approx c_{\hat{k}}&\left[\left(K_1K_2\cdots K_{\hat{k}-2}\right)^{\zeta}\left(\frac{\sigma_{\mathrm{p}}}{\sigma_{\delta_e}}\right)^{\left(\hat{k}-1\right)\zeta}\left(\frac{\delta\left(t_{\mathrm{p}}\right)}{\delta_e}\right)^{\left(\hat{k}-2\right)}\right]\\&\times\left(1-\left(\frac{K_{\hat{k}-1}\sigma_{\mathrm{p}}}{\sigma_{\delta_e}}\right)^{\zeta}\frac{\delta\left(t_{\mathrm{p}}\right)}{\delta_e}\right)^{N_{\hat{k}-1}}\left(\frac{K_{\hat{k}-1}\bar{\sigma}}{\sigma_{\delta_e}}\right)^{\zeta}\left[\frac{\delta\left(t\right)-\delta\left(t_{\mathrm{p}}\right)}{\delta_e}\right],\quad t>t_{\mathrm{p}}\end{aligned} \tag{6.61}$$

Note that the combinatorial factor, c_k, has incorporated $N_{\hat{k}-1}$ to become $c_{\hat{k}}$.

In the case of a 2D planar array, where $c_{\hat{k}}$ is given as in (6.26), (6.57) can be rearranged to give

$$\begin{aligned}W_{\hat{k},\mathrm{p},\hat{k}-1}\left(t;\bar{\sigma},\sigma_{\mathrm{p}}\right)\approx 2^{\hat{k}-1}&\left(K_1K_2\cdots K_{\hat{k}-2}K_{\hat{k}-1}\right)^{\zeta}\left(\frac{\sigma_{\mathrm{p}}}{\sigma_{\delta_e}}\right)^{\left(\hat{k}-1\right)\zeta}\left(\frac{\delta\left(t_{\mathrm{p}}\right)}{\delta_e}\right)^{\left(\hat{k}-2\right)}\\&\times\left(1-\left(\frac{K_{\hat{k}-1}\sigma_{\mathrm{p}}}{\sigma_{\delta_e}}\right)^{\zeta}\frac{\delta\left(t_{\mathrm{p}}\right)}{\delta_e}\right)^{2}\left(\frac{\bar{\sigma}}{\sigma_{\delta_e}}\right)^{\zeta}\left[\frac{\delta\left(t\right)-\delta\left(t_{\mathrm{p}}\right)}{\delta_e}\right]\end{aligned}. \tag{6.62}$$

Using (6.9) to describe the growth of the overload, (6.62) becomes:

$$W_{\hat{k},\mathrm{p},\hat{k}-1}\left(t;\bar{\sigma},\sigma_{\mathrm{p}}\right)\approx 2^{\hat{k}-1}\left(K_1K_2\cdots K_{\hat{k}-2}K_{\hat{k}-1}\right)^{\zeta}\left(\frac{\sigma_{\mathrm{p}}}{\sigma_{\delta_e}}\right)^{(\hat{k}-1)\zeta}\left(1+\left(\frac{t_{\mathrm{p}}}{t_c}\right)^{\theta}\right)^{\frac{\hat{k}-2}{2}}$$
$$\times\left(1-\left(K_{\hat{k}-1}\sigma_{\mathrm{p}}/\sigma_{\delta_e}\right)^{\zeta}\sqrt{1+\left(\frac{t_{\mathrm{p}}}{t_c}\right)^{\theta}}\right)^2\left(\frac{\bar{\sigma}}{\sigma_{\delta_e}}\right)^{\zeta}\left[\sqrt{1+\left(\frac{t}{t_c}\right)^{\theta}}-\sqrt{1+\left(\frac{t_{\mathrm{p}}}{t_c}\right)^{\theta}}\right] \quad (6.63)$$

In the 2D planar case, the multiplicative factor $\left(1-\left(K_{\hat{k}-1}\sigma_{\mathrm{p}}/\sigma_{\delta_e}\right)^{\zeta}\delta\left(t_{\mathrm{p}}\right)/\delta_e\right)^2$ can be shown to be near unity, since typically $\sigma_{\mathrm{p}}<3\hat{\sigma}_V/4$, whereas all other multiplicative factors are very small. Thus we may conservatively simplify (6.62), using (6.9), by neglecting this factor to obtain

$$W_{\hat{k},\mathrm{p},\hat{k}-1}\left(t;\bar{\sigma},\sigma_{\mathrm{p}}\right)\approx 2^{\hat{k}-1}\left(K_1K_2\cdots K_{\hat{k}-1}\right)^{\zeta}\left(\sigma_{\mathrm{p}}/\sigma_{\delta_e}\right)^{(\hat{k}-1)\zeta}$$
$$\times\left(1+\left(\frac{t_{\mathrm{p}}}{t_c}\right)^{\theta}\right)^{\frac{\hat{k}-2}{2}}\left(\frac{\bar{\sigma}}{\sigma_{\delta_e}}\right)^{\zeta}\left[\sqrt{1+\left(\frac{t}{t_c}\right)^{\theta}}-\sqrt{1+\left(\frac{t_{\mathrm{p}}}{t_c}\right)^{\theta}}\right] \quad (6.64)$$

Remember that equations (6.62) through (6.64) are all for a 2D planar array. For a hexagonal array, where $c_{\hat{k}}$ is as in (6.27) and $N_{\hat{k}-1}$ is as in (6.24), equation (6.63) becomes

$$W_{\hat{k},\mathrm{p},\hat{k}-1}\left(t;\bar{\sigma},\sigma_{\mathrm{p}}\right)\approx \pi^{k-1}\prod_{j=1}^{k-1}\left(\sqrt{4j/\pi}+1\right)\left(K_1K_2\cdots K_{\hat{k}-2}K_{\hat{k}-1}\right)^{\zeta}\left(\sigma_{\mathrm{p}}/\sigma_{\delta_e}\right)^{(\hat{k}-1)\zeta}$$
$$\times\left(1+\left(\frac{t_{\mathrm{p}}}{t_c}\right)^{\theta}\right)^{\frac{\hat{k}-2}{2}}\left(1-\left(\frac{K_{\hat{k}-1}\sigma_{\mathrm{p}}}{\sigma_{\delta_e}}\right)^{\zeta}\sqrt{1+\left(\frac{t_{\mathrm{p}}}{t_c}\right)^{\theta}}\right)^{\pi\left(\sqrt{4(\hat{k}-1)/\pi}+1\right)}, \quad (6.65)$$
$$\times\left(\frac{\sigma}{\sigma_{\delta_e}}\right)^{\zeta}\left[\sqrt{1+\left(\frac{t}{t_c}\right)^{\theta}}-\sqrt{1+\left(\frac{t_{\mathrm{p}}}{t_c}\right)^{\theta}}\right]$$

where we have not neglected the multiplicative factor $\left(1-\left(K_{\hat{k}-1}\sigma_{\mathrm{p}}/\sigma_{\delta_e}\right)^{\zeta}\delta\left(t_{\mathrm{p}}\right)/\delta_e\right)^{N_{\hat{k}-1}}$, as was the case in (6.64).

6.4.2.2 Cluster of size $\hat{k}-1$ forms initially, where $\hat{k}-1<k_{\mathrm{p}}$

Equations (6.57) through (6.64) assume the case where $k_{\mathrm{p}}\le\hat{k}-1$, i.e. the overloads, caused by the cluster after time t_{p}, are larger than the previously applied load σ_{p}. If, on the other hand, we have $k_{\mathrm{p}}\ge\hat{k}$, but a cluster of size $\hat{k}-1$ has resulted from the proof test, we have the second situation described above.

In this case, all overloads during the sustained loading, $\bar{\sigma}$, will be less than σ_{p}, and thus no new fiber breaks will occur due to the expanding overload length. However, the proof load σ_{p} will still have broken fibers, and now we simply must wait for the overload region to reach exactly one previously broken fiber flaw in order to grow the cluster to the size $\hat{k}$, which is the failure size. As such, the characteristic distribution takes the form

$$\begin{aligned}W_{\hat{k},\mathrm{p},\hat{k}-1}\left(t;\bar{\sigma},\sigma_{\mathrm{p}}\right)\approx c_{\hat{k}-1}F_{\delta_e}\left(\sigma_{\mathrm{p}}\right)\left[\prod_{i=2}^{\hat{k}-1}F_{\delta_e}\left(K_{i-1}\sigma_{\mathrm{p}},t_{\mathrm{p}}\right)\right]\left[1-F_{\delta_e}\left(K_{\hat{k}-1}\sigma_{\mathrm{p}},t_{\mathrm{p}}\right)\right]^{N_{\hat{k}-1}}\\ \times N_{\hat{k}-1}\left[F_{\delta_e}\left(\sigma_{\mathrm{p}},t\right)-F_{\delta_e}\left(\sigma_{\mathrm{p}},t_{\mathrm{p}}\right)\right],\qquad t>t_{\mathrm{p}}\end{aligned}\tag{6.66}$$

The key difference between equations (6.57) and (6.66) is that instead of searching for newly exposed flaws that are weaker than $K_{\hat{k}-1}\bar{\sigma}$, in this case we want to search for flaws weaker than σ_{p} – i.e. flaws that already failed during the proof test. Thus only the last term changes from equation (6.58) to become $F_{\delta_e}\left(\sigma_{\mathrm{p}},t\right)-F_{\delta_e}\left(\sigma_{\mathrm{p}},t_{\mathrm{p}}\right)$.

Substituting (6.41) into (6.66) gives:

$$W_{\hat{k},\mathrm{p},\hat{k}-1}\left(t;\bar{\sigma},\sigma_{\mathrm{p}}\right)\approx c_{\hat{k}-1}N_{\hat{k}-1}\left[\left(K_1K_2\cdots K_{\hat{k}-2}\right)^{\zeta}\left(\frac{\sigma_{\mathrm{p}}}{\sigma_{\delta_e}}\right)^{(\hat{k}-1)\zeta}\left(\frac{\delta\left(t_{\mathrm{p}}\right)}{\delta_e}\right)^{\hat{k}-2}\right] \times\left(1-\left(\frac{K_{\hat{k}-1}\sigma_{\mathrm{p}}}{\sigma_{\delta_e}}\right)^{\zeta}\frac{\delta\left(t_{\mathrm{p}}\right)}{\delta_e}\right)^{N_{\hat{k}-1}}\left(\frac{\bar{\sigma}}{\sigma_{\delta_e}}\right)^{\zeta}\left[\frac{\delta(t)-\delta\left(t_{\mathrm{p}}\right)}{\delta_e}\right] \tag{6.67}$$

In the case of a planar 2D array, where $N_{\hat{k}-1}=2$ and $c_{\hat{k}}$ is as in (6.26), (6.67) becomes

$$W_{\hat{k},\mathrm{p},\hat{k}-1}\left(t;\bar{\sigma},\sigma_{\mathrm{p}}\right)\approx 2^{\hat{k}-1}\left(K_1K_2\cdots K_{\hat{k}-2}\right)^{\zeta}\left(\sigma_{\mathrm{p}}/\sigma_{\delta_e}\right)^{(\hat{k}-1)\zeta}\left(\delta\left(t_{\mathrm{p}}\right)/\delta_e\right)^{\hat{k}-2} \times\left(1-\left(K_{\hat{k}-1}\sigma_{\mathrm{p}}/\sigma_{\delta_e}\right)^{\zeta}\delta\left(t_{\mathrm{p}}\right)/\delta_e\right)^{2}\left(\sigma_{\mathrm{p}}/\sigma_{\delta_e}\right)^{\zeta}\left(\delta(t)-\delta\left(t_{\mathrm{p}}\right)\right)/\delta_e \tag{6.68}$$

which upon again neglecting the factor $\left(1-\left(K_{\hat{k}-1}\sigma_{\mathrm{p}}/\sigma_{\delta_e}\right)^{\zeta}\delta\left(t_{\mathrm{p}}\right)/\delta_e\right)^{2}$, and substituting (6.9) into (6.68) to describe the growth of the overload, becomes:

$$W_{\hat{k},\mathrm{p},\hat{k}-1}\left(t;\bar{\sigma},\sigma_{\mathrm{p}}\right)\approx\ 2^{\hat{k}-1}\left(K_1K_2\cdots K_{\hat{k}-1}\right)^{\zeta}\left(\frac{\sigma_{\mathrm{p}}}{\sigma_{\delta_e}}\right)^{\hat{k}\zeta}\left(\sqrt{1+\left(\frac{t_{\mathrm{p}}}{t_c}\right)^{\theta}}\right)^{\hat{k}-2} \times\left[\sqrt{1+\left(\frac{t}{t_c}\right)^{\theta}}-\sqrt{1+\left(\frac{t_{\mathrm{p}}}{t_c}\right)^{\theta}}\right]K_{\hat{k}-1}^{-\zeta} \tag{6.69}$$

Remember that equations (6.68) and (6.69) are for a 2D planar array. For a hexagonal array, where $c_{\hat{k}}$ is as in (6.27) and $N_{\hat{k}-1}$ is as in (6.24), equation (6.68) becomes

$$W_{\hat{k},\mathrm{p},\hat{k}-1}\left(t;\bar{\sigma},\sigma_{\mathrm{p}}\right)\approx\ \pi^{k-1}\prod_{j=1}^{k-1}\left(\sqrt{4j/\pi}+1\right)\left(K_1K_2\cdots K_{\hat{k}-1}\right)^{\zeta}\left(\frac{\sigma_{\mathrm{p}}}{\sigma_{\delta_e}}\right)^{\hat{k}\zeta}$$
$$\times\left(\sqrt{1+\left(\frac{t_{\mathrm{p}}}{t_c}\right)^{\theta}}\right)^{\hat{k}-2}\left(1-\left(\frac{K_{\hat{k}-1}\sigma_{\mathrm{p}}}{\sigma_{\delta_e}}\right)^{\zeta}\sqrt{1+\left(\frac{t_{\mathrm{p}}}{t_c}\right)^{\theta}}\right)^{\pi\left(\sqrt{4\left(\hat{k}-1\right)/\pi}+1\right)} \qquad (6.70)$$
$$\times\left[\sqrt{1+\left(\frac{t}{t_c}\right)^{\theta}}-\sqrt{1+\left(\frac{t_{\mathrm{p}}}{t_c}\right)^{\theta}}\right]K_{\hat{k}-1}^{-\zeta}$$

again not neglecting the multiplicative factor $\left(1-\left(K_{\hat{k}-1}\sigma_{\mathrm{p}}/\sigma_{\delta_e}\right)^{\zeta}\delta\left(t_{\mathrm{p}}\right)/\delta_e\right)^{N_{\hat{k}-1}}$.

In order to obtain $k_{\mathrm{p}}\geq\hat{k}$ you must have a small value of $\hat{k}$ and a very high proof ratio, $\sigma_{\mathrm{p}}/\bar{\sigma}$. This situation, where $\sigma_{\mathrm{p}}/\bar{\sigma}>\sigma_{\delta_e}/\hat{\sigma}_V$, is extremely unlikely compared to probabilities for other sequences, and thus we will ignore this term when we later sum up the probabilities for the various configurations in Section 6.4.4.

6.4.3 Cluster of size k forms initially

Again suppose that during time t_{p} a cluster of k fiber breaks forms. In section 6.4.3.1 we look at the first situation where $k_{\mathrm{p}}\leq k<\hat{k}-1$, whereas in Section 6.4.3.2 we will consider the second situation, where $\hat{k}>k_{\mathrm{p}}>k$.

6.4.3.1 Cluster of size k forms initially with $k_{\mathrm{p}}\leq k<\hat{k}-1$

When a cluster of $k < \hat{k} - 1$ fiber breaks forms by time t_{p}, then composite failure by some time, t after the proof test (which requires a cluster of $\hat{k}$ breaks)is caused by a sequence of $\hat{k} - k > 1$ additional failures, beginning with the failure of a fiber flanking the stalled k cluster. Since $k_{\mathrm{p}} \le k$, the overloads, for $t > t_{\mathrm{p}}$, are larger than the previously applied load σ_{p}. In this event the characteristic distribution function takes the form:

$$W_{\hat{k},\mathrm{p},k}\left(t;\bar{\sigma},\sigma_{\mathrm{p}}\right) \approx c_k F_{\delta_e}\left(\sigma_{\mathrm{p}}\right)\left[\prod_{i=2}^{k} F_{\delta_e}\left(K_{i-1}\sigma_{\mathrm{p}},t_{\mathrm{p}}\right)\right]\left(1-F_{\delta_e}\left(K_k\sigma_{\mathrm{p}},t_{\mathrm{p}}\right)\right)^{N_k} \times N_k\left[F_{\delta_e}\left(K_k\bar{\sigma},t\right)-F_{\delta_e}\left(K_k\bar{\sigma},t_{\mathrm{p}}\right)\right]\left[\prod_{i=k+2}^{\hat{k}} N_i F_{\delta_e}\left(K_{i-1}\bar{\sigma},t-t_{\mathrm{p}}\right)\right] \tag{6.71}$$

The first line in (6.71) directly follows from arguments made above, while the second line in (6.71) requires a bit more explanation. The first term of the first line, $c_k F_{\delta_e}\left(\sigma_{\mathrm{p}}\right)\prod_{i=2}^{k} F_{\delta_e}\left(K_{i-1}\sigma_{\mathrm{p}},t_{\mathrm{p}}\right)$, is the probability that exactly k fibers failed during time t_{p}. The second term of the first line, $\left(1-F_{\delta_e}\left(K_k\sigma_{\mathrm{p}},t_{\mathrm{p}}\right)\right)^{N_k}$, is the probability that none of the N_k neighboring fibers failed during time t_{p}. To explain the second line, we first note that during the proof time, t_{p}, a cluster of exactly k fibers is assumed to have formed, and then cluster growth stalled. The applied load was then reduced from σ_{p} to $\bar{\sigma}$. At this point the portions of the neighboring fibers exposed to the overload are stronger than $K_k\sigma_{\mathrm{p}} > K_k\bar{\sigma}$. Thus for the next fiber to break the overload length must grow until a new flaw is uncovered. The first term in the second line, $N_k\left[F_{\delta_e}\left(K_k\bar{\sigma},t\right)-F_{\delta_e}\left(K_k\bar{\sigma},t_{\mathrm{p}}\right)\right]$, is exactly this – the failure probability of the newly exposed portions of the N_k neighboring fibers. Once that neighboring fiber has failed, it now exposes

new fibers whose maximum load before this point was σ_{p}. Since $K_{k+1}\bar{\sigma} > \sigma_{\mathrm{p}}$, we must search the whole overloaded region for flaws to fail. The final term, $\prod_{i=k+2}^{\hat{k}} N_i F_{\delta_e}\left(K_{i-1}\bar{\sigma}, t-t_{\mathrm{p}}\right)$, reflects this, though it does not differentiate between the remaining fibers that were neighbors to the stalled cluster vs. the neighbors newly created by the $k+1$, $k+2 \ldots$ $\hat{k}-1$ fibers breaking. Thus, this term is precisely the probability of failure for the remaining $k+2$ through $\hat{k}$ fibers, where the overload growth starts at time t_{p}. Thus, this final term is an approximation for the desired term.

Taking (6.71) and substituting in (6.41) to approximate the failure probability, we get

$$\begin{aligned} W_{\hat{k},\mathrm{p},k}\left(t;\bar{\sigma},\sigma_{\mathrm{p}}\right) \approx\ & c_{\hat{k}}\left(K_1 K_2 \cdots K_{k-1}\right)^{\zeta}\left(\sigma_{\mathrm{p}}/\sigma_{\delta_e}\right)^{k\zeta}\left(\frac{\delta\left(t_{\mathrm{p}}\right)}{\delta_e}\right)^{k-1}\left(1-\left(\frac{K_k\sigma_{\mathrm{p}}}{\sigma_{\delta_e}}\right)^{\zeta}\frac{\delta\left(t_{\mathrm{p}}\right)}{\delta_e}\right)^{N_k} \\ & \times\left(\frac{\delta(t)-\delta\left(t_{\mathrm{p}}\right)}{\delta_e}\right)\left(\frac{\delta\left(t-t_{\mathrm{p}}\right)}{\delta_e}\right)^{\hat{k}-k-1} \\ & \times\left(K_k\bar{\sigma}/\sigma_{\delta_e}\right)^{\zeta}\left(K_{k+1}\bar{\sigma}/\sigma_{\delta_e}\right)^{\zeta}\ldots\left(K_{\hat{k}-1}\bar{\sigma}/\sigma_{\delta_e}\right)^{\zeta} \end{aligned} \tag{6.72}$$

In the case of a 2D planar array (6.72) simplifies to

$$\begin{aligned} W_{\hat{k},\mathrm{p},k}\left(t;\bar{\sigma},\sigma_{\mathrm{p}}\right) \approx\ & 2^{k-1}\left(K_1 K_2 \cdots K_{k-1}\right)^{\zeta}\left(\sigma_{\mathrm{p}}/\sigma_{\delta_e}\right)^{k\zeta}\left(\frac{\delta\left(t_{\mathrm{p}}\right)}{\delta_e}\right)^{k-1}\left(1-\left(\frac{K_k\sigma_{\mathrm{p}}}{\sigma_{\delta_e}}\right)^{\zeta}\frac{\delta\left(t_{\mathrm{p}}\right)}{\delta_e}\right)^{2} \\ & \times 2^{\hat{k}-k}\left(\frac{\delta(t)-\delta\left(t_{\mathrm{p}}\right)}{\delta_e}\right)\left(\frac{\delta\left(t-t_{\mathrm{p}}\right)}{\delta_e}\right)^{\hat{k}-k-1} \\ & \times\left(K_k\bar{\sigma}/\sigma_{\delta_e}\right)^{\zeta}\left(K_{k+1}\bar{\sigma}/\sigma_{\delta_e}\right)^{\zeta}\ldots\left(K_{\hat{k}-1}\bar{\sigma}/\sigma_{\delta_e}\right)^{\zeta} \end{aligned} \tag{6.73}$$

which reduces to

$$W_{\hat{k},\mathrm{p},k}\left(t;\bar{\sigma},\sigma_{\mathrm{p}}\right)\approx 2^{\hat{k}-1}\left(K_1K_2\cdots K_{\hat{k}-1}\right)^{\zeta}\left(\frac{\sigma_{\mathrm{p}}}{\sigma_{\delta_e}}\right)^{\hat{k}\zeta}\left(\sqrt{1+\left(\frac{t_{\mathrm{p}}}{t_c}\right)^{\theta}}\right)^{k-1}$$
$$\times\left(1-\left(\frac{K_k\sigma_{\mathrm{p}}}{\sigma_{\delta_e}}\right)^{\zeta}\sqrt{1+\left(\frac{t_{\mathrm{p}}}{t_c}\right)^{\theta}}\right)^{2} \tag{6.74}$$
$$\times\left[\sqrt{1+\left(\frac{t}{t_c}\right)^{\theta}}-\sqrt{1+\left(\frac{t_{\mathrm{p}}}{t_c}\right)^{\theta}}\right]\left[\sqrt{1+\left(\frac{t-t_{\mathrm{p}}}{t_c}\right)^{\theta}}\right]^{\hat{k}-k-1}\left(\frac{\bar{\sigma}}{\sigma_{\mathrm{p}}}\right)^{\left(\hat{k}-k\right)\zeta}$$

Neglecting the factor $\left(1-\left(K_{\hat{k}-1}\sigma_{\mathrm{p}}/\sigma_{\delta_e}\right)^{\zeta}\delta\left(t_{\mathrm{p}}\right)/\delta_e\right)^{2}$ we reduce the above expression to

$$W_{\hat{k},\mathrm{p},k}\left(t;\sigma,\sigma_{\mathrm{p}}\right)\approx 2^{\hat{k}-1}\left(K_1K_2\cdots K_{\hat{k}-1}\right)^{\zeta}\left(\frac{\sigma_{\mathrm{p}}}{\sigma_{\delta_e}}\right)^{\hat{k}\zeta}\left(\frac{\bar{\sigma}}{\sigma_{\mathrm{p}}}\right)^{\left(\hat{k}-k\right)\zeta}\left(\sqrt{1+\left(\frac{t_{\mathrm{p}}}{t_c}\right)^{\theta}}\right)^{k-1}$$
$$\times\left[\sqrt{1+\left(\frac{t}{t_c}\right)^{\theta}}-\sqrt{1+\left(\frac{t_{\mathrm{p}}}{t_c}\right)^{\theta}}\right]\left[\sqrt{1+\left(\frac{t-t_{\mathrm{p}}}{t_c}\right)^{\theta}}\right]^{\hat{k}-k-1},\quad t>t_{\mathrm{p}} \tag{6.75}$$

Remember again that equations (6.73) through (6.75) are for a 2D planar array. For a hexagonal array equation (6.73), using (6.9), becomes

$$W_{\hat{k},\mathrm{p},k}\left(t;\sigma,\sigma_{\mathrm{p}}\right)\approx\left[\pi^{\hat{k}-1}\prod_{j=1}^{\hat{k}-1}\left(\sqrt{4j/\pi}+1\right)\right]\left(K_1K_2\cdots K_{\hat{k}-1}\right)^{\zeta}\left(\frac{\sigma_{\mathrm{p}}}{\sigma_{\delta_e}}\right)^{\hat{k}\zeta}\left(\sqrt{1+\left(\frac{t_{\mathrm{p}}}{t_c}\right)^{\theta}}\right)^{k-1}$$
$$\times\left(1-\left(\frac{K_k\sigma_{\mathrm{p}}}{\sigma_{\delta_e}}\right)^{\zeta}\sqrt{1+\left(\frac{t_{\mathrm{p}}}{t_c}\right)^{\theta}}\right)^{\pi\left(\sqrt{4k/\pi}+1\right)}\left[\sqrt{1+\left(\frac{t}{t_c}\right)^{\theta}}-\sqrt{1+\left(\frac{t_{\mathrm{p}}}{t_c}\right)^{\theta}}\right] \tag{6.76}$$
$$\times\left[\sqrt{1+\left(\frac{t-t_{\mathrm{p}}}{t_c}\right)^{\theta}}\right]^{\hat{k}-k-1}\left(\frac{\bar{\sigma}}{\sigma_{\mathrm{p}}}\right)^{\left(\hat{k}-k\right)\zeta}\qquad t>t_{\mathrm{p}}$$

6.4.3.2 Cluster of size k forms initially with $k < k_{\mathrm{p}} < \hat{k}$

Suppose again that during time t_{p} a smaller cluster of $k < \hat{k} - 1$ fiber breaks forms. In this section we look at the case where $k < k_{\mathrm{p}}$. Here, in contrast to above, all overloads during the sustained loading will be less than σ_{p}, and thus no new fibers will break. Thus, the characteristic distribution function takes the form:

$$\begin{aligned} W_{\hat{k},\mathrm{p},k}\left(t;\bar{\sigma},\sigma_{\mathrm{p}}\right) \approx c_k F_{\delta_e}\left(\sigma_{\mathrm{p}}\right)\left[\prod_{i=2}^{k} F_{\delta_e}\left(K_{i-1}\sigma_{\mathrm{p}},t_{\mathrm{p}}\right)\right]\left(1-F_{\delta_e}\left(K_k\sigma_{\mathrm{p}},t_{\mathrm{p}}\right)\right)^{N_k} \\ \times N_k\left[F_{\delta_e}\left(\sigma_{\mathrm{p}},t\right)-F_{\delta_e}\left(\sigma_{\mathrm{p}},t_{\mathrm{p}}\right)\right]\left[\prod_{i=k+2}^{k_{\mathrm{P}}} N_i F_{\delta_e}\left(\sigma_{\mathrm{p}},t-t_{\mathrm{p}}\right)\right]. \\ \times\left[\prod_{i=k_{\mathrm{p}}+1}^{\hat{k}} N_i F_{\delta_e}\left(K_{i-1}\bar{\sigma},t-t_{\mathrm{p}}\right)\right] \end{aligned} \tag{6.77}$$

As before in (6.71), the first term in the first line, $F_{\delta_e}\left(\sigma_{\mathrm{p}}\right)\prod_{i=2}^{k} F_{\delta_e}\left(K_{i-1}\sigma_{\mathrm{p}},t_{\mathrm{p}}\right)$, is the probability that exactly k fibers failed during time t_{p}, and the second term in the first line, $\left(1-F_{\delta_e}\left(K_k\sigma_{\mathrm{p}},t_{\mathrm{p}}\right)\right)^{N_k}$, is the probability that none of the N_k neighboring fibers have failed. In contrast to (6.71), now $k < k_{\mathrm{p}}$, so all overloads during the sustained loading from size k up to cluster size k_{p} will be less than σ_{p}, and thus no new fibers will break, and only as previous breaks, that occurred under σ_{p}, are encountered to grow the cluster. Thus the second line uses σ_{p} as the applied stress instead of $K_i\sigma$, as in (6.71). However, after that, from size $k_{\mathrm{p}}+1$ up to size $\hat{k}$ there will be new fiber breaks due to the overloads due to the steady stress $\bar{\sigma}$ where from

a probability of failure point of view fibers are essentially ‘fresh’ and unaffected by the previous proof test stress, σ_{p}. The term in the third line reflects that probability.

Using (6.41) to approximate the failure probability, (6.77) becomes:

$$
\begin{aligned}
W_{\hat{k},\mathrm{p},k}\left(t;\bar{\sigma},\sigma_{\mathrm{p}}\right) \approx c_k & \left[\left(K_1 K_2 \cdots K_{k-1}\right)^{\zeta}\left(\frac{\sigma_{\mathrm{p}}}{\sigma_{\delta_e}}\right)^{k\zeta}\left(\frac{\delta\left(t_{\mathrm{p}}\right)}{\delta_e}\right)^{k-1}\right] \\
& \times\left(1-\left(\frac{K_k\sigma_{\mathrm{p}}}{\sigma_{\delta_e}}\right)^{\zeta}\left(\frac{\delta\left(t_{\mathrm{p}}\right)}{\delta_e}\right)\right)^{N_k} N_k\left(\frac{K_k\bar{\sigma}}{\sigma_{\delta_e}}\right)^{\zeta} \\
& \times\left[\frac{\delta(t)-\delta\left(t_{\mathrm{p}}\right)}{\delta_e}\right]\left[\prod_{i=k+2}^{k_{\mathrm{p}}} N_i\frac{\delta\left(t_{\mathrm{p}}\right)}{\delta_e}\left(\frac{\sigma_{\mathrm{p}}}{\sigma_{\delta_e}}\right)^{\zeta}\right] \\
& \times\left[\prod_{i=k_{\mathrm{p}}+1}^{\hat{k}} N_i\sqrt{1+\left(\frac{t-t_{\mathrm{p}}}{t_c}\right)^{\theta}}\left(\frac{K_{i-1}\bar{\sigma}}{\sigma_{\delta_e}}\right)^{\zeta}\right]
\end{aligned}
\tag{6.78}
$$

Using (6.9) to describe the length of the overload, (6.78) becomes

$$
\begin{aligned}
W_{\hat{k},\mathrm{p},k}\left(t;\bar{\sigma},\sigma_{\mathrm{p}}\right) \approx c_k & \left[\left(K_1K_2\cdots K_{k-1}\right)^{\zeta}\left(\frac{\sigma_{\mathrm{p}}}{\sigma_{\delta_e}}\right)^{k\zeta}\sqrt{1+\left(\frac{t_{\mathrm{p}}}{t_c}\right)^{\theta}}^{k-1}\right] \\
& \times\left(1-\left(\frac{K_k\sigma_{\mathrm{p}}}{\sigma_{\delta_e}}\right)^{\zeta}\sqrt{1+\left(\frac{t_{\mathrm{p}}}{t_c}\right)^{\theta}}\right)^{N_k} N_k\left(\frac{K_k\bar{\sigma}}{\sigma_{\delta_e}}\right)^{\zeta} \\
& \times\left[\sqrt{1+\left(\frac{t}{t_c}\right)^{\theta}}-\sqrt{1+\left(\frac{t_{\mathrm{p}}}{t_c}\right)^{\theta}}\right]\left[\prod_{i=k+2}^{k_{\mathrm{P}}} N_i\sqrt{1+\left(\frac{t-t_{\mathrm{p}}}{t_c}\right)^{\theta}}\left(\frac{\sigma_{\mathrm{p}}}{\sigma_{\delta_e}}\right)^{\zeta}\right] \\
& \times\left[\prod_{i=k_{\mathrm{p}}+1}^{\hat{k}} N_i\sqrt{1+\left(\frac{t-t_{\mathrm{p}}}{t_c}\right)^{\theta}}\left(\frac{K_{i-1}\bar{\sigma}}{\sigma_{\delta_e}}\right)^{\zeta}\right]
\end{aligned}
\tag{6.79}
$$

In the case of a 2D planar array (6.79) becomes

$$
\begin{aligned}
W_{\hat{k},\mathrm{p},k}\left(t;\bar{\sigma},\sigma_{\mathrm{p}}\right) \approx 2^{\hat{k}-1} & \left[\left(K_1K_2\cdots K_{k-1}\right)^{\zeta}\left(\frac{\sigma_{\mathrm{p}}}{\sigma_{\delta_e}}\right)^{k\zeta}\sqrt{1+\left(\frac{t_{\mathrm{p}}}{t_c}\right)^{\theta}}^{k-1}\right] \\
& \times\left(1-\left(\frac{K_k\sigma_{\mathrm{p}}}{\sigma_{\delta_e}}\right)^{\zeta}\sqrt{1+\left(\frac{t_{\mathrm{p}}}{t_c}\right)^{\theta}}\right)^{2}\left(\frac{K_k\bar{\sigma}}{\sigma_{\delta_e}}\right)^{\zeta} \\
& \times\left[\sqrt{1+\left(\frac{t}{t_c}\right)^{\theta}}-\sqrt{1+\left(\frac{t_{\mathrm{p}}}{t_c}\right)^{\theta}}\right]\left[\prod_{i=k+2}^{k_{\mathrm{P}}}\sqrt{1+\left(\frac{t-t_{\mathrm{p}}}{t_c}\right)^{\theta}}\left(\frac{\sigma_{\mathrm{p}}}{\sigma_{\delta_e}}\right)^{\zeta}\right] \\
& \times\left[\prod_{i=k_{\mathrm{p}}+1}^{\hat{k}}\sqrt{1+\left(\frac{t-t_{\mathrm{p}}}{t_c}\right)^{\theta}}\left(\frac{K_{i-1}\bar{\sigma}}{\sigma_{\delta_e}}\right)^{\zeta}\right]
\end{aligned}
\tag{6.80}
$$

while for a hexagonal array (6.79) becomes

$$W_{\hat{k},\mathrm{p},k}\left(t;\bar{\sigma},\sigma_{\mathrm{p}}\right)\approx\left[\pi^{k-1}\prod_{j=1}^{k-1}\left(\sqrt{4j/\pi}+1\right)\right]\left[\left(K_1K_2\cdots K_{k-1}\right)^{\zeta}\left(\frac{\sigma_{\mathrm{p}}}{\sigma_{\delta_e}}\right)^{k\zeta}\sqrt{1+\left(\frac{t_{\mathrm{p}}}{t_c}\right)^{\theta}}^{k-1}\right]$$
$$\times\left(1-\left(\frac{K_k\sigma_{\mathrm{p}}}{\sigma_{\delta_e}}\right)^{\zeta}\sqrt{1+\left(\frac{t_{\mathrm{p}}}{t_c}\right)^{\theta}}\right)^{\pi\left(\sqrt{4j/\pi}+1\right)}\left(\frac{K_k\bar{\sigma}}{\sigma_{\delta_e}}\right)^{\zeta}$$
$$\times\left[\sqrt{1+\left(\frac{t}{t_c}\right)^{\theta}}-\sqrt{1+\left(\frac{t_{\mathrm{p}}}{t_c}\right)^{\theta}}\right]\left[\prod_{i=k+2}^{k_{\mathrm{P}}}\sqrt{1+\left(\frac{t-t_{\mathrm{p}}}{t_c}\right)^{\theta}}\left(\frac{\sigma_{\mathrm{p}}}{\sigma_{\delta_e}}\right)^{\zeta}\right]$$
$$\times\left[\prod_{i=k_{\mathrm{p}}+1}^{\hat{k}}\sqrt{1+\left(\frac{t-t_{\mathrm{p}}}{t_c}\right)^{\theta}}\left(\frac{K_{i-1}\bar{\sigma}}{\sigma_{\delta_e}}\right)^{\zeta}\right] \tag{6.81}$$

6.4.4 Summation of mutually exclusive events

The general probability of failure after a proof test is calculated by summing the mutually exclusive probabilities of the cluster of broken fibers after the proof test, $1\le k\le\hat{k}$. There are Thus the general failure probability is obtained by summing equations (6.56) for $\hat{k}$ breaks in the proof, (6.57) and (6.66) for $\hat{k}-1$ breaks in the proof, with all possible values of k in equation (6.71) and all possible values of k in equation (6.77):

$$
\begin{aligned}
W_{\hat{k},\mathrm{p},k}\left(t;\bar{\sigma},\sigma_{\mathrm{p}}\right) \approx c_{\hat{k}} \Bigg\{ & \left[F_{\delta_e}\left(\sigma_{\mathrm{p}}\right) \prod_{i=2}^{\hat{k}} F_{\delta_e}\left(K_{i-1}\sigma_{\mathrm{p}}, t_{\mathrm{p}}\right) \right] \\
& + \left[F_{\delta_e}\left(\sigma_{\mathrm{p}}\right) \prod_{i=2}^{\hat{k}-1} F_{\delta_e}\left(K_{i-1}\sigma_{\mathrm{p}}, t_{\mathrm{p}}\right) \right] \left(1 - F_{\delta_e}\left(K_{\hat{k}-1}\sigma_{\mathrm{p}}, t_{\mathrm{p}}\right)\right)^{N_{\hat{k}-1}} \\
& \quad \times \left[F_{\delta_e}\left(K_{\hat{k}-1}\bar{\sigma}, t\right) - F_{\delta_e}\left(K_{\hat{k}-1}\bar{\sigma}, t_{\mathrm{p}}\right) \right] \\
& + \sum_{k=k_{\mathrm{p}}}^{\hat{k}-2} \left[F_{\delta_e}\left(\sigma_{\mathrm{p}}\right) \prod_{i=2}^{k} F_{\delta_e}\left(K_{i-1}\sigma_{\mathrm{p}}, t_{\mathrm{p}}\right) \right] \left(1 - F_{\delta_e}\left(K_k\sigma_{\mathrm{p}}, t_{\mathrm{p}}\right)\right)^{N_k} \\
& \quad \times \left[F_{\delta_e}\left(K_k\bar{\sigma}, t\right) - F_{\delta_e}\left(K_k\bar{\sigma}, t_{\mathrm{p}}\right) \right] \left[\prod_{i=k+2}^{\hat{k}} F_{\delta_e}\left(K_{i-1}\bar{\sigma}, t - t_{\mathrm{p}}\right) \right] \\
& + \sum_{k=1}^{k_{\mathrm{p}}-1} \left[F_{\delta_e}\left(\sigma_{\mathrm{p}}\right) \prod_{i=2}^{k} F_{\delta_e}\left(K_{i-1}\sigma_{\mathrm{p}}, t_{\mathrm{p}}\right) \right] \left(1 - F_{\delta_e}\left(K_k\sigma_{\mathrm{p}}, t_{\mathrm{p}}\right)\right)^{N_k} \\
& \quad \times \left[F_{\delta_e}\left(\sigma_{\mathrm{p}}, t\right) - F_{\delta_e}\left(\sigma_{\mathrm{p}}, t_{\mathrm{p}}\right) \right] \left[\prod_{i=k+2}^{k_{\mathrm{P}}} F_{\delta_e}\left(\sigma_{\mathrm{p}}, t - t_{\mathrm{p}}\right) \right] \\
& \quad \times \left[\prod_{i=k_{\mathrm{p}}+1}^{\hat{k}} F_{\delta_e}\left(K_{i-1}\bar{\sigma}, t - t_{\mathrm{p}}\right) \right] \Bigg\}
\end{aligned}
\tag{6.82}
$$

Using (6.9) to describe the length of the overload, and (6.41) to approximate the failure probability, (6.82) becomes:

$$
\begin{aligned}
W_{\hat{k},\mathrm{p},k}\left(t;\boldsymbol{\sigma},\sigma_{\mathrm{p}}\right) \approx c_{\hat{k}} \Bigg\{ & \left[\left(\frac{\sigma_{\mathrm{p}}}{\sigma_{\delta_e}}\right)^{\zeta} \prod_{i=2}^{\hat{k}} \left(\frac{K_{i-1}\sigma_{\mathrm{p}}}{\sigma_{\delta_e}}\right)^{\zeta} \sqrt{1+\left(\frac{t_{\mathrm{p}}}{t_c}\right)^{\theta}}\right] \\
& + \left[\left(\frac{\sigma_{\mathrm{p}}}{\sigma_{\delta_e}}\right)^{\zeta} \prod_{i=2}^{\hat{k}-1} \left(\frac{K_{i-1}\sigma_{\mathrm{p}}}{\sigma_{\delta_e}}\right)^{\zeta} \sqrt{1+\left(\frac{t_{\mathrm{p}}}{t_c}\right)^{\theta}}\right] \left(1-\left(\frac{K_{\hat{k}-1}\sigma_{\mathrm{p}}}{\sigma_{\delta_e}}\right)^{\zeta} \sqrt{1+\left(\frac{t_{\mathrm{p}}}{t_c}\right)^{\theta}}\right)^{N_{\hat{k}-1}} \\
& \quad \times \left[\left(\frac{K_{\hat{k}-1}\sigma}{\sigma_{\delta_e}}\right)^{\zeta} \sqrt{1+\left(\frac{t}{t_c}\right)^{\theta}} - \left(\frac{K_{\hat{k}-1}\sigma}{\sigma_{\delta_e}}\right)^{\zeta} \sqrt{1+\left(\frac{t_{\mathrm{p}}}{t_c}\right)^{\theta}}\right] \\
& + \sum_{k=k_{\mathrm{p}}}^{\hat{k}-2} \left[\left(\frac{\sigma_{\mathrm{p}}}{\sigma_{\delta_e}}\right)^{\zeta} \prod_{i=2}^{k} \left(\frac{K_{i-1}\sigma_{\mathrm{p}}}{\sigma_{\delta_e}}\right)^{\zeta} \sqrt{1+\left(\frac{t_{\mathrm{p}}}{t_c}\right)^{\theta}}\right] \left(1-\left(\frac{K_{k}\sigma_{\mathrm{p}}}{\sigma_{\delta_e}}\right)^{\zeta} \sqrt{1+\left(\frac{t_{\mathrm{p}}}{t_c}\right)^{\theta}}\right)^{N_k} \\
& \quad \times \left[\left(\frac{K_{k}\sigma}{\sigma_{\delta_e}}\right)^{\zeta} \sqrt{1+\left(\frac{t}{t_c}\right)^{\theta}} - \left(\frac{K_{k}\sigma}{\sigma_{\delta_e}}\right)^{\zeta} \sqrt{1+\left(\frac{t_{\mathrm{p}}}{t_c}\right)^{\theta}}\right] \left[\prod_{i=k+2}^{\hat{k}} \left(\frac{K_{i-1}\sigma}{\sigma_{\delta_e}}\right)^{\zeta} \sqrt{1+\left(\frac{t-t_{\mathrm{p}}}{t_c}\right)^{\theta}}\right] \\
& + \sum_{k=1}^{k_{\mathrm{p}}-1} \left[\left(\frac{\sigma_{\mathrm{p}}}{\sigma_{\delta_e}}\right)^{\zeta} \prod_{i=2}^{k} \left(\frac{K_{i-1}\sigma_{\mathrm{p}}}{\sigma_{\delta_e}}\right)^{\zeta} \sqrt{1+\left(\frac{t_{\mathrm{p}}}{t_c}\right)^{\theta}}\right] \left(1-\left(\frac{K_{k}\sigma_{\mathrm{p}}}{\sigma_{\delta_e}}\right)^{\zeta} \sqrt{1+\left(\frac{t_{\mathrm{p}}}{t_c}\right)^{\theta}}\right)^{N_k} \\
& \quad \times \left[\left(\frac{\sigma_{\mathrm{p}}}{\sigma_{\delta_e}}\right)^{\zeta} \sqrt{1+\left(\frac{t}{t_c}\right)^{\theta}} - \left(\frac{\sigma_{\mathrm{p}}}{\sigma_{\delta_e}}\right)^{\zeta} \sqrt{1+\left(\frac{t_{\mathrm{p}}}{t_c}\right)^{\theta}}\right] \\
& \quad \times \left[\prod_{i=k+2}^{k_{\mathrm{p}}} \left(\frac{\sigma_{\mathrm{p}}}{\sigma_{\delta_e}}\right)^{\zeta} \sqrt{1+\left(\frac{t-t_{\mathrm{p}}}{t_c}\right)^{\theta}}\right] \prod_{i=k_{\mathrm{p}}+1}^{\hat{k}} \left(\frac{K_{i-1}\bar{\sigma}}{\sigma_{\delta_e}}\right)^{\zeta} \sqrt{1+\left(\frac{t-t_{\mathrm{p}}}{t_c}\right)^{\theta}} \Bigg\}
\end{aligned}
\tag{6.83}
$$

Rearranging and consolidating terms gives:

$$
\begin{aligned}
W_{\hat{k},\mathrm{p},k}\left(t;\sigma,\sigma_{\mathrm{p}}\right) \approx c_{\hat{k}}\left(\prod_{i=1}^{\hat{k}-1}K_i\right)\left(\frac{\sigma_{\mathrm{p}}}{\sigma_{\delta_e}}\right)^{\hat{k}\zeta}\left(1+\left(\frac{t_{\mathrm{p}}}{t_c}\right)^{\theta}\right)^{\frac{\left(\hat{k}-1\right)}{2}}\Bigg\{1 \\
+\sum_{k=k_{\mathrm{p}}}^{\hat{k}-1}\left(1-\left(\frac{K_k\sigma_{\mathrm{p}}}{\sigma_{\delta_e}}\right)^{\zeta}\sqrt{1+\left(\frac{t_{\mathrm{p}}}{t_c}\right)^{\theta}}\right)^{N_k}\left[\sqrt{1+\left(\frac{t}{t_c}\right)^{\theta}}-\sqrt{1+\left(\frac{t_{\mathrm{p}}}{t_c}\right)^{\theta}}\right] \\
\times\left(1+\left(\frac{t_{\mathrm{p}}}{t_c}\right)^{\theta}\right)^{\frac{\left(k-\hat{k}\right)}{2}}\left(\frac{\bar{\sigma}}{\sigma_{\mathrm{p}}}\right)^{\left(\hat{k}-k\right)\zeta}\left(1+\left(\frac{t-t_{\mathrm{p}}}{t_c}\right)^{\theta}\right)^{\frac{\left(\hat{k}-k-1\right)}{2}} \\
+\sum_{k=1}^{k_{\mathrm{p}}-1}\left(1-\left(\frac{K_k\sigma_{\mathrm{p}}}{\sigma_{\delta_e}}\right)^{\zeta}\sqrt{1+\left(\frac{t_{\mathrm{p}}}{t_c}\right)^{\theta}}\right)^{N_k}\left[\sqrt{1+\left(\frac{t}{t_c}\right)^{\theta}}-\sqrt{1+\left(\frac{t_{\mathrm{p}}}{t_c}\right)^{\theta}}\right] \\
\times\frac{1}{\prod_{i=k}^{k_{\mathrm{p}}-1}K_i}\left(1+\left(\frac{t_{\mathrm{p}}}{t_c}\right)^{\theta}\right)^{\frac{\left(k-\hat{k}\right)}{2}}\left(\frac{\bar{\sigma}}{\sigma_{\mathrm{p}}}\right)^{\left(\hat{k}-k_{\mathrm{p}}\right)\zeta}\left(1+\left(\frac{t-t_{\mathrm{p}}}{t_c}\right)^{\theta}\right)^{\frac{\left(\hat{k}-k-1\right)}{2}}\Bigg\}
\end{aligned}
\tag{6.84}
$$

In the case of a 2D planar array (6.84) becomes:

$$
\begin{aligned}
W_{\hat{k},\mathrm{p},k}\left(t;\boldsymbol{\sigma},\boldsymbol{\sigma}_{\mathrm{p}}\right) \approx 2^{\hat{k}-1}&\left(\prod_{i=1}^{\hat{k}-1}K_i\right)\left(\frac{\sigma_{\mathrm{p}}}{\sigma_{\delta_e}}\right)^{\hat{k}\zeta}\left(1+\left(\frac{t_{\mathrm{p}}}{t_c}\right)^{\theta}\right)^{\frac{\left(\hat{k}-1\right)}{2}}\left\{1\right.\\
&+\sum_{k=k_{\mathrm{p}}}^{\hat{k}-1}\left(1-\left(\frac{K_k\sigma_{\mathrm{p}}}{\sigma_{\delta_e}}\right)^{\zeta}\sqrt{1+\left(\frac{t_{\mathrm{p}}}{t_c}\right)^{\theta}}\right)^2\left[\sqrt{1+\left(\frac{t}{t_c}\right)^{\theta}}-\sqrt{1+\left(\frac{t_{\mathrm{p}}}{t_c}\right)^{\theta}}\right]\\
&\quad\times\left(1+\left(\frac{t_{\mathrm{p}}}{t_c}\right)^{\theta}\right)^{\frac{\left(k-\hat{k}\right)}{2}}\left(\frac{\bar{\sigma}}{\sigma_{\mathrm{p}}}\right)^{\left(\hat{k}-k\right)\zeta}\left(1+\left(\frac{t-t_{\mathrm{p}}}{t_c}\right)^{\theta}\right)^{\frac{\left(\hat{k}-k-1\right)}{2}}\\
&+\sum_{k=1}^{k_{\mathrm{p}}-1}\left(1-\left(\frac{K_k\sigma_{\mathrm{p}}}{\sigma_{\delta_e}}\right)^{\zeta}\sqrt{1+\left(\frac{t_{\mathrm{p}}}{t_c}\right)^{\theta}}\right)^2\left[\sqrt{1+\left(\frac{t}{t_c}\right)^{\theta}}-\sqrt{1+\left(\frac{t_{\mathrm{p}}}{t_c}\right)^{\theta}}\right]\\
&\quad\times\frac{1}{\prod_{i=k}^{k_{\mathrm{p}}-1}K_i}\left(1+\left(\frac{t_{\mathrm{p}}}{t_c}\right)^{\theta}\right)^{\frac{\left(k-\hat{k}\right)}{2}}\left(\frac{\bar{\sigma}}{\sigma_{\mathrm{p}}}\right)^{\left(\hat{k}-k_{\mathrm{p}}\right)\zeta}\left(1+\left(\frac{t-t_{\mathrm{p}}}{t_c}\right)^{\theta}\right)^{\frac{\left(\hat{k}-k-1\right)}{2}}\left.\right\}
\end{aligned}
\qquad . \qquad (6.85)
$$

In the case of a hexagonal array (6.84) becomes:

$$W_{\hat{k},\mathrm{p},k}\left(t;\sigma,\sigma_{\mathrm{p}}\right)\approx\left[\pi^{\hat{k}-1}\prod_{j=1}^{\hat{k}-1}\left(\sqrt{\frac{4j}{\pi}}+1\right)\right]\left(\prod_{i=1}^{\hat{k}-1}K_i\right)\left(\frac{\sigma_{\mathrm{p}}}{\sigma_{\delta_e}}\right)^{\hat{k}\zeta}\left(1+\left(\frac{t_{\mathrm{p}}}{t_c}\right)^{\theta}\right)^{\frac{\left(\hat{k}-1\right)}{2}}\left\{1\right.$$
$$+\sum_{k=k_{\mathrm{p}}}^{\hat{k}-1}\left(1-\left(\frac{K_k\sigma_{\mathrm{p}}}{\sigma_{\delta_e}}\right)^{\zeta}\sqrt{1+\left(\frac{t_{\mathrm{p}}}{t_c}\right)^{\theta}}\right)^{\sqrt{4\pi k}+\pi}\left[\sqrt{1+\left(\frac{t}{t_c}\right)^{\theta}}-\sqrt{1+\left(\frac{t_{\mathrm{p}}}{t_c}\right)^{\theta}}\right]$$
$$\times\left(1+\left(\frac{t_{\mathrm{p}}}{t_c}\right)^{\theta}\right)^{\frac{\left(k-\hat{k}\right)}{2}}\left(\frac{\bar{\sigma}}{\sigma_{\mathrm{p}}}\right)^{\left(\hat{k}-k\right)\zeta}\left(1+\left(\frac{t-t_{\mathrm{p}}}{t_c}\right)^{\theta}\right)^{\frac{\left(\hat{k}-k-1\right)}{2}} \qquad (6.86)$$
$$+\sum_{k=1}^{k_{\mathrm{p}}-1}\left(1-\left(\frac{K_k\sigma_{\mathrm{p}}}{\sigma_{\delta_e}}\right)^{\zeta}\sqrt{1+\left(\frac{t_{\mathrm{p}}}{t_c}\right)^{\theta}}\right)^{\sqrt{4\pi k}+\pi}\left[\sqrt{1+\left(\frac{t}{t_c}\right)^{\theta}}-\sqrt{1+\left(\frac{t_{\mathrm{p}}}{t_c}\right)^{\theta}}\right]$$
$$\left.\times\frac{1}{\prod_{i=k}^{k_{\mathrm{p}}-1}K_i}\left(1+\left(\frac{t_{\mathrm{p}}}{t_c}\right)^{\theta}\right)^{\frac{\left(k-\hat{k}\right)}{2}}\left(\frac{\bar{\sigma}}{\sigma_{\mathrm{p}}}\right)^{\left(\hat{k}-k_{\mathrm{p}}\right)\zeta}\left(1+\left(\frac{t-t_{\mathrm{p}}}{t_c}\right)^{\theta}\right)^{\frac{\left(\hat{k}-k-1\right)}{2}}\right\}$$

If we can neglect the term $\left(1-F_{\delta_e}\left(K_k\sigma_{\mathrm{p}},t_{\mathrm{p}}\right)\right)^{N_k}$ as being close to unity, equation (6.84) becomes:

$$W_{\hat{k},\mathrm{p},k}\left(t;\sigma,\sigma_{\mathrm{p}}\right)\approx c_{\hat{k}}\left(\prod_{i=1}^{\hat{k}-1}K_i\right)\left(\frac{\sigma_{\mathrm{p}}}{\sigma_{\delta_e}}\right)^{\hat{k}\zeta}\left(1+\left(\frac{t_{\mathrm{p}}}{t_c}\right)^{\theta}\right)^{\frac{\left(\hat{k}-1\right)}{2}}\left\{1\right.$$
$$+\sum_{k=k_{\mathrm{p}}}^{\hat{k}-1}\left[\sqrt{1+\left(\frac{t}{t_c}\right)^{\theta}}-\sqrt{1+\left(\frac{t_{\mathrm{p}}}{t_c}\right)^{\theta}}\right]\left(1+\left(\frac{t_{\mathrm{p}}}{t_c}\right)^{\theta}\right)^{\frac{\left(k-\hat{k}\right)}{2}}\left(\frac{\bar{\sigma}}{\sigma_{\mathrm{p}}}\right)^{\left(\hat{k}-k\right)\zeta}\left(1+\left(\frac{t-t_{\mathrm{p}}}{t_c}\right)^{\theta}\right)^{\frac{\left(\hat{k}-k-1\right)}{2}}$$
$$\left.+\sum_{k=1}^{k_{\mathrm{p}}-1}\left[\sqrt{1+\left(\frac{t}{t_c}\right)^{\theta}}-\sqrt{1+\left(\frac{t_{\mathrm{p}}}{t_c}\right)^{\theta}}\right]\frac{1}{\prod_{i=k}^{k_{\mathrm{p}}-1}K_i}\left(1+\left(\frac{t_{\mathrm{p}}}{t_c}\right)^{\theta}\right)^{\frac{\left(k-\hat{k}\right)}{2}}\left(\frac{\bar{\sigma}}{\sigma_{\mathrm{p}}}\right)^{\left(\hat{k}-k_{\mathrm{p}}\right)\zeta}\left(1+\left(\frac{t-t_{\mathrm{p}}}{t_c}\right)^{\theta}\right)^{\frac{\left(\hat{k}-k-1\right)}{2}}\right\}$$

(6.87)

Assuming $t \gg t_{\mathrm{p}}$ and $t \gg t_c$, equation (6.87) further simplifies to

$$W_{\hat{k},\mathrm{p},k}\left(t;\bar{\sigma},\sigma_{\mathrm{p}}\right) \approx c_{\hat{k}}\left(\prod_{i=1}^{\hat{k}-1} K_i\right)\left(\frac{\sigma_{\mathrm{p}}}{\sigma_{\delta_e}}\right)^{\hat{k}\zeta}\left(\frac{t_{\mathrm{p}}}{t_c}\right)^{\theta\left(\hat{k}-1\right)/2}\left\{1+\sum_{k=k_p}^{\hat{k}-1}\left(\frac{\bar{\sigma}}{\sigma_{\mathrm{p}}}\right)^{\left(\hat{k}-k\right)\zeta}\left(\frac{t}{t_{\mathrm{p}}}\right)^{\frac{\theta\left(\hat{k}-k-1\right)}{2}}\left[\left(\frac{t}{t_{\mathrm{p}}}\right)^{\frac{\theta}{2}}-1\right]\right.$$
$$\left.+\sum_{k=1}^{k_p-1}\frac{1}{\prod_{i=k}^{\hat{k}-1} K_i}\left(\frac{t}{t_{\mathrm{p}}}\right)^{\frac{\theta\left(\hat{k}-k-1\right)}{2}}\left[\left(\frac{t}{t_{\mathrm{p}}}\right)^{\frac{\theta}{2}}-1\right]\right\} \tag{6.88}$$

Returning to the general exact expression as given in (6.84), and letting

$$q_k = \left[1+\left(\frac{t_{\mathrm{p}}}{t_c}\right)^{\theta}\right]^{\frac{k-\hat{k}}{2}}\left(1-\left(\frac{K_k\sigma_{\mathrm{p}}}{\sigma_{\delta_e}}\right)^{\zeta}\sqrt{1+\left(\frac{t_{\mathrm{p}}}{t_c}\right)^{\theta}}\right)^{N_k}$$
$$\times\left(1+\left(\frac{t-t_{\mathrm{p}}}{t_c}\right)^{\theta}\right)^{\frac{\left(\hat{k}-k-1\right)}{2}}\left[\sqrt{1+\left(\frac{t}{t_c}\right)^{\theta}}-\sqrt{1+\left(\frac{t_{\mathrm{p}}}{t_c}\right)^{\theta}}\right] \tag{6.89}$$

and using equations (6.32) and (6.33), then (6.84) becomes

$$W_{\hat{k},\mathrm{p},k}\left(t;\sigma,\sigma_{\mathrm{p}}\right) \approx \frac{1}{V}\left(\frac{\sigma_{\mathrm{p}}}{\sigma_V}\right)^{\hat{\alpha}}\left(1+\left(\frac{t_{\mathrm{p}}}{t_c}\right)^{\theta}\right)^{\frac{\left(\hat{k}-1\right)}{2}}$$
$$\times\left\{1+\sum_{k=k_{\mathrm{p}}}^{\hat{k}-1} q_k\left(\frac{\bar{\sigma}}{\sigma_{\mathrm{p}}}\right)^{\left(\hat{k}-k\right)\zeta}+\sum_{k=1}^{k_{\mathrm{p}}-1}\frac{q_k}{\prod_{i=k}^{k_{\mathrm{p}}-1} K_i}\left(\frac{\bar{\sigma}}{\sigma_{\mathrm{p}}}\right)^{\left(\hat{k}-k_{\mathrm{p}}\right)\zeta}\right\} \tag{6.90}$$

The probability of overall composite failure is related to (6.90) via (6.14), such that the failure probability following a proof test is given by

$$\begin{aligned} H_V\left(t;\bar{\sigma},\sigma_{\mathrm{p}}\right) &\approx 1-\exp\left[-V\,W_{\hat{k},\mathrm{p}}\left(t;\bar{\sigma},\sigma_{\mathrm{p}}\right)\right] \\ &\approx 1-\exp\Bigg[-\left(\frac{\sigma_{\mathrm{p}}}{\hat{\sigma}_V}\right)^{\hat{\alpha}}\sqrt{1+\left(\frac{t_{\mathrm{p}}}{t_c}\right)^{\theta}}^{\hat{k}-1} \\ &\quad\times\left(1+\sum_{k=k_p}^{\hat{k}-1}\left(\frac{\bar{\sigma}}{\sigma_{\mathrm{p}}}\right)^{(\hat{k}-k)\zeta}q_k+\sum_{k=1}^{k_{\mathrm{p}}-1}\frac{q_k}{\prod_{i=k}^{k_{\mathrm{p}}-1}K_i}\left(\frac{\bar{\sigma}}{\sigma_{\mathrm{p}}}\right)^{(\hat{k}-k_{\mathrm{p}})\zeta}\right)\Bigg] \end{aligned} \tag{6.91}$$

In the case where we neglect the term $\left(1-F_{\delta_e}\left(K_k\sigma_{\mathrm{p}},t_{\mathrm{p}}\right)\right)^{N_k}$ as being close to unity, we can define

$$q_{k,approx}=\left[1+\left(\frac{t_{\mathrm{p}}}{t_c}\right)^{\theta}\right]^{\frac{k-\hat{k}}{2}}\left[1+\left(\frac{t-t_{\mathrm{p}}}{t_c}\right)^{\theta}\right]^{\frac{\hat{k}-k-1}{2}}\left[\sqrt{1+\left(\frac{t}{t_c}\right)^{\theta}}-\sqrt{1+\left(\frac{t_{\mathrm{p}}}{t_c}\right)^{\theta}}\right] \tag{6.92}$$

and thus the probability of overall composite failure after a proof test becomes

$$\begin{aligned} H_{V,approx}\left(t;\bar{\sigma},\sigma_{\mathrm{p}}\right) &\approx 1-\exp\left[-V\,W_{\hat{k},\mathrm{p},approx}\left(t;\bar{\sigma},\sigma_{\mathrm{p}}\right)\right] \\ &\approx 1-\exp\Bigg[-\left(\frac{\sigma_{\mathrm{p}}}{\hat{\sigma}_V}\right)^{\hat{\alpha}}\sqrt{1+\left(\frac{t_{\mathrm{p}}}{t_c}\right)^{\theta}}^{\hat{k}-1} \\ &\quad\times\left(1+\sum_{k=k_p}^{\hat{k}-1}\left(\frac{\bar{\sigma}}{\sigma_{\mathrm{p}}}\right)^{(\hat{k}-k)\zeta}q_{k,approx}+\sum_{k=1}^{k_{\mathrm{p}}-1}\frac{q_{k,approx}}{\prod_{i=k}^{k_{\mathrm{p}}-1}K_i}\left(\frac{\bar{\sigma}}{\sigma_{\mathrm{p}}}\right)^{(\hat{k}-k_{\mathrm{p}})\zeta}\right)\Bigg] \end{aligned} \tag{6.93}$$

6.4.5 Conditional reliability following a proof test

Of particular interest is the reliability conditional on surviving a proof test. This is calculated using Bayes theorem:

$$R_p\left(t\middle|\sigma_p\right)=\frac{R\left(t\right)}{R\left(t_p\right)}=\frac{1-F\left(t\right)}{1-F\left(t_p\right)}. \tag{6.94}$$

The conditional reliability for lifetime on surviving loading for time $t \geq t_p$

$$R_{\hat{k},\mathrm{p}}\left(t\middle|\overline{\sigma}\right)\approx\exp\left[\left(\frac{\overline{\sigma}}{\hat{\sigma}_V}\right)^{\hat{\alpha}}\sqrt{1+\left(\frac{t_\mathrm{p}}{t_c}\right)^{\theta}}^{\hat{k}-1}-\left(\frac{\overline{\sigma}}{\hat{\sigma}_V}\right)^{\hat{\alpha}}\sqrt{1+\left(\frac{t}{t_c}\right)^{\theta}}^{\hat{k}-1}\right] \qquad t\geq t_p \tag{6.95}$$

Thus equation (6.91) becomes

$$R_{\hat{k},\mathrm{p}}\left(t\middle|\overline{\sigma},\sigma_\mathrm{p}\right)\approx\exp\left[\left(\frac{\sigma_\mathrm{p}}{\hat{\sigma}_V}\right)^{\hat{\alpha}}\sqrt{1+\left(\frac{t_\mathrm{p}}{t_c}\right)^{\theta}}^{\hat{k}-1}\times\left[1-\left(1+\sum_{k=k_p}^{\hat{k}-1}\left(\frac{\overline{\sigma}}{\sigma_\mathrm{p}}\right)^{\left(\hat{k}-k\right)\zeta}q_k+\sum_{k=1}^{k_\mathrm{p}-1}\frac{q_k}{\prod_{i=k}^{k_\mathrm{p}-1}K_i}\left(\frac{\overline{\sigma}}{\sigma_\mathrm{p}}\right)^{\left(\hat{k}-k_\mathrm{p}\right)\zeta}\right)\right]\right] \qquad t\geq t_p \tag{6.96}$$

Similarly equation (6.93) becomes:

$$R_{\hat{k},\mathrm{p},approx}\left(\bar{\sigma}\right) \approx \exp\left[\left(\frac{\sigma_{\mathrm{p}}}{\hat{\sigma}_V}\right)^{\hat{\alpha}} \sqrt{1+\left(\frac{t_{\mathrm{p}}}{t_c}\right)^{\theta}}^{\hat{k}-1} \times\left\{1-\left(1+\sum_{k=k_p}^{\hat{k}}\left(\frac{\bar{\sigma}}{\sigma_{\mathrm{p}}}\right)^{\left(\hat{k}-k\right)\zeta} q_{k,approx}+\sum_{k=1}^{k_{\mathrm{p}}-1}\frac{q_{k,approx}}{\prod_{i=k}^{k_{\mathrm{p}}-1}K_i}\left(\frac{\bar{\sigma}}{\sigma_{\mathrm{p}}}\right)^{\left(\hat{k}-k_{\mathrm{p}}\right)\zeta}\right)\right\}\right] \qquad t \geq t_p \tag{6.97}$$

6.5. Discussion

6.5.1 Determining parameters

The four independent parameters, $\hat{\sigma}_V$, $\hat{\alpha}$, $\hat{\rho}$, and t_c, that are most closely connected to experimentally observed behavior can be determined from test data using maximum likelihood estimation, as is described in chapters 2-3. The strength and lifetime distributions for the stochastic fiber breakage model are similar in most respects to the CPL-W model, with the exception that for the stochastic fiber breakage model $\hat{\alpha} = \hat{\rho}\hat{\beta}$, whereas in the CPL-W model $\alpha = \left(\rho+1\right)\beta$. The CPL-W model also has a constraint on the parameter t_{ref}, such that t_{ref} can be written in terms of the other parameters. This gives the CPL-W model three independent parameters. However, because of this constraint, the CPL-W model always has the Weibull distribution for strength, and particularly the scale parameter, tied to the loading rate used in strength testing, R.

Since the value of $\hat{\rho}$ is typically fairly large, there is little difference between $\hat{\rho}$ and $\hat{\rho}+1$, thus the CPL-W model and the stochastic fiber breakage model are highly similar for

similar values of t_c and t_{ref}. Given a set of CPL-W model parameters $\{\sigma_{\text{ref}}, \alpha, \rho\}$, and the loading rate used in the strength testing, R, the basic strength and lifetime parameters for the stochastic fiber breakage model are as follows:

$$\hat{\sigma}_V = \sigma_{\text{ref}}$$

$$\hat{\alpha} = \alpha \tag{6.98}$$

$$\hat{\rho} = \rho$$

$$t_c = t_{\text{ref}} = \frac{\sigma_{\text{ref}}}{R(\rho+1)}$$

Additional parameters are required to describe the failure probability following a proof test, as given in equations (6.89) and (6.91), namely the parameters $\hat{k}$, θ, ζ, σ_{δ_e}, and k_{p}. By assuming $\left[1-\left(K_k\sigma_{\text{p}}/\sigma_{\delta_e}\right)^{\zeta}\sqrt{1+\left(t_{\text{p}}/t_c\right)^{\theta}}\right]^{N_k}$ is close to unity, this decreases to three additional parameters: θ, $\hat{k}$, and k_{p}.

Typically ζ is already known based on fiber strength tests. For single carbon fibers, for example, ζ is typically around 5.

The parameter k_{p} is given by equation (6.53) for the planar case and equation (6.54) for the hexagonal case. The parameter σ_{δ_e} can be calculated, given $\hat{k}$, ζ, $\hat{\sigma}_V$ and the volume V, using equation (6.32). Using equation (6.47), $\hat{\rho} = 2\zeta\hat{k}/\left(\theta\left(\hat{k}-1\right)\right)$, we can get θ in terms of $\hat{k}$ and the CPL-W parameters:

$$\theta = \frac{2\alpha}{\rho\left(\hat{k}-1\right)} \tag{6.99}$$

In the planar case, combining equations (6.26), (6.28), (6.32), (6.35) and (6.99), we get an expression for $\hat{k}$ solely in terms of ζ and the volume V:

$$\begin{aligned}
&K_{\hat{k}-1} < \frac{\sigma_{\delta_e}}{\hat{\sigma}_V} < K_{\hat{k}} \\
&\sqrt{1+\frac{\pi\left(\hat{k}-1\right)}{4}} < \frac{\sigma_{\delta_e}}{\sigma_{\delta_e}\left(Vc_{\hat{k}}\right)^{-1/\left(\hat{k}\zeta\right)}\left(K_1K_2\cdots K_{\hat{k}-1}\right)^{-1/\hat{k}}} < \sqrt{1+\frac{\pi\hat{k}}{4}} \\
&\sqrt{1+\frac{\pi\left(\hat{k}-1\right)}{4}} < \left(Vc_{\hat{k}}\right)^{1/\left(\hat{k}\zeta\right)}\left(K_1K_2\cdots K_{\hat{k}-1}\right)^{1/\hat{k}} < \sqrt{1+\frac{\pi\hat{k}}{4}} \\
&\frac{\pi\left(\hat{k}-1\right)}{4} < \left(Vc_{\hat{k}}\right)^{\frac{2}{\hat{k}\zeta}}\left(\prod_{j=1}^{\hat{k}-1}\sqrt{1+\frac{\pi j}{4}}\right)^{\frac{2}{\hat{k}}} - 1 < \frac{\pi\hat{k}}{4} \\
&\hat{k}-1 < \frac{4}{\pi}\left[\left(2^{\hat{k}-1}V\right)^{\frac{2}{\hat{k}\zeta}}\left(\prod_{j=1}^{\hat{k}-1}\sqrt{1+\frac{\pi j}{4}}\right)^{\frac{2}{\hat{k}}} - 1\right] < \hat{k} \\
&-1 < \frac{4}{\pi}\left[\left(2^{\hat{k}-1}V\right)^{\frac{2}{\hat{k}\zeta}}\left(\prod_{j=1}^{\hat{k}-1}\sqrt{1+\frac{\pi j}{4}}\right)^{\frac{2}{\hat{k}}} - 1\right] - \hat{k} < 0
\end{aligned} \tag{6.100}$$

Likewise for the hexagonal case, combining equations (6.27), (6.29), (6.32), (6.36) and (6.99), we get an expression for $\hat{k}$ solely in terms of ζ and the volume V:

$$
\begin{aligned}
&K_{\hat{k}-1}\hat{\sigma}_V < \sigma_{\delta_e} < K_{\hat{k}}\hat{\sigma}_V \\
&\sqrt{1+\sqrt{\frac{4\left(\hat{k}-1\right)}{\pi^3}}} < \frac{\sigma_{\delta_e}}{\sigma_{\delta_e}\left(Vc_{\hat{k}}\right)^{-1/\left(\hat{k}\zeta\right)}\left(K_1K_2\cdots K_{\hat{k}-1}\right)^{-1/\hat{k}}} < \sqrt{1+\sqrt{\frac{4\hat{k}}{\pi^3}}} \\
&\sqrt{\frac{4\left(\hat{k}-1\right)}{\pi^3}} < \left(Vc_{\hat{k}}\right)^{\frac{2}{\hat{k}\zeta}}\left(\prod_{j=1}^{\hat{k}-1}\sqrt{1+\sqrt{\frac{4j}{\pi^3}}}\right)^{\frac{2}{\hat{k}}} - 1 < \sqrt{\frac{4\hat{k}}{\pi^3}} \qquad (6.101) \\
&\hat{k}-1 < \frac{\pi^3}{4}\left[\left(V\pi^{\hat{k}-1}\prod_{j=1}^{\hat{k}-1}\left(\sqrt{\frac{4j}{\pi}}+1\right)\right)^{\frac{2}{\hat{k}\zeta}}\left(\prod_{j=1}^{\hat{k}-1}\left(1+\sqrt{\frac{4j}{\pi^3}}\right)\right)^{\frac{1}{\hat{k}}} - 1\right]^2 < \hat{k} \\
&\hat{k}-1 < \frac{\pi^3}{4}\left[\left(V\pi^{\hat{k}-1}\right)^{\frac{2}{\alpha}}\prod_{j=1}^{\hat{k}-1}\left[\left(\sqrt{\frac{4j}{\pi}}+1\right)^{\frac{2}{\hat{k}\zeta}}\left(1+\sqrt{\frac{4j}{\pi^3}}\right)^{\frac{1}{\hat{k}}}\right] - 1\right]^2 < \hat{k}
\end{aligned}
$$

Equations (6.100) and (6.101) do not necessarily uniquely identify one value of $\hat{k}$, but actually a range of values that satisfy these equations. We are interested in the smallest value of $\hat{k}$ that satisfies equations (6.100) and (6.101). It is worth noting that $\hat{k}$, ζ, and $\hat{\alpha}$ should satisfy equation (6.33), namely $\hat{\alpha} = \hat{k}\zeta$.

We thus now have a method for calculating all five additional parameters, namely $\hat{k}$, θ, ζ, σ_{δ_e}, and k_{p}, assuming the volume V, the three CPL-W parameters, σ_{ref}, α, and ρ as well as the CPL-W loading rate, R, are all known. First we use the known value of ζ to determine $\hat{k}$ dependent on V using equation (6.100) in the planar case, and equation (6.101) for the hexagonal case. Then θ may be determined using α, ρ, and (6.99). The parameter σ_{δ_e} can be calculated next, given $\hat{k}$, ζ, $\hat{\sigma}_V$, V, and (6.32). Finally the parameter k_{p} is given by equation (6.53) for the planar case and equation (6.54) for the hexagonal case.

Table 6.1 gives a selection of parameters. These parameters can be said to loosely represent materials such as Kevlar, Vectran, and Zylon, as well as various types of carbon, such as AS4, T700 and T1000. To aid comparisons, the value for the parameter t_c is set at 0.05, though generally this value would change for the different materials. The assumptions made in the stochastic fiber breakage model are for carbon fibers, yet for completeness we have included the polymer fibers where typically $\hat{\beta} > 1$.

Table 6.1 Sample material parameters, normalized for comparison purposes, for the newly proposed model, chosen to reflect fiber properties including Kevlar, Vectran, and Zylon, as well as various carbon fibers. Table 6.1 (a) contains the values chosen, and Table 6.1 (b) contains the parameter values calculated from Table 6.1 (a)

(a)

Possible material	Chosen parameters				
	ζ	t_c	V	$\hat{\sigma}_V$	$\hat{\rho}$
Kevlar	5	0.05	10^6	1	25
Vectran or Zylon	5	0.05	10^6	1	33 1/3
Carbon 1	5	0.05	10^6	1	50
Carbon 2	5	0.05	10^6	1	100
Carbon 3	5	0.05	10^6	1	200

(b)

Possible material	Chosen parameters				
	$\hat{k}$	$\hat{\alpha}$	θ	σ_{δ_e}	$\hat{\beta}$
Kevlar	10	50	4/9	2.924	2
Vectran or Zylon	10	50	1/3	2.924	1 ½
Carbon 1	10	50	2/9	2.924	1
Carbon 2	10	50	1/9	2.924	½
Carbon 3	10	50	1/18	2.924	¼

Using the material parameters given in Table 6.1, Figures 6.6 through 6.12 show the conditional failure probability following a proof test as given by both the stochastic fiber breakage model and the CPL-W model.

6.5.2 Comparison with the classic power-law in a Weibull framework model

For the CPL-W model the conditional reliability for times, t, greater than t_p is given by:

$$\begin{aligned} R_{\text{CPL-W}\,p}(t) &= \exp\left\{\left[\left(\frac{\sigma_p}{\sigma_{\text{ref}}}\right)^{\rho}\frac{t_p}{t_{\text{ref}}}\right]^{\beta} - \left[\left(\frac{\sigma_p}{\sigma_{\text{ref}}}\right)^{\rho}\frac{t_p}{t_{\text{ref}}} + \left(\frac{\bar{\sigma}}{\sigma_{\text{ref}}}\right)^{\rho}\frac{t-t_p}{t_{\text{ref}}}\right]^{\beta}\right\} \\ &= \exp\left\{\left[\left(\frac{\sigma_p}{\sigma_{\text{ref}}}\right)^{\rho}\frac{t_p}{t_{\text{ref}}}\right]^{\beta}\left(1-\left[1+\left(\frac{\bar{\sigma}}{\sigma_p}\right)^{\rho}\frac{t-t_p}{t_p}\right]\right)^{\beta}\right\}, \quad t > t_p \end{aligned}. \tag{6.102}$$

Thus the failure probability for the CPL-W model conditional on surviving a proof test is:

$$H_{\text{CPL-W}\,p}(t) = 1-\exp\left\{\left[\left(\frac{\sigma_p}{\sigma_{\text{ref}}}\right)^{\rho}\frac{t_p}{t_{\text{ref}}}\right]^{\beta}\left(1-\left[1+\left(\frac{\bar{\sigma}}{\sigma_p}\right)^{\rho}\frac{t-t_p}{t_p}\right]\right)^{\beta}\right\}, \quad t > t_p. \tag{6.103}$$

Similarly, the conditional failure probability following a proof test for the stochastic fiber breakage model (FB), using (6.96), becomes

$$\begin{aligned} H_{\hat{k},\text{p}}\left(t\middle|\bar{\sigma},\sigma_{\text{p}}\right) \approx 1-\exp\Bigg[&\left(\frac{\sigma_{\text{p}}}{\hat{\sigma}_V}\right)^{\hat{\alpha}}\sqrt{1+\left(\frac{t_{\text{p}}}{t_c}\right)^{\theta}}^{\hat{k}-1} \\ &\times\left[1-\left(1+\sum_{k=k_p}^{\hat{k}-1}\left(\frac{\bar{\sigma}}{\sigma_{\text{p}}}\right)^{\left(\hat{k}-k\right)\xi}q_k+\sum_{k=1}^{k_{\text{p}}-1}\frac{q_k}{\prod_{i=k}^{k_{\text{p}}-1}K_i}\left(\frac{\bar{\sigma}}{\sigma_{\text{p}}}\right)^{\left(\hat{k}-k_{\text{p}}\right)\xi}\right)\right]\Bigg], \qquad t \geq t_p \end{aligned} \tag{6.104}$$

Also, the approximation of the conditional failure probability following a proof test for the stochastic fiber breakage model (FB), using the approximation (6.97), becomes

$$H_{\hat{k},\mathrm{p},approx}\left(\bar{\sigma}\right) \approx 1-\exp\left[\left(\frac{\sigma_{\mathrm{p}}}{\hat{\sigma}_V}\right)^{\hat{\alpha}}\sqrt{1+\left(\frac{t_{\mathrm{p}}}{t_c}\right)^{\theta}}^{\hat{k}-1} \times\left\{1-\left(1+\sum_{k=k_p}^{\hat{k}}\left(\frac{\bar{\sigma}}{\sigma_{\mathrm{p}}}\right)^{\left(\hat{k}-k\right)\xi} q_{k,approx}+\sum_{k=1}^{k_{\mathrm{p}}-1}\frac{q_{k,approx}}{\prod_{i=k}^{k_{\mathrm{p}}-1}K_i}\left(\frac{\bar{\sigma}}{\sigma_{\mathrm{p}}}\right)^{\left(\hat{k}-k_{\mathrm{p}}\right)\xi}\right)\right\}\right], \qquad t \geq t_p \tag{6.105}$$

Figures 6.6 through 6.12 show comparisons of the conditional failure probability, following a proof test for the planar version of the stochastic fiber breakage model (FB), (6.104) for the exact expression and (6.105) as an approximate version, as well as the conditional reliability following a proof test for the CPL-W (6.103), and the lifetime distribution without a proof test, which is the same for the FB model and the CPL-W model, and is given in (6.45). The key value that changes from Figure 6.6 to Figure 6.10 is $\hat{\rho}$, which in turn causes $\hat{\beta}$ and θ to change as well. Figure 6.6 has $\hat{\beta}=2$, while Figure 6.7 has $\hat{\beta}=1.5$, Figure 6.8 has $\hat{\beta}=1$, Figure 6.9 has $\hat{\beta}=0.5$, and finally Figure 6.10 has $\hat{\beta}=0.25$. These can be grouped into two regimes: $\hat{\beta}>1$ and $\hat{\beta}\leq 1$, where $\hat{\beta}=1$ exhibits special behavior. Broadly speaking, $\hat{\beta}>1$ occurs in polymer fiber/epoxy composites, such as Kevlar, Vectran and Zylon, whereas $\hat{\beta}\leq 1$ occurs in various carbon fiber/epoxy composites. The stochastic fiber breakage model and the CPL-W model both have distinctly different predictions between these two regimes.

Results for the regime where $\hat{\beta}>1$, which typically involve polymer fibers, are shown in Figures 6.6 and 6.7. Note first that the case with no proof testing, i.e. the failure probability for a simple sustained load, is shown by the blue line, and is virtually the same straight line for both the stochastic fiber breakage model and the CPL_W model. In the cases involving proof testing

at various proofing ratios, $\sigma_p/\bar{\sigma}$, however, the failure probability is increased relative to the failure probability for a sustained lifetime load, particurally earlier in time. The severity of the increase depends on the proof ratio, where higher proof ratios lead to a greater increase in failure probability for short times. Also, the stochastic fiber breakage model predicts a higher failure probability than the CPL-W model, for proofing ratios greater than one.

In the special case where $\hat{\beta} = 1$, shown in Figure 6.8, differences now emerge, whereby the CPL-W model with proof testing is virtually the same as that without proof testing. However, the stochastic fiber breakage model shows considerably higher condtional failure probability, particularly early in time.

In the regime where $\hat{\beta} < 1$, seen in Figures 6.9 and 6.10, the CPL-W model clearly exhibits a benefit, i.e. reduced conditional failure probability, as a result of the proof test. Increasing the proofing ratio increases the extent of this improvement, beyond the point of credibility. On the other hand, the FB model clearly shows an increase in the conditional failure probability after proof testing, especially for larger proofing ratios, $\sigma_p/\bar{\sigma}$. For a proofing ratio of 1, the FB model does predict a slight short-term benefit from the proof test, as we might expect to happen in reality.

Comparing Figures 6.6 and 6.11 shows the effects of changing the parameter t_c, namely to scale the distributions horizontally. Figure 6.11 reflects a value of t_c more in line with polymer fibers than Figure 6.6. This has the effect of simply shifting the plot on the log time scale by two orders of magnitude.

Comparing Figures 6.6 and 6.12 shows the effects of changing the parameter ζ, assuming the regime where $\hat{\beta} > 1$. While differences can be seen, the magnitude of the changes

are surprisingly small compared to the changes caused by changing $\hat{\beta}$.

Regardless of $\hat{\beta}$, the approximation as given in (6.105) works very well, with very little difference between (6.105) and (6.104), particurally for low proofing stresses and lower lifetime load levels. Furthermore, the approximation appears to be conservative, predicting a higher failure probability than the exact version.

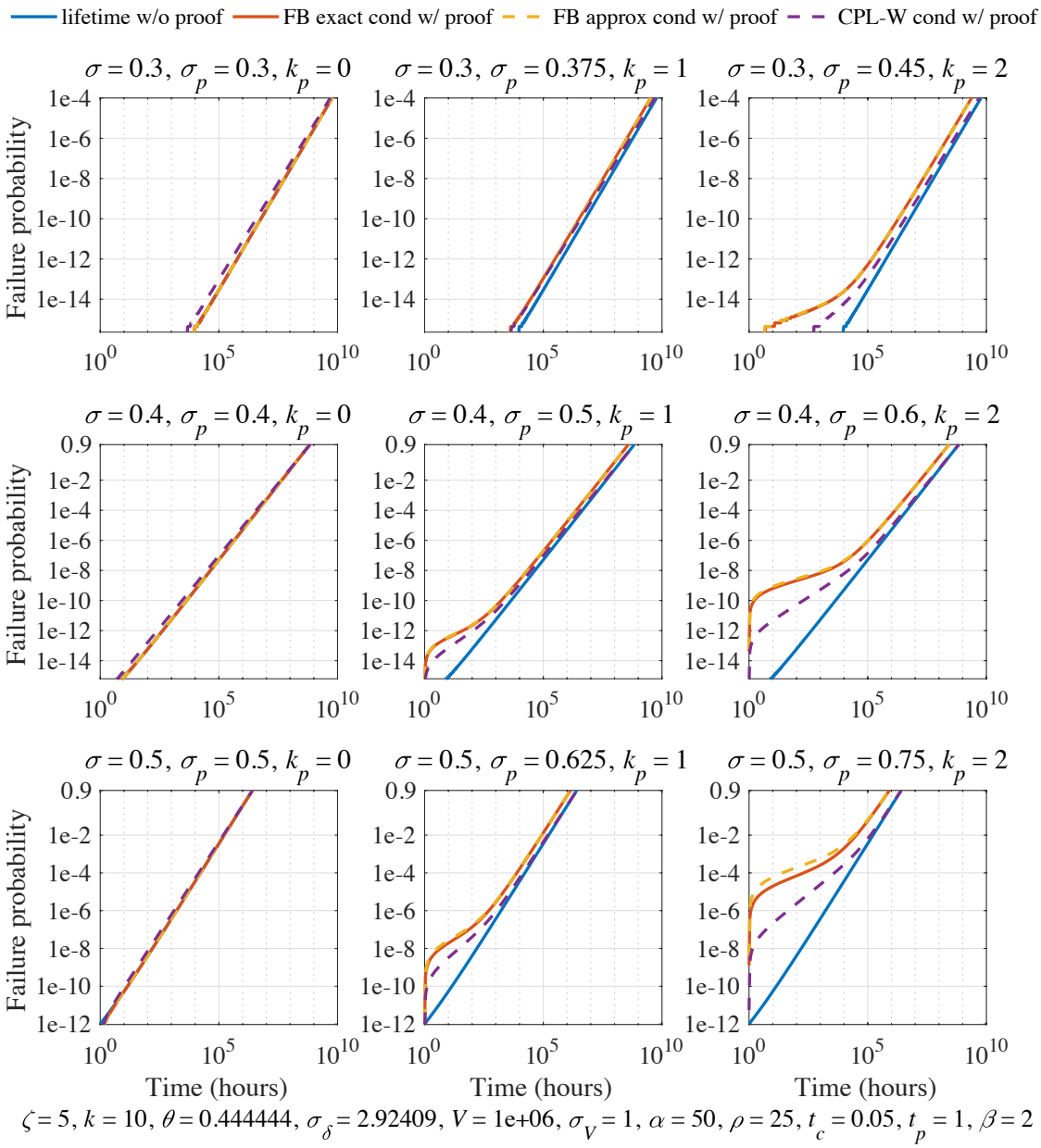

Figure 6.6 Plots of the conditional failure probability for a planar array after a proof test (equation (6.104) for 'exact' and equation (6.105) for 'approx.') as compared to the lifetime reliability without a proof test (equation (6.45)) and to the conditional reliability for the CPL-W model, (6.103), where $\hat{\sigma}_V = 1$, $\zeta = 5$, $V = 10^6$, $t_c = 0.05$, and $\hat{\rho} = 25$, and where $\bar{\sigma}$ takes values $\{0.3, 0.4, 0.5\}$, σ_p takes values $\{1, 1.25, 1.5\}\,\bar{\sigma}$, and where k_p accordingly varies from zero to two

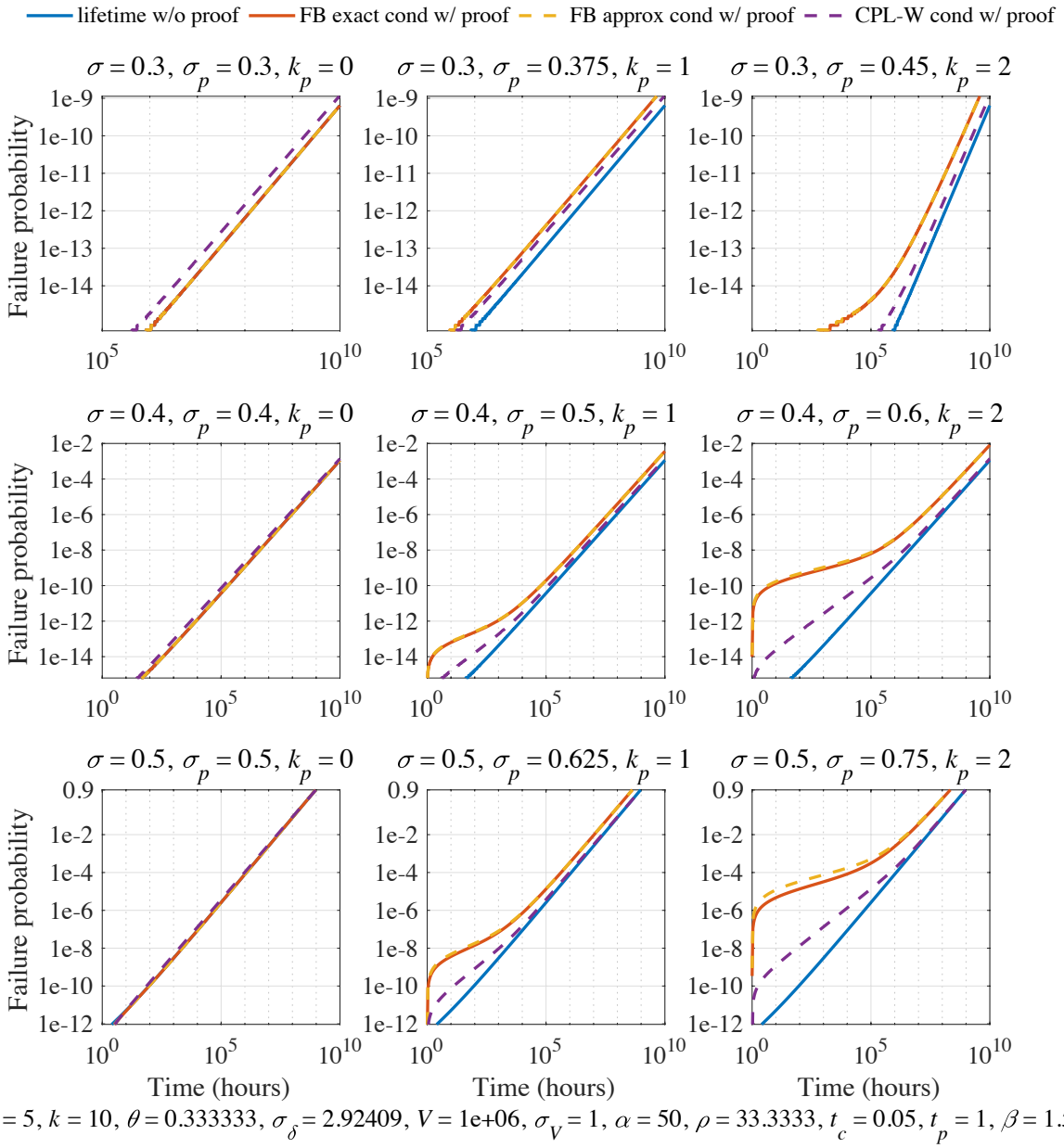

Figure 6.7 Plots of the conditional failure probability for a planar array after a proof test (equation (6.104) for 'exact' and equation (6.105) for 'approx.') as compared to the lifetime reliability without a proof test (equation (6.45)) and to the conditional reliability for the CPL-W model, (6.103), where $\hat{\sigma}_V = 1$, $\zeta = 5$, $V = 10^6$, $t_c = 0.05$, and $\hat{\rho} = 33\frac{1}{3}$, and where $\bar{\sigma}$ takes values {0.3, 0.4, 0.5}, σ_p takes values {1, 1.25, 1.5}$\bar{\sigma}$, and where k_p accordingly varies from zero to two

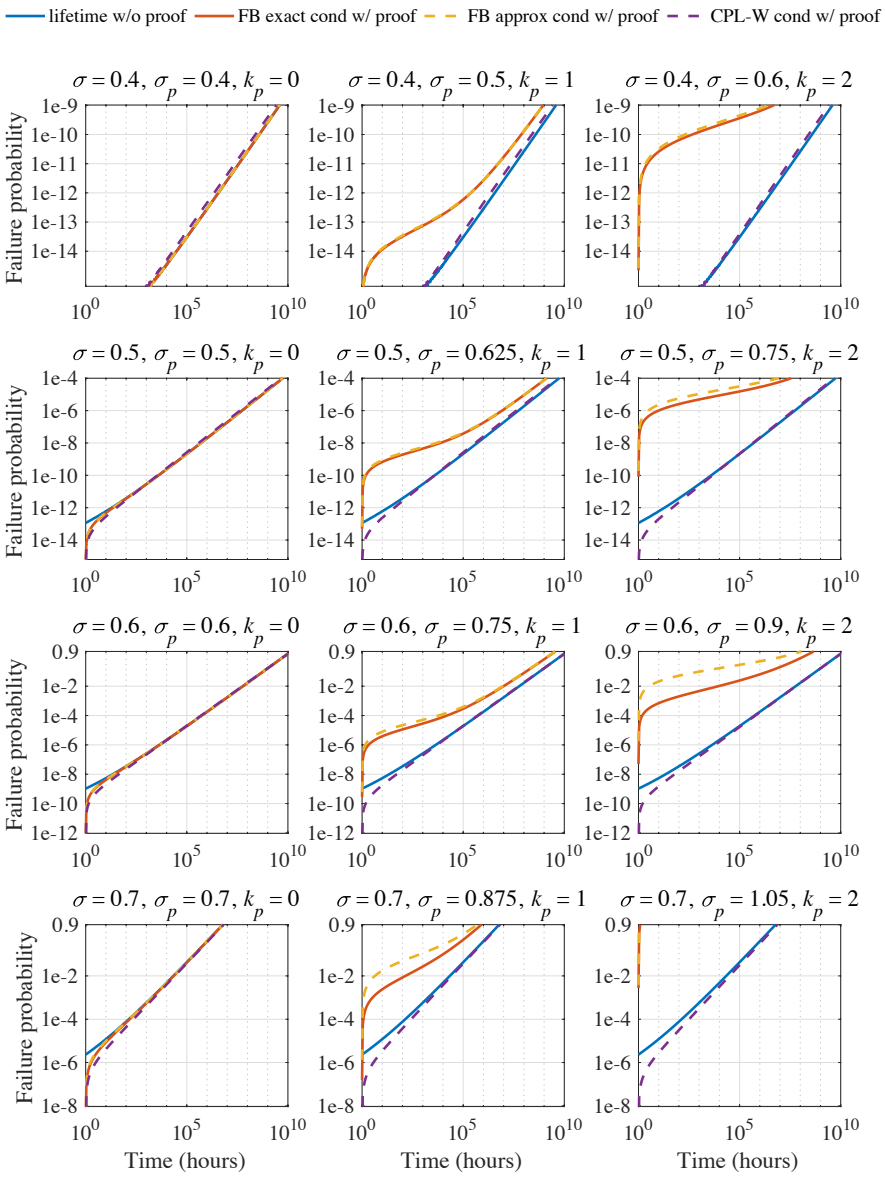

Figure 6.8 Plots of the conditional failure probability for a planar array after a proof test (equation (6.104) for 'exact' and equation (6.105) for 'approx.') as compared to the lifetime reliability without a proof test (equation (6.45)) and to the conditional reliability for the CPL-W model, (6.103), where $\hat{\sigma}_V = 1$, $\zeta = 5$, $V = 10^6$, $t_c = 0.05$, and $\hat{\rho} = 50$, and where $\bar{\sigma}$ takes values {0.4, 0.5, 0.6 0.7}, σ_p takes values {1, 1.25, 1.5} $\bar{\sigma}$, and where k_p accordingly varies from zero to two

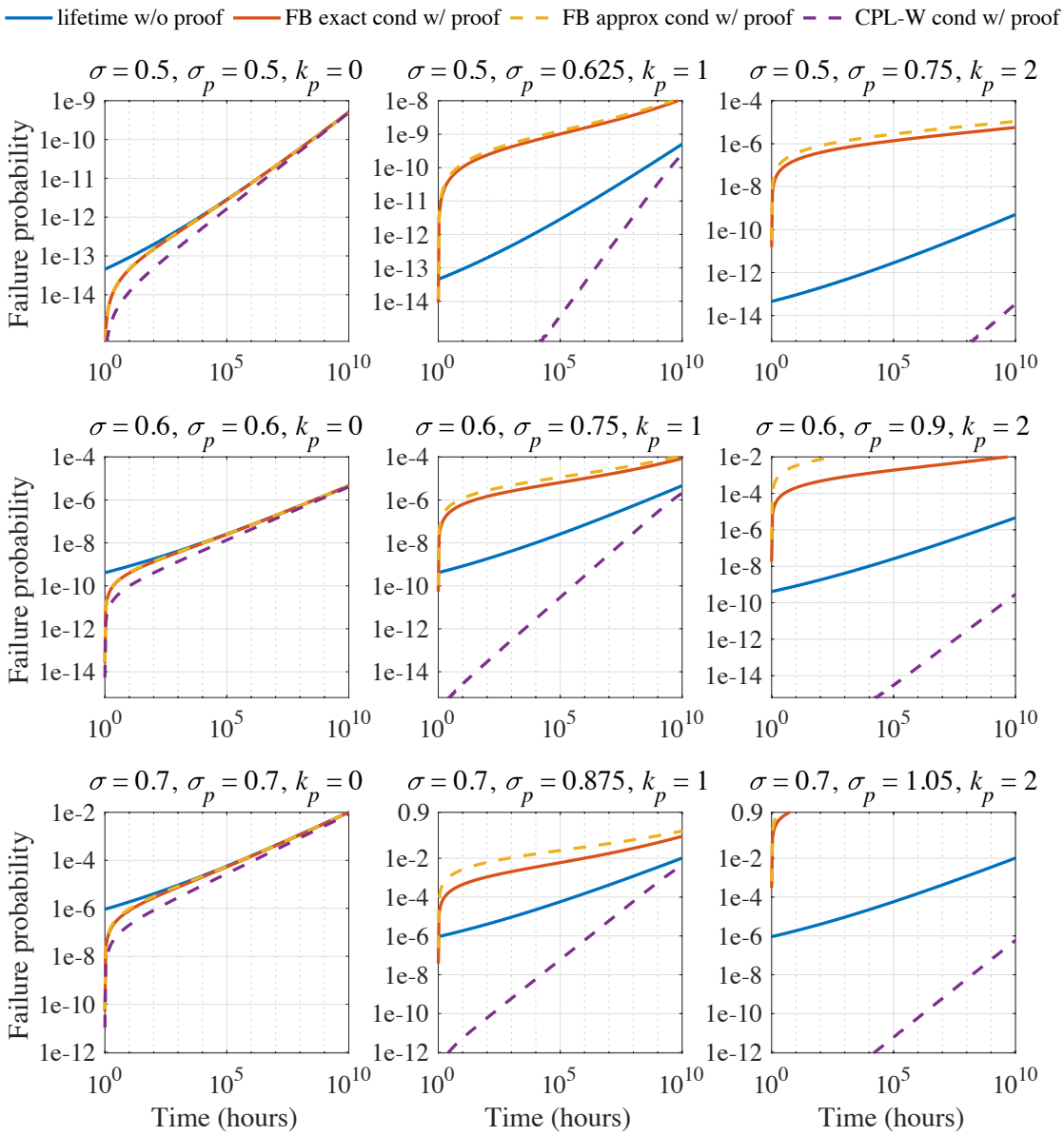

Figure 6.9 Plots of the conditional failure probability for a planar array after a proof test (equation (6.104) for 'exact' and equation (6.105) for 'approx.') as compared to the lifetime reliability without a proof test (equation (6.45)) and to the conditional reliability for the CPL-W model, (6.103), where $\hat{\sigma}_V = 1$, $\zeta = 5$, $V = 10^6$, $t_c = 0.05$, and $\hat{\rho} = 100$, and where $\bar{\sigma}$ takes values {0.5, 0.6 0.7}, σ_p takes values {1, 1.25, 1.5} $\bar{\sigma}$, and where k_p accordingly varies from zero to two

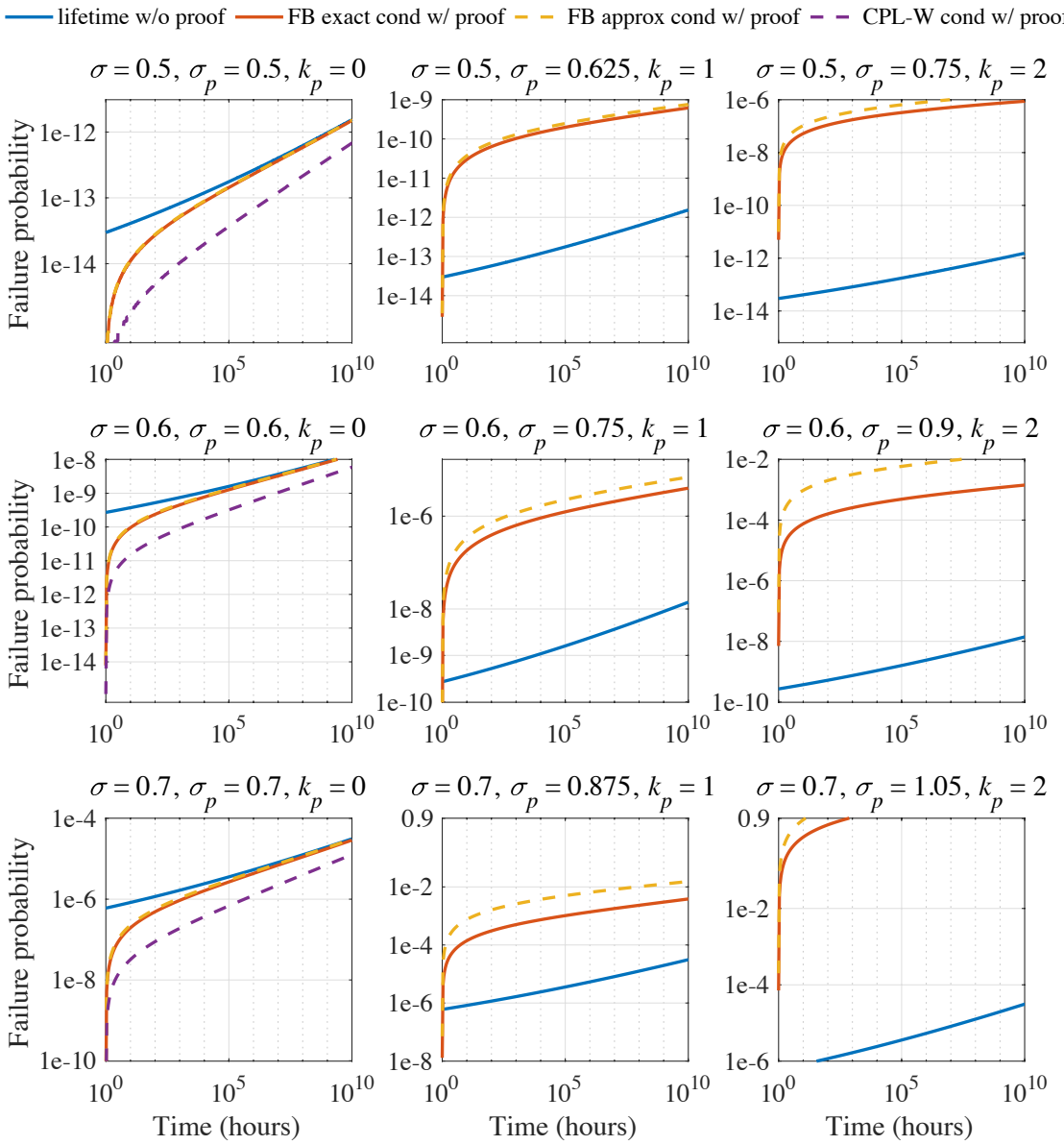

Figure 6.10 Plots of the conditional failure probability for a planar array after a proof test (equation (6.104) for 'exact' and equation (6.105) for 'approx.') as compared to the lifetime reliability without a proof test (equation (6.45)) and to the conditional reliability for the CPL-W model, (6.103), where $\hat{\sigma}_V = 1$, $\zeta = 5$, $V = 10^6$, $t_c = 0.05$, and $\hat{\rho} = 200$, and where $\bar{\sigma}$ takes values {0.5, 0.6 0.7}, σ_p takes values {1, 1.25, 1.5} $\bar{\sigma}$, and where k_p accordingly varies from zero to two

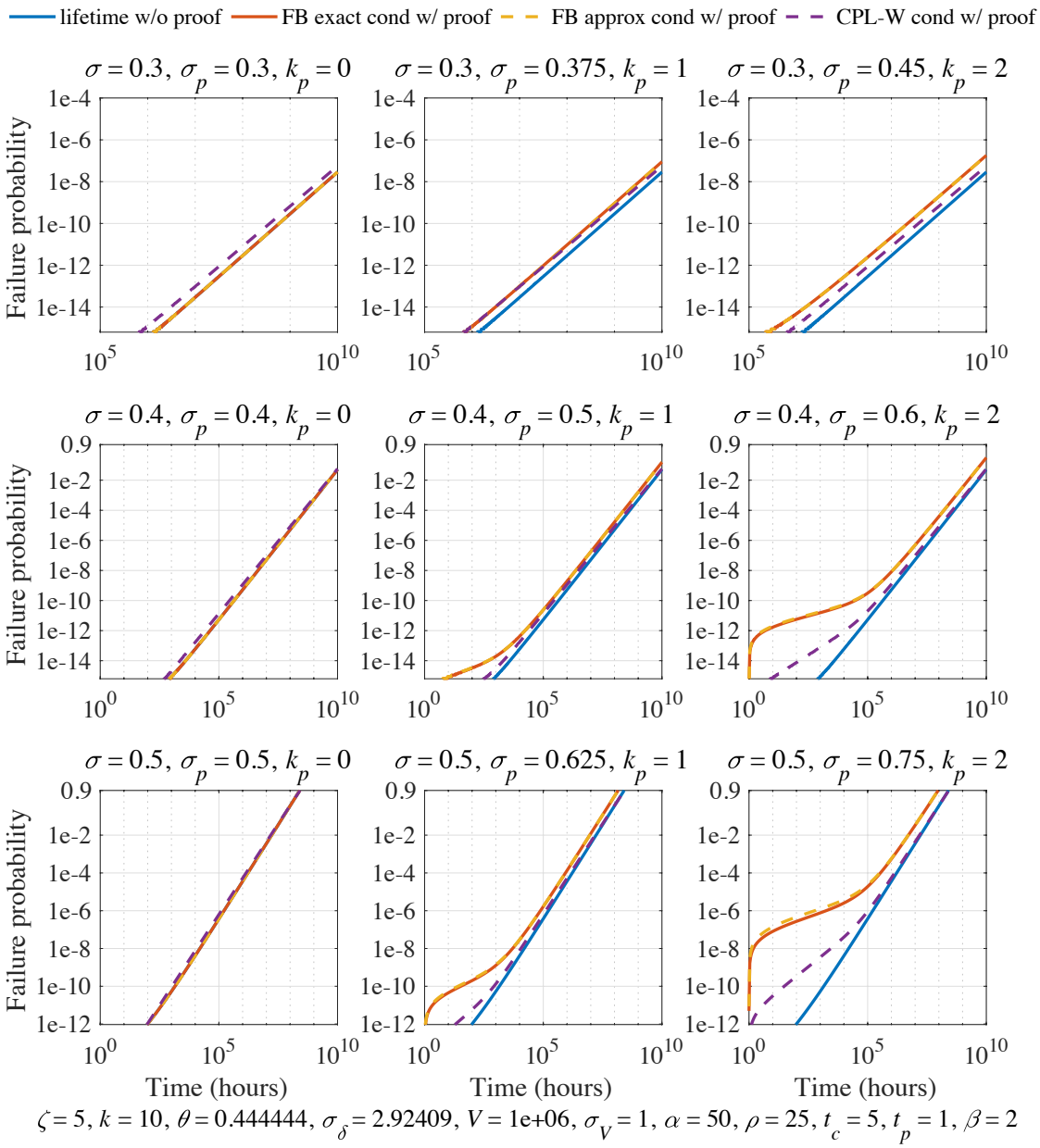

Figure 6.11 Plots of the conditional failure probability for a planar array after a proof test (equation (6.104) for 'exact' and equation (6.105) for 'approx.') as compared to the lifetime reliability without a proof test (equation (6.45)) and to the conditional reliability for the CPL-W model, (6.103), where $\hat{\sigma}_V = 1$, $\zeta = 5$, $V = 10^6$, $t_c = 5$, and $\hat{\rho} = 25$, and where $\bar{\sigma}$ takes values {0.3, 0.4 0.5}, σ_p takes values {1, 1.25, 1.5} $\bar{\sigma}$, and where k_p accordingly varies from zero to two

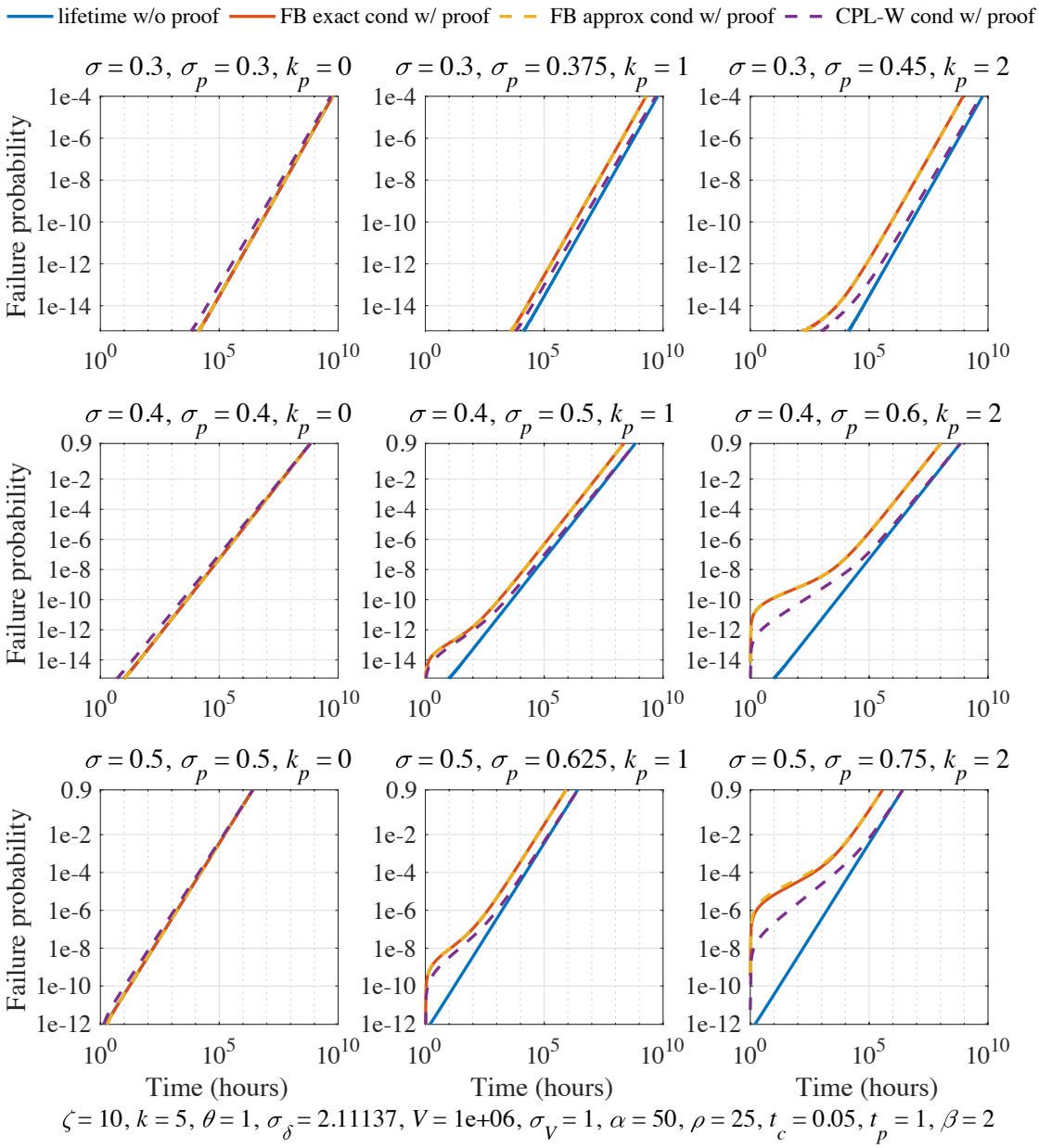

Figure 6.12 Plots of the conditional failure probability for a planar array after a proof test (equation (6.104) for 'exact' and equation (6.105) for 'approx.') as compared to the lifetime reliability without a proof test (equation (6.45)) and to the conditional reliability for the CPL-W model, (6.103), where $\hat{\sigma}_V = 1$, $\zeta = 10$, $V = 10^6$, $t_c = 0.05$, and $\hat{\rho} = 25$, and where $\bar{\sigma}$ takes values {0.3, 0.4, 0.5}, σ_p takes values {1, 1.25, 1.5} $\bar{\sigma}$, and where k_p accordingly varies from zero to two

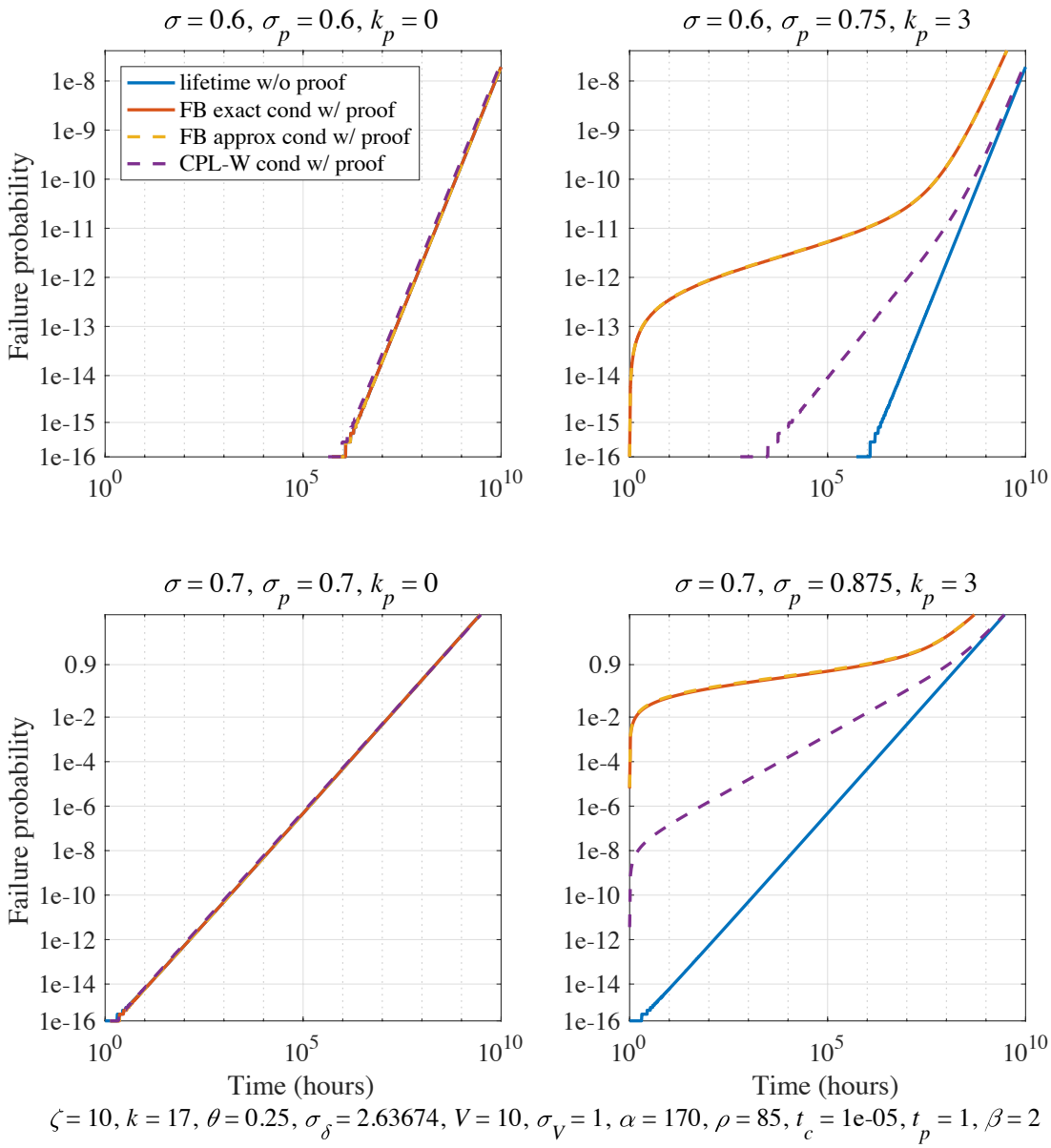

Figure 6.13 Plots of the conditional failure probability for a hexagonal array after a proof test (equation (6.104) for 'exact' and equation (6.105) for 'approx.') as compared to the lifetime reliability without a proof test (equation (6.45)) and to the conditional reliability for the CPL-W model, (6.103), where $\hat{\sigma}_V = 1$, $\xi = 10$, $V = 10$, $t_c = 10^{-5}$, and $\hat{\rho} = 85$, and where $\bar{\sigma}$ takes values $\{0.6, 0.7\}$, σ_p takes values $\{1, 1.25\}\,\bar{\sigma}$, and where k_p accordingly varies from zero to three

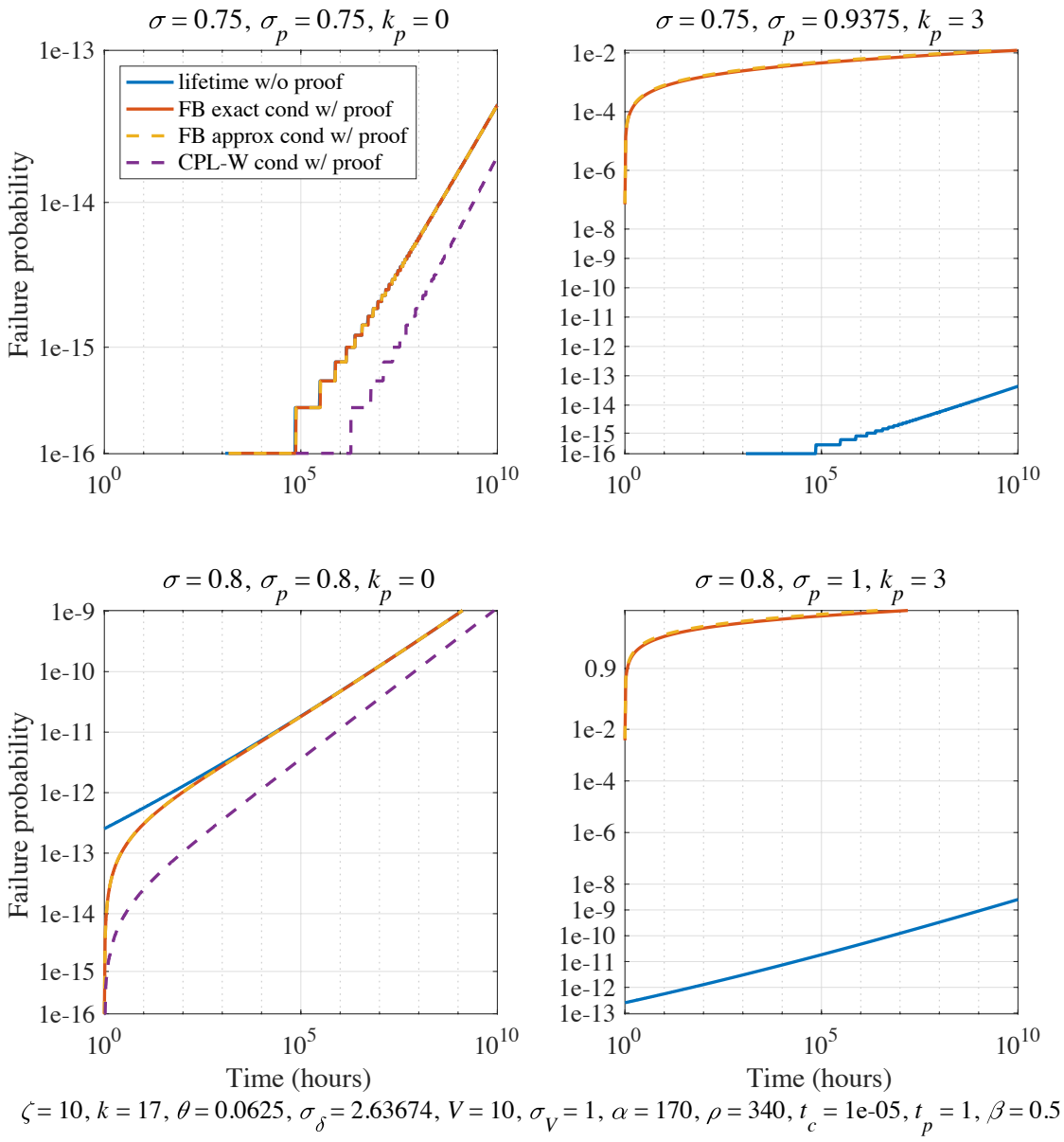

Figure 6.14 Plots of the conditional failure probability for a hexagonal array after a proof test (equation (6.104) for 'exact' and equation (6.105) for 'approx.') as compared to the lifetime reliability without a proof test (equation (6.45)) and to the conditional reliability for the CPL-W model, (6.103), where $\hat{\sigma}_V = 1$, $\zeta = 10$, $V = 10$, $t_c = 10^{-5}$, and $\hat{\rho} = 340$, and where $\bar{\sigma}$ takes values {0.6, 0.7}, σ_p takes values {1, 1.25} $\bar{\sigma}$, and where k_p accordingly varies from zero to three

For the case of a 3D hexagonal array, Figures 6.13 and 6.14 present the two different regimes of $\hat{\beta} > 1$ and $\hat{\beta} \leq 1$ respectively. In the case of a hexagonal array, $\hat{\alpha}$ becomes very large, even when choosing a smaller volume, V. Thus the overall failure probability becomes much less, and we have to switch to higher loads to have failure probabilities greater than 10^{-16}, Matlab's computational limit. Be aware that the steps at very low failure proabilities in Figures 6.13 and 6.14 are numerical artifacts. In Figure 6.14, on the right hand plots, the conditional failure probability for the CPL-W model does not appear because the failure probability is below 10^{-16}.

The trends in the hexagonal case, Figures 6.13 and 6.14, are largely the same as for the planar case, Figures 6.6 to 6.12, with the features being exaggerated between the CPL-W model and the stochastic fiber breakage model.

6.6. Conclusions

There is anecdotal evidence that proof testing carbon COPVs does more harm than good, in terms of creating many clusters of broken fibers that would otherwise not occur, and despite weeding out the rare weak specimen. However, none of the current statistical stress rupture models can predict a weakening due to the proof test. In this paper we have developed the stochastic fiber breakage model, a statistical model for stress rupture failure based on the mechanics of local load sharing. This model, while very similar to the strength and lifetime cases of the current models, does predict a conditional reliability following a proof test that is lower than that of a simple sustained lifetime load. In some cases, mostly those that relate to polymer fibers, this increase is negligible. However, for carbon fibers this decrease in predicted reliability can be very large.

6.7 Appendix

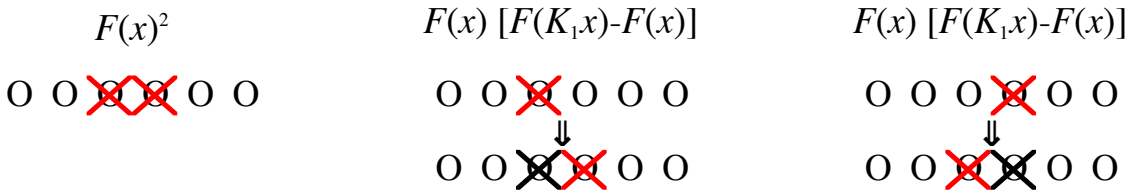

Figure 6.15 All possible sequences for two fibers to break, along with the associated failure probability for each sequence

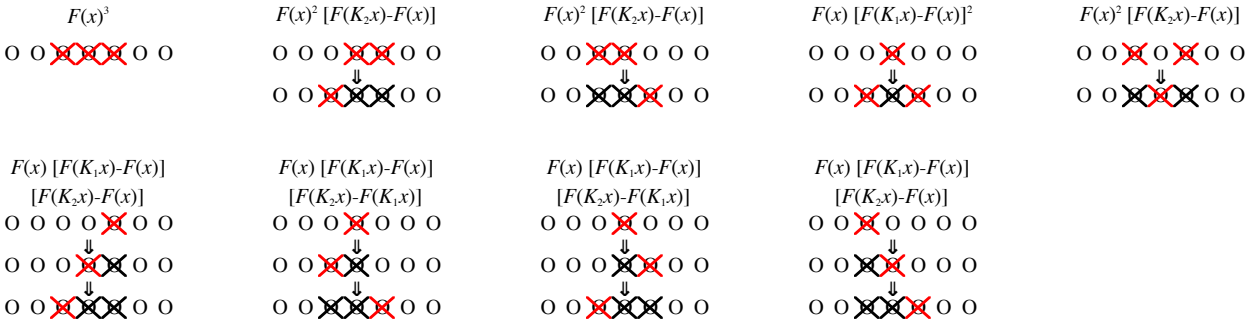

Figure 6.16 All possible sequences for three fibers to break, along with the associated failure probability for each sequence

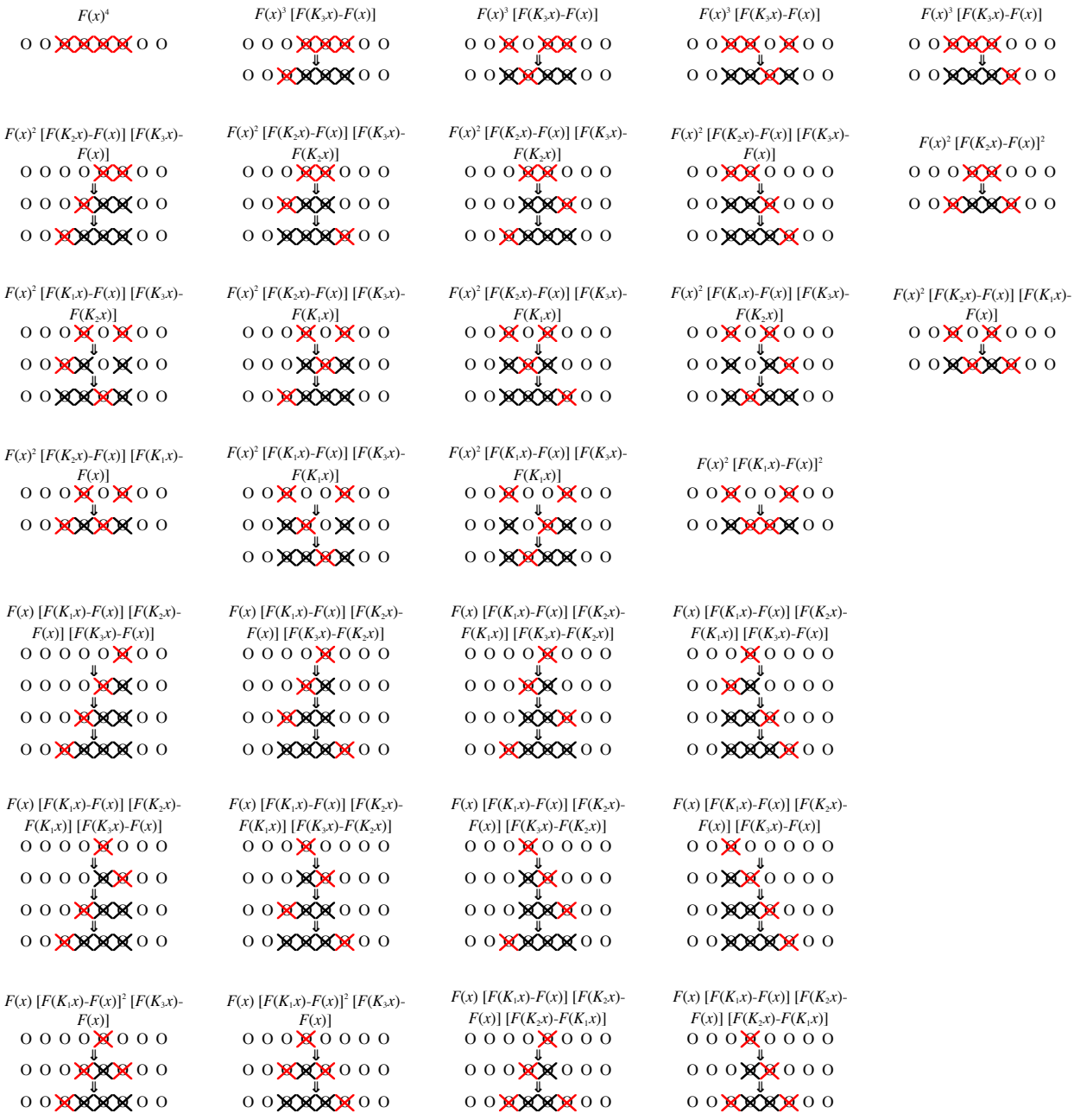

Figure 6.17 All possible sequences for four fibers to break, along with the associated failure probability for each sequence

$F(x)^5$
$F(x)^4\ [F(K_4x)\text{-}F(x)]$
$F(x)^4\ [F(K_4x)\text{-}F(x)]$
$F(x)^4\ [F(K_4x)\text{-}F(x)]$
$F(x)^4\ [F(K_4x)\text{-}F(x)]$
$F(x)^4\ [F(K_4x)\text{-}F(x)]$
$F(x)^3\ [F(K_3x)\text{-}F(x)]\ [F(K_4x)\text{-}F(x)]$
$F(x)^3\ [F(K_3x)\text{-}F(x)]\ [F(K_4x)\text{-}F(K_3x)]$
$F(x)^3\ [F(K_3x)\text{-}F(x)]\ [F(K_4x)\text{-}F(K_3x)]$
$F(x)^3\ [F(K_3x)\text{-}F(x)]\ [F(K_4x)\text{-}F(x)]$
$F(x)^3\ [F(K_3x)\text{-}F(x)]^2$
$F(x)^3\ [F(K_1x)\text{-}F(x)]\ [F(K_4x)\text{-}F(K_3x)]$
$F(x)^3\ [F(K_3x)\text{-}F(x)]\ [F(K_4x)\text{-}F(K_1x)]$
$F(x)^3\ [F(K_3x)\text{-}F(x)]\ [F(K_4x)\text{-}F(K_2x)]$
$F(x)^3\ [F(K_2x)\text{-}F(x)]\ [F(K_4x)\text{-}F(K_3x)]$
$F(x)^3\ [F(K_2x)\text{-}F(x)]\ [F(K_4x)\text{-}F(K_3x)]$
$F(x)^3\ [F(K_3x)\text{-}F(x)]\ [F(K_4x)\text{-}F(K_2x)]$
$F(x)^3\ [F(K_3x)\text{-}F(x)]\ [F(K_4x)\text{-}F(K_1x)]$
$F(x)^3\ [F(K_1x)\text{-}F(x)]\ [F(K_4x)\text{-}F(K_3x)]$
$F(x)^3\ [F(K_1x)\text{-}F(x)]\ [F(K_3x)\text{-}F(x)]$
$F(x)^3\ [F(K_2x)\text{-}F(x)]\ [F(K_3x)\text{-}F(x)]$
$F(x)^3\ [F(K_2x)\text{-}F(x)]\ [F(K_3x)\text{-}F(x)]$
$F(x)^3\ [F(K_1x)\text{-}F(x)]\ [F(K_3x)\text{-}F(x)]$
$F(x)^3\ [F(K_2x)\text{-}F(x)]\ [F(K_4x)\text{-}F(K_2x)]$
$F(x)^3\ [F(K_2x)\text{-}F(x)]\ [F(K_4x)\text{-}F(K_2x)]$
$F(x)^3\ [F(K_2x)\text{-}F(x)]^2$
$F(x)^3\ [F(K_1x)\text{-}F(x)]\ [F(K_4x)\text{-}F(K_2x)]$
$F(x)^3\ [F(K_2x)\text{-}F(x)]\ [F(K_4x)\text{-}F(K_1x)]$
$F(x)^3\ [F(K_2x)\text{-}F(x)]\ [F(K_1x)\text{-}F(x)]$
$F(x)^3\ [F(K_2x)\text{-}F(x)]\ [F(K_4x)\text{-}F(K_1x)]$
$F(x)^3\ [F(K_1x)\text{-}F(x)]\ [F(K_4x)\text{-}F(K_2x)]$
$F(x)^3\ [F(K_2x)\text{-}F(x)]\ [F(K_1x)\text{-}F(x)]$
$F(x)^2\ [F(K_2x)\text{-}F(x)]\ [F(K_3x)\text{-}F(x)]\ [F(K_4x)\text{-}F(x)]$
$F(x)^2\ [F(K_2x)\text{-}F(x)]\ [F(K_3x)\text{-}F(x)]\ [F(K_4x)\text{-}F(K_3x)]$
$F(x)^2\ [F(K_2x)\text{-}F(x)]\ [F(K_3x)\text{-}F(K_2x)]\ [F(K_4x)\text{-}F(K_3x)]$
$F(x)^2\ [F(K_2x)\text{-}F(x)]\ [F(K_3x)\text{-}F(K_2x)]\ [F(K_4x)\text{-}F(x)]$
$F(x)^2\ [F(K_2x)\text{-}F(x)]\ [F(K_3x)\text{-}F(K_2x)]\ [F(K_4x)\text{-}F(x)]$
$F(x)^2\ [F(K_2x)\text{-}F(x)]\ [F(K_3x)\text{-}F(K_2x)]\ [F(K_4x)\text{-}F(K_3x)]$
$F(x)^2\ [F(K_2x)\text{-}F(x)]\ [F(K_3x)\text{-}F(x)]\ [F(K_4x)\text{-}F(K_3x)]$
$F(x)^2\ [F(K_2x)\text{-}F(x)]\ [F(K_3x)\text{-}F(x)]\ [F(K_4x)\text{-}F(x)]$
$F(x)^2\ [F(K_2x)\text{-}F(x)]^2\ [F(K_4x)\text{-}F(x)]$
$F(x)^2\ [F(K_2x)\text{-}F(x)]^2\ [F(K_4x)\text{-}F(x)]$
$F(x)^2\ [F(K_2x)\text{-}F(x)]\ [F(K_3x)\text{-}F(x)]\ [F(K_3x)\text{-}F(K_2x)]$
$F(x)^2\ [F(K_2x)\text{-}F(x)]\ [F(K_3x)\text{-}F(x)]\ [F(K_3x)\text{-}F(K_2x)]$
$F(x)^2\ [F(K_1x)\text{-}F(x)]\ [F(K_2x)\text{-}F(x)]\ [F(K_4x)\text{-}F(K_3x)]$
$F(x)^2\ [F(K_1x)\text{-}F(x)]\ [F(K_2x)\text{-}F(x)]\ [F(K_4x)\text{-}F(K_3x)]$
$F(x)^2\ [F(K_1x)\text{-}F(x)]\ [F(K_3x)\text{-}F(K_2x)]\ [F(K_4x)\text{-}F(K_2x)]$
$F(x)^2\ [F(K_1x)\text{-}F(x)]\ [F(K_3x)\text{-}F(K_2x)]\ [F(K_4x)\text{-}F(K_1x)]$
$F(x)^2\ [F(K_1x)\text{-}F(x)]\ [F(K_3x)\text{-}F(K_2x)]\ [F(K_4x)\text{-}F(K_1x)]$
$F(x)^2\ [F(K_1x)\text{-}F(x)]\ [F(K_3x)\text{-}F(K_2x)]\ [F(K_4x)\text{-}F(K_2x)]$
$F(x)^2\ [F(K_2x)\text{-}F(x)]\ [F(K_3x)\text{-}F(K_1x)]\ [F(K_4x)\text{-}F(x)]$
$F(x)^2\ [F(K_2x)\text{-}F(x)]\ [F(K_3x)\text{-}F(K_1x)]\ [F(K_4x)\text{-}F(K_3x)]$
$F(x)^2\ [F(K_2x)\text{-}F(x)]\ [F(K_3x)\text{-}F(K_1x)]\ [F(K_4x)\text{-}F(K_3x)]$
$F(x)^2\ [F(K_1x)\text{-}F(x)]\ [F(K_3x)\text{-}F(K_1x)]\ [F(K_4x)\text{-}F(x)]$
$F(x)^2\ [F(K_1x)\text{-}F(x)]\ [F(K_3x)\text{-}F(K_2x)]\ [F(K_2x)\text{-}F(x)]$
$F(x)^2\ [F(K_2x)\text{-}F(x)]\ [F(K_3x)\text{-}F(K_1x)]^2$
$F(x)^2\ [F(K_1x)\text{-}F(x)]\ [F(K_3x)\text{-}F(K_2x)]\ [F(K_2x)\text{-}F(x)]$
$F(x)^2\ [F(K_1x)\text{-}F(x)]\ [F(K_2x)\text{-}F(x)]\ [F(K_4x)\text{-}F(K_1x)]$
$F(x)^2\ [F(K_2x)\text{-}F(x)]\ [F(K_1x)\text{-}F(x)]\ [F(K_4x)\text{-}F(x)]$
$F(x)^2\ [F(K_2x)\text{-}F(x)]\ [F(K_1x)\text{-}F(x)]\ [F(K_4x)\text{-}F(x)]$
$F(x)^2\ [F(K_2x)\text{-}F(x)]\ [F(K_1x)\text{-}F(x)]\ [F(K_4x)\text{-}F(K_1x)]$
$F(x)^2\ [F(K_1x)\text{-}F(x)]^2\ [F(K_4x)\text{-}F(K_2x)]$
$F(x)^2\ [F(K_1x)\text{-}F(x)]^2\ [F(K_2x)\text{-}F(x)]$
$F(x)^2\ [F(K_1x)\text{-}F(x)]^3$
$F(x)^2\ [F(K_1x)\text{-}F(x)]^3$
$F(x)^2\ [F(K_1x)\text{-}F(x)]\ [F(K_3x)\text{-}F(K_1x)]\ [F(K_2x)\text{-}F(K_1x)]$

Figure 6.18 All possible sequences for five fibers to break, along with the associated failure probability for each sequence

REFERENCES

[42] Phoenix, S.L. and Beyerlein, I.J. (2001). Statistical Strength Theory for Fibrous Composite Materials, In: Chou, T.W. and Zweben, C. (eds), Chapter 19 in Comprehensive Composites, 1: 559–640.

[43] Beyerlein, IJ and S. L. Phoenix. Statistics for the strength and size effects of microcomposites with four carbon fibers in epoxy resin. Composites Science and Technology 56(1), pp. 75-92. 1996. . DOI: 10.1016/0266-3538(95)00131-X.

[44] Hedgepeth JM. Stress concentrations in filamentary structures. NASA TN D-882, 1961.

[45] Fuminori Hikami and Tsu-Wei Chou. Explicit crack problem solutions of unidirectional composites - Elastic stress concentrations, AIAA Journal, Vol. 28, No. 3 (1990), pp. 499-505.

[46] Hedgepeth, J.M. and Van Dyke, P. (1967). Local Stress Concentration in Imperfect Filamentary Composite Materials, J. Comp. Mater., 1: 294–309.

[47] Beyerlein, IJ and S. L. Phoenix. Stress concentrations around multiple fiber breaks in an elastic matrix with local yielding or debonding using quadratic influence superposition. Journal of the Mechanics and Physics of Solids 44(12), pp. 1997-2039. 1996. . DOI: 10.1016/S0022-5096(96)00068-3.

[48] Beyerlein, IJ S. L. Phoenix and A. M. Sastry. Comparison of shear-lag theory and continuum fracture mechanics for modeling fiber and matrix stresses in an elastic cracked composite lamina. International Journal of Solids and Structures 33(18), pp. 2543-2574. 1996. . DOI: 10.1016/0020-7683(95)00172-7.

[49] Beyerlein, IJ and C. M. Landis. Shear-lag model for failure simulations of unidirectional fiber composites including matrix stiffness. Mechanics of Materials 31(5), pp. 331-350. 1999. . DOI: 10.1016/S0167-6636(98)00075-1.

[50] Beyerlein, I.J., Amer, M., Schadler, L.S. and Phoenix, S.L. (1998). New Methodology for Determining in situ Fiber, Matrix and Interface Stresses in Damaged Multifiber Composites, Sci. Eng. Comp. Mater., 7: 151–204.

[51] Mahesh, S, and S. L. Phoenix. Lifetime distributions for unidirectional fibrous composites under creep-rupture loading. International Journal of Fracture 127(4), pp. 303-360. 2004. . DOI: 10.1023/B:FRAC.0000037675.72446.7c.

[52] Mahesh, S, I. J. Beyerlein and S. L. Phoenix. Size and heterogeneity effects on the strength of fibrous composites. Physica D: Nonlinear Phenomena 133(1), pp. 371-389. 1999. . DOI: 10.1016/S0167-2789(99)00082-2.

[53] Mahesh, S, S. L. Phoenix and I. J. Beyerlein. Strength distributions and size effects for 2D and 3D composites with weibull fibers in an elastic matrix. International Journal of Fracture 115(1), pp. 41-85. 2002. . DOI: 10.1023/A:1015729607223.

[54] Ibnabdeljalil, M, and W. A. Curtin. Strength and reliability of fiber-reinforced composites: Localized load-sharing and associated size effects. International Journal of Solids and Structures 34(21), pp. 2649-2668. 1997.

[55] Iyengar, N and W. A. Curtin. Time-dependent failure in fiber-reinforced composites by matrix and interface shear creep. Acta Materialia 45(8), pp. 3419-3429. 1997. . DOI: 10.1016/S1359-6454(96)00412-0.

[56] Zhou, C.H., Beyerlein, I.J. and Schadler, L.S. (2003). Time-dependent Micromechanical Behavior in Graphite/Epoxy Composites under Constant Load at Elevated Temperatures, J. Mater. Sci., 38: 877–884.

[57] Zhou, C.H., Schadler, L.S. and Beyerlein, I.J. (2002). Time-dependent Micromechanical Behavior in Graphite/Epoxy Composites under Constant Load: a Combined Experimental and Theoretical Study, Acta Materialia, 50: 365–377

[58] Zhou, C.H., Schadler, L.S. and Beyerlein, I.J. (2004). Stress Concentrations in Graphite/Epoxy Model Composites during Creep at Room Temperature and Elevated Temperatures, J. Composite Materials 38: 417-433.

[59] Rossettos, J. N. and K. Sakkas. 1991. "Effect of Fiber Modulus Variations on Stress Concentration in Hybrid Composites," AIAA Jnl., 29(3):482-484.

[60] Dharani, L. R., W. F. Jones, and J. G. Goree. "Mathematical Modeling of Damage in Unidirectional Composites." Engineering Fracture Mechanics, vol. 17, no. 6, 1983, pp. 555-573.

[61] Goree, James G., and Robert S. Gross. "Analysis of a Unidirectional Composite Containing Broken Fibers and Matrix Damage." Engineering Fracture Mechanics, vol. 13, no. 3, 1980, pp. 563-578. Nairn, JA and H. Wagner. A revised shear-lag analysis of an energy model for fiber-matrix debonding. Advanced Composites Letters 5(5), pp. 131-135. 1996.

[62] Nairn, JA. A variational mechanics analysis of the stresses around breaks in embedded fibers. Mechanics of Materials 13(2), pp. 131-154. 1992. . DOI: 10.1016/0167-6636(92)90042-C.

[63] Nairn, JA. Fracture mechanics of unidirectional composites using the shear-lag model I: Theory. Journal of Composite Materials 22(6), pp. 561-588. 1988. . DOI: 10.1177/002199838802200604.

[64] Nairn, JA. Fracture mechanics of unidirectional composites using the shear-lag model II: Experiment. Journal of Composite Materials 22(6), pp. 589-600. 1988. . DOI: 10.1177/002199838802200605.

[65] Nairn, JA. On the use of shear-lag methods for analysis of stress transfer in unidirectional composites. Mechanics of Materials 26(2), pp. 63-80. 1997. . DOI: 10.1016/S0167-6636(97)00023-9.

[66] Beyerlein,IJ S. L. Phoenix and R. Raj. Time evolution of stress redistribution around multiple fiber breaks in a composite with viscous and viscoelastic matrices. International Journal of Solids and Structures 35(24), pp. 3177-3211. 1998. . DOI: 10.1016/S0020-7683(98)00010-9.

[67] Brinson, Hal F., and L. C. Brinson. Polymer Engineering Science and Viscoelasticity: An Introduction. Springer US, Boston, MA, 2015, doi:10.1007/978-1-4899-7485-3.

[68] Lagoudas, DC, C.Y. Hui, S.L. Phoenix. Time evolution of overstress profiles near broken fibers in a composite with a viscoelastic matrix. Int. J. Solids Structures, 25 (1989), pp. 45–66

[69] Smith, R. L., Phoenix, S. L., Greenfield, M. R., Henstenburg, R. B., Pitt, R. E. 1983. Proc. R. Soc. Lond. A, 388:353–391.

[70] Phoenix, S.L., Schwartz, P. and Robinson, H.H. (1988). Statistics for the Strength and Lifetime in Creep-rupture of Model Carbon/Epoxy Composites, Comp. Sci. Tech., 32: 81–120.

CHAPTER 7

CONCLUSIONS AND FUTURE DIRECTIONS

From the research presented in this dissertation, we now know how to analyze a dataset in terms of the CPL-W model. We also know that there are very few differences across models that match the 1979 functional form, and practically no differences that one would expect to see in an experimental dataset. However it unknown how an analysis assuming the CPL-W model would compare to a similar analysis for a different 1979 model in terms of accurate failure probability estimates. In particular, if data is simulated from a version of the 1979 model as disparate as possible from the CPL-W model, would it be better to analyze the dataset using the CPL-W method detailed in Chapter 3, or a unified MLE approach assuming the 1979 functional form, which requires estimation of two additional parameters.

Better material characterization is also a future area of interest. Good material characterization requires well planed tests, as stress rupture testing is expensive. The expense is partly due to the cost of samples, but also due to programs frequently taking up to ten years involving expensive equipment. Careful test design results in more meaningful and useful data – while each specimen results in a single point of data, not all points contain equal 'information' when used in MLE. For example, a group of specimens that happen to be loaded at too low a load level will have no failures, thus adding very little information to the dataset, while tying up equipment and precluding the opportunity to reload the equipment with new specimens. A well planned test design based on preliminary information would avoid these difficulties.

Past stress rupture datasets frequently show minimal planning. One particular dataset of Toray T1000 carbon/epoxy strands (the highest performing fiber available) has five different

lifetime load levels – while most have two or three – and at three of those levels fewer than four specimens were tested, while the other two levels had at least 25 specimens each. In addition the test time for each specimen, within a single load level, varied by as much as a factor of five. In a different dataset for T1000 COPVs with 30 specimens at each of three load levels, the lowest load level was set so low as to have no failures after five years, and the mid load level only had two failures. Even the small amount of preliminary data available would have predicted that these levels were too low and likely to be unproductive.

Designing a test that is optimal, in terms of both the cost and also the accuracy of reliability estimates based on the dataset to be generated, will improve material characterization. Stress rupture datasets are limited, so it is critical to maximize the amount of information contained in each point of data. Maximizing information reduces the variance in the resulting reliability estimates, which is highly important as generally the variance is fairly high. Testing more specimens would also reduce the variance, but this can be too expensive when the specimens are COPVs.

Test design variables to optimize over are:

- How many specimens tested in strength testing
- What loading rate should be used in strength testing
- How many distinct lifetime load levels
- What are the lifetime load levels
- How many specimens at each load level
- How long should each specimen be tested
- Best strategy for reloading test stations with new specimens after specimens have failed

There are two related sensitivity questions. The first is on the material parameters: how accurately do the parameters need to be known ahead of time to be able to design an optimal test, and how much does the optimal test differ for different materials. The second is on the number of specimens and maximum censor time: with more specimens and more time the variance in the reliability estimate should decrease, but does it do so smoothly, or is there a point at which a few more specimens means a large drop in the variance?

By determining better test setups we can get better characterization of materials with no extra cost. Currently we are not producing enough data for T1000 carbon with the type of testing that is being done in order to be able to predict the reliability with reasonable confidence. To compensate for this, industry currently uses a very large safety factor. Better characterization will allow for better-informed safety decisions regarding COPVs and systems using COPVs.

Another aspect of better characterization is determining the effects of proof testing. Proof testing is commonly preformed on a COPV. In proof testing the COPV is raised to a pressure considerably higher than its mean effective operating pressure (MEOP), and held there for some amount of time. Proof testing is performed to weed out weak vessels due to manufacturing anomalies, yet damage is done during the test since fibers break during testing. It is a current matter of debate as to whether or not the damage done out weighs the benefit. The FB model predicts very different results after a proof test than the CPL-W model. As it currently stands there is no test data that allows for any determination of which model is more accurate.

A final area of future interest is predicting the reliability of a large COPV from tests of smaller structures of the same material. Currently to predict the stress rupture behavior of a particular size and type of COPV, we need a stress rupture dataset generated from identical COPVs. The cost of such testing on large COPVs makes this infeasible, so it is necessary to

predict the reliability of a large COPV based on tests run on smaller samples and models of the failure mechanisms to bridge the scales.

COPV testing is expensive, yet the material can be tested more economically. Large COPVs can cost upwards of $50,000 each. Testing facilities for such COPVs need to be large with controlled temperature and humidity. Each COPV requires equipment to maintain the desired pressure and protect the COPV from failures of neighboring COPVs. By testing the material in smaller structures, such as strands, tows, rings (split D or NOL), or even laboratory scale COPVs, we can reduce many of the expenses. Thus by testing smaller samples we can in principal get larger data sets, but we need to be able to scale up those results.

There is theory to describe how reliability scales with length for fibers, which was described in Chapter 6. This theory also works when scaling strength with length for fiber/epoxy strands, but the parameters are different. Scaling from strands to small and large COPVs is more challenging; on a case-by-case basis it has been done successfully, once the controlling mechanisms were appreciated. Difficulties arise because of the massive material volume difference and the differences in fiber/matrix load sharing brought about by crossing layers and uneven stress distributions in a COPV, particularly at the ends. What is needed is a formalized approach to predicting large COPV reliability from material testing of smaller structures.